

**SERI/TR-217-3036**

**DE88001132**

**UC Category: 261**

**The MOD-2 Wind  
Turbine:  
Aeroacoustical Noise  
Sources, Emissions, and  
Potential Impact**

**N. D. Kelley**

**H. E. McKenna**

**E. W. Jacobs**

**R. R. Hemphill**

**N. J. Birkenheuer**

**January 1988**

**Prepared under Task No. WE721201**

**FTP No. 562**

**Solar Energy Research Institute**

A Division of Midwest Research Institute

1617 Cole Boulevard

Golden, Colorado 80401-3393

Prepared for the

**U.S. Department of Energy**

Contract No. DE-AC02-83CH10093

#### NOTICE

This report was prepared as an account of work sponsored by the United States Government. Neither the United States nor the United States Department of Energy, nor any of their employees, nor any of their contractors, subcontractors, or their employees, makes any warranty, expressed or implied, or assumes any legal liability or responsibility for the accuracy, completeness or usefulness of any information, apparatus, product or process disclosed, or represents that its use would not infringe privately owned rights.

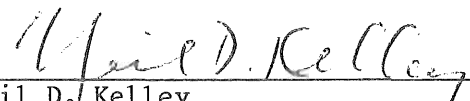
Printed in the United States of America  
Available from:  
National Technical Information Service  
U.S. Department of Commerce  
5285 Port Royal Road  
Springfield, VA 22161

Price: Microfiche A01  
Printed Copy A10

Codes are used for pricing all publications. The code is determined by the number of pages in the publication. Information pertaining to the pricing codes can be found in the current issue of the following publications, which are generally available in most libraries: *Energy Research Abstracts (ERA)*; *Government Reports Announcements and Index (GRA and I)*; *Scientific and Technical Abstract Reports (STAR)*; and publication, NTIS-PR-360 available from NTIS at the above address.

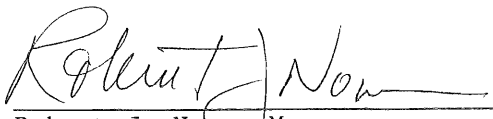
## PREFACE

This report summarizes extensive research by the staff of the Solar Energy Research Institute into characteristics of acoustic noise emissions of the DOE/NASA MOD-2 wind turbine. The results of this study have shown that the MOD-2 noise levels are well below annoyance thresholds within residential structures a kilometer or more from the turbine rotor. It was also found that the inflow turbulent structure has a major influence on the level and characteristics of the low-frequency (2-160 Hz) range acoustic emissions which, in turn, have implications for the associated structural response of the rotor assembly. The high-frequency range (A-weighted) levels were found to vary primarily with the mean hub-height wind speed. In addition, the rotor inflow turbulence characteristics at the Goodnoe Hills Site were found to be controlled almost entirely by the diurnal variation in the vertical stability of the first 100 m of the atmospheric boundary layer.

  
\_\_\_\_\_  
Neil D. Kelley  
Principal Scientist  
Wind Energy Research Branch

Approved for

SOLAR ENERGY RESEARCH INSTITUTE

  
\_\_\_\_\_  
Robert J. Noun, Manager  
Wind Energy Research Branch

  
\_\_\_\_\_  
Jack L. Stone, Director  
Solar Electric Research Division

### ACKNOWLEDGMENTS

The authors wish to acknowledge the excellent support and assistance of the following organizations in SERI's MOD-2 research effort:

- Boeing Aerospace Corporation
- Bonneville Power Administration
- Cornell University, Sibley School of Mechanical and Aerospace Engineering
- Engineering Dynamics, Inc.
- Fairchild-Weston, Inc.
- NASA Langley Research Center
- NASA Lewis Research Center
- Oregon State University, Atmospheric Sciences Department
- Pacific Northwest Laboratories
- B.C. Willmarth Co.

Special thanks are extended to Larry Gordon of NASA Lewis and Ron Holeman of the Bonneville Power Administration who provided the scheduling and support services so necessary to our effort. The support of Ron Schwemmer and Don Fries of Boeing was without reproach. We salute the dedicated efforts of Ben Willmarth who expertly operated the tethered balloon system under very adverse circumstances. We also extend our deepest thanks to David Long of Fairchild-Weston who provided us with outstanding data support services.

## SUMMARY

### Objective

This document summarizes the results of an extensive investigation by the Solar Energy Research Institute (SERI) into the factors relating to acoustic emissions associated with the operation of a MOD-2 wind turbine. The MOD-2 was the sixth in a series of turbine designs developed for the U.S. Department of Energy (DOE) by the Lewis Research Center of the National Aeronautics and Space Administration (NASA) as part of the Federal Wind Energy Program. The MOD-2 turbine has a rotor diameter of 91 m (300 ft) and is capable of generating 2.5 MW of electrical power at its rated wind speed of about 13 m/s (28 mph), measured at a rotor hub elevation of 61 m (200 ft). A cluster of three MOD-2 turbines installed on the Goodnoe Hills near Goldendale, Wash., was used for the experiments described in this report.

An investigation of the characteristics of the MOD-2's acoustic emissions was undertaken as a result of the experience SERI gained with its predecessor, the 2-MW MOD-1 turbine. One of the primary motivations for designing the MOD-2 turbine with its rotor upwind of the support tower was to avoid the impulsive, low-frequency noise associated with the downwind MOD-1. It was expected that placing the MOD-2 rotor upwind would largely eliminate the community annoyance problem that was characteristic of the impulsive MOD-1 emissions. It was not known, however, whether similar or perhaps greater levels of nonimpulsive, low-frequency noise that radiated from the large MOD-2 rotor as a result of inflow turbulence interactions would annoy the residents nearby. We designed our MOD-2 test program to answer these questions, including the following specific objectives:

- A general characterization of both low- (under 200 Hz) and high-frequency-range acoustic emissions
- The development of a methodology for making acoustic measurements in a windy environment
- The development of a methodology relating low-frequency acoustic emissions to the turbulent inflow structure
- The development of a methodology for predicting the interior annoyance potential of nearby residential structures from a wind turbine's low-frequency acoustic loadings
- The application of the annoyance potential criteria using MOD-2 emission levels measured under a range of operating conditions and a comparison of the results with similar ones for the MOD-1 turbine.

### Discussion

We undertook a series of five experiments from February 1981 to August 1986 to characterize the MOD-2's acoustic emissions. The primary experiments, however, were performed during May 1982 and August 1983, using Turbine No. 2 at the Goodnoe Hills site. The 1982 experiments collected statistical measurements of high-frequency-range emissions as well as low-frequency data. The 1983 experiment was designed to be more narrow in scope but included additional parameters not available in 1982, such as rotor surface pressures and

high-frequency turbulence measurements made from a fixed tower location and a tethered balloon flown in the turbine inflow. Major modifications were made to Turbine No. 2 between the 1982 and 1983 experiments as a result of operational instabilities. These included installing vortex generators along the rotor's leading edge over 70% of the blade span and establishing a different blade pitch sequence in the control system software. These changes required us to stratify the low-frequency data collected during these two experiments by year.

In order to make low-frequency noise measurements in a windy environment, we developed a technique that employs a pair of ground-mounted microphones spaced 15 m apart. Cross-correlation signal processing procedures were then used to obtain the in-phase acoustic portion of the signal while largely rejecting the random, turbulence-induced contribution. Inflow measurements were made from fixed meteorological towers located outside the turbine induction zone and from a tethered balloon flown approximately 1.5 rotor diameters (1.5D) upwind of the rotor plane. Both standard-response and high-frequency anemometers were used on both platforms. Twelve surface-mounted pressure transducers were attached to the upper and lower surfaces of Blade No. 1 on Turbine No. 2 at two span locations during the 1983 experiment.

The data categories--acoustic, atmospheric, and blade surface pressures--each necessitated somewhat different processing procedures. Because of the random or stochastic nature of the inflow turbulence responsible for exciting the acoustic response of the turbine, we developed a statistical sampling approach for presenting and quantifying the radiated acoustic spectra. Consistent with this approach, we characterized the turbulent inflow using the methods of statistical fluid mechanics and calculated a range of "bulk" flow parameters. We employed standard time-series analysis procedures in determining the MOD-2 aeroacoustic and surface pressure response functions.

Our detailed measurements of the inflow to Turbine No. 2 revealed a regime that is often stably stratified and contains multiple, thin layers of small-scale, anisotropic turbulence. There is strong evidence of the development of an internal boundary layer within the rotor disk's vertical envelope, whose formation and depth vary diurnally. Further, the vertical layer encompassing the rotor disk is influenced by the presence and breakdown of internal wave motions, accompanied by intense, small-scale turbulence. For example, under stable conditions, typical longitudinal or axial turbulence component length scales are in the neighborhood of 200 m, but those of the vertical or upwash (in-plane) component are often more than an order of magnitude smaller.

Measurements of emissions in the high-frequency range (400-8000 Hz) have shown that close to the rotor disk the radiation pattern resembles that of a classic quadrupole source. This pattern is then distorted by the prevailing wind at larger distances, i.e., extended downstream and contracted upstream of the rotor disk. Statistical measures of the A-weighted emissions over periods of several hours have shown the observed levels to be essentially normally distributed. The decay of these emission levels with distance (at Goodnoe Hills) can be described by the following polynomial:

$$L_{eq}(A) = -3.89464 x^4 + 46.6729 x^3 - 191.884 x^2 + 287.15 x - 28.4 ,$$

where  $x$  is the  $\log_{10}$  of the downwind distance, in feet. The departure from an  $r^2$  dependence is apparently the result of local propagation effects. The average audible range of a single MOD-2 at the Goodnoe Hills site has been estimated to be 1220 m (4000 ft) downwind of the turbine. Statistical measurements of the acoustic environment downwind of the site with up to three turbines operating show that the turbine noise level experienced by an observer is dominated by the closest turbine. The effects of multiple turbine operation, however, are most noticeable when the turbines are located at nearly the same upstream distance from the observer.

The A-weighted, equivalent sound pressure level or  $L_{eq}(A)$  at a distance of  $1.5D$  (137 m or 450 ft) from the rotor disk was found to vary primarily with the hub-height wind speed, though some slight dependency was noted on the vertical stability (Richardson number) and wind direction. The  $L_{eq}(A)$  variation, at this reference distance, can be expressed to within  $\pm 0.5$  dB by  $1/2 U_H + 57$  over a hub wind speed ( $U_H$ ) range of 6-15 m/s (13 to 34 mph).

An examination of the variation of 1/3-octave band spectra with inflow characteristics revealed that there was essentially a uniform increase in the observed average band pressure levels [ $L_{eq}(f_{1/3})$ ] across the spectrum with wind speed and stability. A "peaking behavior" (distinct peaks in the exceedence level, 1/3-octave band spectra) was noted, principally in the  $L_{10}$ ,  $L_5$ , and  $L_1$  levels of the 2500-Hz band. This was most noticeable in measurements made in the plane of the rotor, and it appears to be load-related. We believe this peaking characteristic may be related to some form of oscillatory fluctuations in the rotor's aerodynamic boundary layer.

Comparisons made between on-axis measurements taken during the 1982 and 1983 experiments revealed a sharp spectral cut-off in the 1983 emissions above 1600 Hz. While some of the "peaking" behavior we noted above was present in 1983, a downshift appears to have occurred in the 1/3-octave band in which it was dominant, i.e., 2500 Hz in 1982 to 1000 Hz in 1983. We have attributed the lower spectral cut-off and lower "peaking" frequency in the 1983 emissions directly to the vortex generators, with their inherent ability to limit boundary-layer separation. It is also possible that these changes may be somehow related to the modifications in the pitch angle schedule, i.e., perhaps because they reduced the maximum attack angles encountered.

No significant, steady-tone noise components were found in analyses of representative narrowband (25-Hz resolution) spectra. This indicates that mechanical noise sources associated with the drivetrain are well controlled and that there are no discrete aeroacoustic sources of consequence.

We measured the MOD-2 low-frequency (LF)-range acoustic transfer function directly by means of balloon-borne instruments flown in the turbine inflow. We found that the radiated acoustic spectrum changes characteristics at inflow turbulent scales less than the measured longitudinal or axial integral scale, i.e., for turbulent eddies less than this scale length. Statistical correlations between five characteristic scales of the inflow and the mean and the first three moments of the 1/3-octave band spectrum level distributions (expressed as the variance, skewness, and relative kurtosis coefficients) were derived from the 1983 data set. Using these five inflow scales as predictors in a linear, multivariate model of the band spectral levels, we found that a

high degree of convergence of the model could be obtained; i.e., a high percentage of the observed variation of the mean and the first three moments could be explained. The most efficient predictors included the following:

- (1) A reference mean wind speed ( $U_z$ ) measured at a height  $z$  within the rotor disk layer (vertical layer occupied by the rotor disk)
- (2) The gradient Richardson number (Ri) stability parameter measured over the rotor disk layer
- (3) The Monin-Obukov length scale,  $L$  (see Section 2.4.2), or
- (4) The vertical or in-plane turbulence component scale length along the vertical  $z$ -direction,  $I_w^z$ , measured at the height noted in (3).

The statistical distributions of the emitted 1/3-octave band spectra were most highly correlated with the  $U_z$ , Ri, and  $I_w^z$  predictors or scales. The inclusion of (1) and (4) agrees with the generalized theory of Homicz and George for subsonic rotor noise generated in homogeneous, isotropic turbulence. The need to include the Richardson number reflects the inhomogeneous, vertically stratified characteristics of the rotor inflow at the Goodnoe Hills site. We found that an increase in the stability above critical values ( $Ri > +0.25$ ) led to a decrease in the vertical or in-plane turbulence scales. This in turn had the effect of increasing the LF acoustic output below a frequency of 10 Hz, with a corresponding decrease above that.

We attempted to relate the spectral characteristics of the tower-measured axial and in-plane (upwash) turbulence components to the shape of the LF acoustic mean 1/3-octave band spectra. We suggest using

$$f' = (2_{\pi} \Omega R_o / I_w^z) f$$

as a fixed to rotating space frequency ( $f'$ ) transformation, where  $\Omega$  is the rotor rotation rate and  $R_o$  is the effective radius (75% span length). Using this conversion, we found that

- (1) There is a small positive slope change in the mean acoustic pressure spectra, in the vicinity of the rotor effective chord length. This also seems to coincide with the isotropic turbulence region (indicated by the two turbulence component spectra becoming parallel).
- (2) The acoustic pressure spectral roll-off approximates a  $-5/3$  slope for reference wind speeds less than about 10 m/s.

Because of the substantive changes made to Turbine No. 2 between the 1982 and 1983 experiments, we made an effort to compare the acoustic emission characteristics and their relation to the inflow for both years. We were limited to comparing the LF-range results, since we did not have sufficient high-frequency (HF)-range acoustic data from the 1983 experiment. We determined that the 1983 configuration of the turbine was far more acoustically sensitive to inflow stability. We also determined that the 1982 configuration was influenced by flow stability at all frequencies. We found that the 1983 emissions exhibited less coherent (impulsive) tendencies above 9-10 m/s than those of the 1982 configuration. It is clear that, because of whatever instabilities were present, the upwind 1982 MOD-2 turbine at times performed

acoustically in a manner similar to its predecessor, the downwind MOD-1. Thus, a definite improvement was achieved in reducing the degree of coherency in the LF-range emissions by adding the vortex generators and making the pitch schedule modifications.

In order to better understand the physical processes responsible for aero-acoustic noise generation, we performed a space-time correlation analysis using three parameters measured on the blade itself and the far-field acoustic pressure as measured in the 8-Hz octave band. Our results showed, at least at the 87% span station, that the processes related to the observed flap and chordwise moments, the blade normal surface pressures, and the radiated acoustic pressure field are correlated over time periods of 65-75 ms, which translate to a movement of the rotor through about 5 m in space.

Our experience with the MOD-1 turbine reinforced the desirability of assessing the MOD-2's potential to cause interior annoyance problems in nearby residential structures by means of low-frequency acoustical loads. Through a limited, interior low-frequency noise evaluation experiment, using volunteer subjects, we identified what we believe to be an efficient descriptor or metric for measuring the degree of annoyance from such stimuli. From data available to us, we modified the derivation of this descriptor to include internal dynamic pressure effects resulting from the application of external, low-frequency acoustical loads. Using this modified descriptor, we then developed a procedure for establishing a "figure-of-merit" for a given turbine, which attempted to take into account worst-case conditions of surface reflection and atmospheric focusing. By using 1/3-octave band acoustic spectra measured at a reference distance from a turbine's rotor plane, we were then able to establish a predicted worst-case figure for the MOD-2. We were then able to compare that result with the documented community annoyance associated with emissions from the MOD-1 operating at both 35 and 23 RPM.

### Conclusion

We determined from our analysis of both the high- and low-frequency-range acoustic data that annoyance to the community from the 1983 configuration of the MOD-2 turbine can be considered very unlikely at distances greater than 1 km (0.6 mile) from the rotor plane.

## TABLE OF CONTENTS

	<u>Page</u>
1.0 Introduction.....	1
1.1 Characteristics of the MOD-2 Turbine.....	1
1.2 Background.....	1
1.2.1 The MOD-1 Turbine.....	2
1.2.2 Related Studies.....	4
1.3 SERI's MOD-2 Acoustic Characterization Program Objectives.....	4
2.0 Investigative Procedure.....	6
2.1 MOD-2 Field Studies.....	6
2.1.1 February 1981.....	6
2.1.2 May 1982.....	6
2.1.3 August 1983.....	6
2.1.4 August 1986.....	7
2.2 Instrumentation.....	7
2.2.1 Acoustic Measurement Instruments.....	7
2.2.2 Atmospheric Measurement Instruments.....	8
2.2.2.1 Tower-Mounted Measurements.....	8
2.2.2.2 Tethered Balloon Measurements.....	10
2.2.3 Turbine Rotor Surface Pressures.....	12
2.2.4 Turbine Operational Information.....	12
2.2.5 Data Recording.....	12
2.3 Experimental Procedures.....	12
2.3.1 The 1982 Experiment.....	14
2.3.2 The 1983 Experiment.....	19
2.4 Data Reduction Procedures.....	19
2.4.1 Acoustic Data.....	20
2.4.1.1 Low-Frequency-Range, Coherent Random Sampling Technique.....	22
2.4.1.2 High-Frequency-Range, Random Sampling Technique.....	25
2.4.2 Atmospheric Data.....	25
2.4.2.1 Mean Inflow Characteristics.....	25
2.4.2.2 Turbulent Inflow Characteristics.....	35
2.4.3 Rotor Surface Pressures.....	36
3.0 Description of Goodnoe Hills Inflow Structure.....	37
3.1 Identification of the Acoustically Important Inflow Properties.....	37
3.2 Determining the Vertical Distributions of $U_H$ , $I_1^J$ , and $w'^2$ .....	41
3.2.1 Surface Layer Similarity Scaling.....	41
3.2.2 The Vertical Distribution of $U_H$ ( $V_c$ ).....	42
3.2.3 Variation of $w'$ Spectra with Height.....	42
3.3 Inflow Data Statistical Summaries.....	43
3.4 1983 45-m Inflow Turbulence Spectral Content.....	45

## TABLE OF CONTENTS (Continued)

	<u>Page</u>
3.5 Rotor Disk Inflow Vertical Profiles.....	45
3.5.1 PNL Tower Vertical Profiles of Wind Speed and Turbulence Intensity.....	46
3.5.2 Representative Tethered Balloon Vertical Profiles in Turbine No. 2 Inflow.....	46
4.0 Characteristics of MOD-2 High-Frequency-Range Emissions.....	60
4.1 Observed Directivity Pattern.....	60
4.2 Statistical A-Weighted Emission Distributions.....	60
4.2.1 Single Turbine Operation.....	62
4.2.2 Multiple Turbine Operation.....	64
4.3 Influence of Rotor Inflow on HF Noise Generation.....	65
4.3.1 A-Weighted, Equivalent Sound Pressure Level Variation....	65
4.3.2 Spectral Variation in High-Frequency-Range Emissions.....	67
4.3.2.1 High-Frequency-Range Measurement Locations.....	67
4.3.2.2 Establishment of Background Spectral Reference.....	69
4.3.2.3 Rotor Inflow Influence on Spectral Distribution.....	71
4.4 Typical High-Frequency-Range Narrowband Spectra.....	85
5.0 Characteristics of Low-Frequency-Range Emissions.....	90
5.1 Influence of Rotor Inflow Structure on LF Noise Spectra.....	90
5.1.1 MOD-2 Aeroacoustic Response Function.....	90
5.1.1.1 Direct Measurement Approach.....	90
5.1.1.2 Inflow Bulk Scaling Parameter/Multivariate Modeling Approach.....	93
5.1.1.3 Model Interpretation.....	114
5.1.1.4 Case Studies of the Role of Inflow Structure on Radiated Spectral Characteristics.....	118
5.1.1.5 Relationship of Inflow Spectral Characteristics to the Mean LF Acoustic Spectrum.....	147
5.2 Comparison of 1982 and 1983 Results via Regression Modeling.....	151
5.2.1 Regression Modeling of 1982/83 Data.....	151
5.3 Comparison of MOD-2 and MOD-2 LF Emissions Characteristics.....	153
5.3.1 Statistical Measures of Impulsiveness or Coherency.....	157
5.3.1.1 Adjacent Band Correlated Spectral Levels.....	157
5.3.1.2 Statistical BSL Exceedence Values.....	159
5.3.2 Degree of 1982/83 MOD-2 vs. MOD-1 Emissions Coherency....	159
5.3.3 Comparison of 1982/83 MOD-2 Exceedence Analysis.....	161
5.4 Observed Physical Scales of MOD-2 LF Noise Generation.....	161

**TABLE OF CONTENTS (Concluded)**

	<u>Page</u>
6.0 Measuring the Annoyance Potential of a Single MOD-2 Turbine.....	168
6.1 Additional Comparisons of MOD-1 and MOD-2 Emissions Characteristics and Their Relationship to Interior Annoyance Potential.....	168
6.2 Use of the PLSL Metric in Assessing Potential Interior Annoyance.....	170
6.2.1 Synopsis of Results of Interior Low-Frequency Noise Evaluation Experiment.....	170
6.2.1.1 Identifying an Efficient Estimator of Interior LF Annoyance.....	171
6.2.1.2 Establishing an LSL Annoyance Scale.....	173
6.2.2 A Methodology for Predicting Interior LSL Values.....	173
6.2.2.1 Predicting an Interior LSL Level.....	173
6.2.2.2 Establishing a Reference External Acoustic Loading.....	174
6.3 Estimating the Community Annoyance Potential of Both an Individual MOD-2 Turbine and Clusters of Turbines.....	176
6.3.1 Annoyance Potential from High-Frequency-Range Emissions.....	176
6.3.2 Interior Annoyance Potential of Low-Frequency-Range Emissions.....	177
7.0 Conclusions.....	178
7.2 Low-Frequency-Range Acoustic Characteristics.....	178
7.3 Comparisons of MOD-2 Low-Frequency Emission Characteristics with Those of the MOD-1.....	179
7.4 Community Annoyance Potential of a Single MOD-2 Turbine.....	179
8.0 Recommendations.....	180
9.0 References.....	181

## LIST OF FIGURES

	<u>Page</u>
1-1 The MOD-2 Wind Turbine.....	2
1-2 Schematic of the MOD-2 Configuration.....	3
1-3 Cluster Arrangement of MOD-2 Turbines at Goodnoe Hills Site.....	5
2-1 Microphone Measurement Station.....	8
2-2 Acoustic Instrumentation Configuration for 1982 Experiments.....	9
2-3 Triad of VLF Microphones Used for 1983 Experiments.....	9
2-4 Site Layout Schematic Showing Locations of Meteorological Towers with Respect to the Turbines.....	10
2-5 Detail of Inflow Instrumentation Carried by Tethered Balloon.....	11
2-6 Typical Position of Tethered Balloon in Turbine No. 2 Inflow.....	11
2-7 Data Flow Path for Inflow Measurements.....	13
2-8 Surface Pressure Tap Installation at Blade No. 1, Station 1562, 15% Chord Position.....	14
2-9 Data Sources and Recording Systems Configuration.....	15
2-10 Schematic Representation of an Averaged Radiated Sound Pressure Spectrum from a Large Wind Turbine.....	21
2-11 Schematic Sound Spectrum of Figure 2-10 with Residential Construction Vibration Modes and Applicative Damping Mechanisms Added.....	21
2-12 Low-Frequency-Range Coherent Processing Flow.....	24
2-13 Example of Low-Frequency Acoustic Data Reduction Output: Observed Frequency Distributions of 8-Hz 1/3-Octave Band Spectrum Level for Turbine Operating (Run #1) and Background Conditions (Run #2).....	26
2-14 Example of Low-Frequency Acoustic Data Reduction Output: Mean and Peak 1/3-Octave BSL Spectra for Turbine Operating (Run #1) and Background Conditions (Run #2).....	27
2-15 Example of Low-Frequency Acoustic Data Reduction: Exceedence Level ( $L_1$ ) Comparison for Turbine Operating (Run #1) and Background Conditions (Run #2).....	28
2-16 High-Frequency-Range Acoustic Data Processing.....	29

LIST OF FIGURES (continued)

	<u>Page</u>
2-17 Example of High-Frequency Acoustic Data Reduction Output: Observed Frequency Distributions of A-Weighted BPL for Turbine Operating (Run #1) and Shut-Down Conditions (Run #2) in High Winds.....	30
2-18 Example of High-Frequency Acoustic Data Reduction Output: Mean and Peak 1/3-Octave BPL Spectra for Turbine Operating (Run #1) and Shut-Down Conditions (Run #2) in High Winds.....	31
2-19 Example of High-Frequency Acoustic Data Reduction Output: Exceedence Level ( $L_1$ ) Distribution Comparisons for the Case of Figures 2-17 and 2-18.....	32
3-1 Rotor Geometry Used by Homicz and George.....	38
3-2 Schematic of $L_{ur}^x$ , $L_w^x$ , $L_w^z$ Length Scales with Respect to Turbine Rotor.....	40
3-3 BPA Tower 45-m Level Longitudinal (u) and Vertical (w) Inflow Spectra for 1983--Run A05.....	47
3-4 BPA Tower 45-m Level Longitudinal (u) and Vertical (w) Inflow Spectra for 1983-Run A03.....	48
3-5 BPA Tower 45-m Level Longitudinal (u) and Vertical (w) Inflow Spectra for 1983 Run A14-1.....	47
3-6 BPA Tower 45-m Level Longitudinal (u) and Vertical (w) Inflow Spectra for 1983-Run A14-2.....	49
3-7 BPA Tower 45-m Level Longitudinal (u) and Vertical (w) Inflow Spectra for 1983-Run A18.....	48
3-8 BPA Tower 45-m Level Longitudinal (u) and Vertical (w) Inflow Spectra for 1983-Run All.....	49
3-9 Smoothed Vertical Profile (PNL Tower) of $U_{hub}$ -Normalized Horizontal Wind Speed (a) and Turbulence Intensity (b) for 1983--Run A03.....	50
3-10 Smoothed Vertical Profile (PNL Tower) of $U_{hub}$ -Normalized Horizontal Wind Speed (a) and Turbulence Intensity (b) for 1983--Run A14-1.....	51
3-11 Smoothed Vertical Profile (PNL Tower) of $U_{hub}$ -Normalized Horizontal Wind Speed (a) and Turbulence Intensity (b) for 1983--Run A14-2.....	52
3-12 Smoothed Vertical Profile (PNL Tower) of $U_{hub}$ -Normalized Horizontal Wind Speed (a) and Turbulence Intensity (b) for 1983--Run A18.....	53

## LIST OF FIGURES (continued)

	<u>Page</u>
3-13 Smoothed Vertical Profile (PNL Tower) of $U_{hub}$ -Normalized Horizontal Wind Speed (a) and Turbulence Intensity (b) for 1983--Run All.....	54
3-14 Smoothed Vertical Profile (PNL Tower) of $U_{hub}$ -Normalized Horizontal Wind Speed (a) and Turbulence Intensity (b) for 1983--Run A05.....	55
3-15 Smoothed and High-Resolution Vertical Profiles of Wind Speed for Run A05.....	56
3-16 Smoothed and High-Resolution Vertical Profiles for Wind Direction for Run A05.....	57
3-17 Smoothed and High-Resolution Vertical Profiles of Sensible Temperature for Run A05.....	58
3-18 Narrowband Longitudinal Turbulence Spectrum Measured at 78-m ( $\pm 6$ m) Height for Run A05.....	59
4-1 Microphone Locations Used in High-Frequency-Range Measurements.....	65
4-2 A-Weighted Sound Pressure Level Directivity Pattern for a Single MOD-2 Turbine.....	62
4-3 Cumulative Distributions of A-Weighted SPL at Three Downwind Distances from a Single MOD-2 Turbine.....	63
4-4 Average Turbine $L_{eq}$ (A) Emissions Decay Downwind of a Single MOD-2 Turbine.....	63
4-5 Cumulative Distributions of A-Weighted SPL at Site No. 2 (see Figure 4-1) for Two and Three Operating MOD-2 Turbines.....	64
4-6 $L_{eq}$ (A) Levels as a Function of Hub-Height Wind Speed.....	66
4-7 Observed Frequency Distributions of A-Weighted SPL for Highest and Lowest Mean Hub-Height Wind Speeds.....	68
4-8 Comparison of Background Mean BPL Spectra for Highest and Lowest Mean Hub-Height Wind-Speed Conditions.....	69
4-9 Comparisons of Observed Mean SPL Spectra for Operating and Background Conditions in High (a) and Low (b) Winds.....	70
4-10 Comparison of Background HF Acoustic Spectra at On-Axis Microphone Location for the Same Mean Hub-Height Wind Speed during 1982 and 1983 Experiments.....	71

## LIST OF FIGURES (continued)

	<u>Page</u>
4-11 1982 HF-Range Acoustic Spectral Distribution for On-Axis (solid) and In-Plane (dashed) Locations as a Function of Wind Speed and Stability.....	72
4-12 Comparison of the On-Axis Component of the HF Spectral Distribution between 1982 and 1983 under High Loading Conditions...	74
4-13 Comparison of On-Axis (solid) versus In-Plane (dashed) HF Spectral Emissions for Neutral to Slightly Stable Inflow Conditions.....	75
4-14 Comparison of $L_1$ , $L_5$ , $L_{10}$ , $L_{20}$ , and $L_{50}$ 1/3-Octave Level Spectra at 1.5D at the On-Axis and In-Plane Measurement Locations for 1982 Runs: (a) 17-2; (b) 19-1; and (c) 26-1.....	76
4-15 Comparison of Mean 1/3-Octave BPL Spectra for Mean Wind Speeds of 9.3 and 10.3 mps under Stable Conditions.....	77
4-16 Comparison of $L_1$ , $L_5$ , $L_{10}$ , $L_{20}$ , and $L_{50}$ 1/3-Octave Level Spectra at 1.5D at the On-Axis (a) and In-Plane (b) Measurement Stations...	78
4-17 Comparison of Mean 1/3-Octave BPL Spectra for High and Moderate Wind Speeds under Stable Inflow Conditions.....	79
4-18 Comparison of $L_1$ , $L_5$ , $L_{10}$ , $L_{20}$ , and $L_{50}$ 1/3-Octave Level Spectra for High and Moderate Wind Speeds under Stable Inflow Conditions...	80
4-19 Comparison of Mean 1/3-Octave BPL Spectra for a Mean Wind Speed of 13.3 mps and Stable Conditions (Run 27) and a Mean Wind Speed of 14.5 mps and Unstable Conditions (Run 25-1).....	81
4-20 Comparison of $L_1$ , $L_5$ , $L_{10}$ , $L_{20}$ , and $L_{50}$ 1/3-Octave Level Spectra for High-Wind, Stable vs. High-Wind, Unstable Inflow Conditions....	82
4-21 Mean and $L_{20}$ BPL Spectra for 1982 Run R27 and 1983 Run A-11.....	83
4-22 Mean and $L_{20}$ BPL Spectra for 1982 Run 26-1 and 1983 Run A18.....	84
4-23 Comparison of Acoustic Environment at 1.5D, On-Axis Measurement Location with and without the Turbine Operating under High Wind Conditions.....	85
4-24 Comparison of $L_1$ , $L_5$ , $L_{10}$ , $L_{20}$ , and $L_{50}$ On-Axis 1/3-Octave Level Spectra for Identical Mean Wind Conditions during 1982 and 1983 Experiments.....	86
4-25 Comparison of $L_1$ , $L_5$ , $L_{10}$ , $L_{20}$ , and $L_{50}$ On-Axis 1/3-Octave Level Spectra for Similar Wind Speed Regimes in 1982 and 1983.....	86
4-26 Representative 1982 HF-Range Narrowband ( $B_e = 1.25$ Hz) Spectra for Very Low Wind Conditions.....	87

LIST OF FIGURES (continued)

	<u>Page</u>
4-27 Representative 1982 HF-Range Narrowband Spectra for Moderated but Below-Rated Wind Conditions.....	87
4-28 Representative 1982 HF-Range Narrowband Spectra for Above-Rated, Unstable Inflow Conditions.....	88
4-29 1983 On-Axis HF-Range Narrowband Spectra for Above-Rated, Very Stable Inflow Conditions.....	88
4-30 1983 On-Axis HF-Range Narrowband Spectra for Near-Rated, Stable Inflow Conditions.....	89
5-1 Relationship of Location of Measurements on Blade No. 1, Rotor Disk Geometry, and Height of Elevated Turbulent Layer.....	92
5-2 Measured Low-Frequency Acoustic Response Function.....	92
5-3 Measured Low-Frequency Acoustic Response as a Function of Turbulent Space Scale.....	93
5-4 Comparisons of the Observed Run-to-Run Variations of the BSL Mean and First Three Statistical Moments and the Variations Expected from a Purely Random Process.....	94
(a) mean BSL comparison.	
(b) variance coefficient comparison.	
(c) skewness coefficient comparison.	
(d) kurtosis coefficient comparison.	
5-5 Spectral Run-to-Run Variation ANOVA Results for the 45-m Longitudinal (u) and Vertical or In-Plane (w) Turbulence Components.....	97
(a) longitudinal component.	
(b) vertical or in-plane component.	
5-6 Observed Variation of the Disk Gradient Richardson Number as a Function of the Time-of-Day for the Combined 1982/83 Experimental Periods.....	98
5-7 Observed Variation of the Disk Gradient Richardson Number as a Function of the Time-of-Day for the 1983 Experimental Period.....	98
5-8 Observed Variation of the Mean Hub-Height Wind Speed as a Function of the Disk Gradient Richardson Number for the Combined 1982/83 Experimental Periods.....	99

## LIST OF FIGURES (continued)

	<u>Page</u>
5-9 Observed Variation of the Mean Hub-Height Wind Speed as a Function of the Time-of-Day for the Combined 1982/83 Experimental Period...	100
5-10 Observed Variation of the Height of the Mean Wind Speed Maximum as a Function of the Gradient Richardson Number for the 1983 Experimental Period.....	101
5-11 Observed Rotor Disk Maximum Mean Wind Speed as a Function of the Richardson Number for the 1983 Experimental Period.....	101
5-12 Observed Rotor Disk Maximum Mean Wind Speed as a Function of the Time-of-Day for the 1983 Experimental Period.....	102
5-13 Observed Variation in the Mean Wind Speed at the Five Levels of the PNL Tower as a Function of the Gradient Richardson Number for the 1983 Experimental Period.....	102
5-14 Observed Variation of the Mean 45-m Horizontal Wind Speed ( $U$ ) and the Horizontal ( $I_U^X$ ) and Vertical ( $I_W^Z$ ) Length Scales as a Function of the Richardson Number.....	103
5-15 Observed Variation of the Mean 45-m Horizontal Wind Speed ( $U$ ) and Horizontal ( $f_{\mu}$ ) and Vertical ( $f_{mw}$ ) Spectral Peak Reduced Frequencies as a Function of the Richardson Number.....	103
5-16 Observed Variations of the 45-m Horizontal and Vertical Length Scales as Functions of the Spectral Frequency Reduced Frequencies.....	104
(a) variation of $I_U^X$ versus $f_{\mu}$ .	
(b) variation of $I_W^Z$ versus $f_{mw}$ .	
5-17 Ratio of Hourly-to-Diurnal Mean Hub-Height Wind Speed as a Function of Time-of-Day for Summer and Winter of 1985/86 Wind Season.....	105
5-18 Observed Diurnal Variation of Actual Hub-Height Mean Wind Speed for Summer and Winter of the 1985/86 Wind Season.....	105
5-19 Observed Variation of the 45-m Mean Wind Speed ( $U_H$ ) and the Brunt-Väisälä Frequency ( $N$ ) as a Function of the Disk Richardson Number.....	106
5-20 Observed Variation of the Brunt-Väisälä Frequency ( $N$ ) and the Horizontal ( $I_U^X$ ) and Vertical ( $I_W^Z$ ) Length Scales as a Function of the Disk Richardson Number.....	106
5-21 Same as Fig. 5-20 except for Spectral Peak Reduced Frequencies $f_{\mu}$ (Horizontal Component) and $f_{mw}$ (Vertical Component).....	107

## LIST OF FIGURES (continued)

	<u>Page</u>
5-22 ANOVA Analysis of the Observed Run-to-Run Variation in the Longitudinal or Axial (u) Turbulence Component.....	108
5-23 Same as Fig. 5-22 but for the Vertical or In-Plane (w) Turbulence Component.....	108
5-24 ANOVA Analysis of the Efficiency of Multivariate Models Using a Series of Predictors for the Observed Run-to-Run Variation of the Acoustic MBSL Spectra.....	109
5-25 ANOVA Analysis of the Observed Run-to-Run Variation of the Acoustic MBSL Spectra as a Function of Four Inflow Predictor Scales.....	110
5-26 Same as Fig. 5-24 but for the Observed Variation in the Acoustic BSL Variance Coefficient $\langle b_2 \rangle$ Spectra.....	110
5-27 Same as Fig. 5-25 but for the Observed Variation in the Acoustic BSL Variance Coefficient $\langle b_2 \rangle$ Spectra.....	111
5-28 Same as Fig. 5-24 but for the Observed Variation in the Acoustic BSL Skewness Coefficient $\langle b_3 \rangle$ Spectra.....	112
5-29 Same as Fig. 5-25 but for the Observed Variation in the Acoustic BSL Skewness Coefficient $\langle b_3 \rangle$ Spectra.....	112
5-30 Same as Fig. 5-24 but for the Observed Variation in the Acoustic BSL Kurtosis Coefficient $\langle b_4 \rangle$ Spectra.....	113
5-31 Same as Fig. 5-25 but for the Observed Variation in the Acoustic BSL Kurtosis Coefficient $\langle b_4 \rangle$ Spectra.....	113
5-32 Characteristic Scaling Sensitivities for Mean Band Spectrum Levels.....	115
5-33 Characteristic Scaling Sensitivities for BSL Variance Coefficients.....	115
5-34 Characteristic Scaling Sensitivities for BSL Skewness Coefficients.....	116
5-35 Characteristic Scaling Sensitivities for BSL Kurtosis Coefficients.....	117
5-36 Normalized 45-m Turbulence Spectra for Runs A18 and A05.....	119
5-37 Ensemble Statistical Moments of 1/3-Octave Acoustic Band Spectral Levels for Runs A18 and A05.....	120

## LIST OF FIGURES (continued)

	<u>Page</u>
5-38a Smoothed (a) and High-Resolution (b) Vertical Profiles of Wind Speed for Run A05.....	123
5-38b Smoothed (a) and High-Resolution (b) Vertical Profiles of Wind Direction for Run A05.....	124
5-38c Smoothed (a) and High-Resolution (b) Vertical Profiles of Sensible Temperature for Run A05.....	125
5-39 Normalized 45-m Turbulence Spectra for Runs A18 and A14-1.....	126
5-40 Ensemble Statistical Moments of 1/3-Octave Acoustical Band Spectrum Levels for Runs A18 and A14-1.....	127
5-41 Normalized 45-m Turbulence Spectra for Runs A14-2 and A11.....	129
5-42 Ensemble Statistical Moments of 1/3-Octave Acoustical Band Spectrum Levels for Runs A14-2 and A11.....	130
5-43 Normalized 45-m Turbulence Spectra for Runs A03 and A14-1.....	132
5-44 Ensemble Statistical Moments of 1/3-Octave Acoustic Band Spectrum Levels for Runs A03 and A14-1.....	133
5-45 Normalized 45-m Turbulence Spectra for Runs A03 and A05.....	136
5-46 Ensemble Statistical Moments of Acoustic 1/3-Octave Band Spectral Levels for Runs A03 and A05.....	137
5-47a Detailed Vertical Profiles (3-m Resolution) of Wind Direction for Runs A03 and A05.....	139
5-47b Detailed Vertical Profiles of Wind Speed for Runs A03 and A05.....	139
5-47c Detailed Vertical Profile of Thermal Structure (Potential Temperature) for Runs A03 and A05.....	140
5-48 Normalized 45-m Turbulence Spectra for Runs A11 and A18.....	141
5-49 Ensemble Statistical Moments of Acoustic 1/3-Octave Band Spectrum Levels for Runs A11 and A18.....	142
5-50 Normalized 45-m Turbulence Spectra for Runs A14-1 and A14-2.....	144
5-51 Ensemble Statistical Moments of Acoustic 1/3-Octave Band Spectrum Levels for Runs A14-1 and A14-2.....	145
5-52 Relationship of Mean Acoustic Pressure Spectral Distribution $S_{ap}(f)$ to 45-m Axial $S_u(f')$ and Upwash $S_w(f')$ Turbulence Components for Run A05.....	148

## LIST OF FIGURES (continued)

	<u>Page</u>
5-53 Relationship of Mean Acoustic Pressure Spectral Distribution $S_{ap}(f)$ to 45-m Axial $S_u(f')$ and Upwash $S_w(f')$ Turbulence Components for Run A03.....	148
5-54 Relationship of Mean Acoustic Pressure Spectral Distribution $S_{ap}(f)$ to 45-m Axial $S_u(f')$ and Upwash $S_w(f')$ Turbulence Components for Run A14-1.....	149
5-55 Relationship of Mean Acoustic Pressure Spectral Distribution $S_{ap}(f)$ to 45-m Axial $S_u(f')$ and Upwash $S_w(f')$ Turbulence Components for Run A14-2.....	149
5-56 Relationship of Mean Acoustic Pressure Spectral Distribution $S_{ap}(f)$ to 45-m Axial $S_u(f')$ and Upwash $S_w(f')$ Turbulence Components for Run A18.....	150
5-57 Relationship of Mean Acoustic Pressure Spectral Distribution $S_{ap}(f)$ to 45-m Axial $S_u(f')$ and Upwash $S_w(f')$ Turbulence Components for Run A11.....	150
5-58 Difference in Mean Band Spectrum Levels for 1982 and 1983.....	153
5-59 Results of ANOVA Analysis for Mean Band Spectrum Level Inflow Parameter Sensitivities.....	154
(a) 1982 turbine configuration	
(b) 1983 turbine configuration	
5-60 Normalized Inflow Parameter Predictor Slopes for Observed Mean Band Spectrum Levels.....	155
(a) 1982	
(b) 1983	
5-61 Relative MBSL Spectral Sensitivity to Inflow Stability (Richardson Number) for 1982 and 1983 Configurations.....	156
5-62 Relative MBSL Spectral Sensitivity to Inflow Stability for Mean Hub-Height ( $U_H$ ) Wind Speed.....	156
5-63 Relative MBSL Spectral Sensitivity to Inflow Stability for Hub-Height Wind Speed Variance ( $u'$ ).....	157
5-64 Comparison of 8/16-Hz CBSLs vs. Hub-Height Wind Speed for 1982 and 1983 MOD-2 Configurations and the MOD-1 Turbine.....	159
5-65 Comparison of 16/31.5-Hz CBSLs vs. Hub-Height Wind Speed for 1982 and 1983 MOD-2 Configurations and MOD-1 Turbine.....	160

## LIST OF FIGURES (concluded)

	<u>Page</u>
5-66 Comparison of 31.5/63-Hz CBSLs vs. Hub-Height Wind Speed for 1982 and 1983 MOD-2 Configurations and MOD-1 Turbine.....	160
5-67 Comparison of Inflow Predictor Sensitivities on Adjacent CBSLs and Ccoefs for 1982 nd 1983 Turbine Configurations.....	162
5-68 Sensitivity of Inflow Predictors on Adjacent CBSLs and Correlation Coefficients for 1983 MOD-2 Configurations.....	164
6-1 MOD-1 Mean 1/3-Octave Band Acoustic Spectra Associated with Numerous Complaints of Community Annoyance at 1 km from the Turbine.....	169
6-2 Comparison of MOD-1 Acoustic Spectra of Figure 6-1 with Spectra from the 1983 MOD-2 under Lowest (Run A05) and Highest (Runs A11 and A18) Wind Conditions.....	169
6-3 Comparison of MOD-1 Acoustic Spectra of Figure 6-1 with Spectra from the 1982 MOD-2 Operating in a Severe Off-Design Condition (Run 25-1).....	170
6-4 Low-Frequency Noise Metrics Spectral Weightings.....	172
6-5 Typical Indoor/Outdoor Transmissibility Functions for Impulsive and Nonimpulsive Acoustic Loadings.....	175
6-6 Modification of Original LSL Frequency Weighting for Impulsive and Nonimpulsive PLSL Measurements.....	175

## LIST OF TABLES

	<u>Page</u>
1-1 MOD-2 Configuration Characteristics and Features.....	4
2-1 Original Test Matrix for 1982/1983 MOD-2 Experiment.....	17
2-2 Excerpt of Run Configurations for 1982 Single Turbine Experiments..	18
2-3 ISO Octave and 1/3-Octave Low-Frequency Analysis Bands.....	22
2-4 ISO/1/3-Octave Bands Used for High Frequency Analysis.....	23
2-5 Magnetic Recorder Bandwidths and Dynamic Ranges for HF Acoustic Recordings during 1982 and 1983 Experiments.....	23
2-6 Bulk Surface Layer Parameters Measured during 1983 Goodnoe Hills Experiments from Towers and Tethered Balloon.....	34
2-7 Pressure Tap Locations on Turbine No. 2, Blade No. 1.....	36
3-1 Comparison of 1982 and 1983 Inflow Statistics from the BPA Meteorological Tower.....	44
3-2 Summary BPA Tower Statistics of Reduced 1982/1983 Data Sets.....	44
3-3a 1983 Mean Inflow Characteristics Summary from BPA Tower: Wind Speeds.....	45
3-3b 1983 Mean Inflow Characteristics: Characteristic Scaling Parameters.....	45
3-3c 1983 Mean Inflow Characteristics: Spectral Scaling and Rotor Disk Layer Parameters.....	46
4-1 Inflow Conditions and Resulting $L_{eq}(A)$ Levels for Representative 1982 and 1983 Data Runs at 1.5D.....	65
4-2 Multivariate Regression Correlations of MOD-2 $\langle L_{eq}(A) \rangle$ Levels with Hub-Height Wind Vector and Vertical Stability.....	66
5-1 Summary of Important Turbulence Excitation and Turbine Operating Flow Angles for the Analyzed Segment of Run A05.....	91
5-2 Bivariate Correlation Coefficients for Inflow Turbulence Scales and Intensities versus Stability, Velocity, and Roughness.....	96
5-3 Cross-Correlation Matrix for Stability, Velocity, and Roughness....	96
5-4 Inflow Structure Comparisons Data.....	118
5-5 Overlap Ranges of Reduced 1982/83 Inflow Data Sets.....	152

## LIST OF TABLES (concluded)

	<u>Page</u>
5-6 Comparison of Mean 1/3-Octave Band Spectral Levels for the Conditions in Tables 3-2 and 5-9 for 1982 and 1983 Runs.....	152
5-7 Statistical Summary of Correlated or Coherent Octave Band Spectrum Levels Measured On-Axis at 1.5D for 1982/83 MOD-2 Data Runs Compared with the MOD-1 Turbine at 35 and 23 RPM.....	158
5-8 Comparison Summary of 1982/83 Adjacent-Band Correlated Spectrum Levels for Reduced Meteorological Data Set of Table 3-2 and the 23-RPM Operation of the MOD-1.....	163
5-9 Comparison Summary of 1982/83 LF-Range Octave Band Exceedence Levels for Reduced Meteorological Data Set of Table 3-2 and the 23-RPM Operation of the MOD-1.....	165
5-10 Exceedence Level Summary for 1983 LF-Range Octave BSL Values.....	166
5-11 MOD-2 Rotor Space-Time Correlation Scales for Four Aeroacoustic/Aeroelastic Parameters.....	167
6-1 Low-Frequency Noise Environments Subjective Ranking Criteria.....	172
6-2 Correlation Coefficients of Volunteer Ratings of Low-Frequency Noise Stimuli versus Six Noise Metrics.....	173
6-3 SERI Interior Low-Frequency Annoyance Criteria Employing the LSL Metric.....	174
6-4 Predicted Interior LSL (PLSL) Values at 1 km from the MOD-2 Turbine (1983 Configuration).....	176

## NOMENCLATURE

A	ISO "A" spectral weighting
ANSI	American National Standards Institute
$a_0$	local acoustic velocity
B	Bowen ratio; number of blades in rotor
b	blade span length
$b_2$	variance coefficient
$b_3$	skewness coefficient
$b_4$	kurtosis coefficient
BAC	Boeing Aerospace Corporation
BPA	Bonneville Power Administration
BPF	blade passage frequency
BPL	band pressure level
BSL	band spectrum level
BUREC	Bureau of Reclamation
C	ISO "C" spectral weighting
c	rotor chord dimension
CBSL	coherent octave band spectrum level
Ccoef	cross-correlation coefficient
CNA	community noise analyzer
$c_0$	rotor chord length at effective radius $R_0$
$c_p$	specific heat at constant pressure for air
D	turbine rotor diameter
dB	decibel <sup>a</sup>
DOE	U.S. Department of Energy
DOI	U.S. Department of the Interior
$D_r$	rotor-surface force fluctuation spectral density
EDS	Engineering Data System
f	reduced frequency parameter, $f=nz/U$
FM	frequency modulation
$f_{mi}$	i-th component $S_i(f)$ peak reduced frequency
g	local gravity acceleration
$G_1, G_2$	proposed ISO spectral weightings
H	vertical heat flux

## NOMENCLATURE (continued)

$H_o$	surface vertical heat flux
HF	high frequency
Hz	SI unit of cyclic frequency (cycles per second)
ISO	International Organization for Standardization
$I_u^x$	longitudinal length scale along x-axis
$I_w^x$	vertical length scale along x-axis
$I_w^z$	vertical length scale along vertical (z) axis
K	degrees Kelvin
$k_a$	von Karman constant
L	Monin-Obukov length
$L_{1/3}$	one-third octave band level
$L_{eq}$	time-averaged sound pressure level
LF	low frequency
$L_i$	sound level exceeded i-th percent of time
LSL	low-frequency sound level
LSPL	low-frequency sound pressure level
$M_c$	axial convection Mach number
$M_o$	rotor speed Mach number
MOD-1	DOE/NASA 2-MW wind turbine design
MOD-2	DOE/NASA 2.5-MW wind turbine design
MSL	mean spectrum level
N	Brunt-Väisälä frequency
n	cyclic frequency (Hz); BPF harmonic number
NASA	National Aeronautics and Space Administration
$n_o$	rotational-broadband transition frequency
$n_r$	inflow/rotor scaling frequency
octave	2:1 frequency ratio
Pa	SI unit of pressure
PG&E	Pacific Gas and Electric Company
$P_{hub}$	hub elevation barometric pressure
$P_i$	i-th component peak turbulence energy
PLSL	predicted interior LSL value
PNL	Pacific Northwest Laboratories

## NOMENCLATURE (continued)

$P_{sfc}$	surface barometric pressure
$Q_o$	surface kinematic heat flux
$R,r$	slant-range distance to observer
$Ri$	Richardson number
$R_{ij}$	autocorrelation function
$R_o$	effective rotor radius
$S_{ap}$	far-field acoustic pressure spectral density
SERI	Solar Energy Research Institute
SI	International System of Units
$S_i$	i-th component logarithmic spectral density
$T$	absolute air temperature
$T_*$	surface layer temperature scale
$T_{BV}$	Brunt-Väisälä period
$T_u$	longitudinal time scale
$T_w$	vertical time scale
$u',w'$	1-10 Hz band, mean square turbulence values
$u_*$	friction velocity
$U_{45}$	mean along-wind component at 45 m height
$U_H$	mean horizontal windspeed at hub height
$U_{max}$	rotor-disk peak mean horizontal wind speed
$U_z$	mean horizontal wind speed at height z
$V_c$	axial convection velocity
VLF	very low frequency
$W_{45}$	mean vertical wind component at 45 m height
$W_H$	mean vertical wind component at hub height
x	along-the-ground downwind distance
z	geometric height above the ground
$z_{max}$	height of peak mean wind speed in rotor 'disk
$z_o$	surface roughness length

Greek

$\rho_o$	local air density
$\gamma$	rotor plane-to-observer angle

## NOMENCLATURE (concluded)

$\theta$	potential temperature
$\theta_0$	rotor disk mean potential temperature
$\tau_s$	surface Reynolds stress
$\Omega$	rotor rotational frequency
$\zeta$	non-dimensional turbulence wavenumber
$\langle \rangle$	ensemble statistical quantity

---

<sup>a</sup>referenced to 20  $\mu\text{Pa}$  unless usage indicates otherwise.

## 1.0 INTRODUCTION

This document summarizes the results of an extensive investigation into the factors relating to the acoustic emissions associated with the operation of a MOD-2 wind turbine. Three of the turbines used for the work reported here were located at the Goodnoe Hills Wind Turbine Site near Goldendale, Wash., which was operated by the Bonneville Power Administration (BPA) for the U.S. Department of Energy (DOE). The data for this study were taken primarily from the Unit No. 2 turbine at Goodnoe Hills. However, some measurements of high-frequency-range acoustic emissions from all three of the turbines were made and are reported on. The investigations herein were conducted by the Solar Energy Research Institute (SERI) on the MOD-2 turbine since 1981.

### 1.1 Characteristics of the MOD-2 Turbine

The subject of this study, referred to as the MOD-2 wind turbine, was the sixth in a series of turbine designs developed for DOE by the National Aeronautics and Space Administration (NASA) Lewis Research Center as part of the Federal Wind Energy Program. Five turbines of this design were constructed by the Boeing Aerospace Corporation (BAC). Three were located in a cluster at the Goodnoe Hills Wind Site near Goldendale, Wash. One was installed near Medicine Bow, Wyo. for the U.S. Department of the Interior (DOI), Bureau of Reclamation (BUREC). A fifth and privately financed unit was installed in the Solano Hills near San Francisco, Calif. for the Pacific Gas and Electric Company (PG&E). Only the PG&E unit remains in operation.

The MOD-2 turbine has a rotor diameter of 91 m (300 ft) and is capable of generating 2.5 MW of power at its rated wind speed of about 13 mps (28 mph). The rotor is located upwind of the supporting tower and turns on a hub 61 m (200 ft) above the ground. Figures 1-1 and 1-2 show a photograph and a schematic of the turbine, respectively. Table 1-1 summarizes the turbine's design and mechanical specifications. Figure 1-3 illustrates the turbine cluster arrangement at the BPA Goodnoe Hills wind turbine site.

### 1.2 Background

An extensive investigation of the characteristics of the MOD-2 acoustic emissions was undertaken as a result of the experience we gained with the MOD-1, a large downwind turbine. One of the primary reasons for moving the MOD-2 rotor upstream of the support tower was to avoid the impulsive, low-frequency noise generated by its predecessor. An extensive study of the MOD-1 was made by SERI and others and is reported in Ref. [1]. We expected that the MOD-2 upwind configuration would largely eliminate the low-frequency, impulsive characteristic of the MOD-1 emissions. We did not know, however, whether similar or perhaps greater levels of nonimpulsive, low-frequency noise (radiated from the larger MOD-2 rotor) would excite the interiors of nearby residential structures enough to reach or exceed the detection threshold of the occupants. SERI designed its MOD-2 test program to answer these questions.



Figure 1-1. The MOD-2 Wind Turbine

### 1.2.1 The MOD-1 Turbine

From the extensive investigation of the MOD-1 noise situation detailed in Ref. [1], we arrived at the following conclusions:

- The annoyance to the affected residents near the turbine was caused by a low-frequency noise phenomenon.
- The source of the phenomenon was a more or less steady stream of acoustic impulses, caused by the unsteady aerodynamic loading of the MOD-1 rotor blades as they passed through the wake of the support tower.
- The severity of the situation was enhanced by the focusing of this low-frequency, coherent acoustic energy on the homes of complaining residents by a combination of terrain reflection and atmospheric refraction.

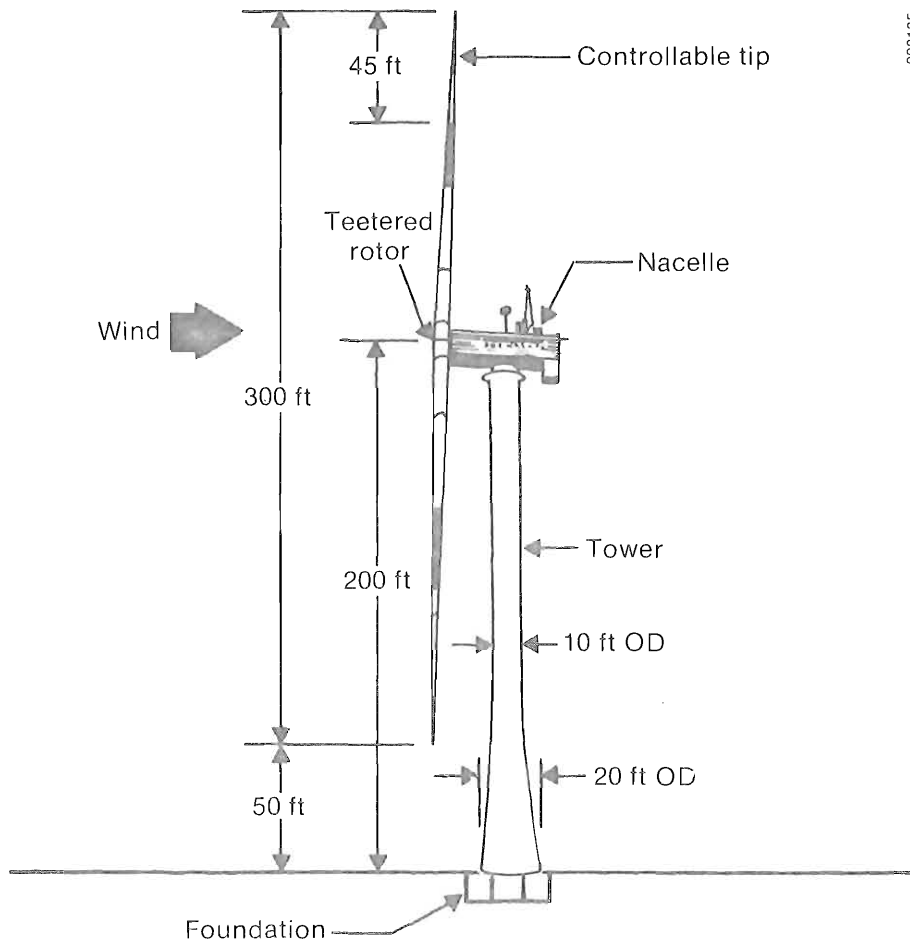


Figure 1-2. Schematic of the MOD-2 Configuration

- The impulsive acoustic loading of the homes produced strong, short-lived resonances in the structures, which were transmitted to the occupants by both direct and secondary acoustic emissions within the vibrating structures.

As a part of the MOD-1 investigation, several analysis techniques were developed along with criteria for measuring the degree of coherency in the radiated acoustic field. On at least three occasions we had detailed responses from at least two of the affected homes when measurements at the turbine were available. We also were able to make simultaneous acoustic and vibration measurements indoors and outside on two of the homes, and correlate these along with residents' comments, during the varying acoustic loads of the turbine. Thus, we had a very good idea of what was responsible for the annoyance from the MOD-1 turbine and were in a position to employ this knowledge in evaluating the annoyance potential of a large, upwind turbine such as the MOD-2.

**Table 1-1. MOD-2 Configuration Characteristics and Features**

Parameter	Design Feature
Rated power	2,500 KW
Rotor diameter	91 m (300 ft)
Rotor type	Teetered, tip controlled
Rotor airfoil shape	NACA 230XX
Rotor orientation	Upwind, 2.5° tilt
Rated wind at hub	13 mps (28 mph)
Cut-off wind speed at hub	20 mps (45 mph) <sup>a</sup>
Rotor tip speed	84 mps (275 fps)
Rotor rpm	17.5
Generator rpm	1,800
Generator type	Synchronous
Gear box	Compact planetary gear
Hub height	61 m (200 ft)
Tower	Soft-shell type
Pitch control	Hydraulic
Yaw control	Hydraulic
Electronic control	Microprocessor
System power coefficient	0.382 (max)

<sup>a</sup>The Medicine Bow and Solano turbines have cut-offs of 27 mps (60 mph).

### 1.2.2 Related Studies

The NASA Langley Research Center has been involved in a companion effort in studying acoustic emissions and impacts of large wind turbines. The Center's primary focus has been on field measurements, propagation studies, and turbine characterization as well as studies of psychoacoustical response to wind turbine noise. A number of reports that summarize their efforts are available, including Refs. [2], [3], and [4].

### 1.3 SERI's MOD-2 Acoustic Characterization Program Objectives

SERI's program for MOD-2 noise characterization had the following objectives:

- A general characterizing of both low- (under 200 Hz) and high-frequency-range acoustic emissions.
- The development of a methodology for making acoustic measurements in a windy environment.
- The development of a methodology for relating low-frequency acoustic emissions to the turbulent inflow structure.
- The development of a methodology for predicting the interior annoyance potential of nearby residential structures from acoustic loading from wind turbine emissions.
- The application of the annoyance potential criteria to measured MOD-2 emissions under a range of operating conditions and a comparison of the predictions with similar ones for the downwind MOD-1 turbine.



008136

**Figure 1-3. Cluster Arrangement of MOD-2 Turbines at Goodnoe Hills Site**

## 2.0 INVESTIGATIVE PROCEDURE

### 2.1 MOD-2 Field Studies

Five field experiments were undertaken by SERI from February 1981 to August 1986 to support the characterization of MOD-2 acoustic emissions. Three of the five were major activities requiring up to four weeks in the field. These major experiments were performed in May 1982 and August 1983 at the Goodnoe Hills site and in October and November 1983 at the Medicine Bow site. Although wake measurements were the primary objective of the Medicine Bow experiment, acoustic emission characterization in that environment was also programmed. Unfortunately, the acoustic data were affected by the presence of another large, downwind turbine which operated during the bulk of the MOD-2 data-taking periods, corrupting the recordings. The sole source of the MOD-2 acoustic data utilized in this report was Turbine No. 2 at the Goodnoe Hills site.

#### 2.1.1 February 1981

A brief survey was performed early, during the acceptance tests of Turbine No. 1 in February 1981. The purpose of these measurements was to see if any impulsiveness could be detected in the MOD-2 emissions, similar to those of the large downwind turbines. An analysis of the resulting tape records did not reveal a tendency for impulsive characteristics.

#### 2.1.2 May 1982

A major field measurement was planned for May 1982 at the Goodnoe Hills site using all three turbines. While continuous statistical distributions of high-frequency-range noise levels for one, two, and three operating turbines were collected, low-frequency-range noise data were collected from Turbine No. 2 only. SERI's tethered balloon system was used to obtain detailed descriptions of Turbine No. 2 inflow on runs that were within its wind-speed operating range. Unfortunately, at that stage in the program's development the turbines were operating erratically, particularly in high winds. As a result, major revisions were made in the control algorithms and vortex generators were installed on the rotors after our measurements were completed.

#### 2.1.3 August 1983

A second major experiment was performed using Turbine No. 2 during the last two weeks of August 1983. While the experiment's scope was more limited than that of the previous year, considerably more information was collected. Twelve surface pressure taps were installed on Blade No. 1 of the turbine and an improved hot-film anemometer was flown on the SERI tethered balloon system. A two-axis, hot-film anemometer was also installed at the 45-m level of the BPA meteorological tower, about 400 m from Turbine No. 2.

A very limited amount of high-frequency-range acoustic data was collected since the primary objective of this test series was to ascertain low-frequency emission characteristics and their relationship to the turbulent inflow. As mentioned above, the turbine had undergone a number of major revisions, including a different pitch angle schedule and vortex generators installed on 70% of the rotor surface. These changes have made it very difficult to

compare the 1982 and 1983 data sets since the operating characteristics of the turbine were substantially altered. Thus, the 1983 data set is considered a reference for the MOD-2; four of the five turbines were converted to essentially the same configuration.

#### 2.1.4 August 1986

Analysis of the 1982 and 1983 inflow data revealed the existence of wave structures that would successively form and then break down into high-frequency turbulence over a period of 30 minutes to an hour. A monostatic acoustic sounder and minimal wind recording equipment were installed in August 1986 to aid in verifying that (1) the wave structure and breakdown were actually occurring, and (2) the phenomena were characteristic of the Goodnoe Hills site.

### 2.2 Instrumentation

To understand the complex noise-generation processes, several kinds of instruments were necessary. To characterize the turbine inflow structure both tower- and balloon-supported measurements were needed. Surface pressure taps on one of the turbine blades had to be installed, to understand the unsteady blade loads responsible for low-frequency noise emissions. Multiple measuring microphone systems were used to (1) determine the spatial characteristics of the radiated acoustic pressure field and (2) to reduce the effects of the wind on individual microphones. Multiple data recording systems accommodated the number of data channels required to fully document the noise generation processes on the MOD-2.

#### 2.2.1 Acoustic Measurement Instruments

Two pairs of ground-level, very-low-frequency (VLF) microphone systems (Bruel & Kjaer Model 2631 FM-carrier preamplifiers with Type 4144 back-sealed microphones) were employed during the 1982 measurements. The microphone pairs were spaced 15 m (50 ft) apart, or about a 1/4 acoustic wavelength at 5 Hz. During the 1982 program, one pair was placed on the rotor axis 1.5 rotor diameters (1.5D, 137 m or 450 ft) upwind, and one pair was placed in the rotor plane a similar distance from the turbine hub axis. A single, precision sound level meter (ANSI Type-1, Bruel & Kjaer Model 2209 with a Type 4165 microphone) was located halfway between the two low-frequency microphones. Figure 2-1 shows the placement of one of the microphone stations. In addition to the fixed microphone stations, an averaging Type-1 sound level meter was used to establish the directivity of the MOD-2 A-weighted acoustic emissions making measurements over a predetermined grid pattern around the turbine. Two community noise analyzers (CNA, GenRad Model 1945) were used to obtain statistical distributions of the A-weighted emission levels at several locations. Figure 2-2 summarizes the acoustic measurements used during the 1982 experiment.

A slightly different arrangement was employed during the 1983 experiment. A triad of surface-mounted VLF microphones was located on the rotor axis as shown in Figure 2-3. This arrangement allowed us to use acoustic ranging measurement techniques, such as those discussed by Hemphill [5], for locating emission source regions within the rotor disk. While not part of the original test plan, a Type-1 sound level meter was placed between the VLF microphones



**Figure 2-1. Microphone Measurement Station**

at the 137-m distance for a few data runs. The on-axis VLF microphone placement was the same as for the 1982 tests, to allow for direct comparisons between the two years. All acoustic measurements taken in 1981, 1982, and 1983 were referenced to a Bruel & Kjaer Type 4220 pistonphone corrected for the local barometric pressure.

### **2.2.2 Atmospheric Measurement Instruments**

Information about the details of the turbine inflow during these experiments was very important if any quantitative relationship between the inflow structure and the spectral emission levels was to be achieved. Historically, this information has been gathered from multiple, fixed measurement heights installed on a meteorological tower near the turbine. Some attempts have been made to use remote probing devices such as bi-static acoustic sounders or laser velocimeters, but often with limited success because of operational limitations as well as the long averaging times required. We chose to use both tower measurements and a package carried by a tethered balloon flown directly upwind of the turbine.

#### **2.2.2.1 Tower-Mounted Measurements**

The Goodnoe Hills site has two meteorological towers. One, operated by the Pacific Northwest Laboratories (PNL), is 107 m tall with five levels instrumented with cup and vane anemometry, sensible air temperature at 15 m, a 15- to 107-m temperature difference, and local barometric pressure at the 61 m (200 ft) hub-height level. This tower is located near Turbine No. 1 on the

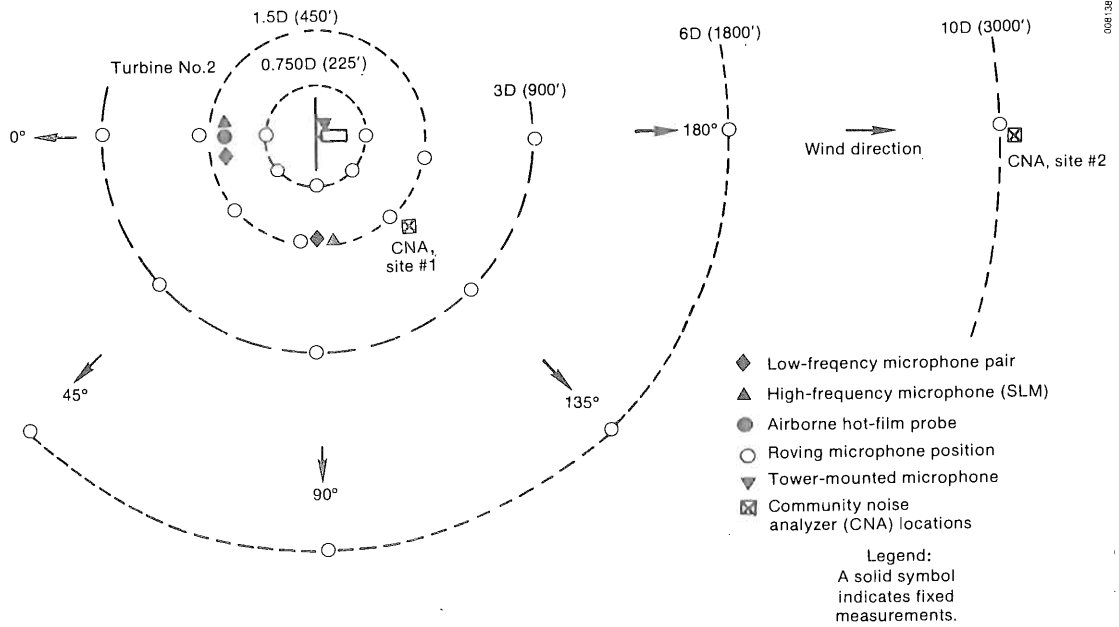


Figure 2-2. Acoustic Instrumentation Configuration for 1982 Experiments

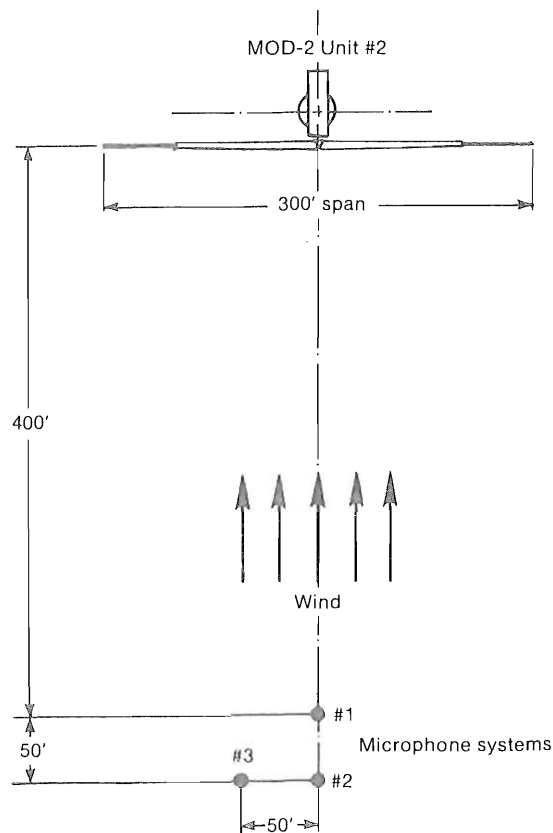


Figure 2-3. Triad of VLF Microphones Used for 1983 Experiments (Plan view)

east side of the site. The second tower, operated by BPA, is located on the west side of the site between Turbine Nos. 2 and 3. It has a maximum elevation of 61 m with propeller-type anemometry at the 15- and 59-m levels, sensible temperature at 15 m, and surface barometric pressure. A three-axis propeller anemometer, with a response of about 1 Hz, was also temporarily installed at the 61-m level. SERI mounted a two-axis, hot-film anemometer with a response of 10 Hz at the 45-m level. Figure 2-4 shows the location of the two towers with respect to Turbine No. 2.

2.2.2.2 Tethered Balloon Measurements

In order to make detailed measurements of both the hub-height wind speed and direction, as well as the vertical distribution of the wind vector and temperature, SERI employed a commercial tethered balloon system (AIR, Inc.) which was modified to carry a 0.15-mm diameter, hot-film anemometer. The standard instrument package transmits wind speed and direction, dry- and wet-bulb temperatures, and barometric pressure (height) once every 10 seconds over a radio link to a ground receiving station where it is displayed and recorded. The hot-film anemometer transmits a nonlinear velocity signal with a 125-Hz bandwidth over a special, digital FM-telemetry link. This link provides a signal dynamic range (maximum Signal-to-noise ratio or SNR) of 70 dB. The received signal is converted to an analog voltage, linearized, and recorded. Figures 2-5 and 2-6, respectively, are photographs of the measuring system

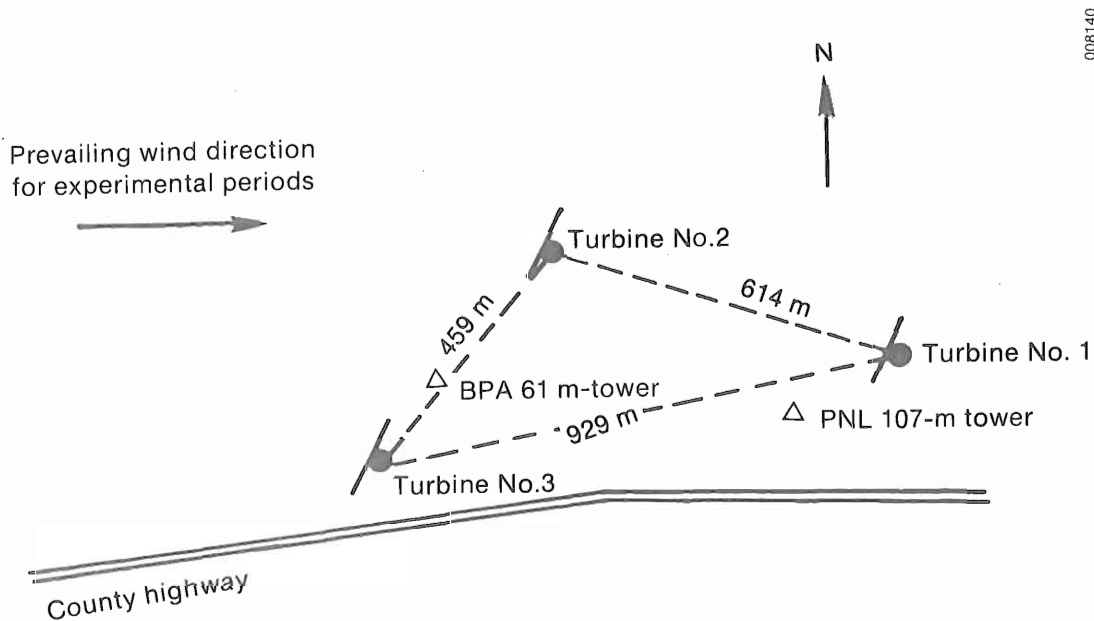
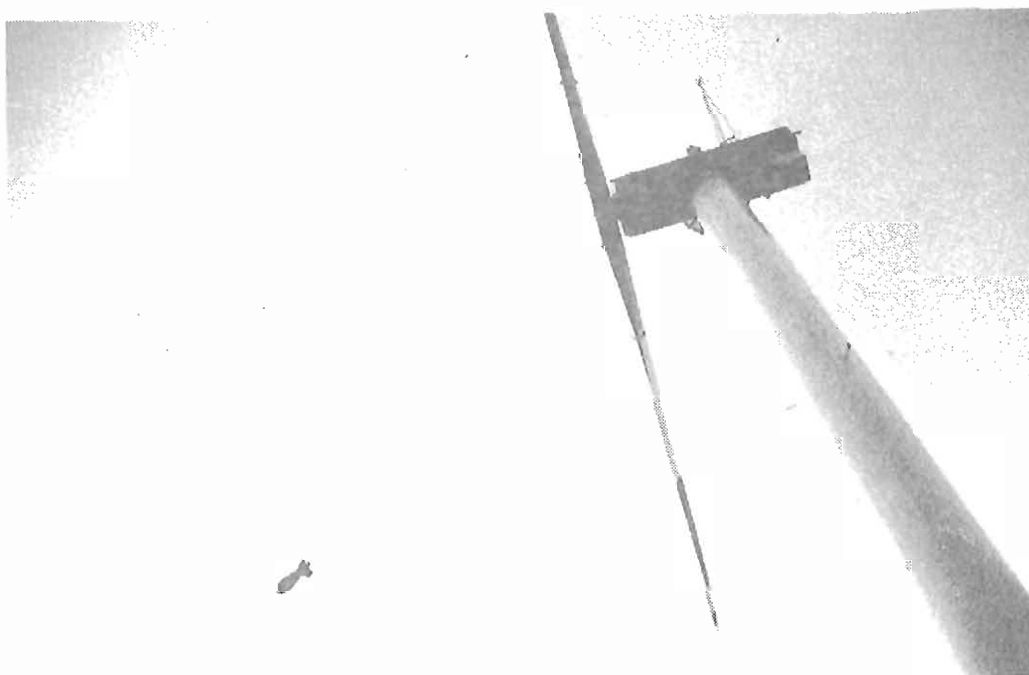


Figure 2-4. Site Layout Schematic Showing Locations of Meteorological Towers with Respect to the Turbines



**Figure 2-5. Detail of Inflow Instrumentation Carried by Tethered Balloon**



**Figure 2-6. Typical Position of Tethered Balloon in Turbine No. 2 Inflow**

carried by the tethered balloon and its position in the turbine inflow. Figure 2-7 schematically shows the data flow paths associated with the hot-film anemometer and meteorological parameter measurements.

### 2.2.3 Turbine Rotor Surface Pressures

During the 1983 experiment, 12 surface-mounted, pressure transducers were attached to the upper and lower surfaces of Blade No. 1 of Turbine No. 2. The transducers were subminiature, 35 kPa (5 psi) capacity semiconductor, strain gage type, each with a frequency response of at least 5 kHz. The site engineering data system (EDS) unfortunately limited the data bandwidth from these transducers to 37.5 Hz (-3 dB point). Six transducers were installed at locations equalling 65% and 87% of the blade span at 15%, 40%, and 85% chord positions on the upper and lower surfaces. Figure 2-8 shows a typical installation at the outer span station.

### 2.2.4 Turbine Operational Information

A number of standard engineering measurements were recorded to support these tests. The parameters included the rotor position angle, Blade No. 1 pitch angle, generator power output, chordwise and flapwise moments at the 21%, 65%, and 87% span locations, and flapwise accelerations at the 21% and 67% span locations.

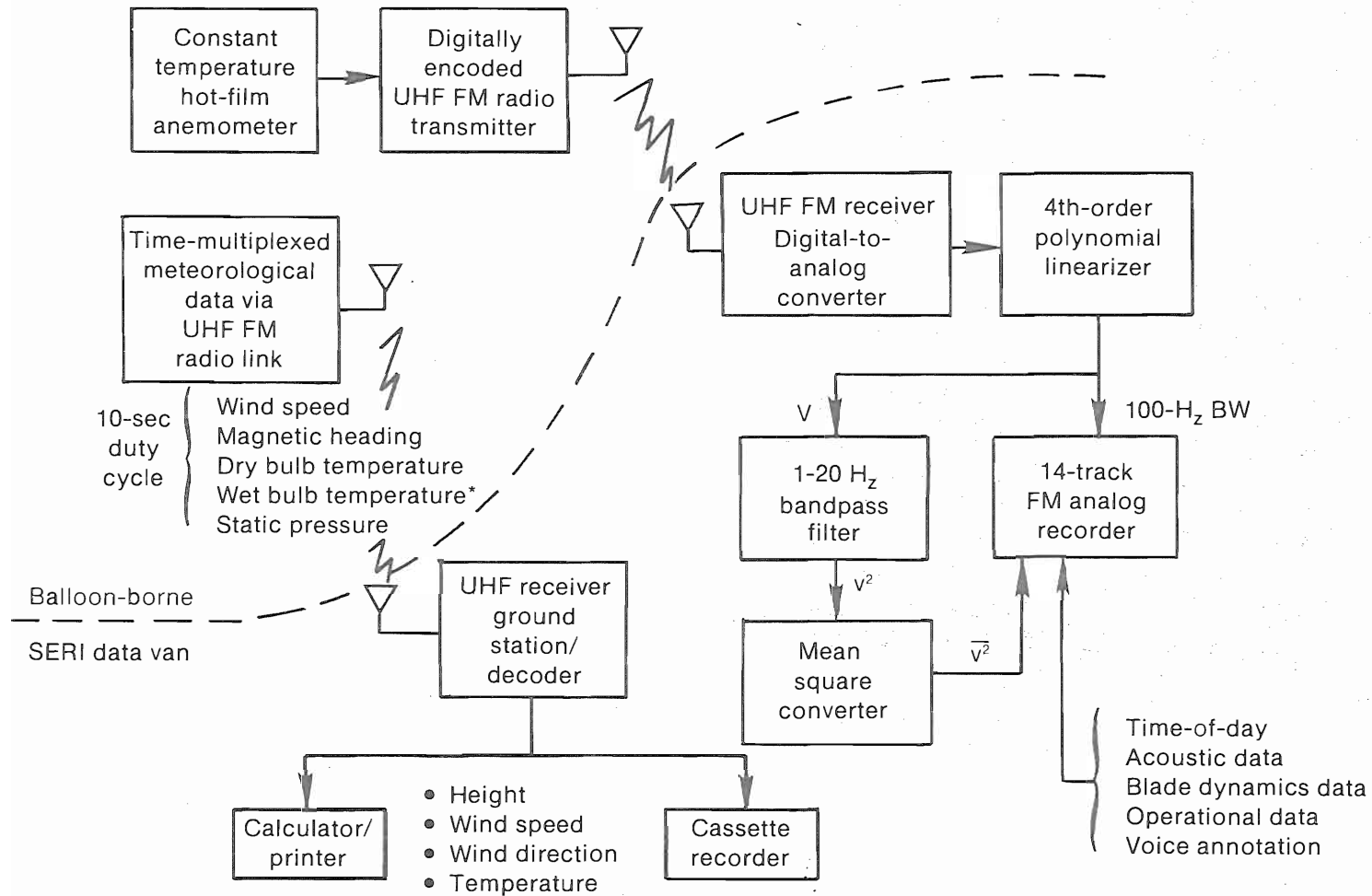
### 2.2.5 Data Recording

Multiple recording systems were required to handle the volume and diversity of data sources for these experiments. Figure 2-9 summarizes the data sources and recording system configurations for the 1983 experiment. Five separate systems were used. Acoustic data were recorded on SERI's 14-channel FM/direct tape together with two of the outer span station pressure taps, the corresponding chord and flapwise moments, and the linearized hot-film anemometer signal from the tethered balloon. The PNL minicomputer-based data logging system was used for the standard meteorological data from both towers. The data were later transferred to digital cassettes for transport to SERI.

The bulk of the pressure tap, aeroelastic information, and operational data from the turbine were recorded using the NASA Data Van in FM multiplex format. The standard 10-second data from the tethered balloon system were logged on its own recorder in serial-digital format. A 7-channel FM recorder was used to acquire the two-axis hot-film and the standard 59-m level wind speed and direction from the BPA tower. All recording systems included time channels that were synchronized at the beginning of each experimental period. The maximum time uncertainty between recording systems is estimated at less than 5 seconds for a given run and less than 1 second for the NASA and SERI recording systems in particular.

## 2.3 Experimental Procedures

A consistent objective of both the 1982 and 1983 experiments was to document the acoustic noise characteristics of an isolated MOD-2 rotor under a range of atmospheric inflow conditions. The primary difference between the two years was that in 1983 the low-frequency-range emissions were of particular interest, rather than both high and low frequencies, which was the case in 1982.



\*Not used.

Figure 2.7 Data Flow Path for Inflow Measurements

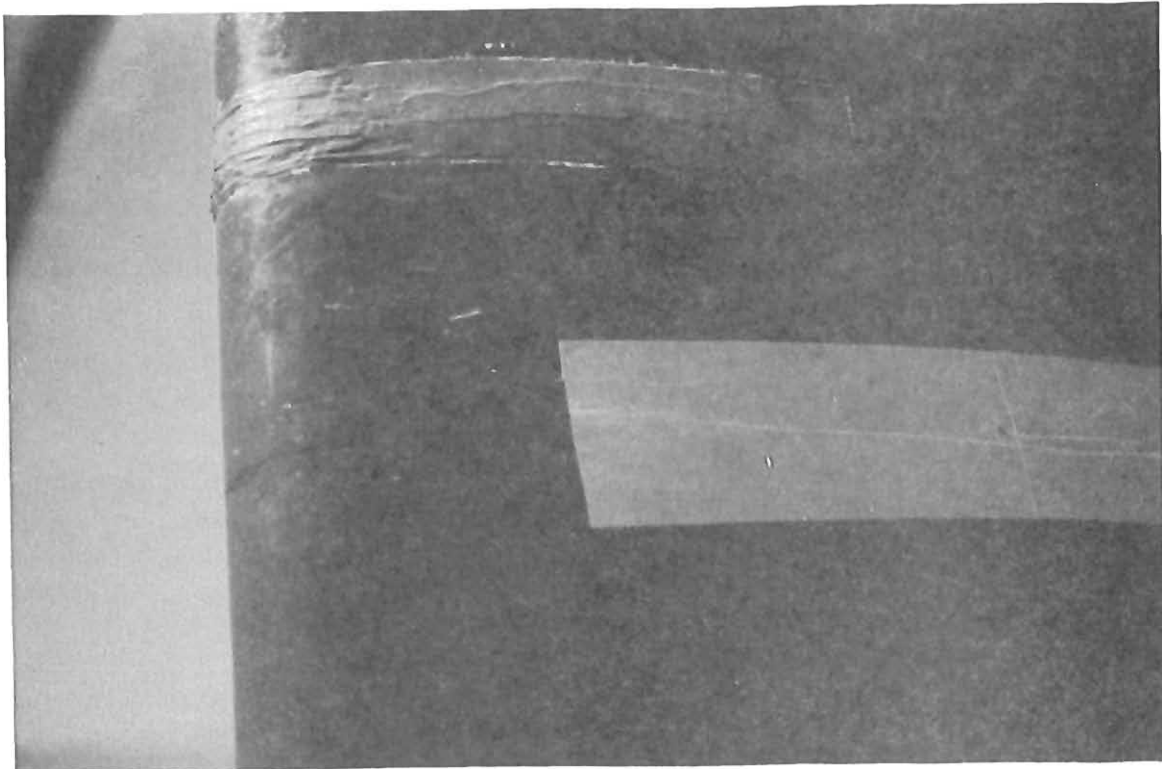


**Figure 2-8. Surface Pressure Tap Installation at Blade No. 1, Station 1562, 15% Chord Position**

Experience gained from acoustic surveys of other large wind turbines showed that the inflow turbulence structure was a major factor in determining not only the level and spectral content of radiated emissions, but the degree of coherence or impulsiveness as well. Furthermore, SERI's wind-tunnel and atmospheric tests [1,6] showed that inflow turbulence length scales, the order of the rotor's mean chord length, were the most important in terms of low-frequency emissions. Therefore, the experimental procedures used were designed to document these key elements: the degree of rotor aerodynamic loading, and the turbulent inflow structure and its relationship to other atmospheric surface layer parameters.

### 2.3.1 The 1982 Experiment

The 1982 experiment was originally planned to document not only the acoustic emission characteristics of a single MOD-2, but the aggregate effects of the cluster triad as well. We recognized that these objectives would require at least two experimental periods. The original plan, therefore, was to complete the individual MOD-2 characterization in 1982 and the cluster effects in 1983. The 1982 objective was basically met. Subsequent material changes in the turbine physical and operational configuration, however (an alteration of the pitch angle schedule and the installation of vortex generators on the rotor), necessitated a reassessment of the modified machine. Either or both of these modifications had the potential to substantially alter the characteristics of the radiated acoustic field.

Data Sources	Recording Systems	Available SNR* (dB)
<b>Acoustics</b>		
Low-frequency noise (0.1-200 Hz)	→ SERI single FM channel/track	55
High-frequency noise (400-8000 Hz)		
Continuous unweighted A-weighted SPL	→ SERI single direct channel/track	40
Statistically-sampled	→ Community noise analyzer (CNA)	95
Spatially-sampled	→ Type-1 sound level meter (SLM)	50
<b>Blade surface pressures/dynamics</b>		
d.c. — 37.5 Hz data bandwidth	→ SERI single FM channel/track	55
	→ NASA data van 16 FM channels/track	35
	→ Site EDS 16 FM channels/track	30-35
<b>Turbine operational data</b>		
d.c. — 37.5 Hz data bandwidth	→ SERI single FM channel/track	55
	→ NASA data van 16 FM channels/track	35
	→ Site EDS 16 FM channels/track	30-35
<b>BPA meteorological tower</b>		
Hot-film anemometry (d.c. — 10 Hz)	→ SERI single FM channel/track	45
Wind direction/speed (d.c. — 1 Hz)	→ SERI single FM channel/track	45
	→ PNL site data system (2-s averages)	46+
<b>PNL meteorological tower</b>		
Wind direction/speed (2-s averages)	→ PNL site data system	46+
Temperature/temp. difference		
<b>Tethered balloon</b>		
Wind direction/speed, Temperature, height (d.c.— 0.1 Hz)	→ Stand-alone digital recording (10-s sampling)	60
Hot-film anemometer (d.c. — 100 Hz)	→ SERI single FM channel/track	55

\*SNR = Signal-to-noise ratio

Figure 2-9. Data Sources and Recording Systems Configuration

008145



The experimental test matrix had to be based not only on field-measurable parameters having a direct influence on the inflow turbulent structure and the degree of rotor aerodynamic loading, but also on the turbine's relative alignments to assess the acoustic impacts of upwind turbine wakes on downwind machines. The turbulent structure reaching the turbine rotor is a function of the wind speed regime, the hydrodynamic stability of the vertical atmospheric layer occupied by the rotor disk, and the upwind fetch or surface conditions (landforms, vegetation, man-made structures, etc.). These parameters are not independent and may be a strong function of the local wind azimuth and time-of-day. The diurnal dependence was automatically determined by the availability of sufficient winds for the turbine's operation and not included directly in the test conditions. The most commonly used measure of the vertical stability, which can be readily determined under field conditions, is the gradient Richardson number (Ri) defined in Eq. (2-1), where  $g$  is the local gravity acceleration,  $\Delta\theta$  and  $\bar{\theta}_0$  are the difference and mean potential temperatures for the layer defined by  $\Delta z$ , and  $\Delta u$  is the difference in wind speed between those two levels.

$$Ri = g/\bar{\theta}_0(\Delta\theta/\Delta Z)/(\Delta u/\Delta z)^2 . \quad (2-1)$$

The potential temperature  $\theta$  is given by

$$\theta(z) = T(z)[100/p(z)]^{0.286} \quad (2-2)$$

where  $T(z)$  and  $p(z)$  are the absolute temperature (K) and barometric pressure (kPa) at height  $z$ . Three turbulence regimes have often been assigned to ranges of the Richardson number and include the unstable ( $0 < Ri$ ), the stable-turbulent ( $0 < Ri < 0.25$ ), and the stable-laminar ( $Ri > 0.25$ ). The turbulent structure has been observed to undergo distinct changes in each of these three regimes.

The test matrix elements chosen for these experiments then were based on 10-minute averages of three locally determined criteria: the hub-height (59 m) wind speed and direction from the BPA tower and the gradient Richardson number as measured from the 15- and 107-m levels on the PNL tower. Table 2-1 summarizes the test condition matrix originally planned to be used for the 1982/83 experiment. The original matrix in Table 2-1 employed three wind direction ranges (SW, W, and NW; see Figure 1-4), two wind-speed ranges (7-11 and 12-20 mps), and the three vertical stability regimes discussed above. The two wind-speed regimes were chosen to separate conditions below and above the turbine's rated operation (12 mps or 28 mph). The upper operational limit of SERI's tethered balloon system at that time was also about 11 mps, so runs in the high-speed regime of Table 2-1 were not planned to be supported with balloon inflow measurements (that limitation was removed by redesigning the balloon rigging system before the October 1983 experiment). Table 2-1 also lists the desired matrix conditions for the multiple turbine portions of the experiment by alignment (see Figure 2-4); i.e., 5 rotor diameters (D) or approximately 450 m (1500 ft) with Turbine 2 and 3 within  $\pm 10^\circ$  of on-axis alignment; 7D (640 m or 2100 ft) with Turbine Nos. 1 and 2 aligned; and 10 D (915 m or 3000 ft) with Turbine Nos. 1 and 3.

Table 2-2 presents an excerpt from the run configuration for the single turbine portion of the experiment. The probability of success was based on what was known about the climatology of the site. For example, while we wanted to

Table 2-1. Original Test Matrix for 1982/1983 MOD-2 Experiment

Average Wind Direction	Average Wind Speed	Ri Average, 15- to 107-m Layer
SW direction <sup>a</sup> (205°-235°)	Low-speed range (7-11 mps)	Unstable
		Stable-turbulent
or		Stable-laminar
5D spacing <sup>b</sup> (210°-230°)	High-speed range (12-20 mps)	Unstable
		Stable-turbulent
		Stable-laminar
W direction (255°-285°)	Low-speed range	Unstable
		Stable-turbulent
or		Stable-laminar
7D spacing (270°-290°)	High-speed range	Unstable
		Stable-turbulent
		Stable-laminar
NW direction (300°-330°)	Low-speed range	Unstable
		Stable-turbulent
or		Stable-laminar
10D spacing (245°-260°)	High-speed range	Unstable
		Stable-turbulent
		Stable-laminar

<sup>a</sup>single turbine experiment; <sup>b</sup>multiple turbine experiment.

evaluate the turbine under southwesterly flow conditions (air flowing up out of the Columbia Gorge), a great percentage of the time the winds are below cut-in speed from this direction; thus, the low-probability rating. Each run with the turbine operating was 30 minutes long while background runs with the turbine shut down were 10 minutes.

Table 2-2. Excerpt of Run Configurations for 1982 Single Turbine Experiments

Run Code Number	Priority	Success Prob.	WD/ Spacing	WS Range	Stability Range	Airborne Config.	Acoustic Config.	Site Data Config.	Operating Turbines			Remarks
									1	2	3	
ST27	2	G	W	II	SL	---	AC1	SD1		*		
ST28	3	F	NW	L	US	AD	AC1	SD1		*		
ST29	1	G	NW	L	US	AC	AC1	SD1		*		background
ST30	1	G	NW	L	US	AC	AC1	SD1		*		
ST31	3	E	NW	L	ST	AD	AC1	SD1				
ST32	1	E	NW	L	ST	AC	AC1	SD1		*		
ST33	1	E	NW	L	ST	AC	AC1	SD1		*		
ST34	3	E	NW	L	SL	AD	AC1	SD1				background
ST35	1	E	NW	L	SL	AC	AC1	SD1		*		
ST36	1	E	NW	L	SL	AC	AC1	SD1				background
ST37	2	G	NW	II	US	--	AC1	SD1		*		
ST38	2	E	NW	II	ST	--	AC1	SD1		*		
ST39	2	E	NW	II	SL	--	AC1	SD1				
ST40	1	E	W	L	US	AD	AC2	SD1		*		
ST41	1	E	W	L	ST	AD	AC2	SD1		*		
ST42	1	G	W	L	SL	AD	AC2	SD1		*		
ST43	1	E	W	L	ST	AC	AC2	SD1		*		

Success Probability

E = Excellent  
 G = Good  
 F = Fair  
 P = Poor

### 2.3.2 The 1983 Experiment

The test matrix was redefined slightly in 1983 in response to the reduced scope of the objectives and also to reflect the shorter testing period available. Because of structural cracks developing within the low-speed shaft of Turbine No. 2, the actual running time was very limited. Enough data were collected during the 1982 experiment to verify that inflow turbulence played a major role in determining the characteristics (intensity, coherency, etc.) of the MOD-2 radiated emissions, particularly for acoustic energy contained in frequencies below 200 Hz. A preliminary analysis indicated that many of these characteristics could be predicted with some accuracy from a knowledge of (1) the mean hub-height wind speed, (2) the turbulence intensity or level, and (3) the vertical stability of the atmospheric layer occupied by the rotor disk.

The major objective of the 1983 experiment, in addition to re-evaluating acoustic performance after the control and rotor modifications, was to attempt a direct measurement of the MOD-2 aeroacoustic/aeroelastic turbulence spectral response. The rotor surface pressure measurements supported this objective. The 1982 experience demonstrated that a single wind-direction range, i.e., 255°-285°, which also happened to be the most prevalent during the desired operating hours, would be sufficient. It was also realistic, in view of the previous year's experience, to slightly modify the Richardson number stability parameter ranges in order to ensure a greater degree of variation in the turbulent characteristics of the inflow. These redefined ranges included the following:

- o Unstable (US):  $-0.5 < Ri$ ,
- o Stable-turbulent (ST):  $-0.5 < Ri < +0.5$ ,
- o Stable-laminar (SL):  $Ri > +0.5$ .

Thus, the modified 1983 test matrix used a single wind-direction range, two hub-height wind-speed ranges (same as the 1982 experiment), and the redefined vertical stability classes US, ST, and SL defined above. Each data run consisted of a 30-minute period when the machine was operational, concluded by a 15-minute period of background conditions. The tethered balloon system (used when the hub-level winds were less than 11 mps or 25 mph) produced a vertical profile of the inflow before the operational run and again at its conclusion, with the instrument package "parked" near the hub elevation and nominally 1.5-2.0 rotor diameters upstream during turbine operation.

### 2.4 Data Reduction Procedures

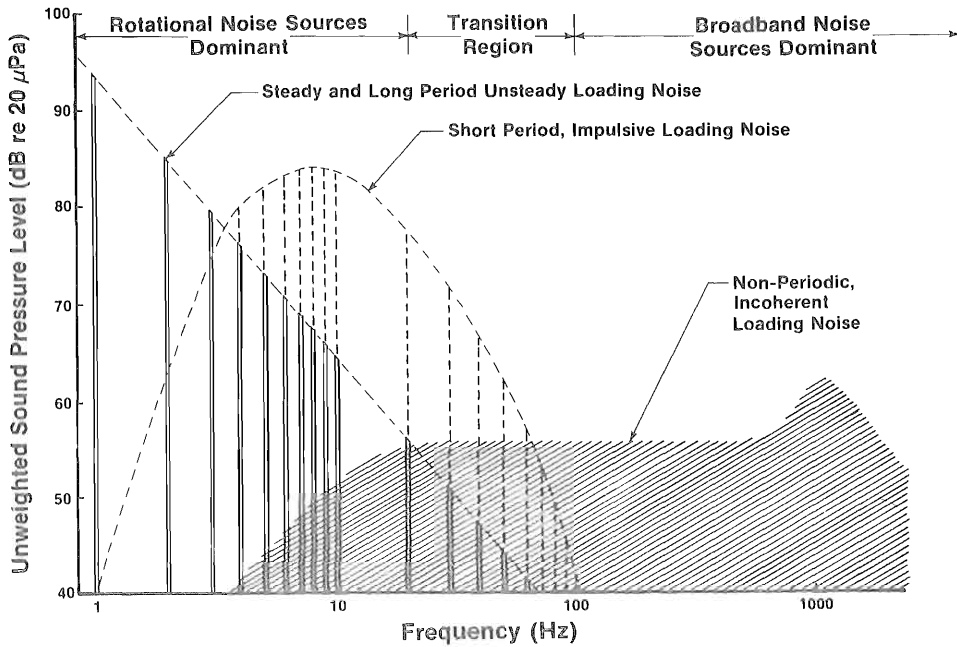
The acoustic, atmospheric, and 1983 surface pressure and hot-film inflow data each required somewhat different processing procedures. Furthermore, because of the stochastic nature of the turbulence exciting the acoustic response of the turbine, a statistical sampling approach has been developed for presenting and quantifying the radiated acoustic spectra. This procedure is explained below. Consistent with the statistical approach, the turbulent inflow was characterized using the methods of statistical fluid mechanics and described in terms of "bulk" flow parameters. To determine direct estimations of the MOD-2 aeroacoustic and surface-pressure response functions, standard continuous time-series analysis procedures were employed.

### 2.4.1 Acoustic Data

It was convenient and reasonable to separate the radiated acoustic spectra presentations into low- and high-frequency ranges. The low-frequency range (< 200 Hz) is essentially controlled by the unsteady airload driven by the inflow turbulence encountered in the rotor disk (rotational noise sources). The high-frequency range, whose emissions dominate the contributions to the A-weighted sound pressure level, is often influenced by so-called broadband "self-noise" mechanisms; i.e., trailing edge vortex shedding, as an example, though rotor/turbulence interaction may still play a significant role. The two-level frequency range classification was further supported by our previous experience with the MOD-1 turbine and an Oregon gas turbine peaking generator [25]. Acoustic emissions in the 5 to 100-Hz range were found to produce resonant interactions with residential structures [1] causing annoyance to the occupants.

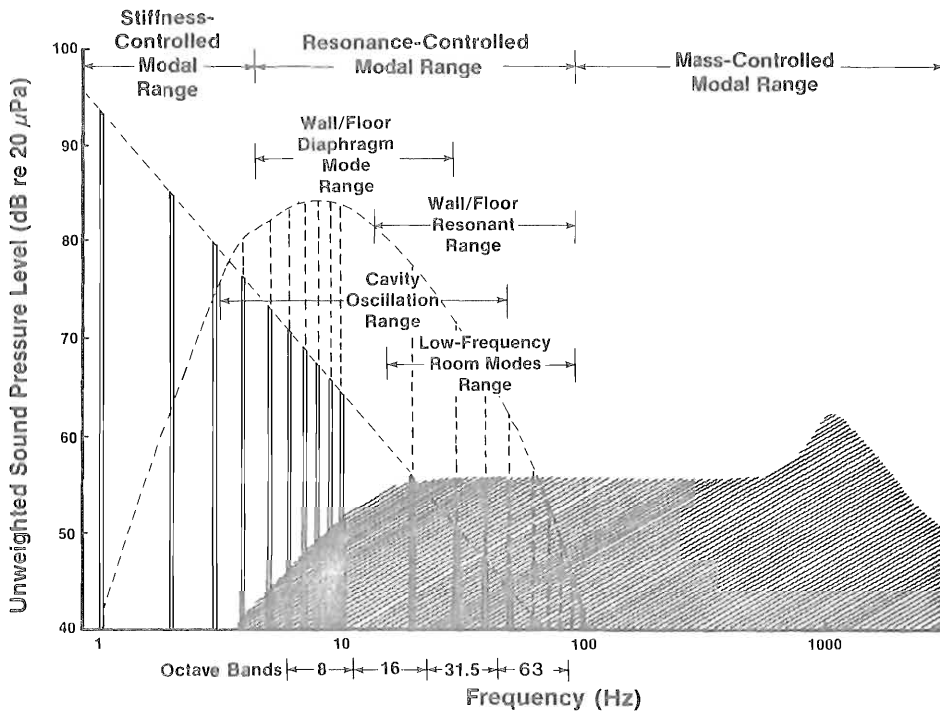
Figure 2-10 illustrates schematically the typical characteristics of a large wind turbine's acoustic spectra, and Figure 2-11 schematically delineates the relationship of these emissions to acoustically sensitive resonances in residential constructions. The 5- to 100-Hz, resonance-controlled modal range shown in the Figure 2-10 damping range can be reasonably described by the 8-, 16-, 31.5-, and 63-Hz ISO (International Organization for Standardization) octave bands or, in more detail, by the corresponding ISO 1/3-octave bands. Table 2-2 lists these bands and their associated frequency ranges, with the frequency range covered by the 8-, 16-, 31.5-, and 63-Hz ISO octave bands highlighted. These four bands encompass 87% of the desired range of 95 Hz from 5 to 100 Hz. Using the 1/3-octave bands as the minimum frequency resolution is justified over this frequency range because (1) the frequency resolution is small, ranging from 1.2 Hz for the 5-Hz band to 22 Hz for the 100-Hz band; and (2) even including the remainder of the bands shown in Table 2-3, the numerical and statistical processing demands remain tractable in comparison with performing the same operations with a narrowband resolution of 0.5 or even 1 Hz over the desired frequency range of 95 Hz. The bookkeeping may be compared by noting the volume of data required for summarizing the multi-dimensional statistics of 20 maximum (ISO 3 to 22) or 12 minimum (ISO 8 to 19) 1/3-octave bands versus 95 bands with 1-Hz resolution and the 190 bands at 0.5-Hz resolution for the desired 5- to 100-Hz range.

The 1/3-octave band resolution was also employed for the high-frequency range emission spectra as well. Table 2-4 lists the ISO 1/3-Octave Bands used for the high range as well as the corresponding A-scale weightings. The high-frequency ranges available in terms of recorder channel bandwidths and dynamic ranges for the 1982 and 1983 experiments were limited, as shown in Table 2-5. The A-weighted values displayed in later sections are based on a truncated frequency range and should be considered estimates rather than strictly defined by ISO and American National Standards Institute (ANSI) standards. We do not believe the values used are seriously deficient, however, since the range of most sensitive human hearing and nominal atmospheric absorption are covered by the bands of Table 2-4 for both experimental years.



008146

Figure 2-10. Schematic Representation of an Averaged Radiated Sound Pressure Spectrum from a Large Wind Turbine



008147

Figure 2-11. Schematic Sound Spectrum of Figure 2-10 with Residential Construction Vibration Modes and Applicative Damping Mechanisms Added

**Table 2-3. ISO Octave and 1/3-Octave Low-Frequency Analysis Bands**

Band No.	Nominal Center Frequency (Hz)	Third-Octave Passband (Hz)		Octave Passband (Hz)	
3	2	1.78-	2.24	1.41-	2.82
4	2.5	2.24-	2.82		
5	3.15	2.82-	3.55		
6	4	3.55-	4.47		
----- <sup>a</sup>					
7	5	4.47-	5.62		
8	6.3	5.62-	7.08		
9	8	7.08-	8.91	5.62-	11.2
10	10	8.91-	11.2		
11	12.5	11.2-	14.1		
12	16	14.1-	17.8	11.2-	22.4
13	20	17.8-	22.4		
14	25	22.4-	28.2		
15	31.5	28.2-	35.5	22.4-	44.7
16	40	35.5-	44.7		
17	50	44.7-	56.2		
18	63	56.2-	70.8	44.7-	89.1
19	80	70.8-	89.1		
-----					
20	100	89.1-	112		
21	125	112-	141	89.1-	178
22	160	141-	178		

<sup>a</sup>Region within dashed lines represents the portion of the 5- to 100-Hz structural resonance range included by the 8-, 16-, 31.5-, and 63-Hz ISO octave bands used in the analysis.

#### 2.4.1.1 Low-Frequency-Range, Coherent Random Sampling Technique

Figure 2-12 summarizes schematically the random, coherent processing technique used for the reduction of MOD-2 low-frequency-range data. The purpose of this technique, which is explained more fully in Ref. [7], is to minimize the effects of wind-induced or "pseudo" noise on the results. The approach is based on the assumption that (1) the wind-induced-noise components will exhibit a random phase characteristic at 5 Hz and above between two microphones spaced a minimum of a quarter wavelength apart at 5 Hz, as compared with the more coherent radiation from the wind turbine rotor; and (2) the use of random sampling will produce statistically significant differences between the turbine's operating acoustic pressure spectra and the local background.

The actual processing consisted of feeding the recorded signal from each of the two microphones into a dual-channel, narrowband (400-line, effective bandwidth of 0.5 Hz) spectrum analyzer and calculating the in-phase or cospectrum for the desired frequency range or time period, or both. The resulting elemental cospectrum frequency-band amplitudes were then summed into the appropriate ISO 1/3-octave and octave bands listed in Table 2-3. Each 30-minute data collection run with the turbine operating was subdivided into three

**Table 2-4. ISO 1/3-Octave Bands Used for High Frequency Analysis**

Band No.	Nominal Center Frequency (Hz)	Third-Octave Passband (Hz)		A-Scale Weighting (db)
23	200	178-	224	-11
24	250	224-	282	-9
25	315	282-	355	-7
----- a				
26	400	355-	447	-5
27	500	447-	562	-3
28	630	562-	708	-2
29	800	708-	891	-1
30	1000	891-	1120	0
31	1250	1120-	1410	+1
32	1600	1410-	1780	+1
33	2000	1780-	2240	+1
34	2500	2240-	2820	+1
35	3150	2820-	3550	+1
36	4000	3550-	4470	+1
37	5000	4470-	5620	+1
38	6300	5620-	7080	0
39	8000	7080-	8910	-1

<sup>a</sup> Available high-frequency-data range for the 1983 experiment (dashed area).

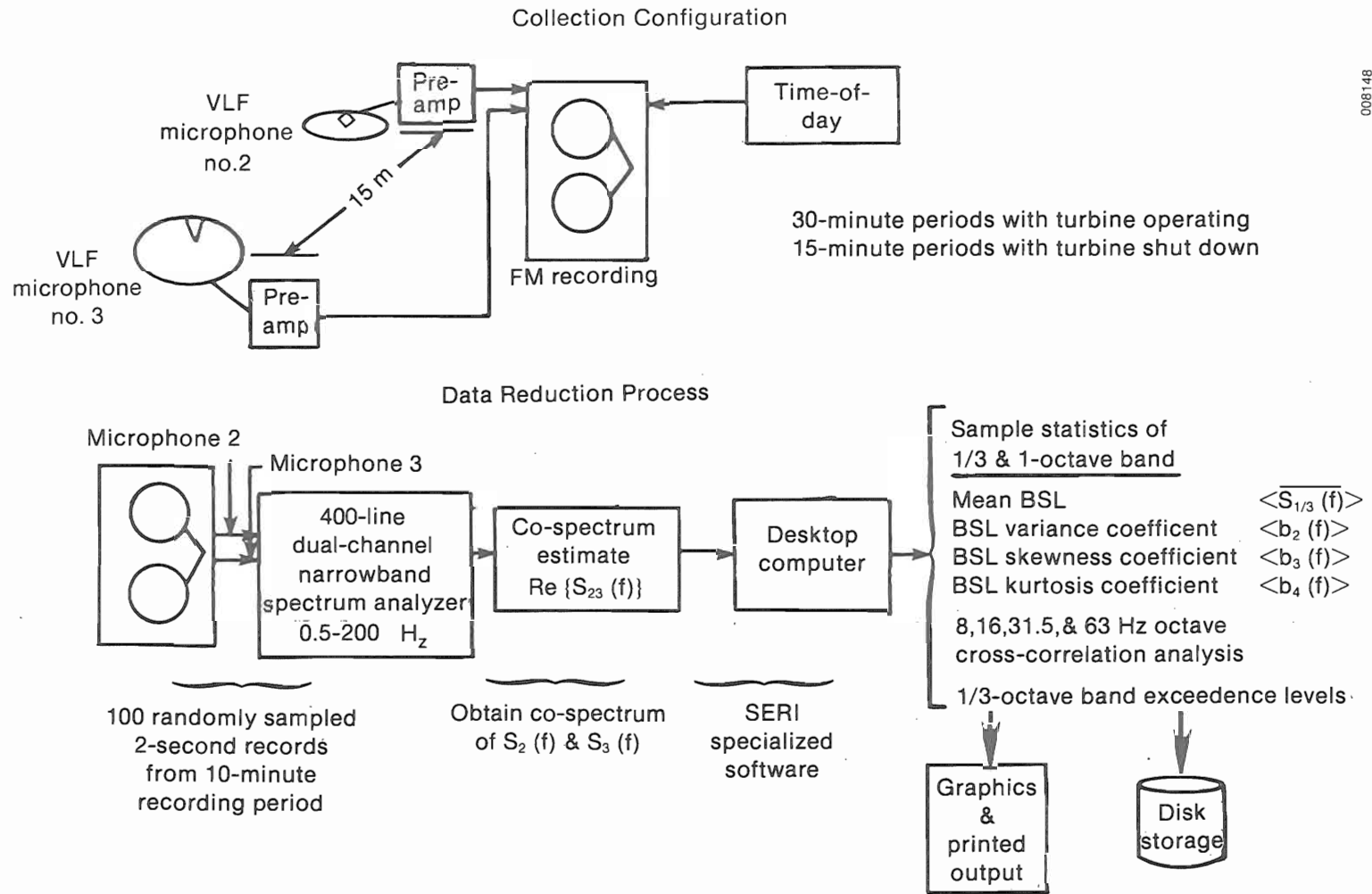
**Table 2-5. Magnetic Recorder Bandwidths and Dynamic Ranges for HF Acoustic Recordings during 1982 and 1983 Experiments**

	Recording Bandwidth (kHz)	Signal Dynamic Range (dB)
<u>1982</u>		
Racal 7DS	0.1 to 19.0	38
<u>1983</u>		
Honeywell 5600E	0.4 to 62.5 <sup>a</sup>	33

<sup>a</sup> Signal bandwidth limited to 20 kHz before recording.

10-minute segments, and individual 1/3-octave and octave cospectra were calculated from 100 2-second, randomly sampled (with replacement) ensemble records. The same processing procedure was applied to the corresponding background recordings.

The statistical distributions of the band spectrum levels (BSL) up through the fourth moment were then calculated for each 1/3-octave and octave band listed in Table 2-3. In addition, both band-to-band cross and conditional correlations as well as frequency distributions were calculated for the four octave



008148



**Figure 2-12. Low-Frequency-Range Coherent Processing Flow**

band amplitudes. The summary statistics as well as the raw band spectrum level distributions for each 10-minute record were then stored in disk files. The aggregate statistics for each 30-minute run were later arrived at from the arithmetic average of these shorter segments. Figures 2-13 through 2-15 present representative examples of the distributions and displays that are available from typical 10-minute analysis segments.

#### 2.4.1.2 High-Frequency-Range Random Sampling Technique

A somewhat similar random sampling technique was used for the 10-minute records of the high-frequency-range measurements, and it is summarized in Figure 2-16. For acoustic emissions in this range, only a single microphone was used. Band pressure levels (BPL) of the 1/3-octave bands listed in Table 2-4 were assembled from an 800-line, narrowband autospectrum with an effective bandwidth ( $B_p$ ) of 25 Hz. Rather than the 100 random samples of a 2-second record, which were used for low frequencies, the high-frequency 1/3-octave spectra were calculated from 31 samples of the average of three consecutive autospectra with a total sample record length of 0.06 seconds. The observed frequency distributions and corresponding 1/3-octave band statistical distributions were calculated (including the A-weighted band level estimate discussed in Section 2.3.1) and stored in a disk file. No band-to-band cross or conditional correlations were derived. As before, the aggregate statistics for a particular 30-minute run were formed from the arithmetic mean of the individual 10-minute-segment statistics. Figures 2-17, 2-18, and 2-19 are representative samples of the resulting high-frequency-range statistical summaries.

#### 2.4.2 Atmospheric Data

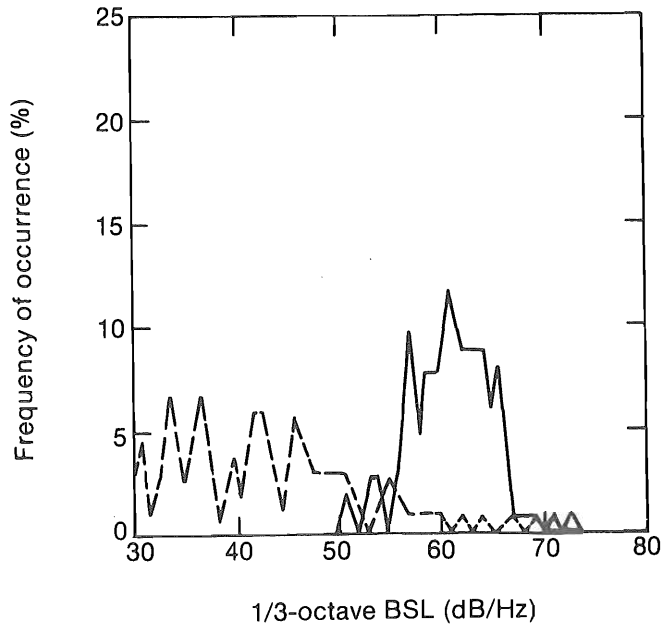
Two approaches to relating the MOD-2 acoustic emissions to the turbine inflow were used in our evaluation. One employed stochastic analysis methods in which the statistical distributions of the 1/3-octave emission spectra were correlated using bivariate and multivariate linear regression techniques with characteristic bulk measures of the turbulent inflow. The other approach relied on more-or-less conventional time-series techniques using continuous records as a basis of comparison. With the exception of continuous analog recordings of the two-axis, hot-film anemometer and the hub-height wind vector on the BPA tower, the majority of the measurements from the two meteorological towers were used to determine the mean inflow characteristics for each 30-minute data collection period. SERI's tethered balloon system was used during many of the low-speed-regime runs of Table 2-1 and its 1983 counterpart to estimate a mean vertical profile of the Turbine No. 2 inflow, with a level of detail unavailable from the tower measurements. The details of the tethered balloon operation and associated data processing may be found in Ref. [8].

##### 2.4.2.1 Mean Inflow Characteristics

Table 2-6 lists the surface-layer bulk characteristic parameters for Goodnoe Hills measured from the PNL and BPA meteorological towers and SERI's tethered balloon system for the 1983 experiments. The BPA tower measurements, except for the vertical stability (Richardson number), were used to correlate the test turbine acoustic emissions, because of the tower's close proximity. The PNL tower measurements were also used in determining the value and height of the rotor disk peak mean wind speed and the Brunt-Vaisala frequency (period)

**1/3-octave BSL Frequency Distribution**

Run #1: A05-C ——— 1/3 oct. band = 8 Hz  
 Run #2: A05-BG - - - - Upper freq. limit = 8.915 Hz  
 Lower freq. limit = 7.085 Hz



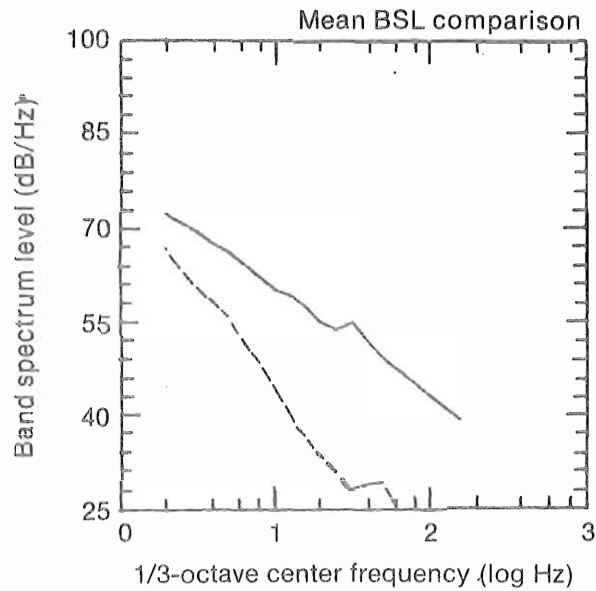
**8.00-Hz band distribution statistics**

		<u>Run #1</u>	<u>Run #2</u>
Mean BSL (dB/Hz)	=	61.9	48.4
Peak BSL (dB/Hz)	=	72.7	69.1
Min. BSL (dB/Hz)	=	50.8	25.7
Coef. variance	=	0.50	1.60
Skewness coef.	=	1.80	3.88
Rel. kurtosis coef.	=	5.59	17.70
Mode BSL (dB/Hz)	=	61.0	37.0
Median BSL (dB/Hz)	=	61.0	42.0

**Figure 2-13. Example of Low-Frequency Acoustic Data Reduction Output: Observed Frequency Distributions of 8-Hz 1/3-Octave Band Spectrum Level for Turbine Operating (Run #1) and Background Conditions (Run #2)**

008150

1/3-Octave BSL Frequency Spectrum  
 Run #1: A05-C ———  
 Run #2: A05-BG - - - -



1/3-Octave BSL Frequency Spectrum  
 Run #1: A05-C ———  
 Run #2: A05-BG - - - -

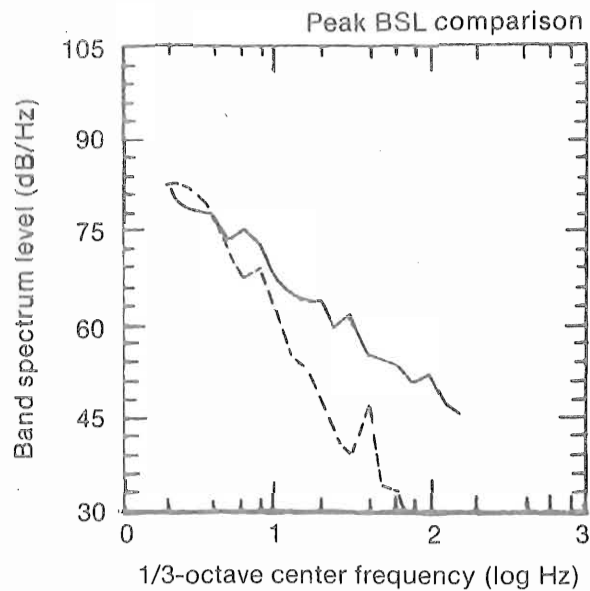


Figure 2-14. Example of Low-Frequency Acoustic Data Reduction Output: Mean and Peak 1/3-Octave BSL Spectra for Turbine Operating (Run #1) and Background Conditions (Run #2)

Run A05-C  
Run #1: 1/3-octave BSL exceedence level summary (dB/Hz)

Center frequency (Hz)	1%	5%	10%	20%	50%
2.00	82	79	78	75	72
2.50	79	77	76	74	71
3.15	78	76	74	72	69
4.00	78	75	73	71	67
5.00	74	73	71	69	66
6.30	75	70	68	66	64
8.00	73	67	66	64	61
10.00	67	65	63	62	60
12.50	65	65	63	62	59
16.00	64	62	61	60	56
20.00	64	60	58	57	54
25.00	60	58	57	55	53
31.50	62	59	58	56	54
40.00	56	54	54	53	51
50.00	54	52	51	50	49
63.00	54	50	49	48	47
80.00	51	48	47	47	45
100.00	52	46	45	44	43
125.00	48	44	43	42	41
160.00	46	41	41	40	40

Run A05-BG  
Run #2: 1/3-octave BSL exceedence level summary (dB/Hz)

Center frequency (Hz)	1%	5%	10%	20%	50%
2.00	83	77	74	71	63
2.50	83	74	70	66	59
3.15	81	71	69	64	57
4.00	77	68	66	61	51
5.00	72	67	65	59	50
6.30	67	62	60	55	46
8.00	69	60	56	50	42
10.00	62	55	52	47	39
12.50	55	52	46	42	34
16.00	53	46	42	39	32
20.00	48	42	39	35	30
25.00	42	39	35	33	29
31.50	39	34	32	29	26
40.00	47	34	31	30	27
50.00	34	33	32	31	29
63.00	33	29	28	27	24
80.00	26	25	23	22	21
100.00	27	25	25	24	22
125.00	28	27	27	27	23
160.00	26	25	24	23	22

**Figure 2-15. Example of Low-Frequency Acoustic Data Reduction: Exceedence Level ( $L_1$ ) Comparison for Turbine Operating (Run #1) and Background Conditions (Run #2)**

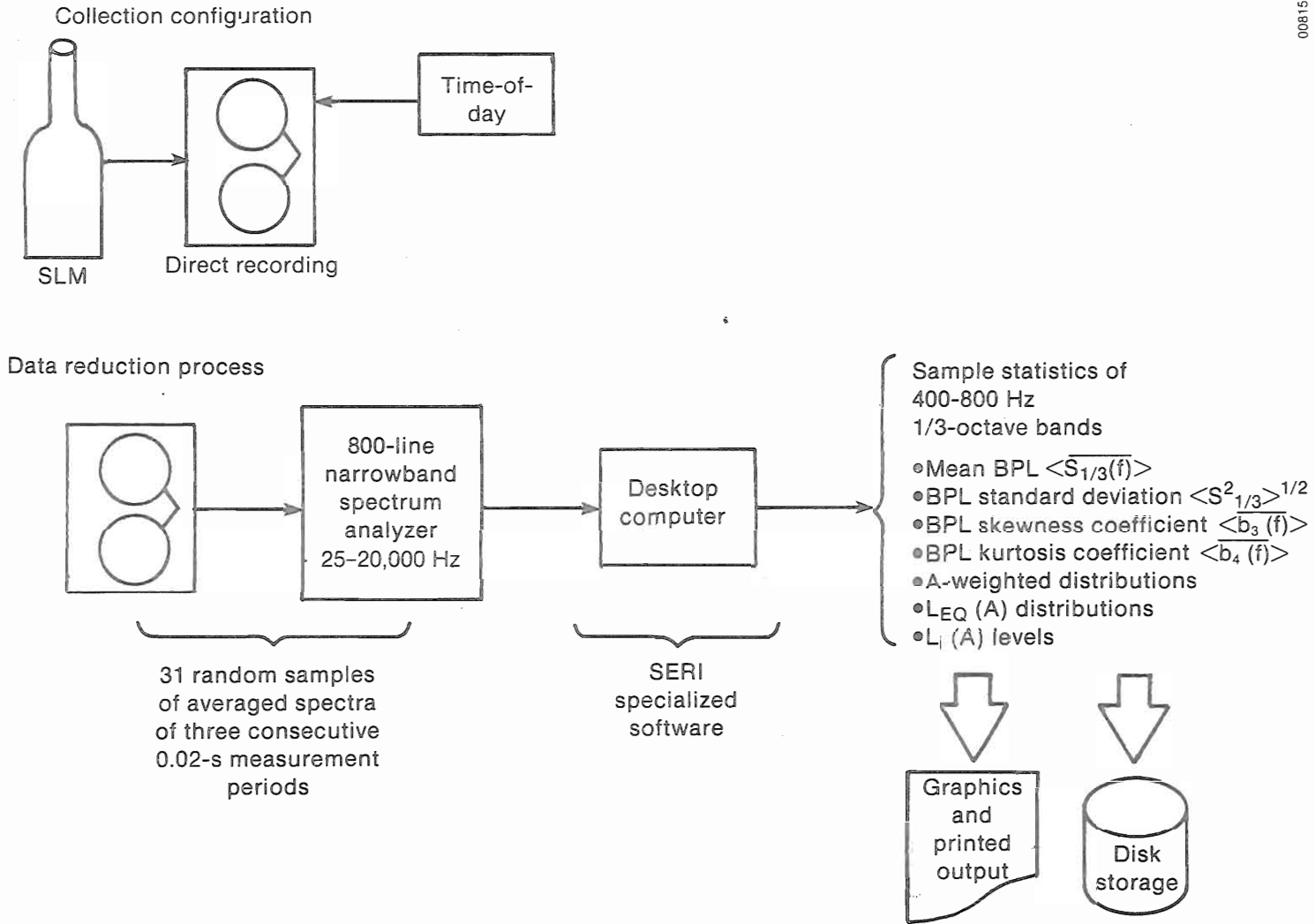
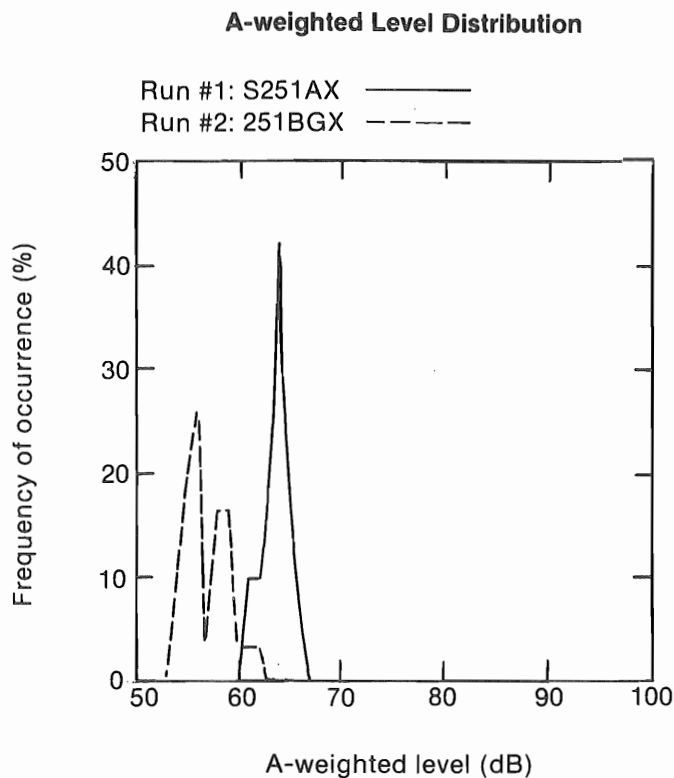


Figure 2-16. High-Frequency-Range Acoustic Data Processing

008153



**A-weighted level distribution statistics**

	Run #1	Run #2
Mean BPL (dB) =	63.7	57.0
Peak BPL (dB) =	66.0	62.2
Min. BPL (dB) =	61.1	53.6
Std. dev. (dB) =	1.26	2.05
Skewness coef. =	-0.50	0.54
Kurtosis coef. =	-0.34	-0.27
Mode (dB) =	64	56
Median (dB) =	64	56

**Figure 2-17. Example of High-Frequency Acoustic Data Reduction Output: Observed Frequency Distributions of A-Weighted BPL for Turbine Operating (Run #1) and Shut-Down Conditions (Run #2) in High Winds (>14 mps)**

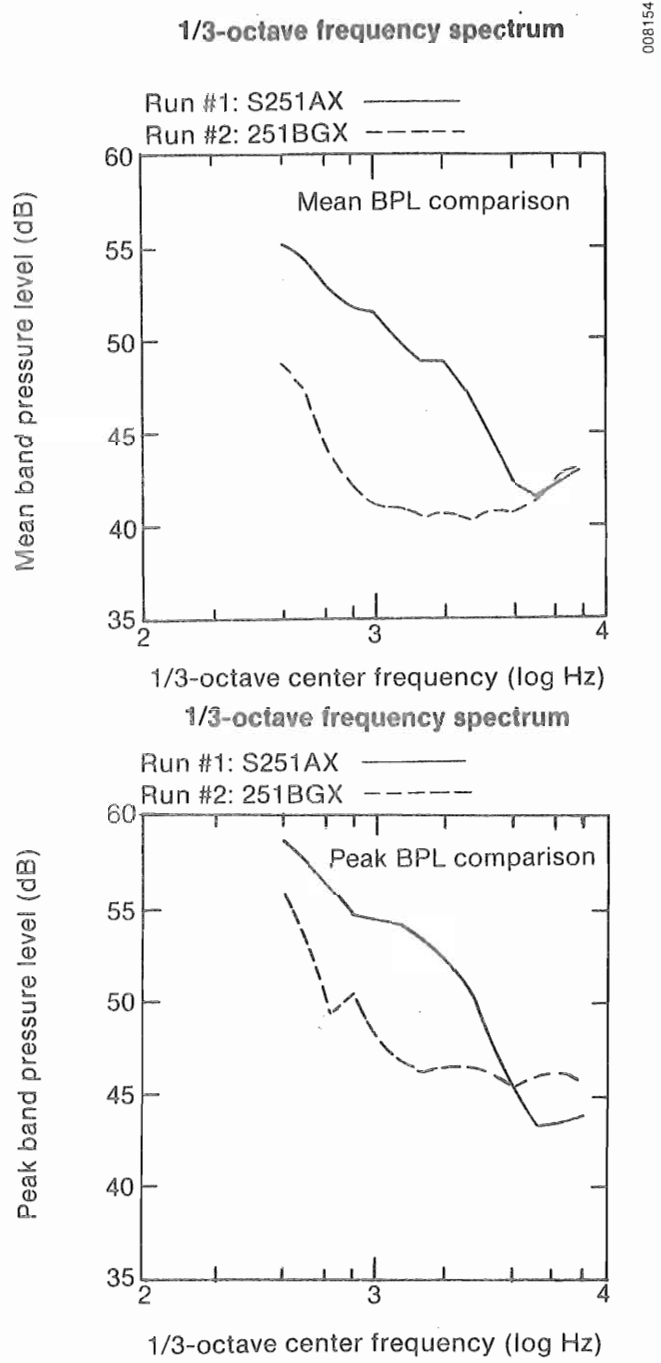


**Figure 2-18. Example of High-Frequency Acoustic Data Reduction Output: Mean and Peak 1/3-Octave BPL Spectra for Turbine Operating (Run #1) and Shut-Down Conditions (Run #2) in High Winds**

**Run S251AX**

**Run #1: 1/3-octave BPL exceedence level summary (dB)**

Center frequency (Hz)	1%	5%	10%	20%	50%
400	59	58	58	57	55
500	57	57	57	56	55
630	56	56	55	54	53
800	55	55	54	53	52
1000	54	54	54	53	51
1250	54	54	52	52	50
1600	53	53	51	50	49
2000	52	52	52	50	49
2500	51	51	50	48	47
3150	48	47	47	46	45
4000	45	45	45	44	42
5000	43	43	42	42	42
6300	44	43	43	43	42
8000	44	44	44	43	43
A-weighted level	66	66	65	65	64

**Run 251BGX**

**Run #2: 1/3-octave BPL exceedence level summary (dB)**

Center frequency (Hz)	1%	5%	10%	20%	50%
400	56	52	52	50	48
500	53	53	51	49	47
630	49	47	46	46	43
800	50	45	45	44	42
1000	48	46	44	43	41
1250	47	45	44	43	41
1600	46	43	43	42	40
2000	47	44	43	43	41
2500	47	43	42	42	40
3150	46	44	43	42	40
4000	45	43	42	42	40
5000	46	43	42	42	41
6300	46	44	43	43	43
8000	46	44	43	43	43
A-weighted level	62	61	59	59	56

Figure 2-19. Example of High-Frequency Acoustic Data Reduction Output: Exceedence Level ( $L_{\%}$ ) Distribution Comparisons for the Case of Figures 2-17 and 2-18

of the rotor disk layer. Unless otherwise specified, the parameters in Table 2-5 were calculated for the 30-minute data collection period.

A number of parameters listed in Table 2-6 and calculated for this experiment have not generally been used in previous wind research field programs. These parameters include the following, with a brief explanation of what they represent.

Surface roughness length,  $z_0$ . The  $z_0$  parameter represents the size of the turbulent eddy at the ground surface and is a measure of the roughness over which air is flowing. It is usually a function of the local wind direction or upstream fetch. Typical values range from  $10^{-4}$  to  $10^+$  m. Roughness lengths of 0.1 to 0.5 m are common for open country similar to that upwind of Turbine Nos. 2 and 3.

Friction velocity,  $u_*$ . The friction or shear velocity is defined by

$$u_*^2 \equiv (\tau_s / \rho_0) = \nu \frac{\partial \bar{u}}{\partial z}, \quad (2-3)$$

where  $\tau_s$  is the surface Reynolds stress,  $\rho_0$  is the local air density, and  $\nu$  is the kinematic viscosity. It is a scaling parameter with the units of velocity and a measure of the stress and considered constant with height in the lower portion of the earth's boundary layer, i.e., the surface layer.

Gradient Richardson number,  $Ri$ . The gradient Richardson number, defined by Eq. (2-1), represents the ratio of buoyant (thermal) to mechanical (shear) turbulence production in the layer  $\Delta z$ . Negative values (unstable) correspond to conditions when turbulence generation is being dominated by thermal convection while positive (stable) ones represent conditions during which energy is transferred from mean to turbulent motions; i.e., that buoyancy-damped, shear-generated turbulence is dominant. A Richardson number of zero represents neutral stability conditions indicating that the conditions for only mechanical turbulence generation are present.

Monin-Obukov length,  $L$ . The Monin-Obukov length is defined by

$$L \equiv (-u_*^3 c_p \rho_0 T) / [k_a g H (1 + 0.07/B)], \quad (2-4)$$

where  $c_p$  is the specific heat at constant pressure;  $T$ , the absolute temperature;  $g$ , the gravity acceleration;  $H$ , the vertical heat flux;  $k_a$ , the von Karman constant; and  $B$ , the Bowen ratio (a measure of the ratio of sensible to latent heat flux at the surface). Since the direct evaluation of Eq. (2-4) requires an array of specialized instrumentation,  $L$  is usually estimated from a knowledge of the Richardson number. Panofsky and Dutton [9] recommend Eqs. (2-5) and (2-6) for estimating  $L$  where  $z$  is the height.

$$z/L = Ri \quad \text{for } Ri < 0 \quad (2-5)$$

$$z/L = Ri / (1 - 5Ri) \quad \text{for } Ri > 0. \quad (2-6)$$

**Table 2-6. Bulk Surface Layer Parameters Measured during 1983 Goodnoe Hills Experiments from Towers and Tethered Balloon**

Rotor Disk Mean Flow Quantities	BPA Tower	PNL Tower
Mean 15-m horiz. wind vector, $U_{15}$	o	o
Mean 38-m horiz. wind vector, $U_{38}$		o
Mean 45-m u-(long.) component, $U_{45}$	o	
Mean 45-m w-(vert.) component, $W_{45}$	o	
Mean hub-ht. horiz. wind vector, $U_H$	o	o
Mean hub-ht. vert. component, $W_H$	o	
Mean 84-m horiz. wind vector, $U_{84}$		o
Mean 107-m horiz. wind vector, $U_{107}$		o
Surface roughness length, $z_o$	o	o
Friction velocity, $u_*$	o	o
Gradient Richardson number, $Ri$		o
Monin-Obukov length, $L$	o	
Rotor disk peak horiz. wind speed, $U_{max}$		o
Rotor disk peak velocity height, $z_{max}$		o
Rotor disk Brunt-Väisälä period, $T_{BV}$		o
Surface barometric pressure, $P_{sfc}$	o	
Hub-height barometric pressure, $P_{hub}$		o

BPA 45 m Bulk Inflow Turbulence Quantities

Longitudinal component (u), x-direction length scale,  $I_u^x$

Vertical component (w), z-direction length scale,  $I_w^z$

Vertical component (w), x-direction length scale,  $I_w^x$

Longitudinal (u) time scale,  $T_u$

Vertical (w) time scale,  $T_w$

Longitudinal (u) frequency spectral estimate,  $S_u(f)$

Vertical (w) frequency spectral estimate,  $S_w(f)$

Longitudinal (u) spectra reduced frequency peak,  $f_u$

Vertical (w) spectra reduced frequency peak,  $f_w$

Longitudinal (u) peak turbulence energy,  $P_u$

Vertical (w) peak turbulence energy,  $P_w$

**Table 2-6. Bulk Surface Layer Parameters Measured during 1983 Goodnoe Hills Experiments from Towers and Tethered Balloon (Continued)**

---

Tethered Balloon Quantities

- Nominal hub-height mean wind speed,  $U_H$
  - Nominal hub-height  $(u^2 + w^2)^{1/2}$  turbulence spectra,  $S_{uw}(n)$
  - Nominal hub-height inflow turbulence length scales,  $I_{uw}$
  - Low and high vertical resolution velocity profiles,  $U(z)$
  - Low and high resolution vertical shear profiles,  $dU/dz$  and  $du/dz$
  - Low and high resolution potential temperature profiles,  $\theta(z)$
  - Low and high resolution sensible temperature profiles,  $\theta_s(z)$
  - Layer, local Richardson numbers profiles,  $Ri_{1y}(z)$  and  $Ri_{10}(z)$
  - Brunt-Väisälä frequency profiles,  $N(z)$
- 

It is a surface layer characteristic scaling length and a measure of the height below which mechanical (shearing) turbulence generation is dominant.  $L$  is defined as negative when convective conditions are present (negative or upward heat flux) and positive when a stable stratification exists (positive or downward heat flux). The dimensionless ratio  $z/L$  can also be thought of as an indicator of the predominant type of turbulence generation going on. Large negative values indicate that convective turbulence generation is dominant; near zero indicates that mechanical turbulence mechanisms dominate; and a positive  $z/L$  indicates a predominance of buoyancy-damped, shear generation [9].

Brunt-Väisälä frequency (period,  $T_{bv}$ ),  $N$ . The Brunt-Väisälä frequency,

$$N^2 = (1/T_{bv})^2 = [(g/\bar{\theta}_0)(\Delta\theta/\Delta z)]^2, \quad (2-7)$$

is a measure of the characteristic period of oscillation of a density-stratified flow. Oscillations in the vertically stratified, stable boundary layer typically have periods of 30-300 s, and  $N$  is an important measure of the existence of such periodic phenomena. As shown in Table 2-6, it has been calculated for the rotor disk layer from the PNL tower measurements and layer and local values from SERI's tethered balloon profiles.

2.4.2.2 Turbulent Inflow Characteristics

Turbulent component length scales,  $I_{ij}$ . The turbulent component integral or length scales are defined by

$$I_{u_i}^j = \bar{u}_i T_i = \bar{u}_i \int_0^\infty R_{ij}(\tau) d\tau \text{ for } i=1,2,3, \quad (2-8)$$

where  $T_i$  is the integral time-scale for the  $i$ th-component and  $R_{ij}(\tau)$  is the cross-correlation function between the  $i$  and  $j$  components. There are nine possible terms in the  $R_{ij}(\tau)$  matrix. Three of these have been computed for the 1983 experiment from the hot-film anemometer measurements and listed in

Table 2-6.  $I_u^x$  is a characteristic scale length of the longitudinal turbulence component,  $u$ , along the  $x$ -direction (positive east). Similarly,  $I_w^x$  is a scale length of the vertical component,  $w$ , along the  $x$ -direction. Finally,  $I_w^z$  is a scale length of the  $w$ -component in the vertical or  $z$ -direction. The time and length scales were calculated from component velocity signals over a frequency range of 0.05 to 10 Hz for the 30-minute data-collection periods.

Normalized turbulence spectra descriptors. Frequency spectra amplitudes of the turbulent wind components ( $u$ ,  $v$ ,  $w$ ) are often normalized by the cyclic frequency or  $nS(n)$ . The corresponding cyclic frequency,  $n$ , is normalized by the ratio  $z/U(z)$  or  $nz/U(z)$  and referred to as the reduced frequency  $f$ , where  $U(z)$  is the mean wind speed at height  $z$ . The quantities  $f_u$  and  $f_w$  in Table 2-6 represent the value of the reduced frequency where  $fS(f)$  has its maximum. Further,  $P_u$  and  $P_w$  parameters in Table 2-6 refer to the maximum values of  $nS_u(f)$  and  $nS_w(f)$ , respectively.

### 2.4.3 Rotor Surface Pressures

Table 2-7 lists the locations of the 12 semiconductor pressure transducers used on Blade No. 1 of Turbine No. 2 in the 1983 experiment. In this volume, only the measurements near the leading edge of the rotor have been analyzed to any great extent. This is because coherent, low-frequency acoustic radiation is associated with turbulence-induced, unsteady blade loads, whose greatest effects tend to be concentrated near the leading edge.

Table 2-7. Pressure Tap Locations on Turbine No. 2, Blade No. 1

Tap No.	Blade Station	Percent Span	Percent Chord	Surface
1	1164 <sup>a</sup>	65	15	Upper <sup>b</sup>
2	1164	65	15	Lower <sup>c</sup>
3	1164	65	40	Upper
4	1164	65	40	Lower
5	1164	65	85	Upper
6	1164	65	85	Lower
7	1562 <sup>d</sup>	87	15	Upper
8	1562	87	15	Lower
9	1562	87	40	Upper
10	1562	87	40	Lower
11	1562	87	85	Upper
12	1562	87	85	Lower

<sup>a</sup>Fixed pitch portion of blade.

<sup>b</sup>Low pressure surface.

<sup>c</sup>High-pressure surface.

<sup>d</sup>Movable tip portion.

### 3.0 DESCRIPTION OF GOODNOE HILLS INFLOW STRUCTURE

A knowledge of the details of the turbulent inflow structure is important if any statistical correlation between the inflow properties and the resulting acoustic emission characteristics is to be made. We must first establish what properties are most important in terms of acoustic noise generation by the MOD-2 in a turbulent atmosphere. Summaries are then given of the available inflow properties for the 1982 and 1983 experimental periods.

#### 3.1 Identification of the Acoustically Important Inflow Properties

Homicz and George [10,11] and George and Kim [17] have developed a unified theory using generalized functions of aeroacoustic noise generated by rotating blades in a turbulent atmosphere. We will use their results as a basis for determining the critical inflow parameters to be used as statistical predictors for correlations with the MOD-2 emissions spectra.

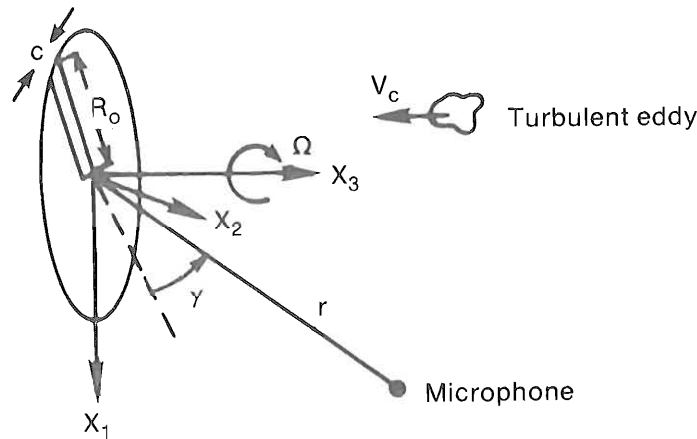
Homicz and George have shown that the generalized function for the far-field radiated acoustic spectrum  $\langle S_{ap}(f) \rangle$ , for a localized disturbance source region is given by

$$\langle S_{ap}(\underline{x}, f) \rangle = \frac{f^2}{4\rho_0 a_0^3} \frac{x_i x_j}{r^4} \int_{-\infty}^{\infty} d^3\eta \langle P_{L_i} L_j(\eta, -\frac{f}{a_0} \hat{n}_0, f) \rangle \quad (3-1)$$

where  $f$  is the acoustic frequency,  $a_0$  is the sound speed,  $\rho_0$  is the air density,  $\gamma$  is the distance between the observation point and the rotor,  $n$  is the harmonic number,  $\eta$  is the position vector of the disturbance on the rotor,  $P_{L_i} L_j$  is the cross-spectral density of the lift, and  $\hat{n}_0$  is the unit vector along  $\underline{x}$ . Figure 3-1 shows the geometry of the rotor and associated angles and symbols. They also have shown that the characteristics of the radiated acoustic spectrum depend on the quasi-static load due to mean loading conditions plus the fluctuating loads due to rotor-turbulence interaction. The far-field radiated spectrum due to a turbulent upwash spectrum is of the form

$$\langle S_{ap}(f) \rangle \propto \int_{\zeta}^{\infty} d\zeta \left[ \sum_{n=n_1}^{n_2} \sum_{\ell=-\infty}^{\infty} G(\zeta, n, \ell) J_{nB-1}^2\left(\frac{f\alpha}{\Omega}\right) \right. \\ \left. \times J_{\ell}^2\left(\frac{M_c}{M_c}\right) \sqrt{\left(\frac{V_c}{I_w^z}\right)^2 \zeta^2 - \left(\frac{f}{\Omega} - nB\right)^2} \right], \quad (3-2)$$

where  $\langle S_{ap}(f) \rangle$ , the acoustic pressure spectrum, is expressed in the form of an integral over  $\zeta$ , the turbulent velocity spectrum dimensionless wavenumber, and where the two series involving Bessel functions arise because of the resolution of the turbulence into polar coordinates and because of the Doppler shift due to the rotation. The function  $G(\zeta, n, \ell)$  includes the ingested turbulence spectrum and unsteady aerodynamic effect and the finite span effect of the rotor blades.  $I_w^z$  is the vertical or upwash turbulence integral scale;  $V_c$  is the axial convection velocity of the turbulence (usually taken as  $0.8U_H$ );  $B$  is the number of blades in the rotor; and  $M_c$  is the axial convection Mach number,  $M_c = V_c/a_0$ .



008156

Figure 3-1. Rotor Geometry Used by Homicz and George [10,11]

The dynamic characteristics of the low-frequency portion of the radiated spectrum is determined by the degree of blade-to-blade correlation with turbulent eddies passing through the rotor plane [10]. Larger eddies may be cut by more than one blade, producing peaked, essentially discrete tones in the low-frequency spectrum. Smaller eddies produce much higher frequency blade loads, but generally there is less likelihood of repeated encounters with the same eddy, and random, broadband noise is radiated. Homicz and George have shown that the frequency at which this transition to broadband takes place is

$$f_0 \approx \frac{B\Omega (1 + M_o/M_c)}{2 (1 - M_o \cos\gamma)} \quad (3-3)$$

They also were able to show that the values of  $\zeta$  that provide significant contributions to the acoustic spectrum at frequency  $f$  are

$$\frac{(f/\Omega) (1 - M_o \cos\gamma)}{(V_c/I_u\Omega) (1 + M_o/M_c)} < \zeta < \frac{(f/\Omega) (1 + M_o \cos\gamma)}{V_c/I_u\Omega} \quad (3-4)$$

When (3-3) and (3-4) are combined, the lower limit of  $\zeta$ , which makes significant contributions for  $f > f_0$  is

$$\zeta_{f_0} > B I_u \Omega / 2 V_c \quad (3-5)$$

For the MOD-2 turbine with  $\zeta$  dimensionalized by the chord  $c_o$  at  $R_o$ , the corresponding turbulent eddy wavelength would be ~10 m or 5 chord lengths for a longitudinal integral scale of 125 m.

Homicz and George assumed that the inflow turbulence could be considered homogeneous and isotropic. This enabled them to use only one length scale. As we see in Sections 3.2.2 and 3.3, even treating the MOD-2 inflow two-dimensionally requires additional length-scale specification, because of the

degree of anisotropy that may be present in the (inflow) acoustically significant eddy wavelengths. In anticipation, we define three integral scales:  $I_u^x$ , the longitudinal or axial scale;  $I_w^x$ , the scale length of the vertical turbulence or upwash component,  $w$ , along the axial direction; and  $I_w^z$ , the scale of the vertical component in the rotor plane. Figure 3-2 sketches the relationship of these length scales to the rotor plane.

Homicz and George arrived at the following general expression for the non-dimensionalized, one-sided acoustic spectrum from a turbulent environment moving through a rotor:

$$\frac{\langle S_{ap}(f) \rangle}{\rho_o a_o^3 \Omega^{-1} M_t^2 (R_t/r)} = \frac{16\pi^4 B^2 M_o^4}{1 - M_o^2} \left(\frac{bc}{R_t}\right)^2 \left(\frac{R_t}{R_o}\right)^2 \left(\frac{\Omega I_w^z}{V_c}\right)^3 \left(\frac{f}{\Omega}\right)^2 \quad (3-6)$$

$$\times \int_{\zeta_{\min}}^{\infty} d\zeta \zeta \sum_{n=n_1}^{n_2} \sum_{l=-\infty}^{\infty} E_{-int} E_l E_{turb} E_{aero} E_{span},$$

where

$$E_{int} = \left[ \cos\mu \sin\gamma - \frac{(nB-1)\sin\mu}{M f_o/\Omega} \right]^2 J_{nB-1}^2 \left( M_o \frac{f}{\Omega} \cos\gamma \right)$$

$$E_l = J_1^2 \left[ \frac{M_o}{M_c} \sqrt{(V_c/I_w^z \Omega)^2 \zeta^2 - (f/\Omega - nB)^2} \right]$$

$$E_{turb} = \left[ (V_c/I_w^z \Omega)^2 \zeta^2 - (f/\Omega - nB)^2 \right] / (1 + 4\pi^2 \zeta^2)^3$$

$$E_{span} = \left\{ 1 + \frac{\tilde{k}_c b}{\pi c} \right\}^{-1}$$

$$E_{aero} = \frac{J_o^2 \left[ \frac{M_o \tilde{k}_T}{1 - M_o^2} \right] + J_1^2 \left[ \frac{M_o^2 \tilde{k}_T}{1 - M_o^2} \right]}{1 + \frac{2\pi}{1 - M_o^2} \tilde{k}_T}$$

$\tilde{k}_c$  and  $\tilde{k}_s$  are the reduced aerodynamic frequencies along the chord ( $c$ ) and span ( $s$ ) averaged over one blade revolution, and  $\tilde{k}_T = (\tilde{k}_c^2 + \tilde{k}_s^2)^{1/2}$ .

$E_l$  gives the relative strengths of the  $l$  loading modes for a given non-dimensional wavenumber,  $\zeta$ ;  $E_{int}$  describes the acoustic interference of these upwash modes with the rotating  $nB$  harmonic modes;  $E_{turb}$  establishes the weighting applied to the contribution from any turbulent wavenumber;  $b$  is the blade span;  $\mu$  is the angle between the lift force vector and the vertical;  $n$  is the harmonic number of the blade passage frequency;  $M_t$  is the tip Mach number; and  $R_t$  is the tip radius. The  $E_{aero}$  and  $E_{span}$  terms reflect the influence of the rotor's unsteady aerodynamic response and a spanwise correction to account for the loss of acoustic compactness at high frequencies. Homicz and George have developed expressions for these terms under what we believe to be highly idealized conditions. For now, we have chosen to lump these effects together with those fixed by design by experimentally determining the MOD-2 aeroacoustic transfer functions.

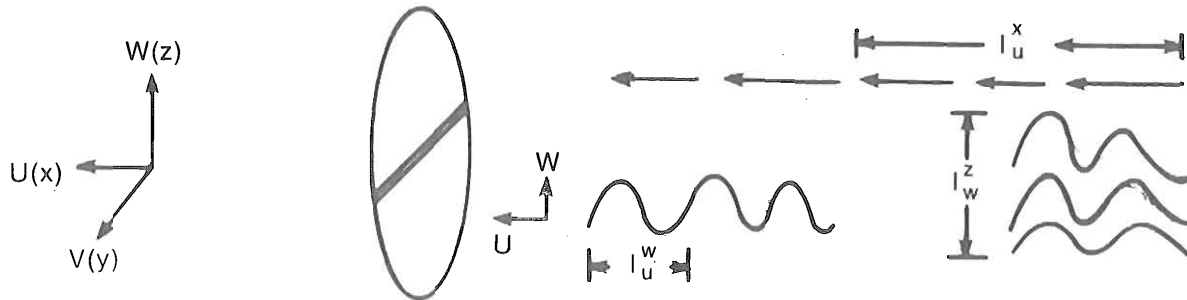


Figure 3-2. Schematic of  $I_u^x$ ,  $I_w^x$ ,  $I_w^z$  Length Scales with Respect to Turbine Rotor

The acoustically significant inflow properties, which need to be determined within a stochastic framework, can now be summarized and include these:

- Axial convection velocity,  $V_c$ , which we will approximate by  $0.8U_H$ , thus making  $U_H$  an inflow parameter
- Upwash velocity turbulence intensity,  $\overline{w'^2}$
- Turbulence integral scale, which we have expanded into three components:  $I_u^x$ ,  $I_w^x$ , and  $I_w^z$ , by treating the problem two-dimensionally
- Local atmospheric state (barometric pressure, temperature), which is used to calculate the air density,  $\rho_0$ , and acoustic velocity,  $a_0$ .

The remainder of the scaling parameters in Eq. (3-6) are fixed for the MOD-2 design and include the

- Rotor rotational frequency,  $\Omega$
- Number of blades,  $B$
- Rotor tip radius,  $R_t$  or  $D/2$
- Blade span,  $b$
- Blade chord,  $c_0$ , at effective radius  $R_0$  (typically taken as  $0.75R_t$ )
- Airfoil shape of the rotor blades.

Furthermore, a reference distance,  $r$ , and its relationship to the rotor disk must be chosen. We have decided to use the upwind, on-axis station located  $1.5D$  ahead of the rotor disk or at an angle of  $24^\circ$  with respect to the turbine hub height as this reference point. It also allows this measuring station to

"see" thrust and torque components of the acoustic radiation. This location is also useful in verifying the predictive methods of Homicz and George by avoiding the complications associated with modeling the conditions in the vicinity of the rotor plane.

### 3.2 Determining the Vertical Distributions of $U_H$ , $I_i^j$ , and $\overline{w'^2}$

In the lower portion of the earth's atmospheric boundary layer (usually referred to as the surface layer),  $U_H$ ,  $I_i^j$ , and  $\overline{w'^2}$  are all functions of height,  $z$ . The rotor blades of large, horizontal-axis wind turbines, such as the MOD-2, traverse deep vertical layers perhaps exceeding the height of the surface or constant flux layer (see Section 3.2.1) a percentage of the time. The existence of strong vertical shearing and layering associated with this layer, particularly under stable flow conditions, makes the specification of acoustically significant parameters essentially impossible except for some well-defined reference atmosphere. What is needed are characteristic or scaling parameters, which by physical processes are efficient predictors of the statistical distribution of the vertical or upwash velocity,  $w'$ , spectrum (or, more generally, the three-dimensional spectrum) and the horizontal wind velocity  $U_H$  across the vertical depth of the turbine's rotor disk. Such scaling is discussed below.

#### 3.2.1 Surface Layer Similarity Scaling

It is known that, within a locally homogeneous and quasi-steady surface layer, the vertical fluxes of heat, momentum, and moisture are essentially constant. Ideally, under such conditions, the turbulent structure should be related to only a few parameters. Monin and Obukov [13,14] proposed that turbulent motions in the homogeneous surface layer scaled with the height  $z$  above the surface, the local buoyancy,  $g/\theta$ , the kinematic surface stress  $\tau_s/\rho_0$  (where  $\tau_s$  is the surface stress), and the surface kinematic heat flux  $Q_0 = H_0/\rho_0 c$ . By combining these parameters, they defined a series of surface-layer scaling factors (known as similarity or M-O scaling), including a velocity scale,  $u_*$  (the friction velocity; see Section 2.4.2.1); a temperature scale,  $T_* = -Q_0/u_*$ ; the M-O length,  $L$  (defined in Section 2.4.2.1); and the geometric height,  $z$ .

When surface layer flow properties are appropriately nondimensionalized (velocities by  $u_*$ , temperatures by  $T_*$ , etc.), M-O theory has shown that they become universal functions of  $z/L$ . It is generally accepted that the "universal function" aspect of M-O similarity applies in surface layers over homogeneous terrain [15]. In the real world, and that includes most wind plant sites, there is often a departure from strict M-O theory as a result of such influences as nonsteady boundary conditions, complex terrain features, local radiative effects, or inhomogeneous flow conditions due to upstream (fetch) effects. These "departures" usually have the effect of changing "universal functions" into site-specific ones.

### 3.2.2 The Vertical Distribution of $U_H$ ( $V_c$ )

Because of the effects of surface friction, the horizontal wind vector increases with height at least part of the way in the surface layer. Under neutral stability conditions ( $Ri = z/L = 0$ ), and over homogeneous terrain, this vertical profile of  $U_H$  can be represented by the familiar log profile, or

$$U_H(z) = (u_* / k_a) \cdot \ln(z/z_0) , \quad (3-7)$$

where  $z_0$  is the roughness length defined in Section 2.4.2.1. Equation (3-7) is modified for non-neutral surface layers by the diabatic wind profile [8], or

$$U_H(z) = (u_* / k_a) \cdot [\ln(z/z_0) - \psi_m(z/L)]$$

where

$$\zeta_m(z/L) = \int_{z_0/L}^{z/L} [1 - \gamma_m(\zeta)] \frac{d\zeta}{\zeta} \quad (3-8)$$

and

$$\zeta_m(z/L) = [(1 - 16(z/L))^{1/4}] .$$

The important point here is the influence of the M-0 scaling parameters  $u_*$ ,  $L$ , and  $z$  on the value of  $U_H$ , or equivalently  $V_c$ , as a function of height within the turbine's rotor disk. If the conditions of true M-0 scaling are met,  $u_*$  and  $L$  are not functions of  $z$ . Thus, we may think of these parameters as potential candidates for predictors of turbine acoustic emissions characteristics.

### 3.2.3 Variation of $w'$ Spectra with Height

If M-0 scaling is applicable, Panofsky and Dutton [9] show the vertical variation of  $w'$  spectra,  $S_w(f, z)$ , is of the form

$$nS_w(n, z) / u_*^2 = F(nz/U_H(z), z/L) = F(f(z), z/L) , \quad (3-9)$$

where  $n$  is the cyclic frequency and  $f$  is the reduced or normalized frequency given by  $f(z) = nz/U_H(z)$ . The relationship defined in Eq. (3-9) has a different form for unstable/neutral and stable environments. For stable conditions, Panofsky and Dutton recommend the equation developed by Kaimal [16]:

$$nS_w(n, z) / u_*^2 = [4.6(P_w / u_*^2) / f / f_m] / [1 + 1.5(f/f_m)]^{5/3} , \quad (3-10)$$

where  $P_w / u_*^2$  is the maximum of  $S_w(f, z)$  at  $f_m = f$  and is a function of  $z/L$ . For unstable and neutral conditions, they recommend the Hojstrup [18] model, or

$$\frac{nS_w(n, z)}{u_*^2} = \frac{32f}{(1+17f)^{5/3}} \left(\frac{z}{-L}\right)^{2/3} + \frac{2f}{(1 + 5.3f)^{5/3}} \quad (3-11)$$

Assuming M-0 similarity holds, Eqs. (3-9), (3-10), and (3-11) demonstrate the statistical dependency of the upwash velocity spectra on the  $U_H(z)$ ,  $u_*$ , and  $z/L$  scale lengths characteristic of the flow. Since the M-0 length,  $L$ , can be estimated from a knowledge of the Richardson number (see Section 2.4.2.1), the  $Ri$  could be substituted for  $L$ .

In addition to the M-O similarity theory scale lengths discussed above, it is also possible to empirically determine characteristic length scales of the inflow itself. These scale lengths, called integral scales, are defined by

$$I_{ij} = \overline{u_i} \int_0^{\infty} R_{ij}(\tau) d\tau, \quad (3-12)$$

where  $u_i = [u, v, w]$  and  $j = [x, y, z]$ , but since

$$R_{ij}(\tau) = \int_{-\infty}^{\infty} S_{ij}(f) e^{-i2\pi f\tau} df, \quad (3-13)$$

$I_{ij}$  contains information about  $S_{ij}(f)$  and should also be related to the M-O scales. The measured  $I_{ij}$  scales contain information about the spectral content of the flow, even if it does not strictly follow M-O similarity.

From the above, it is clear that one would expect  $S_w(f, z_1)$  to have some relationship with  $S_w(f, z_2)$ , with  $z_1 = z_2$ , since both  $S_w(f)$  and  $U_H$  scale with height in the surface layer while  $u_x$  and  $L$  do not. Thus, it seems plausible that detailed spectral measurements made at a given height within the rotor disk layer should be at least statistically related to those at other heights if the scaling laws apply. Since we do not have the ability to gather direct measurements of the upwash or  $w'$  spectra throughout the entire disk, we have chosen to establish a reference to measure the actual flow scale lengths related to it as well as the normal M-O scaling parameters. These parameters include the following:

- o Mean reference or hub-height wind speed,  $U_H$
- o Rotor disk gradient Richardson number,  $Ri$
- o Longitudinal (axial) velocity component length scale,  $I_u^x$
- o Vertical (upwash) velocity component length scale along the axial (x) direction,  $I_w^x$
- o Vertical component length scale parallel to the rotor plane  $I_w^z$ .

Thus, the parameters above provide scales for  $V_c$  ( $1.25U_H$ ), the surface layer vertical stability ( $Ri$  and/or  $z/L$ ), and characteristic flow scale lengths related to  $S_w(f)$ .

### 3.3 Inflow Data Statistical Summaries

As previously stated, no detailed, high-frequency turbulence measurements were taken during the 1982 experiment. This has limited our ability to establish adequate correlations with the MOD-2 acoustic emissions spectra for that experimental period. However, since the current MOD-2 configuration is the one in use during the 1983 series, we believe it is the more important. We have summarized below what information was available for the 1982 data runs. A reduced 1982 data set was selected based on available inflow properties whose values fell within the observed ranges of the same parameters in 1983. This was done to try to establish a common inflow basis for year-to-year comparisons.

A comparison of the 1982 and 1983 overall inflow statistics are given in Table 3-1. While lower wind speeds were, on the average, encountered during 1983, Table 3-1 shows that these data runs were made in conditions that were, on the average, more stable and more turbulent than the 12 runs made in April-May 1982. Table 3-2 lists the reduced data set summary statistics for 1982 and 1983, with its closely overlapping parameter ranges. Missing from Table 3-2, of course, are the measured characteristic scale lengths of the inflow.

Tables 3-3a, b, and c summarize the detailed inflow data for the six 1983 data runs used for the low-frequency-range analysis in Section 5.0. Table 3-3a lists the air motions data from three measuring heights on the BPA tower. The two-axis, hot-film anemometer was installed at the 45-m level, from which the high-frequency turbulence statistics were gathered. Eight runs were made in 1983, but one was lost to a failure in the recorder collecting the hot-film data. The other run was lost when the wind direction moved out of the desired 40° cone for the operation of the two-axis, hot-film anemometer. The inflow characteristic scaling parameters are listed in Table 3-3b; the air motions data were derived largely from the BPA tower but the stability information came from the PNL tower. Table 3-3c summarizes the longitudinal and vertical component spectral scaling parameters  $P_u/u_*^2$  and  $P_w/u_*^2$  discussed in Section 3.2.3 as well as the Brunt-Väisälä period  $T_{BV}$ . The peak mean wind speeds and heights listed in Table 3-3c were determined by vertically smoothing the five speeds available from the PNL tower.

**Table 3-1. Comparison of 1982 and 1983 Inflow Statistics from the BPA Meteorological Tower**

Parameter	1982	1983
Total number of data runs	12	8
59-m mean wind speed, mps	11.4	9.5
59-m mean wind speed variance, (mps) <sup>2</sup>	1.51	1.75
59-m mean turbulence intensity, %	10.8	13.9
Mean Richardson number (PNL tower)	0.30	2.36
Peak 59-m 10-min mean wind speed, mps	14.5	13.6
Minimum 59-m 10-min mean wind speed, mps	7.5	6.9

**Table 3-2. Summary BPA Tower Statistics of Reduced 1982/1983 Data Sets**

Parameter	1982	1983
Number of data runs	6	4
59-m mean wind speed, mps	9.85	9.58
59-m mean wind speed variance, (mps) <sup>2</sup>	1.15	0.99
59-m mean turbulence intensity, %	10.9	10.4
Mean Richardson number	0.25	0.34
Mean M-O z/L parameter	2.86	3.02

**Table 3-3a. 1983 Mean Inflow Characteristics Summary from BPA Tower:  
Wind Speeds**

Data Run	59-m Wind Direction (deg)	59-m $U_H$ (mps)	59-m $(U_H')^{1/2}$ (mps)	45-m $u$ (mps)	45-m $(u')^{1/2}$ (mps)	45-m $(w')^{1/2}$ (mps)	60-m $w$ (mps)
A05	268	7.3	1.02	8.7	1.13	0.16	0.52
A03	261	8.1	1.03	9.0	1.32	0.19	0.76
A14-1	261	9.2	1.31	9.6	1.30	0.19	0.95
A14-2	256	9.9	1.10	10.5	1.37	0.15	0.78
A18	254	12.4	0.89	13.9	0.90	0.12	0.99
A11	257	13.6	0.31	14.3	1.10	0.17	0.52
Means	260	10.1	0.94	11.0	1.19	0.16	0.75

**Table 3-3b. 1983 Mean Inflow Characteristics: Characteristic Scaling Parameters**

Data Run	Ri	$z/L$	$u_*$ (mps)	$z_0$ (cm)	$I_u^x$ (m)	$I_w^x$ (m)	$I_w^z$ (m)	$T_u$ (sec)	$T_w$ (sec)
A05	11.7	5.62	.635	56.7	136	125	7.5	15.6	14.4
A03	-0.12	-0.12	.461	5.6	210	157	13.3	23.4	17.5
A14-1	0.13	.334	1.01	11.9	157	166	16.5	16.4	17.3
A14-2	0.26	5.62	0.736	25.6	86.5	81.7	6.1	8.22	7.76
A18	1.25	5.62	0.943	27.4	125	123	8.8	9.02	8.84
A11	6.68	5.62	1.09	46.3	336	86.8	6.8	23.4	6.06
Means	3.32	3.78	.813	28.9	175	123	9.8	16.0	12.0

### 3.4 1983 45-m Inflow Turbulence Spectral Content

The frequency spectra for six analysis runs of the longitudinal and vertical turbulence components measured at the 45-m level on the BPA tower are presented in Figures 3-3 through 3-8. The corresponding Richardson number ( $Ri$ ), mean hub-height wind speed ( $U_{hub}$ ), and longitudinal ( $I_u^x$ ) and vertical ( $I_w^z$ ) integral scale lengths are listed on each plot.

### 3.5 Rotor Disk Inflow Vertical Profiles

It is important to know the vertical distribution of wind speed and turbulence across the MOD-2 rotor disk. Since the height of the BPA tower extended only to hub height, we were left with two other sources of vertical profiles of wind distribution information: the five levels of the PNL tower and SERI's tethered balloon sounding system. The latter was limited, in 1982/83, to wind speeds under about 11 mps. We have used both resources to assemble a picture of the distribution of the horizontal wind with height.

### 3.5.1 PNL Tower Vertical Profiles of Wind Speed and Turbulence Intensity

The vertical resolution (22.9 m or 75 ft) of the PNL tower is limited, but by regression smoothing we can achieve a reasonable estimate of a mean vertical profile. Also, it is clear that these profiles may not exactly agree with the vertical inflow structure into Turbine No. 2 because of the degree of spatial separation. However, they are useful because they track the vertical structure (shape) of the profiles under the range of stability and speeds encountered during the six 1983 data runs. Figures 3-9 through 3-14 plot the smoothed wind speed normalized by the hub-height value and the un-normalized turbulent intensity for each of the six data runs. We should point out that we consider the turbulent intensity plotted here to be the "long wave" contribution due to the lack of response of the cup anemometers at small wavelengths (high frequencies).

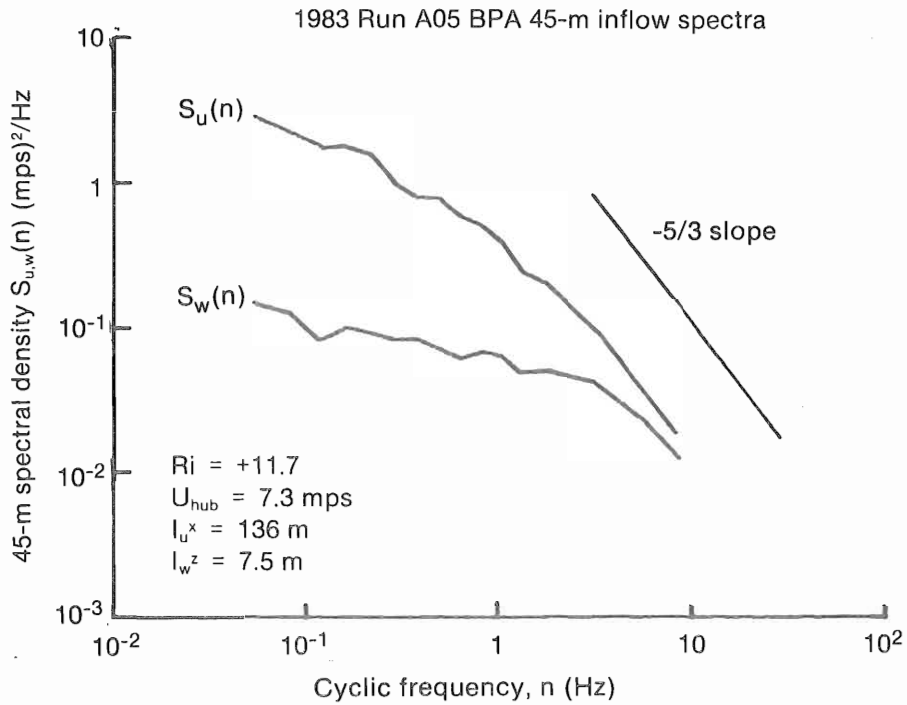
### 3.5.2 Representative Tethered Balloon Profiles in Turbine No. 2 Inflow

A number of 1982 runs were supported by the tethered balloon system but only three were available in 1983 because of equipment problems, high winds, or both. In 1983 the runs that were supported included A03, A03-1, and A05. The 45-m level turbulence data were unavailable from the A03-1 run because of an out-of-tolerance hub wind direction. Figures 3-15 through 3-17 present smoothed, high-resolution vertical profiles of wind direction and speed, sensible temperature, and atmospheric stability taken just before the beginning of Run A05. It is interesting to compare the vertical wind-speed profile measured by the five discrete levels on the PNL tower in Figure 3-14 and the tethered balloon profiles taken in the inflow of Turbine No. 2 in Figure 3-15. A representative sample of a high-resolution inflow turbulence spectrum measured by the hot-film anemometer is plotted in Figure 3-18 for the same run.

Table 3-3c. 1983 Mean Inflow Characteristics: Spectral Scaling and Rotor Disk Layer Parameters

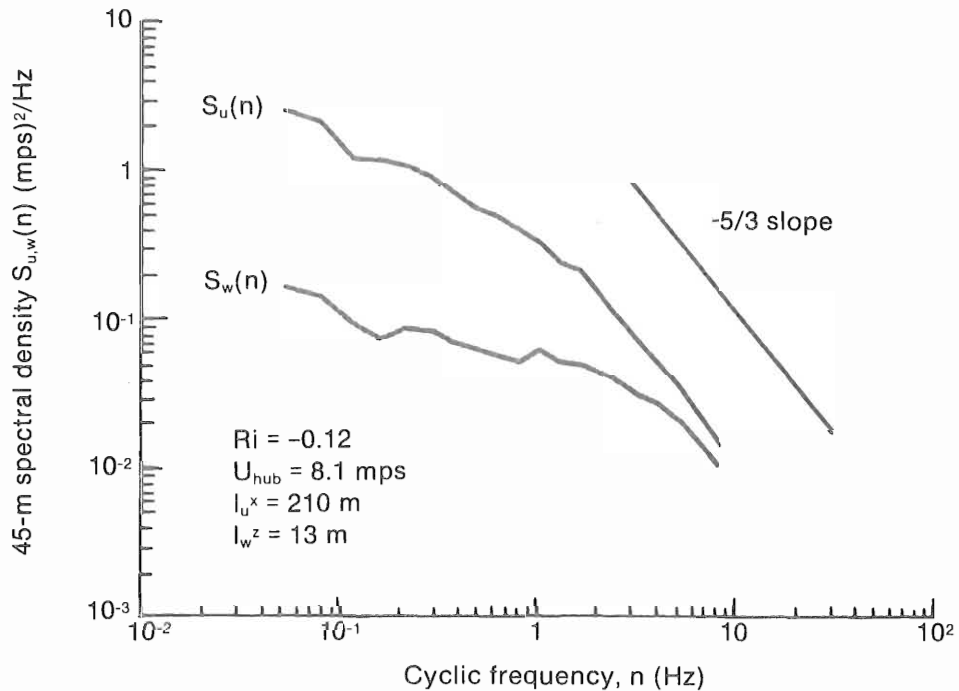
Data Run	$f_{m_u}$	$f_{m_w}$	$P_u/u_*^2$	$P_w/u_*^2$	$T_{BV}$ (sec)	Mean Speed (mps)	Peak Wind <sup>a</sup> Height (m)
A05	.081	.081	0.836	0.038	247	6.8	44.8
A03	.078	.078	0.729	0.162	0	9.0	107
A14-1	.147	.147	0.489	0.061	319	11.5	107
A14-2	.134	.067	0.941	0.050	343	11.3	107
A18	.101	.051	0.324	0.031	234	13.6	97.9
A11	.049	.167	2.43	0.043	177	13.2	68.4
Means	.098	.099	0.958	0.064	264	10.9	88.7

<sup>a</sup>Determined from the PNL tower.



008158

Figure 3-3. BPA Tower 45-m Level Longitudinal (u) and Vertical (w) Inflow Spectra for 1983--Run A05



008159

Figure 3-4. BPA Tower 45-m Level Longitudinal (u) and Vertical (w) Inflow Spectra for 1983--Run A03

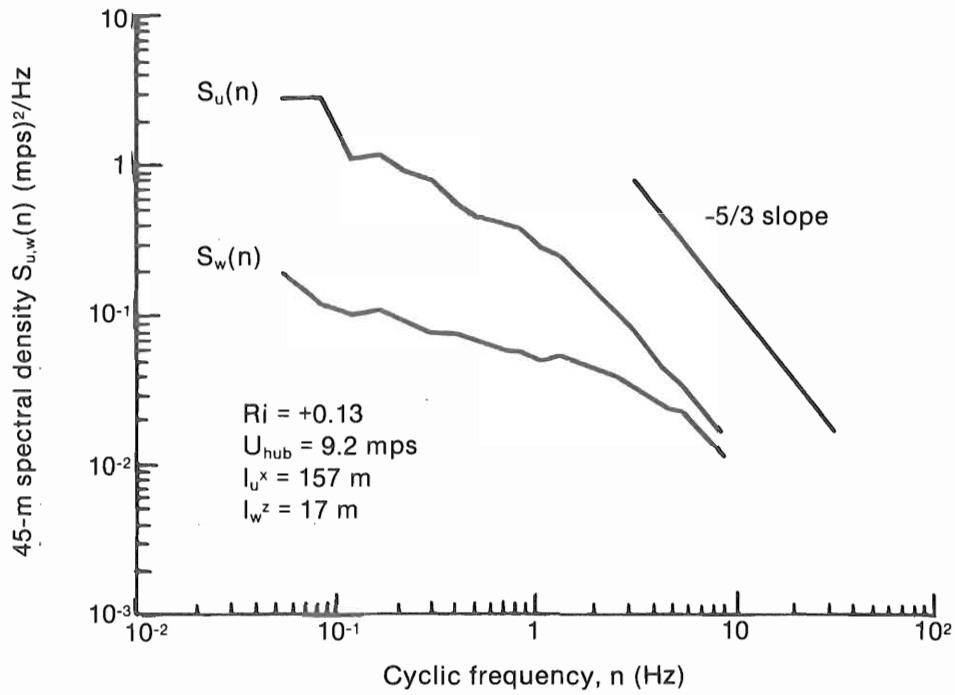


Figure 3-5. BPA Tower 45-m Level Longitudinal (u) and Vertical (w) Inflow Spectra for 1983--Run A14-1

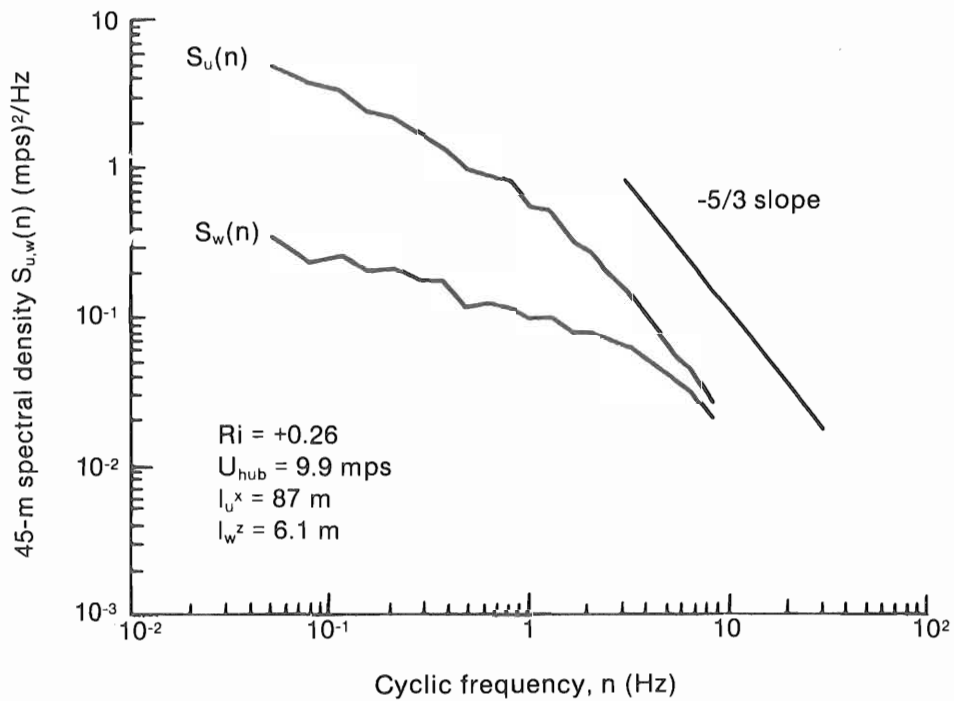
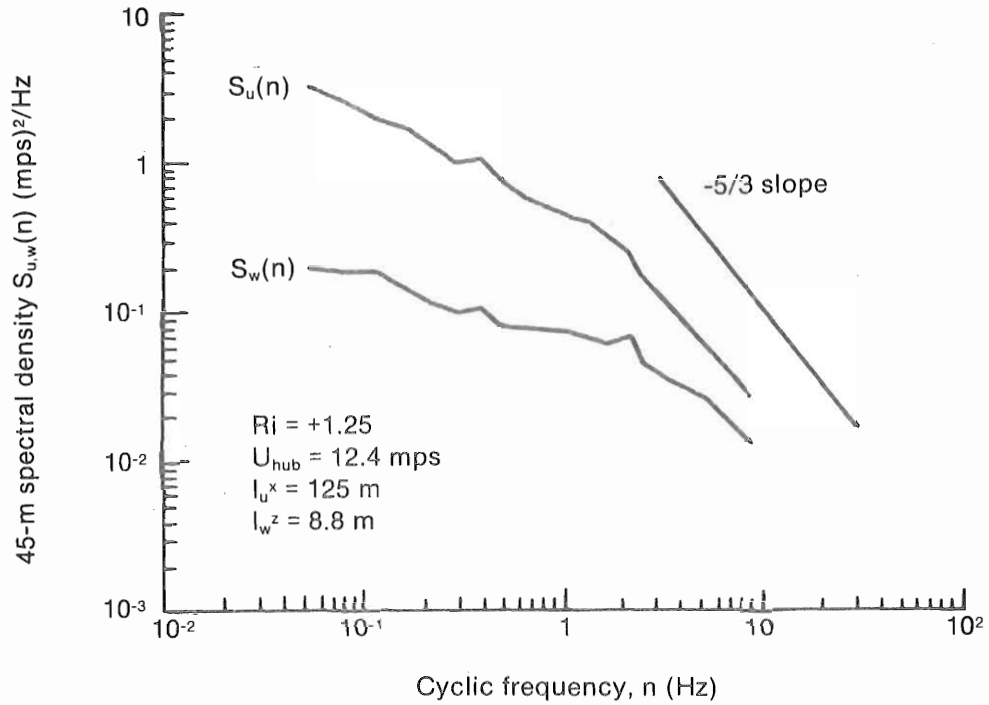
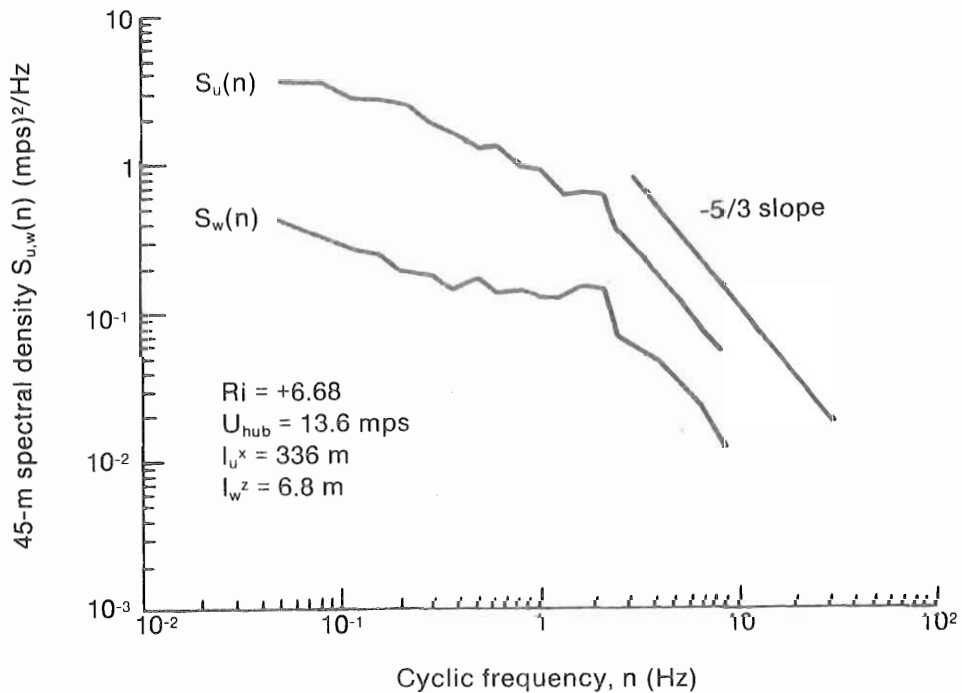


Figure 3-6. BPA Tower 45-m Level Longitudinal (u) and Vertical (w) Inflow Spectra for 1983--Run A14-2



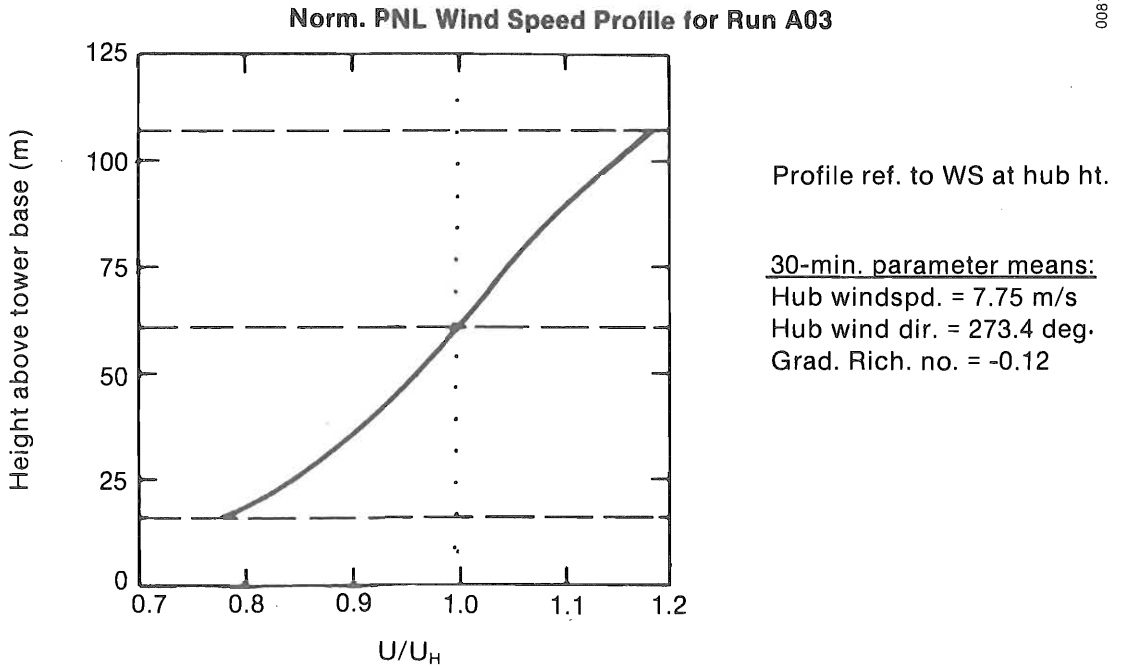
008162

Figure 3-7. BPA Tower 45-m Level Longitudinal (u) and Vertical (w) Inflow Spectra for 1983--Run A18

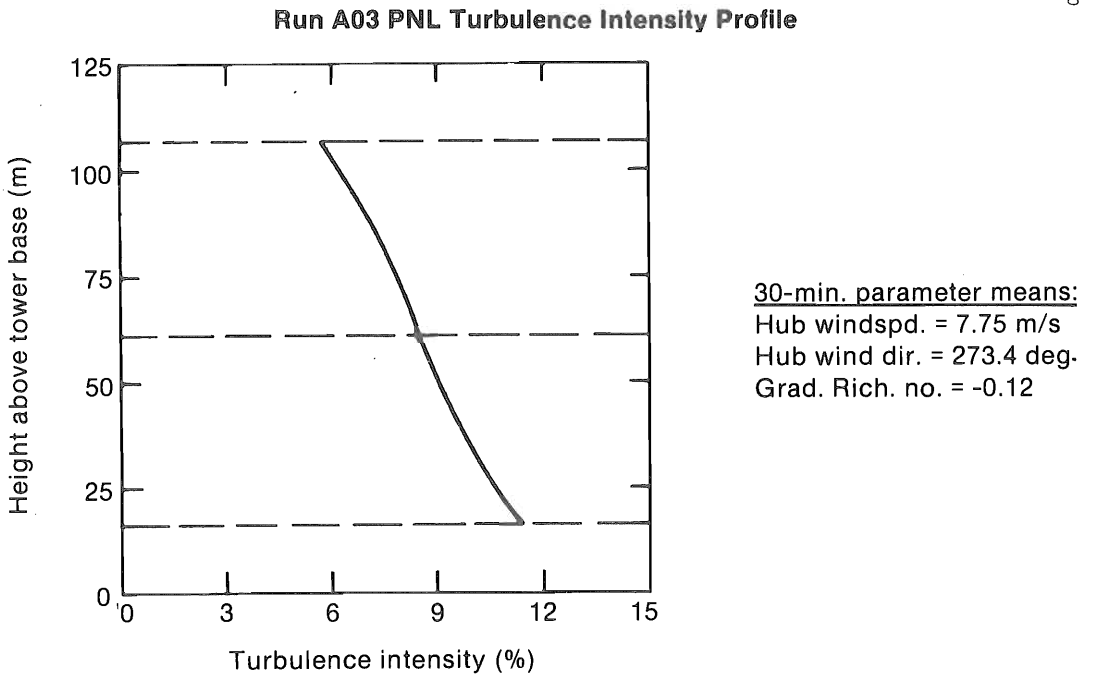


008163

Figure 3-8. BPA Tower 45-m Level Longitudinal (u) and Vertical (w) Inflow Spectra for 1983--Run All

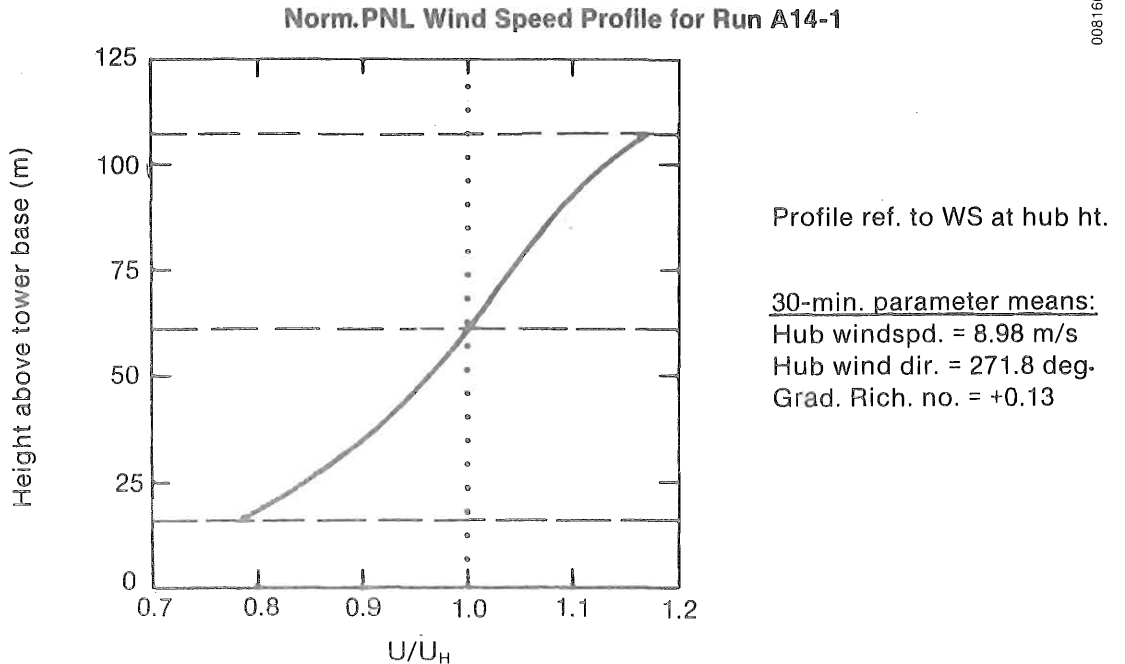


(a)  $U_H$  normalized horizontal wind speed

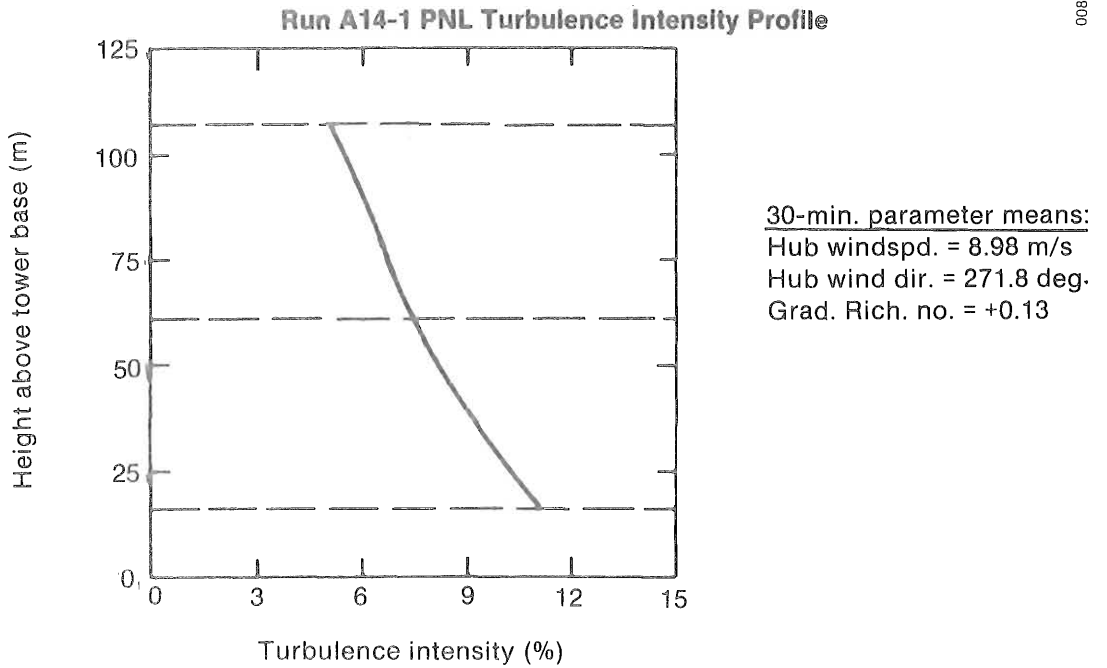


(b) turbulence intensity

Figure 3-9. Smoothed Vertical Profile (PNL Tower) of  $U_{hub}$ -Normalized Horizontal Wind Speed (a) and Turbulence Intensity (b) for 1983--Run A03

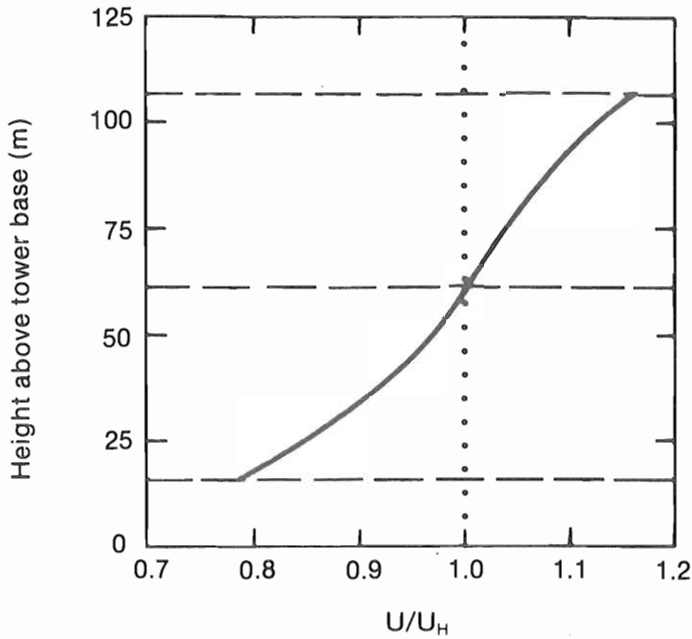


(a)  $U_H$  normalized wind speed



(b) turbulence intensity

Figure 3-10. Smoothed Vertical Profile (PNL Tower) of  $U_{hub}$ -Normalized Horizontal Wind Speed (a) and Turbulence Intensity (b) for 1983--Run A14-1

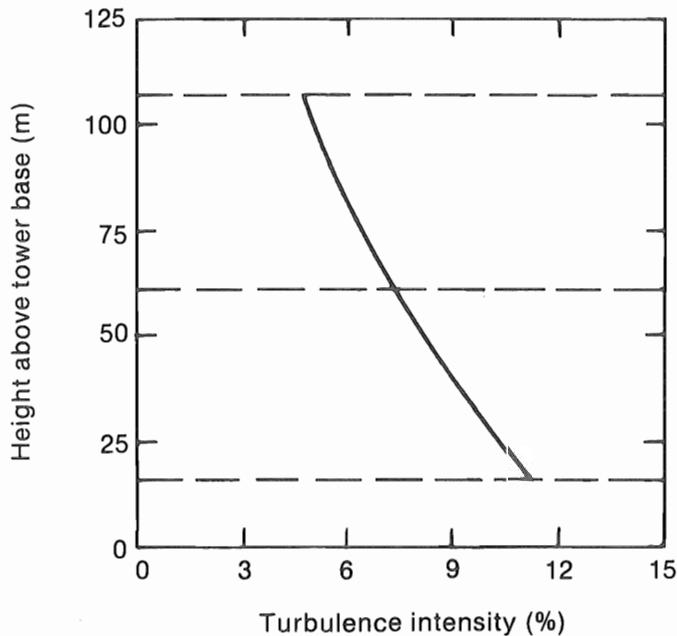


Profile ref. to WS at hub ht.

30-min. parameter means:  
 Hub windspd. = 9.78 m/s  
 Hub wind dir. = 274 deg.  
 Grad. Rich. no. = +0.26

(a)  $U_H$  normalized horizontal wind speed

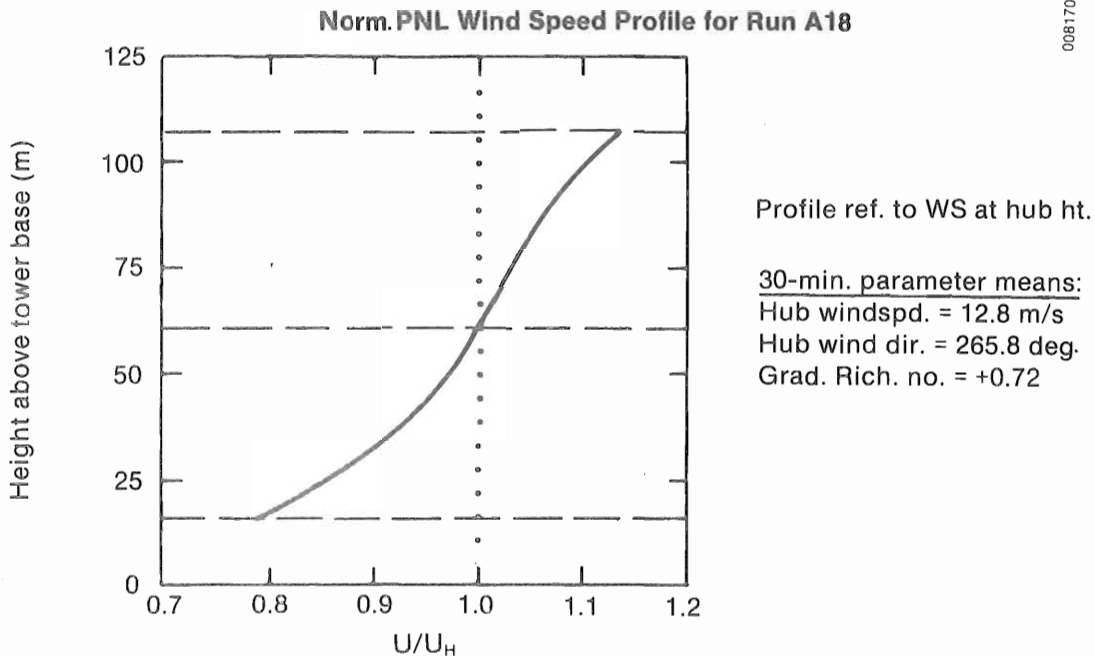
Run A14-2 PNL Turbulence Intensity Profile



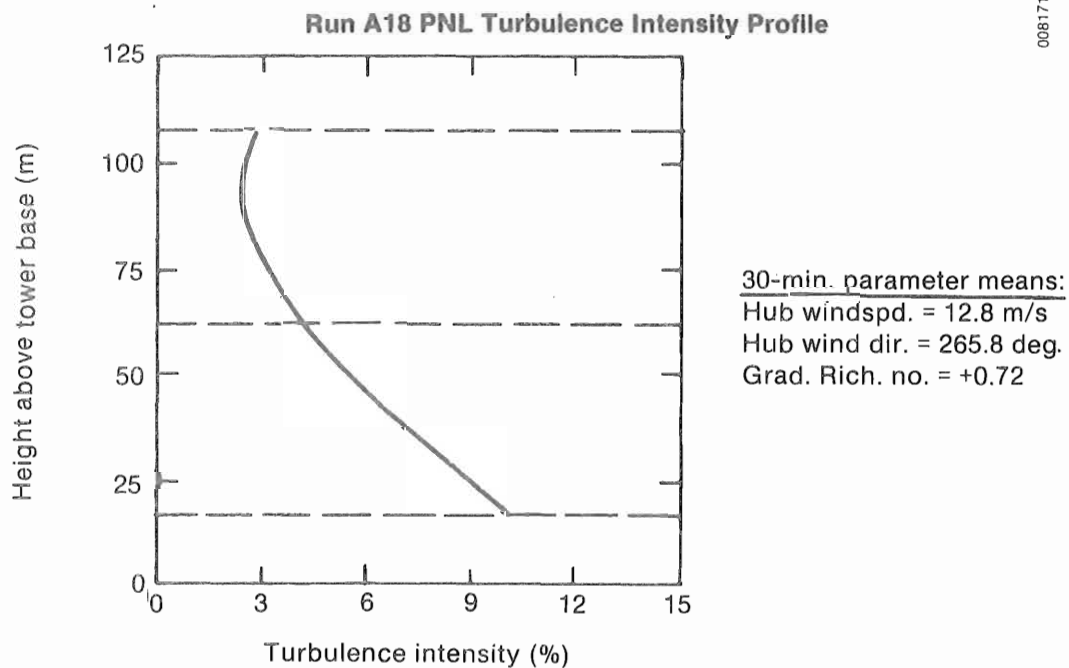
30-min. parameter means:  
 Hub windspd. = 9.78 m/s  
 Hub wind dir. = 274 deg.  
 Grad. Rich. no. = +0.26

(b) turbulence intensity

Figure 3-11. Smoothed Vertical Profile (PNL Tower) of  $U_{hub}$ -Normalized Horizontal Wind Speed (a) and Turbulence Intensity (b) for 1983--Run A14-2

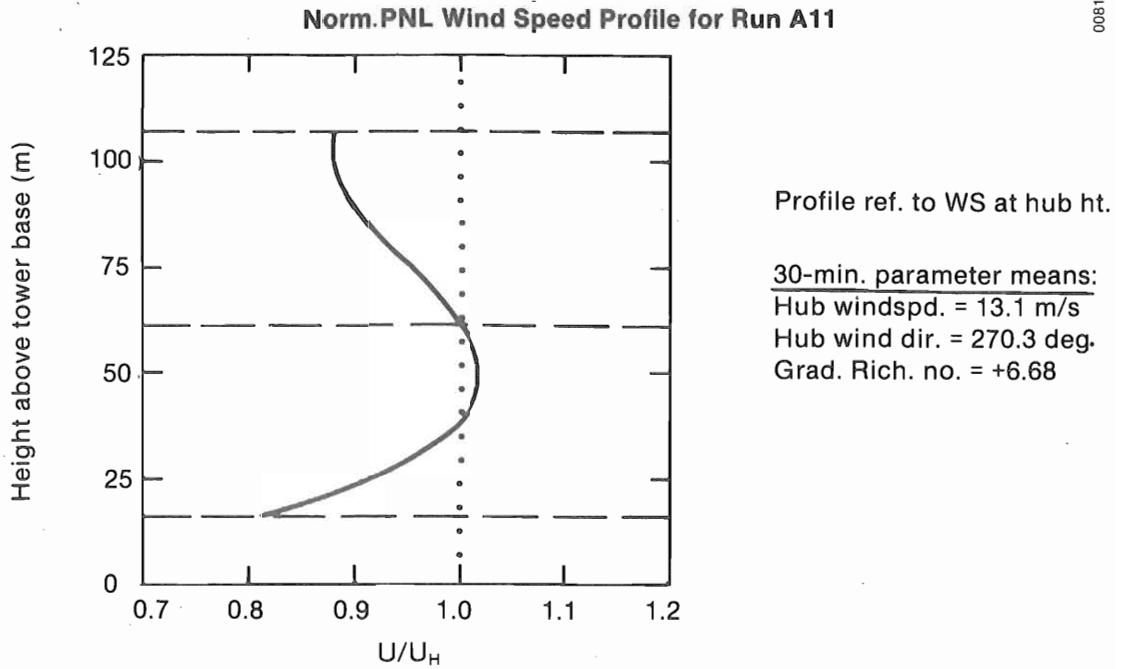


(a)  $U_H$  normalized horizontal wind speed

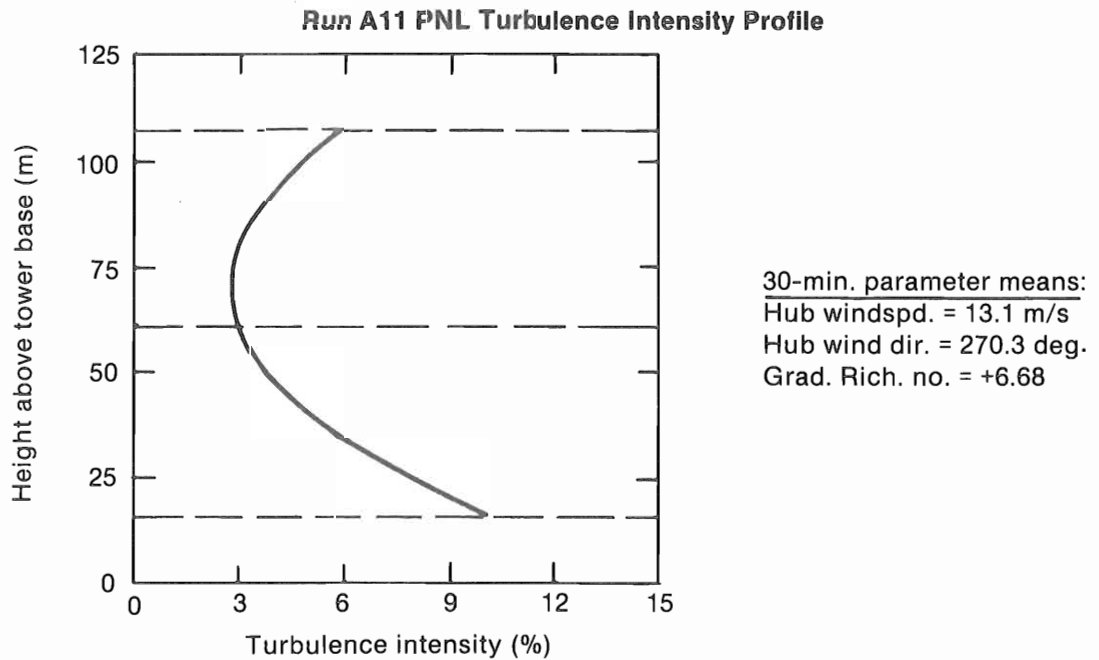


(b) turbulence intensity

Figure 3-12. Smoothed Vertical Profile (PNL Tower) of  $U_{hub}$ -Normalized Horizontal Wind Speed (a) and Turbulence Intensity (b) for 1983--Run A18

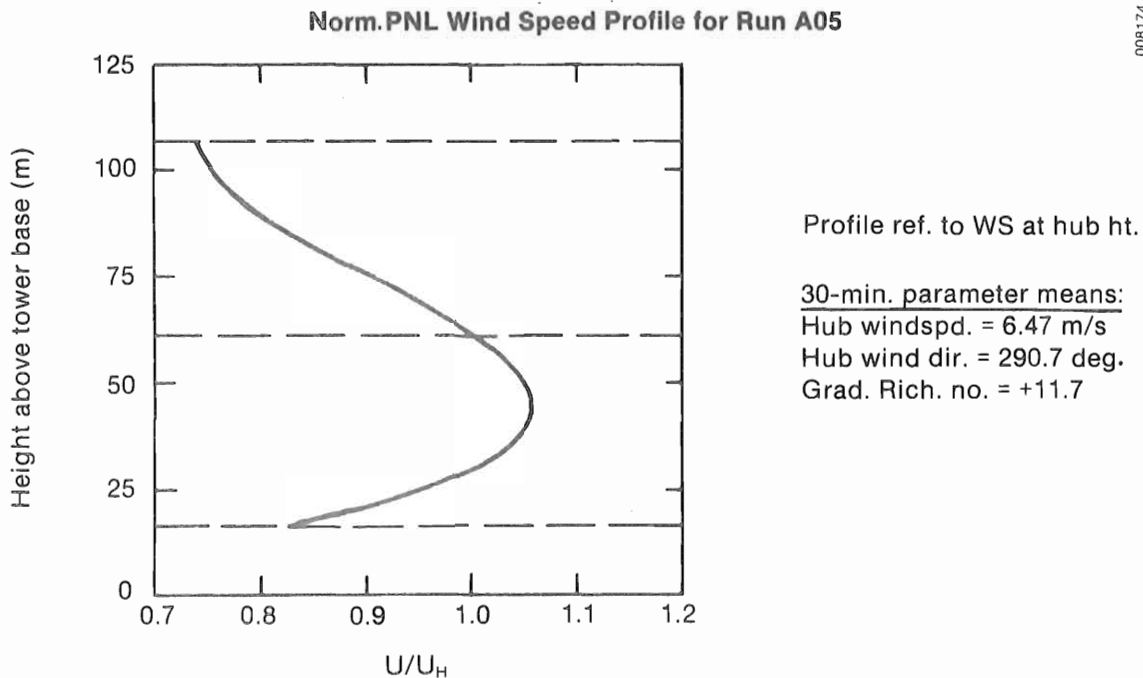


(a)  $U_H$  normalized horizontal wind speed

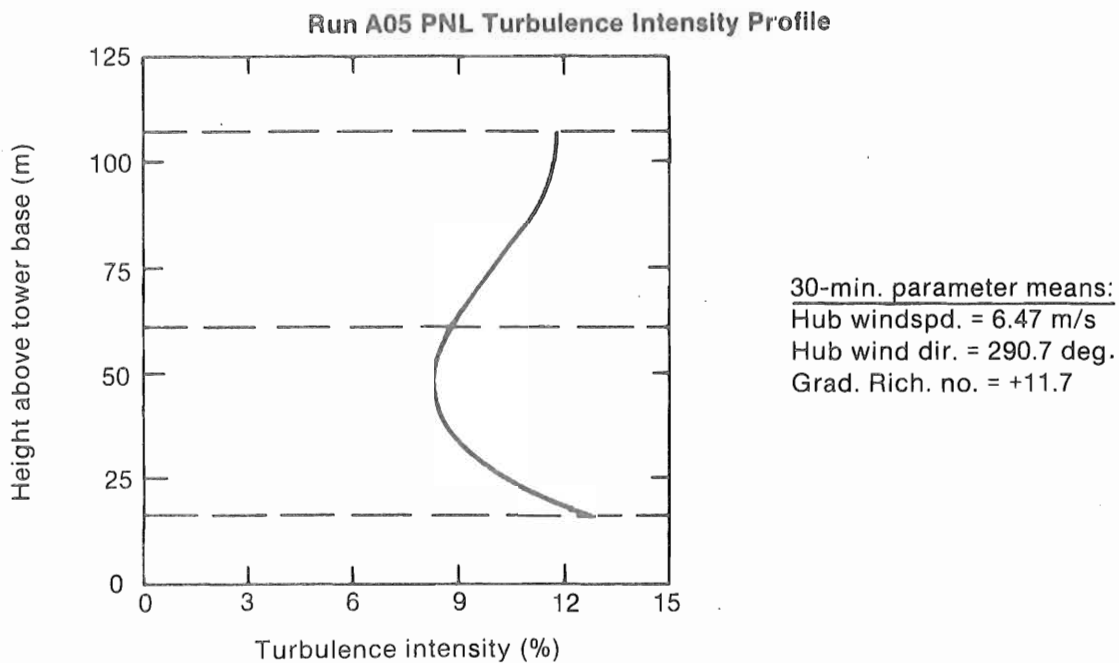


(b) turbulence intensity

Figure 3-13. Smoothed Vertical Profile (PNL Tower) of  $U_{hub}$ -Normalized Horizontal Wind Speed (a) and Turbulence Intensity (b) for 1983--Run A11

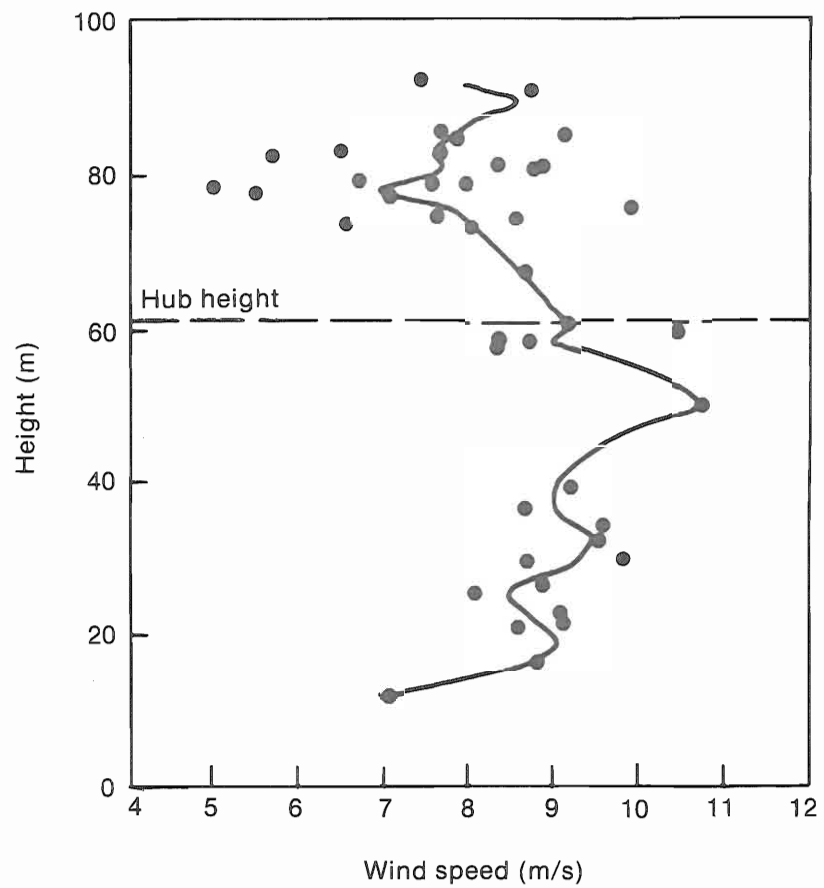
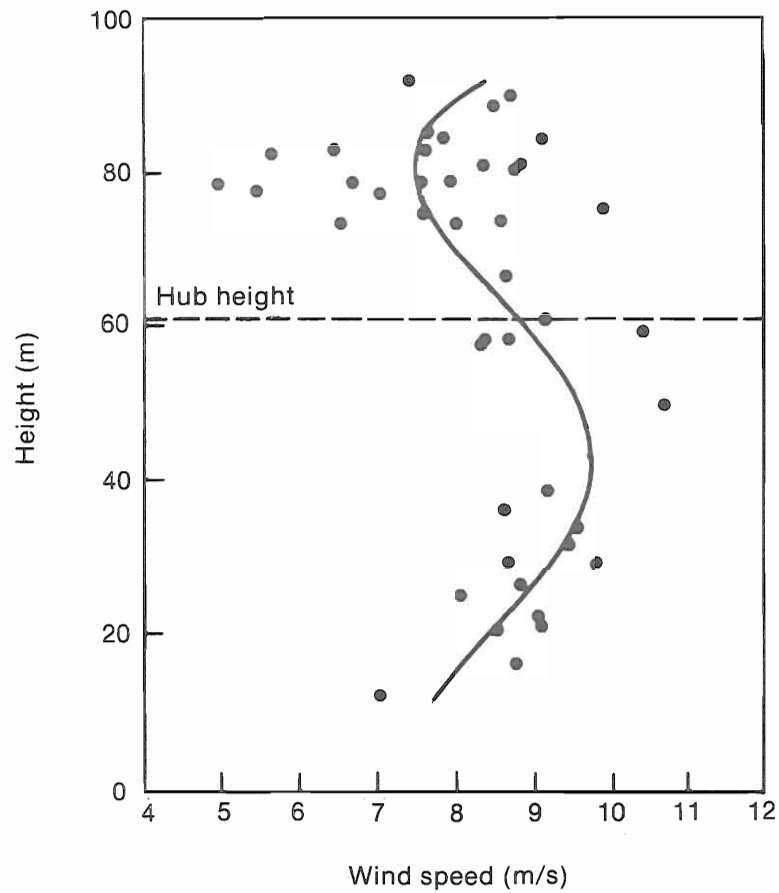


(a)  $U_H$  normalized horizontal wind speed



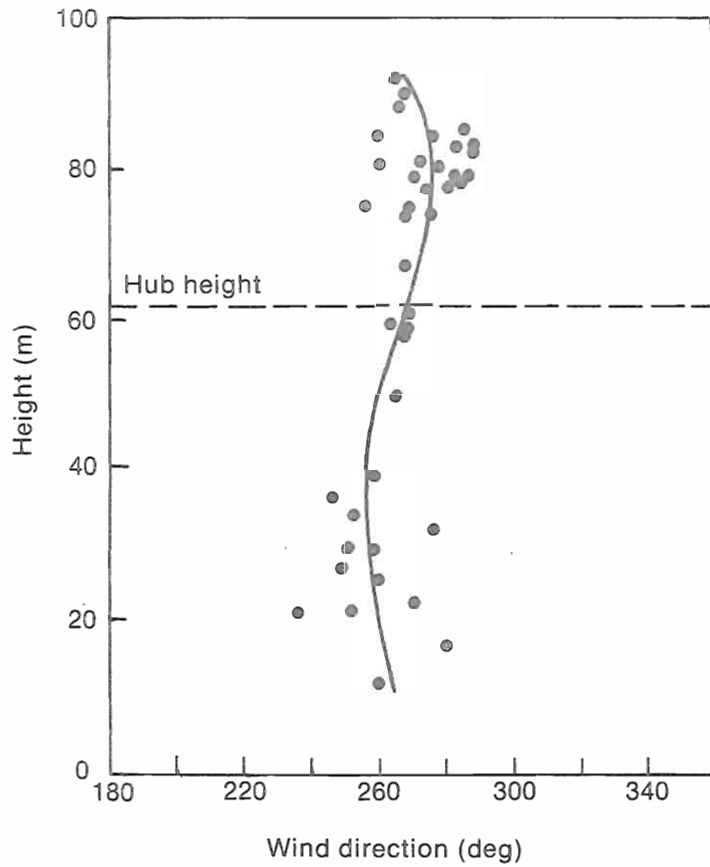
(b) turbulence intensity

Figure 3-14. Smoothed Vertical Profile (PNL Tower) of  $U_{hub}$ -Normalized Horizontal Wind Speed (a) and Turbulence Intensity (b) for 1983--Run A05

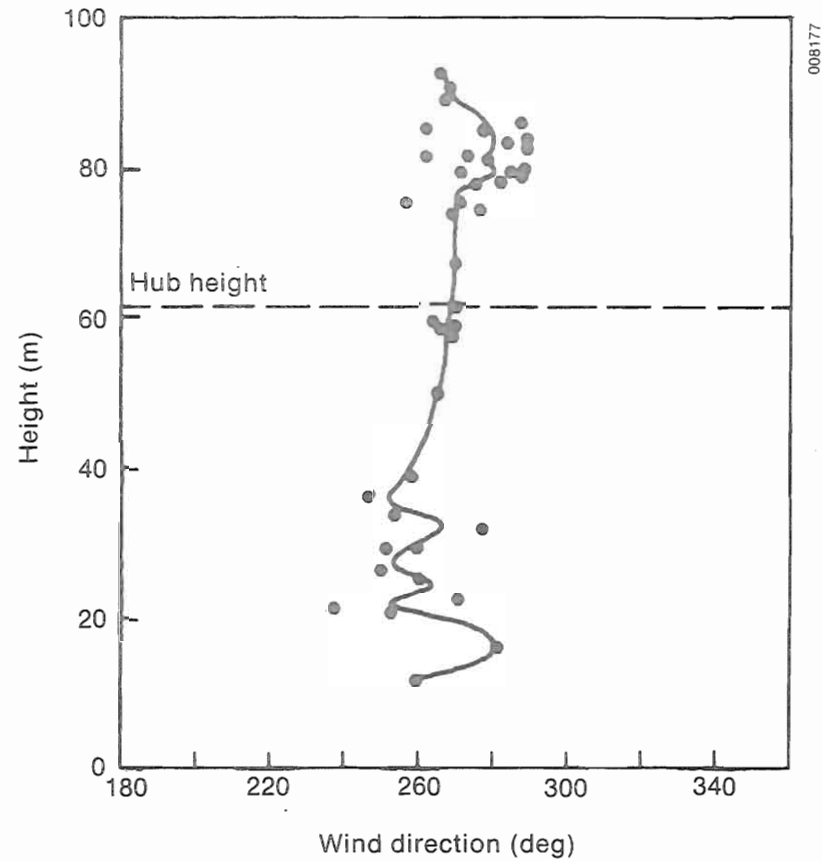


006176

Figure 3-15. Smoothed and High-Resolution Vertical Profiles of Wind Speed for Run A05

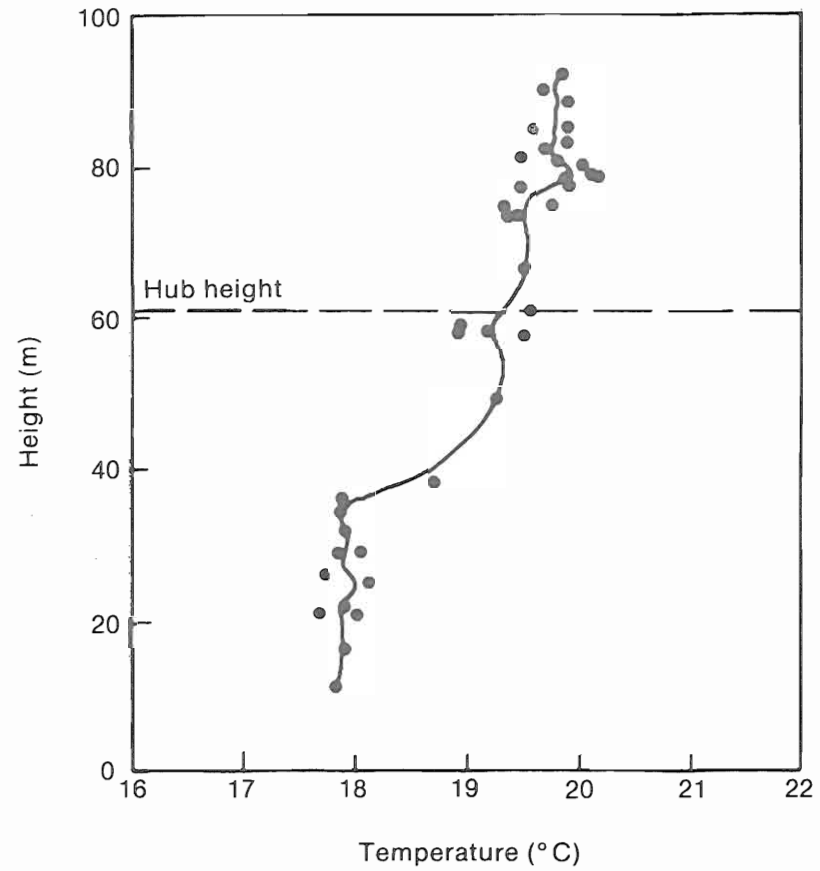
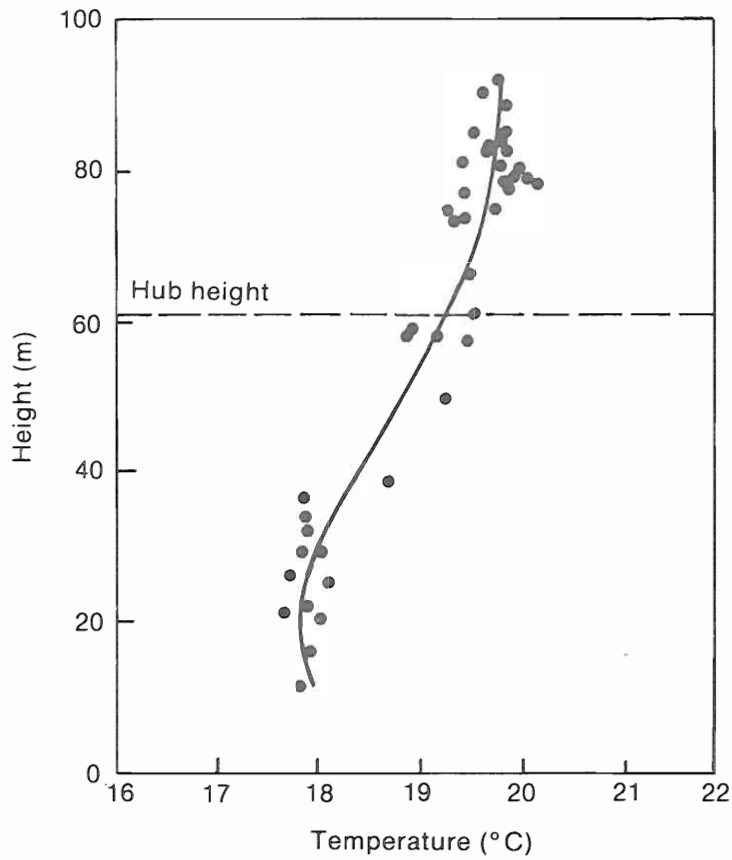


(a) Smoothed profile



(b) High-resolution vertical profile

Figure 3-16. Smoothed and High-Resolution Vertical Profiles for Wind Direction for Run A05



008176

Figure 3-17. Smoothed and High-Resolution Vertical Profiles of Sensible Temperature for Run A05

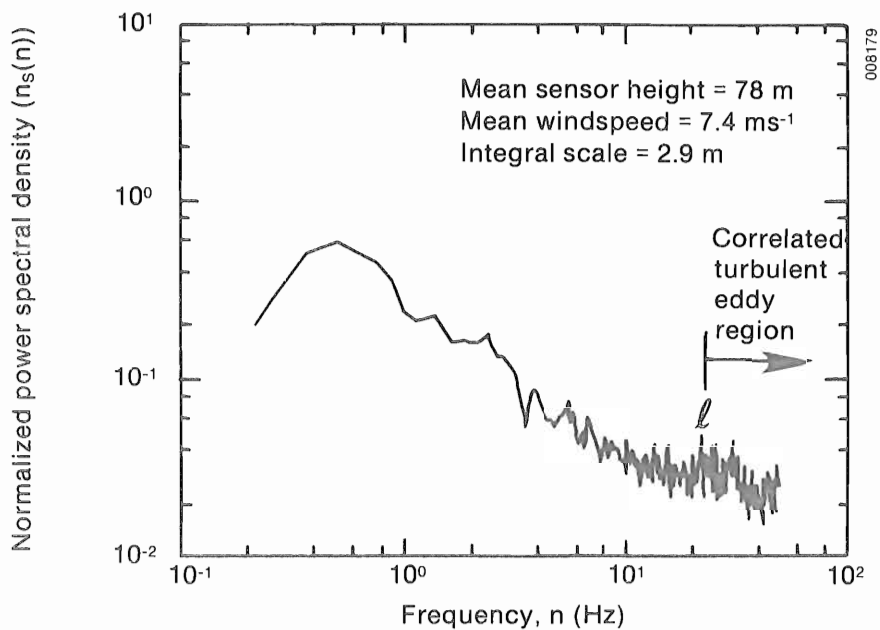


Figure 3-18. Narrowband Longitudinal Turbulence Spectrum Measured at 78-m ( $\pm 6$  m) Height for Run A05

#### 4.0 CHARACTERISTICS OF MOD-2 HIGH-FREQUENCY-RANGE EMISSIONS

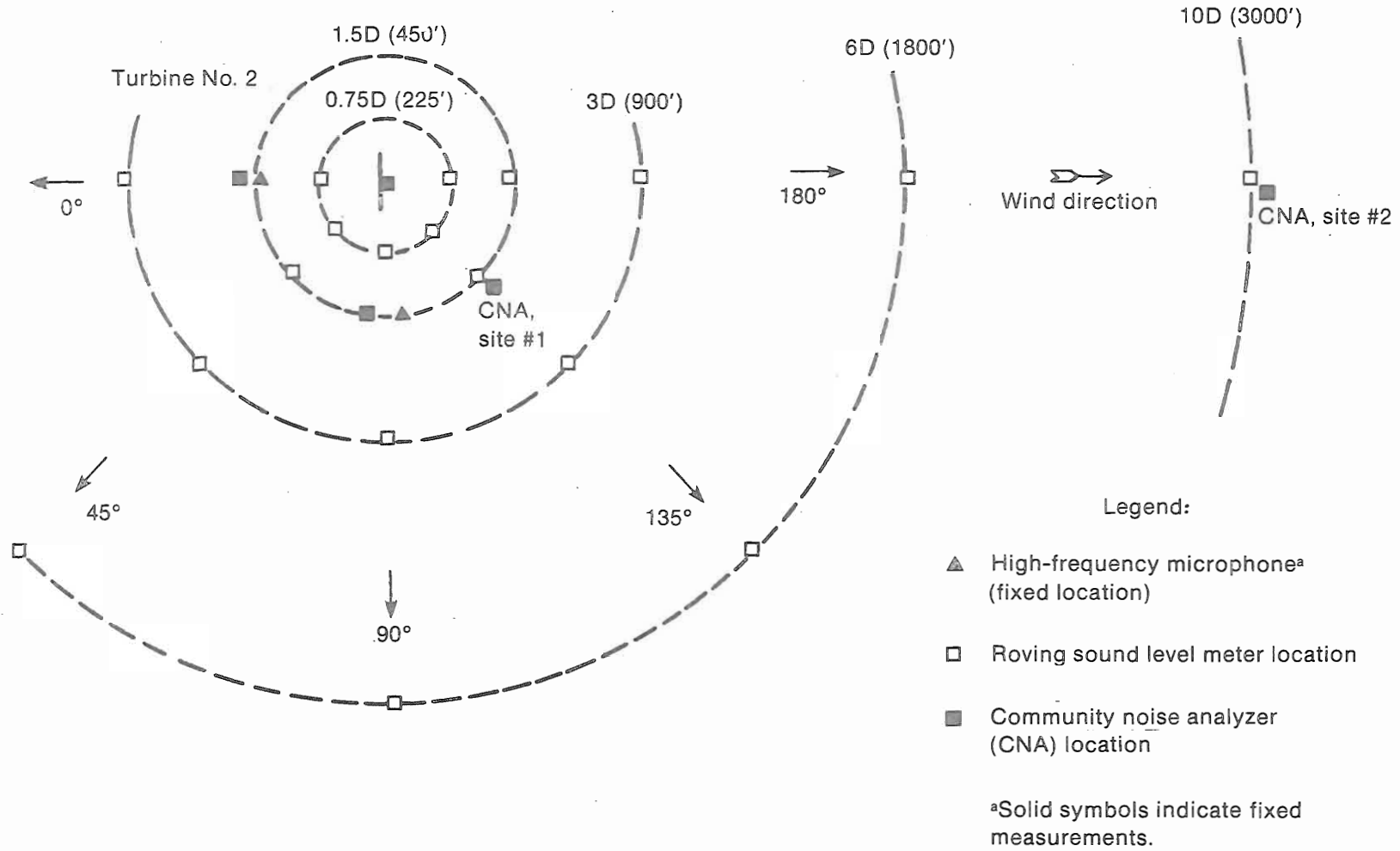
This section summarizes the characteristics of the high-frequency-range (HF) MOD-2 emissions found during both the 1982 and 1983 experiments. The bulk of the data presented reflects measurements made during the 1982 period. As previously stated, the objectives of the 1983 experiment were much more limited and focused on low-frequency-range (LF) emissions. Since an analysis of the 1982 data indicated a relatively small run-to-run variation in emission levels, no additional HF data were initially planned for the 1983 period. During the end of this experimental period, an on-axis HF measurement was added, however. The characteristics of the MOD-2 HF emissions include an estimate of the rotor (source) directivity, temporal statistics of the A-weighted emissions at various downwind distances for both single and multiple turbine operation, and a limited correlation of HF levels with various inflow regimes.

##### 4.1 Observed Directivity Pattern

A survey to estimate the rotor HF radiation pattern was accomplished during the 1982 experimental period. A grid of markers was surveyed from the east to the southwest of Turbine No. 2, as shown in Figure 4-1. Stakes were placed at a minimum range of 0.75D (69 m or 225 ft) to a maximum of 10D (915 m or 3000 ft). On the evening of May 13, 1982, between the hours of 1900 and 2100 (local time), a hand-held precision sound level meter was carried to each marker position as rapidly as practical and a 2-minute average value of the A-weighted sound pressure levels (SPL) was obtained. This period of the day was chosen because it was observed that local propagation effects (e.g., extensive refractive focusing) were at a relative minimum during these hours. The resulting A-weighted SPL directivity pattern is plotted in Figure 4-2 with the readings taken east and south of the turbine reflected to the north and west to form the symmetrical pattern shown. The shape of the contours in Figure 4-2 appears to resemble a classic quadrupole radiation pattern distorted by the prevailing wind at larger distances, i.e., extended downwind and contracted upwind of the rotor plane.

##### 4.2 Statistical A-Weighted Emission Distributions

Important considerations in the future siting of turbines the size of the MOD-2 are the fall-off of the noise with distance and the temporal characteristics of the A-weighted SPL (a measure of loudness). It has been recognized that the A-weighted noise level received is a random variable because of the random nature of the turbulence driving many aeroacoustic mechanisms [10] and the modulation by atmospheric refraction between source and receiver. In order to achieve a measure of both of these MOD-2 HF noise qualities at the Goodnoe Hills site, two community noise analyzers (CNA) were used at various positions downwind of the turbine rotor plane(s). The CNA consists of an integral measurement-quality microphone, a preamplifier, and a specialized computer that continuously calculates the statistical cumulative distribution of the A-weighted SPL over three contiguous preset collection periods ranging from 30 minutes to several hours. Data were collected from the CNAs for both single and multiple turbine operation.



008180



Figure 4-1. Microphone Locations Used in High-Frequency-Range Measurements

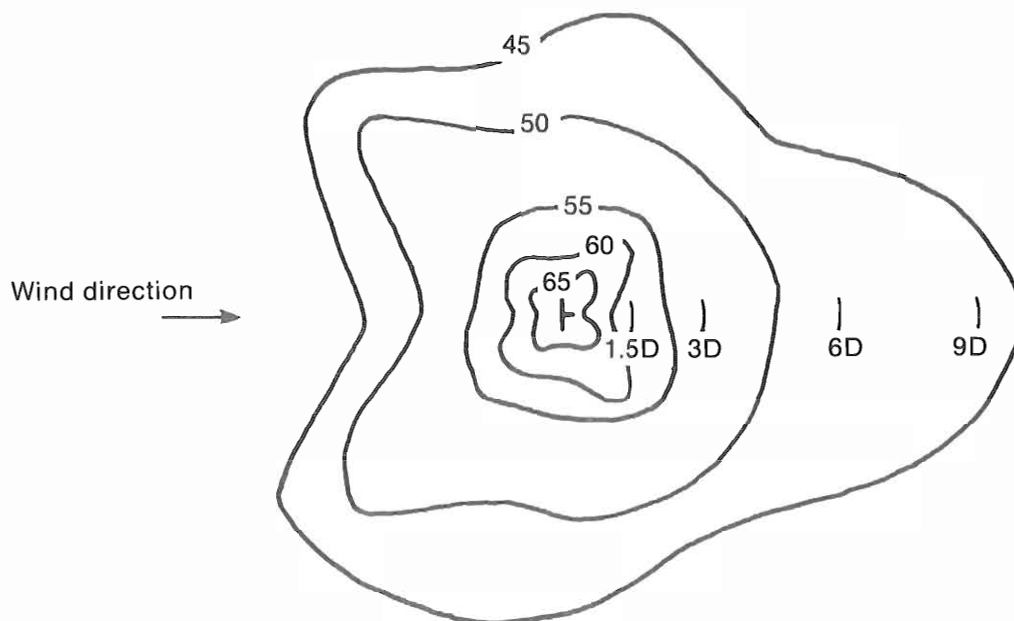


Figure 4-2. A-Weighted Sound Pressure Level Directivity Pattern for a Single MOD-W Turbine. Levels shown are in dB(A).

#### 4.2.1 Single Turbine Operation

For the single turbine evaluation, CNA data were collected from two locations (shown in Figure 4-1). One location was at the geometric center of the three-turbine cluster 1.75D (160 m or 525 ft) from Turbine No. 2. The other was off-site and downwind of Turbine No. 1 at a distance of about 3D (274 m or 900 ft). The majority of the data collected involved turbines cycling on and off during the recording periods, but enough information was obtained with a stable operational configuration (i.e., one, two, or three turbines constantly operating for the entire recording period) to summarize the results.

The fall-off of SPL observed with distance from a single turbine is shown in Figures 4-3 and 4-4. The cumulative distributions of the A-weighted SPL measured at 1.75D, 3D, and 10D downwind distances are plotted in Figure 4-3 along with the equivalent SPL ( $L_{eq}$ ) and a representative background distribution for a surface wind speed of 7-9 mps (15-20 mph). As shown, the observed levels remain essentially normally distributed (a linear decrease with increasing probability level) at the 1.75D and 3D distances. The effect of the background noise becomes evident at the 10D distance, however, as this cumulative distribution shape approaches that of the reference background. It is likely that the HF turbine noises from a single MOD-2 would be heard only intermittently at this distance, under the reference background conditions.

Figure 4-4 plots the equivalent sound level or  $L_{eq}$  as function of downwind distance. The  $L_{eq}$  corresponds to the equivalent sound level of a steady sound which, over a given period of time, would contain the same noise energy as the time-varying sound as the fluctuating turbine or background sounds. The  $L_{eq}$

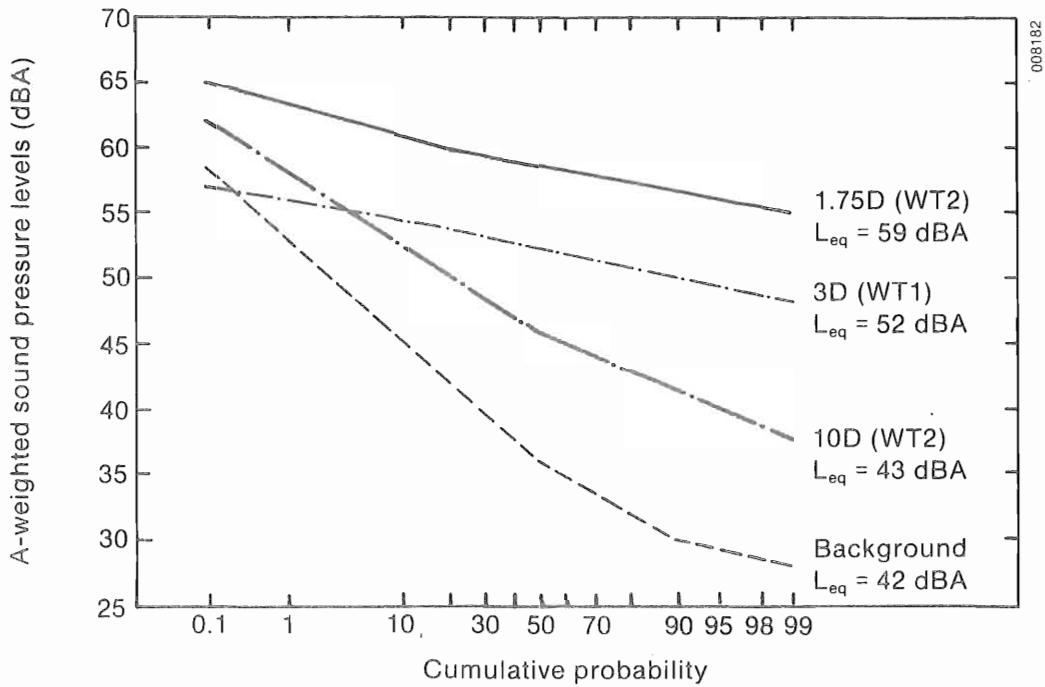


Figure 4-3. Cumulative Distributions of A-Weighted SPL at Three Downwind Distances from a Single MOD-2 Turbine

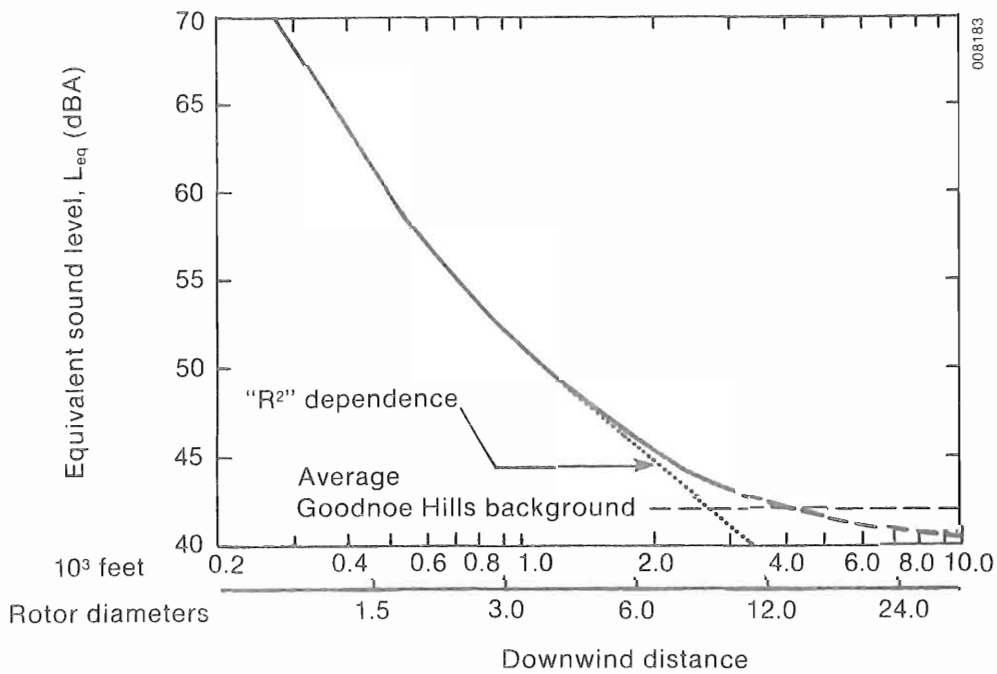
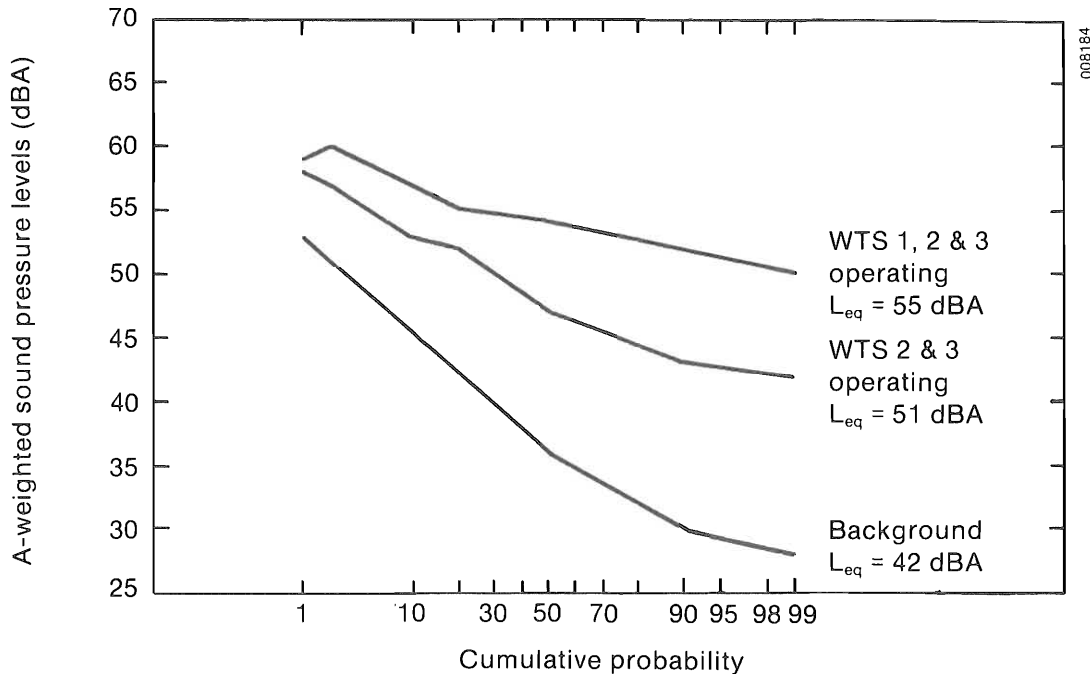


Figure 4-4. Average Turbine  $L_{eq}(A)$  Emissions Decay Downwind of a Single MOD-2 Turbine



**Figure 4-5. Cumulative Distributions of A-Weighted SPL at Site No. 2 (see Figure 4-1) for Two and Three Operating MOD-2 Turbines**

is a preferred noise level metric of the U.S. Environmental Protection Agency (EPA). The plot of Figure 4-5 indicates, on the average, the turbine emissions level and the background noise at the Goodnoe Hills Site become the same at a distance of about 1220 m (4000 ft) or 13+D downwind. This distance may be considered the average audible range for this site. The turbine emission-level decay curve of Figure 4-5 asymptotically approaches the mean background  $L_{eq}$  instead of falling as the " $r^2$ " dependence shown. This is most likely the result of a varying background level and propagation effects. The departure from  $r^2$  dependence began about 5D or 457m (139 ft) downwind of the turbine. This means the detectability of HF-range emissions downwind in the outdoors is almost entirely controlled by the background level in the vicinity of the receiver, as indicated by the shallow  $L_{eq}$  slope. A polynomial that describes the curve of Figure 4-5 to better than 0.5% is

$$L_{eq}(A) = -3.89464 x^4 + 46.67294 x^3 - 191.884 x^2 + 287.1514 x - 28.4, \quad (4-1)$$

where  $x$  is the  $\log_{10}$  of the downwind distance in feet.

#### 4.2.2 Multiple Turbine Operation

The effect of multiple turbine operation at the CNA measuring point east of the site shown in Figure 4-1 is summarized in the  $L_{eq}$  cumulative distribution plots of Figure 4-5. The effect on the local noise level is raised by 3 dB by the operation of all three turbines over Turbine No. 1 (WT1) operating alone. Similarly, the difference between Turbines No. 2 and No. 3 operating and No. 2 operating alone at this location is, on the average, +8 dB. Thus, the local noise environment is dominated by the closest turbine in the cluster, but the effects of multiple turbine operation are most noticeable when sounds are compared from turbines located nearly the same distance upstream from the observer.

### 4.3 Influence of Rotor Inflow on HF Noise Generation

A total of nine data runs were selected from the two experimental years, seven from 1982 and the two available from 1983, to quantify the effects on turbine inflow on the HF noise level radiated from a single turbine rotor. With the exception of the two 1983 runs, the remainder were selected to cover a range of hub-height wind speeds, vertical stabilities, and all with the same microphone placement. Table 4-1 lists the inflow conditions and the on-axis and in-plane A-weighted  $\langle L_{eq}(A) \rangle$  values at the reference distance of 1.5D from the hub axis for these nine runs.

#### 4.3.1 A-Weighted, Equivalent Sound Pressure Level Variation

Table 4-1 indicates, on the average, that there is little difference in the on-axis and in-plane A-weighted emission levels under the range of inflow conditions listed. These conditions vary from an extremely stable ( $Ri = +24$ ), low-wind flow (just at turbine cut-in) to a high-wind (well above rated), convectively unstable ( $Ri = -0.92$ ) surface boundary layer. The information available in Table 4-1 is not sufficient to establish whether or not there is a systematic variation in the on-axis and in-plane levels with wind speed, stability, or experimental year. Similarly, with only two cases from the 1983 experiment available, we cannot identify any statistically significant differences in the on-axis  $\langle L_{eq}(A) \rangle$  levels as a result of the turbine modifications installed between the two experimental periods.

The standard deviation of the entries in Table 4-1 was found to be  $\pm 2$  dB for a wide range of rotor loadings; i.e., a wind speed range covering cut-in to well above rated conditions. There is a noticeable increase in the  $L_{eq}$  level (6 dB) at a slightly more than doubling of the wind speed. This wind speed dependence is plotted in Figure 4-6 for the on-axis and in-plane microphone positions, respectively. The correlation coefficient for the in-plane data is 0.981, with a standard error of  $\pm 0.3$  dB for a linear regression. Similarly, the correlation coefficient for the on-axis readings is 0.889, with a standard

Table 4-1. Inflow Conditions and Resulting  $L_{eq}(A)$  Levels for Representative 1982 and 1983 Data Runs at 1.5D

Run No.	Hub-Height Direction (deg)	Wind Speed (mps)	Richardson Number	On-Axis $\langle L_{eq}(A) \rangle$ (dB)	In-Plane $\langle L_{eq}(A) \rangle$ (dB)	Year
23-1	267	6.3	24	59.0	59.9	1982
21-1	275	9.3	0.46	60.9	61.3	1982
19-1	266	10.3	0.18	61.8	62.5	1982
17-2	258	11.7	-0.01	62.1	62.5	1982
26-1	266	12.0	0.13	61.4	62.5	1982
18	254	12.7	1.26	62.8	n.a.	1983
27	264	13.3	0.42	62.8	63.7	1982
11	256	13.3	6.68	62.8	n.a.	1983
25-1	274	14.5	-0.92	63.0	64.1	1982
Means	264	11.5	3.60	62.0	62.4	

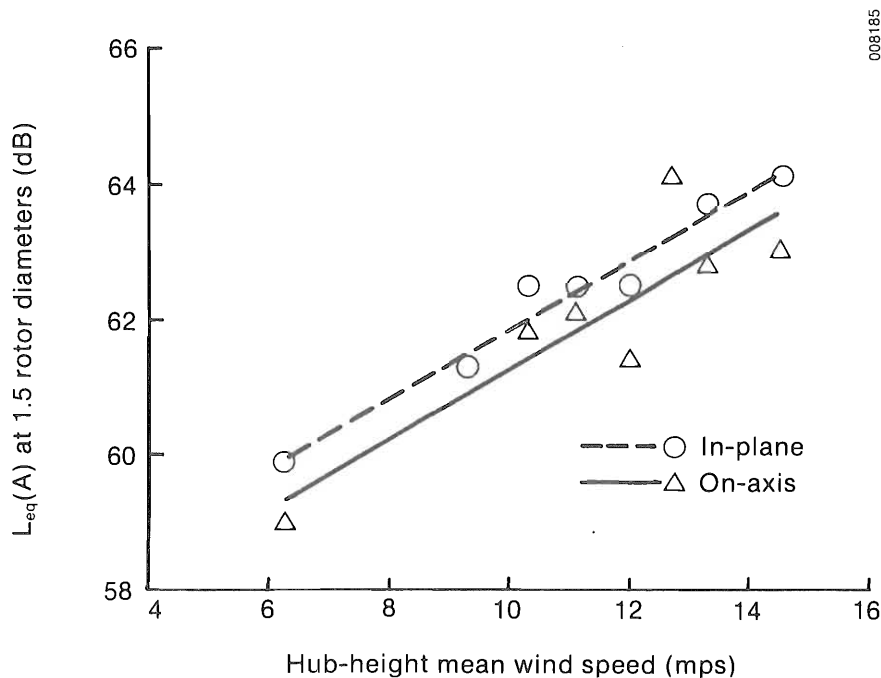


Figure 4-6.  $L_{eq}(A)$  Levels as a Function of Hub-Height Wind Speed

error of  $\pm 0.7$  dB. The regression relations describing the MOD-2 on-axis and in-plane  $\langle L_{eq}(A) \rangle$  dependencies as a function of the mean hub-height wind speed ( $U_H$ ) over a range of 6 to 15 mps are

$$\langle L_{eq}(A) \rangle = 0.52005 U_H + 56 \quad (\text{on-axis}) \quad (4-2)$$

$$\langle L_{eq}(A) \rangle = 0.51327 U_H + 57 \quad (\text{in-plane}). \quad (4-3)$$

A closer examination of Table 4-1 reveals some correlations with the hub-height wind direction and vertical stability. Table 4-2 lists the correlation matrices for the on-axis and in-plane  $\langle L_{eq}(A) \rangle$  values with the hub-height wind direction and speed and the rotor disk vertical stability. While of Table 4-2 confirms that the  $\langle L_{eq}(A) \rangle$  levels are indeed related to the wind direction and vertical stability, these parameters would be site-dependent.

Table 4-2. Multivariate Regression Correlations of MOD-2  $\langle L_{eq}(A) \rangle$  Levels with Hub-Height Wind Vector and Vertical Stability

Parameter	On-Axis $\langle L_{eq}(A) \rangle$ Level	In-Plane $\langle L_{eq}(A) \rangle$ Level
Wind direction	-.468	-.037
Wind speed	0.889	0.981
Richardson number	-.691	-.784
Correlation coefficient	0.945	0.983
Standard error (dB)	0.61	0.36

Because of this dependency, there appears to be little advantage to including the wind direction as a predictor of the  $\langle L_{eq}(A) \rangle$  for the MOD-2 in view of the high degree of correlation in the wind speed (loading) and stability. However, the relationship to the stability expressed here may be valid only for the Goodnoe Hills site. Thus, we suggest that only the hub wind speed be used. We suggest that the on-axis  $\langle L_{eq}(A) \rangle$  value at rated wind speed be considered as a HF emissions figure-of-merit for comparing MOD-2 class machines. For the MOD-2, this value would be 63 dB at the rated hub wind speed of 12.5 mps (28 mph).

An interesting characteristic of the MOD-2 A-weighted levels is the very small temporal or sample-to-sample variation under a given set of conditions. The frequency distributions of the  $\langle SPL(A) \rangle$  parameter for the highest and lowest wind runs (25-1 and 23-1) are plotted in Figure 4-7. As shown in the figure, the sample-to-sample variation is quite small in both cases, enabling us to support the statement that the MOD-2 HF radiation is very steady (as opposed to that of the LF, which is discussed in Section 5.0).

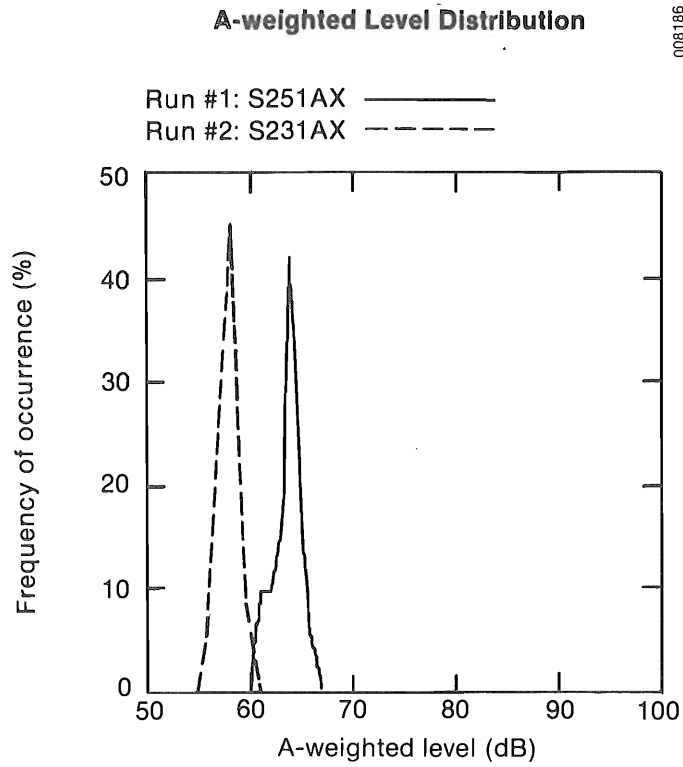
#### 4.3.2 Spectral Variation in High-Frequency-Range Emissions

The spectral content of the high-frequency-range emissions is important not only for its contribution to A-weighted measures of community annoyance, such as the  $L_{eq}(A)$  parameter, but also for assessing whether there are potentially annoying discrete tone radiations. The spectral presentation is also useful for evaluating the relative contributions of various aeroacoustic source mechanisms to the total high-frequency emission level. Such knowledge may be very important if the resulting emission levels are considered too great and some modifications are required.

Two general spectral presentations are currently in use: narrowband and 1/3-octave. The time-averaged, high-frequency resolution of the narrowband spectrum is most useful for examining the turbine emissions for discrete tone noise. Because of the number of elemental frequency bands or spectral lines involved (typically anywhere from 200 to 800), narrowband spectra are not useful for statistical analysis procedures because of the large data volume associated with their use. To make the storage of the spectral representation more tractable for statistical analyses on smaller computers, the 1/10- or 1/3-octave bands are often employed. The elemental spectral frequency band is then bounded by a frequency ratio of  $2^{1/10}$  or  $2^{1/3}$ . The 1/3-octave bandwidths, besides having a smaller number of elemental bands to process and store, approximately correspond to the critical bandwidths used by psychoacousticians to assess tonal noise. We have chosen to use the 1/3-octave resolution for statistical analysis of both the low- and high-frequency-range MOD-2 emissions. The HF-range analysis bands are listed in Table 2-4. In addition, we have employed narrowband spectral techniques to examine the MOD-2 emissions for the existence of discrete tonal noise.

##### 4.3.2.1 High-Frequency-Range Measurement Locations

Figure 4-1 shows the locations of the sound level meters used in the 1982 experimental series. One was placed 137 m (450 ft or 1.5D) upwind and along a line parallel to the rotor axis. This measurement station, referred to as the on-axis location, makes a  $24^\circ$  angle with the rotor plane centered at the hub. The other microphone station, which will be referred to as the in-plane



**A-weighted level distribution statistics**

	<u>Run #1</u>	<u>Run #2</u>
Mean BPL (dB) =	63.7	58.0
Peak BPL (dB) =	66.0	59.8
Min. BPL (dB) =	61.1	56.3
Std. dev. (dB) =	1.26	0.85
Skewness coef. =	-0.50	0.00
Kurtosis coef. =	-0.34	-0.33
Mode (dB) =	64	58
Median (dB) =	64	58

**Figure 4-7. Observed Frequency Distributions of A-Weighted SPL for Highest and Lowest Mean Hub-Height Wind Speeds**

location (as shown in Figure 4-1) was located 137 m or 1.5D perpendicular to the rotor axis and in its plane.

4.3.2.2 Establishment of Background Spectral Reference

To ensure that the spectra are actually emitted from the MOD-2 and not the result of wind-induced or "pseudo" noise, it is important to establish reference spectra for a range of background conditions. We did this by including a 10- to 15-minute recording period with each data run with the turbine shut down. Figure 4-8 shows the range of background acoustic spectra taken at the on-axis and in-plane positions for the upper and lower limits of the average hub-height wind speed observed during the 1982/83 experimental periods. The corresponding wind speeds were 6 and 14.5 mps at the 59-m level on the BPA tower. As we see in this figure, more than a 20-dB range in background noise is typical for the winds encountered at this microphone location during the 1982 experiment, with some differences in the two positions. The ensemble mean band pressure levels (BPLs) with the turbine operating and the associated background for these two cases are shown in Figure 4-9. Only the on-axis microphone position was used for two high-wind data runs during the 1983 experiment. Figure 4-10 plots a representative 1982 on-axis background spectra with one from 1983 with identical average hub-height wind speeds. One notices the changes particularly at high frequencies. We attribute these differences to the condition of the local ground cover in April/May 1982 and August 1983; e.g., grasses were deeper during the former.

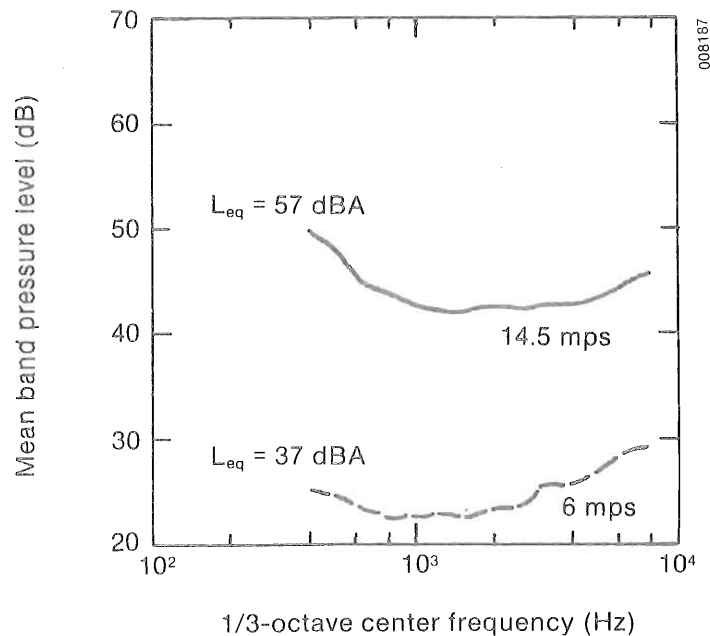
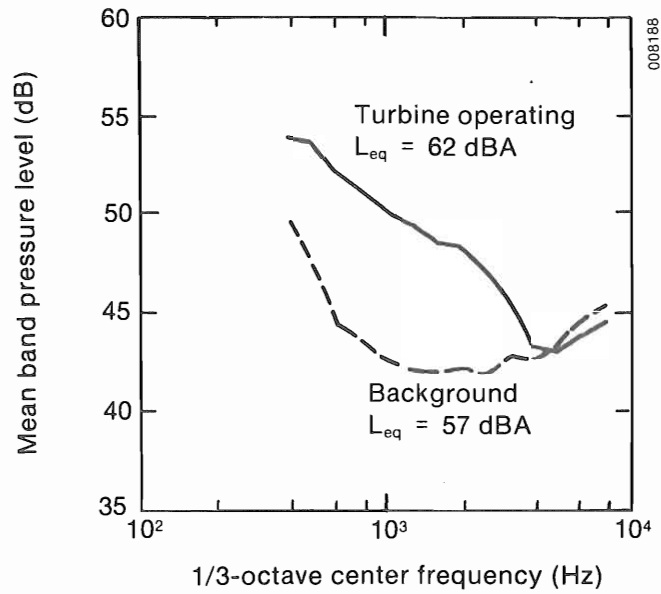
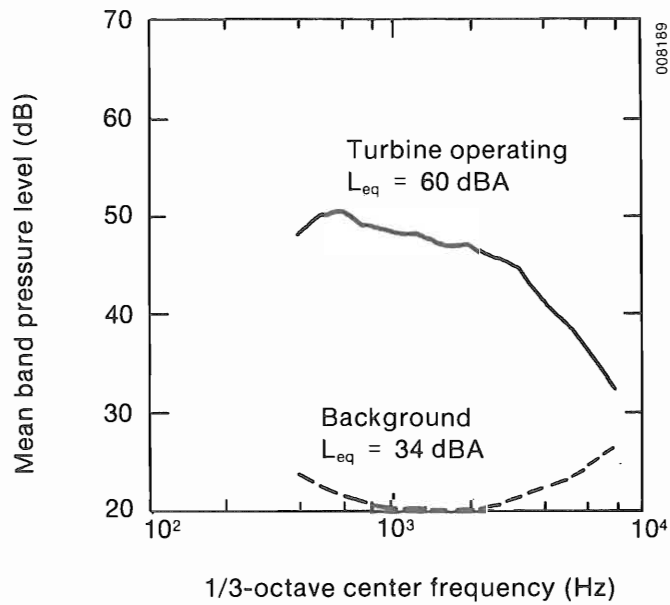


Figure 4-8. Comparison of Background Mean BPL Spectra for Highest and Lowest Mean Hub-Height Wind-Speed Conditions



(a) highest wind observation (14.5 mps)



(b) lowest wind speed observation (6 mps)

Figure 4-9. Comparisons of Observed Mean SPL Spectra for Operating and Background Conditions in High (a) and Low (b) Winds

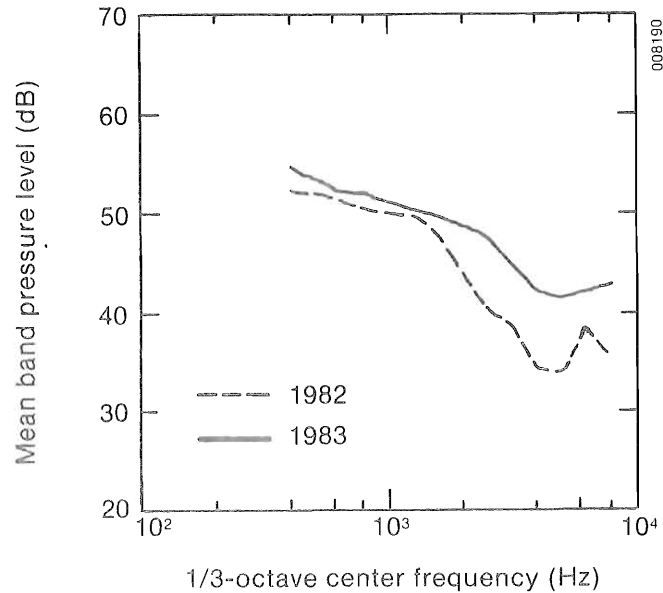


**Figure 4-10. Comparison of Background HF Acoustic Spectra at On-Axis Microphone Location for the Same Mean Hub-Height Wind Speed during 1982 and 1983 Experiments**

4.3.2.3 Rotor Inflow Influence on Spectral Distribution

In Section 4.3.1 the  $\langle L_{eq}(A) \rangle$  dependency on the mean wind speed was discussed. One would logically expect a similar relationship to exist with the 1/3-octave spectral bands, since the A-weighted  $\langle L_{eq} \rangle$  value is a summation of these bands. Figure 4-11 plots the ensemble-averaged 1/3-octave BPLs from the on-axis and in-plane positions for seven mean wind speeds from the 1982 experiment. The wind-speed dependency is less clear in the on-axis spectra than the in-plane. Also, the high-frequency level (above the 2500-Hz band) of the on-axis spectra rises because the local background noise exceeds the turbine radiation level. A comparison is made between two 1983 data runs and three runs from 1982 at similar wind speeds in Figure 4-12. We see that the turbine emission levels were 2-3 dB higher in the 630- to 5000-Hz bands in 1983 for a mean-wind-speed range of 12-13 mps.

We attempted, as in the case of the  $\langle L_{eq}(A) \rangle$  values, to determine if other inflow parameters such as the rotor disk vertical stability (and therefore the turbulence structure) had any influence on the MOD-2 mean and temporal characteristics of the HF acoustic spectral content. Unfortunately, the bulk of the data available was from the 1982 experiment, when we had only a minimal description of the inflow turbulence.

We first examined data runs in which the mean hub-height wind speeds were similar but the stability (turbulence characteristics) varied. Using Table 4-1 as a guide, we chose to compare 1982 Runs 19-1, 17-2, and 26-1. These three runs involved mean wind speeds of 10.3, 11.7, and 12.0 mps and

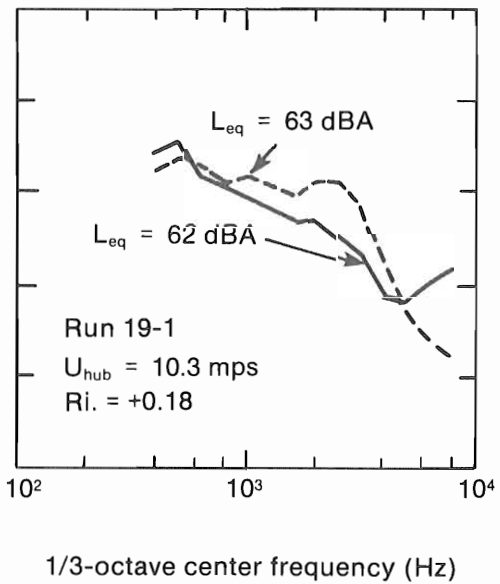
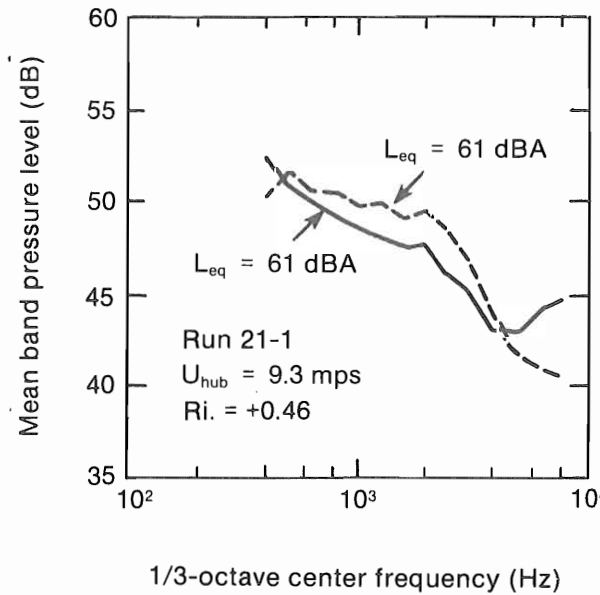
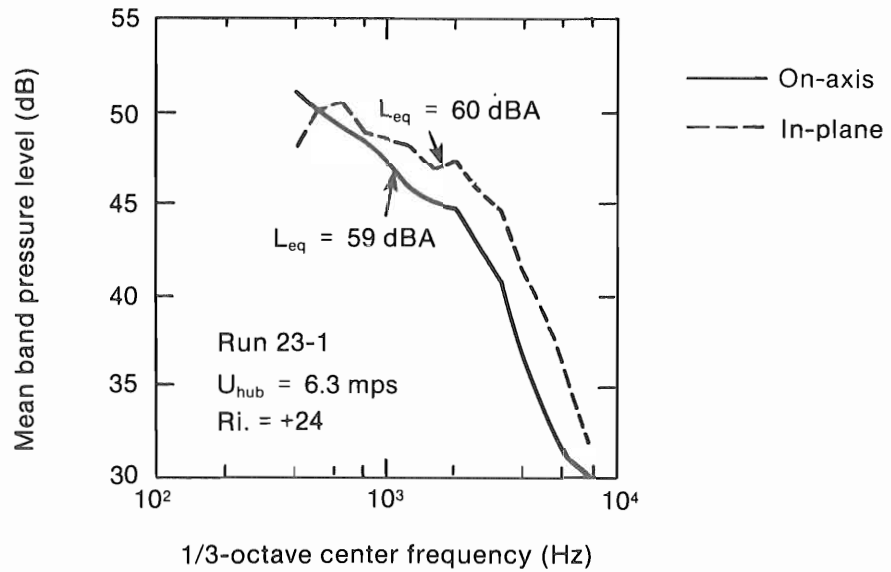


Figure 4-11. 1982 HF-Range Acoustic Spectral Distribution for On-Axis (solid) and In-Plane (dashed) Locations as a Function of Wind Speed and Stability

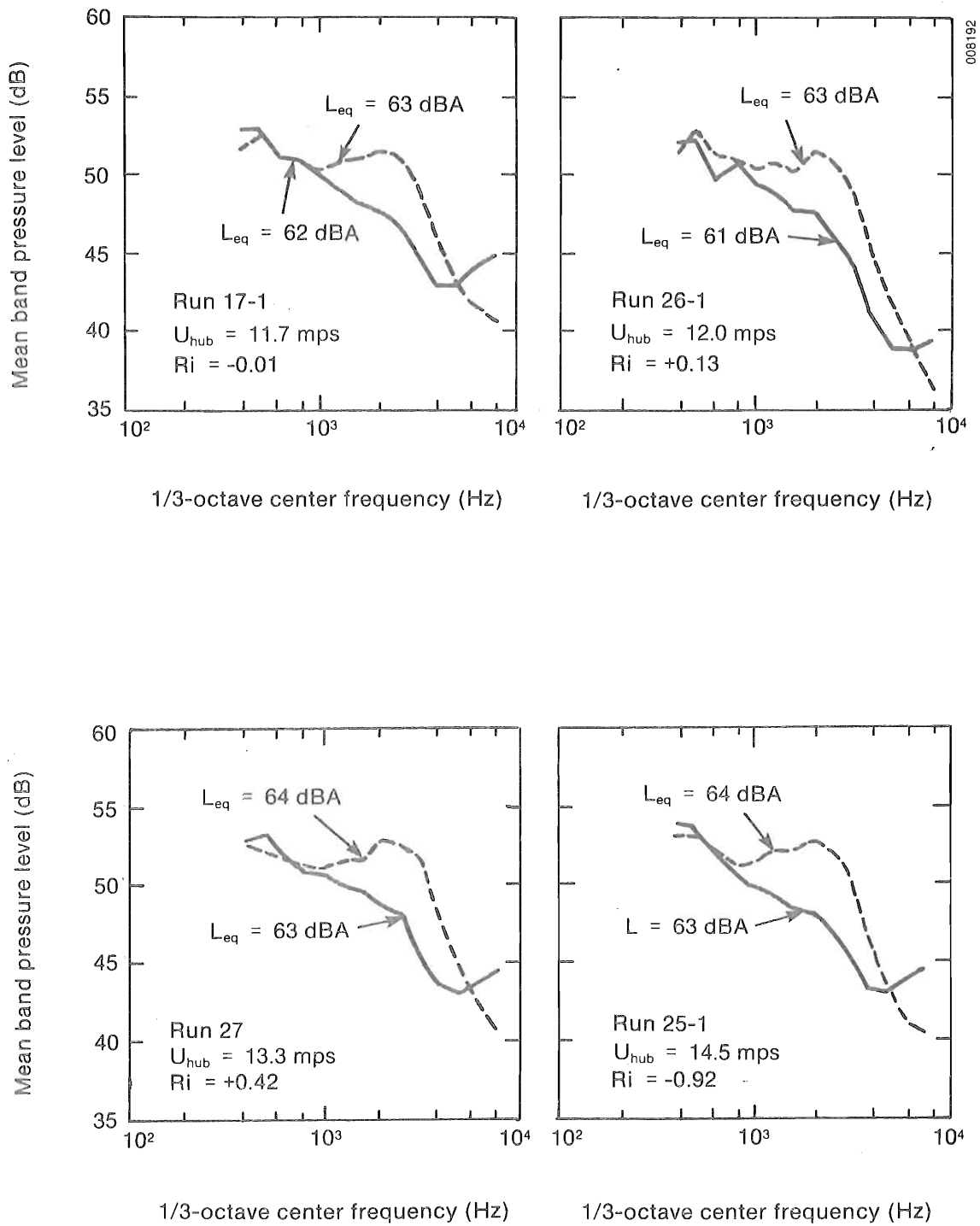


Figure 4-11. 1982 HF-Range Acoustic Spectral Distribution for On-Axis (solid) and In-Plane (dashed) Locations as a Function of Wind Speed and Stability (concluded)

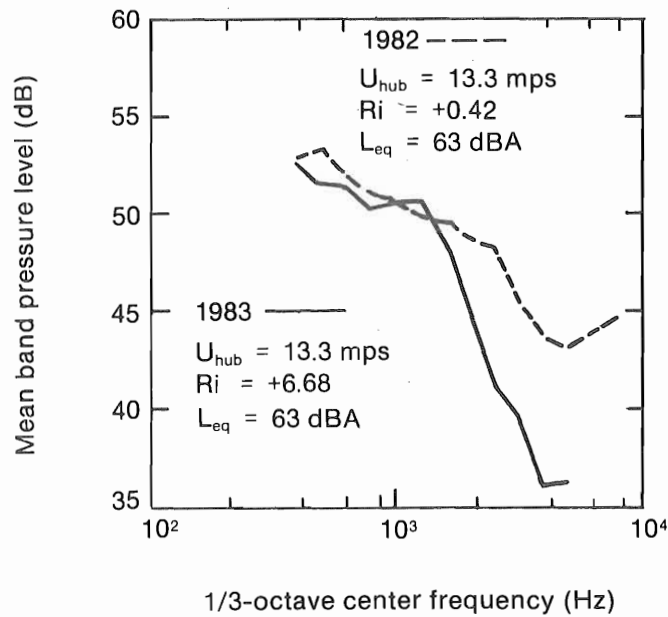
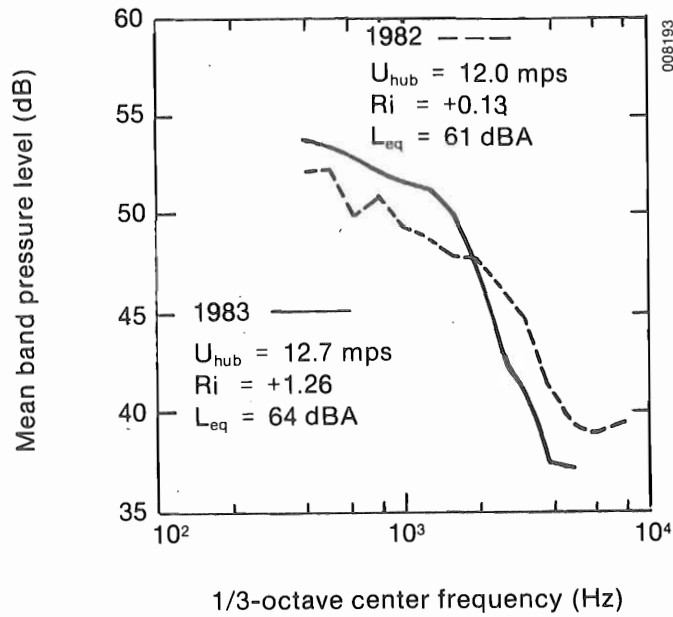


Figure 4-12. Comparison of the On-Axis Component of the HF Spectral Distribution between 1982 and 1983 under High Loading Conditions

Richardson numbers of 0.18, -0.01, and 0.13, respectively. This range of Richardson numbers indicates a neutral to slightly stable surface layer which would be dominated by slightly buoyancy-damped, mechanically (shear) generated turbulence. Figure 4-13 presents the ensemble-averaged mean BPL spectra for the on-axis and in-plane measurement stations for these runs. On the whole, these mean spectra show remarkably little run-to-run variation. The exception is the on-axis station of runs 17-2 and 19-1, where less acoustic energy is present in the high-frequency bands of run 17-2 even though this run has the higher wind speed of the two. The temporal variation of the 1/3-octave BPLs is presented as plots of the ensemble 1%, 5%, 10%, 20%, and 50% BPL exceedence, or  $\langle L_1 \rangle$ ,  $\langle L_5 \rangle$ ,  $\langle L_{10} \rangle$ ,  $\langle L_{20} \rangle$ , and  $\langle L_{50} \rangle$  levels in Figure 4-14. These levels represent the percentage of time the randomly sampled BPL equaled or exceeded that figure. For example, a 1000-Hz, 1/3-octave BPL  $\langle L_{20} \rangle$  of 55 dB means that 20% of the samples contained levels of 55 dB or more. The only obvious difference is the on-axis  $\langle L_1 \rangle$  or 1% exceedence level, which is highly peaked in the 2500-Hz band, compared with the others.

Runs 19-1 and 21-1 were compared, since they differed by 1 mps (10.3 vs. 9.3, respectively), but the inflow with the latter was more stable, i.e., 0.46 as opposed to 0.18. The ensemble mean BPLs are plotted in Figure 4-15 and the

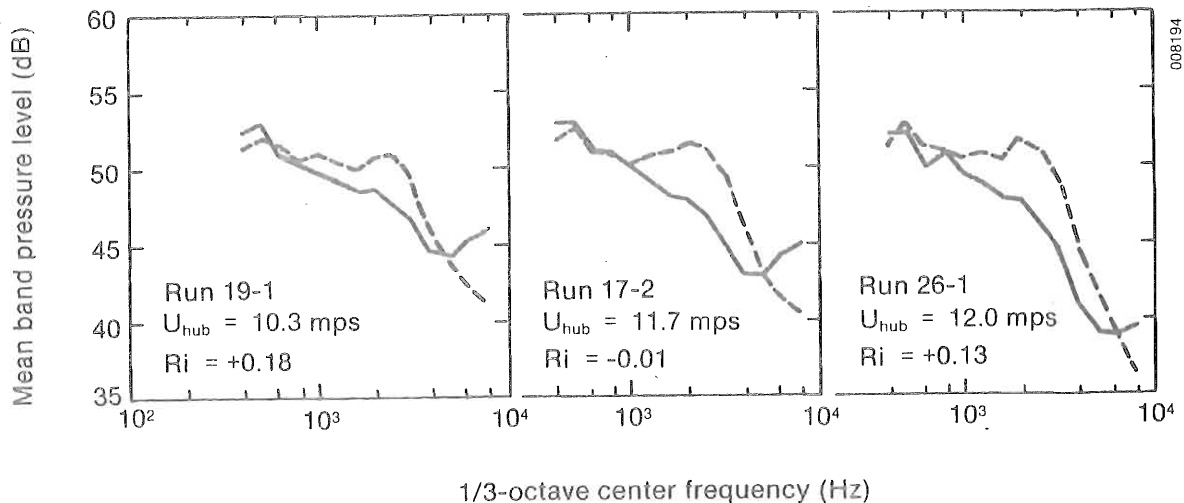


Figure 4-13. Comparison of On-Axis (solid) versus In-Plane (dashed) HF Spectral Emissions for Neutral to Slightly Stable Inflow Conditions

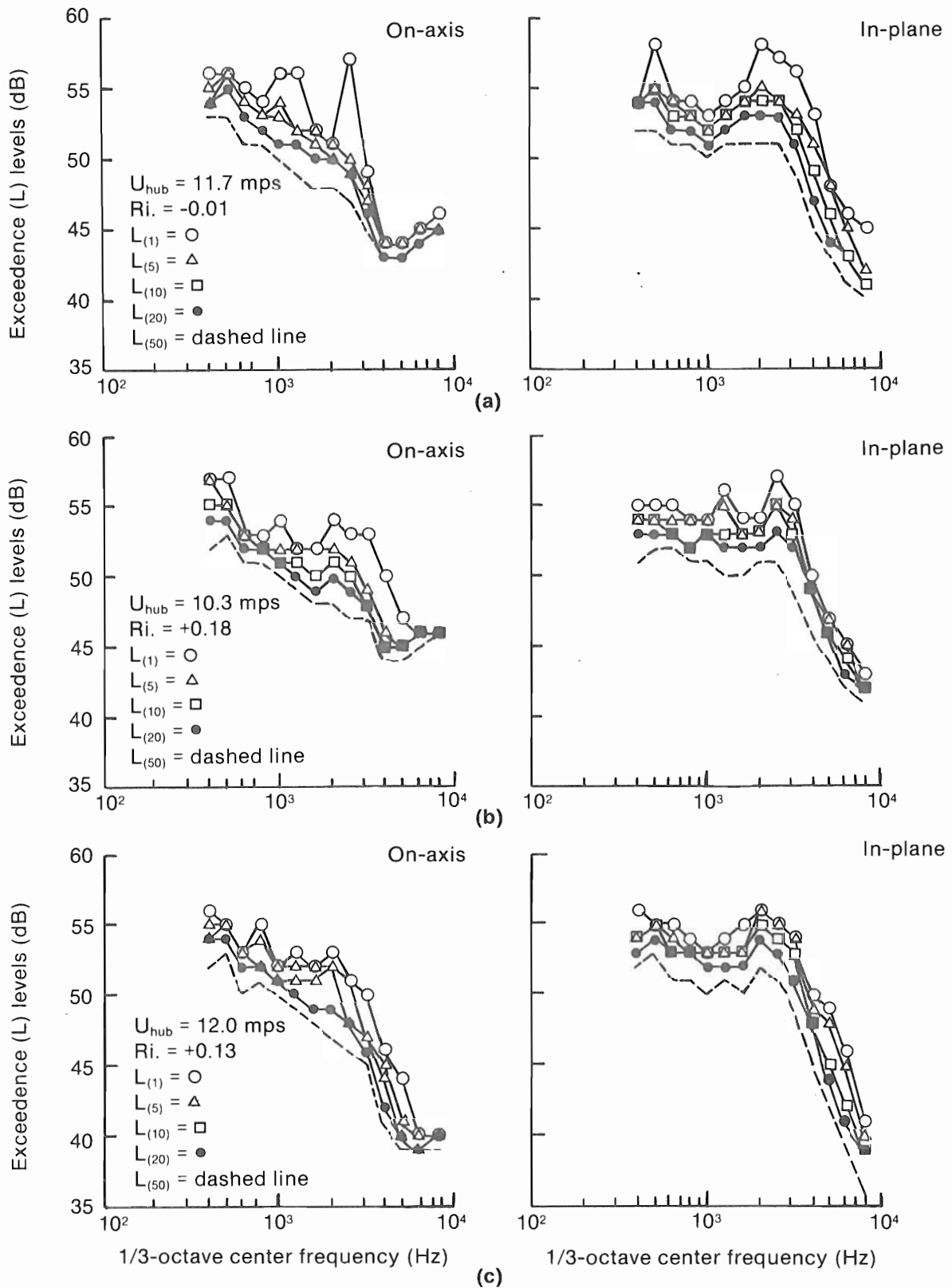
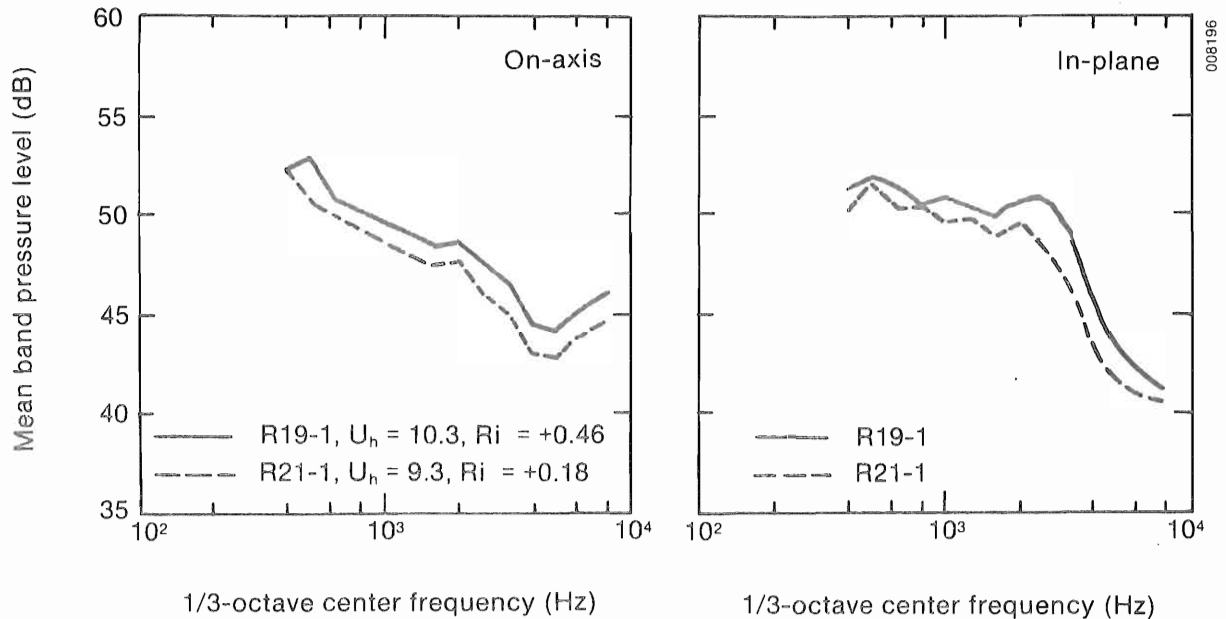


Figure 4-14. Comparison of  $L_1$ ,  $L_5$ ,  $L_{10}$ ,  $L_{20}$ , and  $L_{50}$  1/3-Octave Level Spectra at 1.5D at the On-Axis and In-Plane Measurement Locations for 1982 Runs: (a) 17-2; (b) 19-1; and (c) 26-1

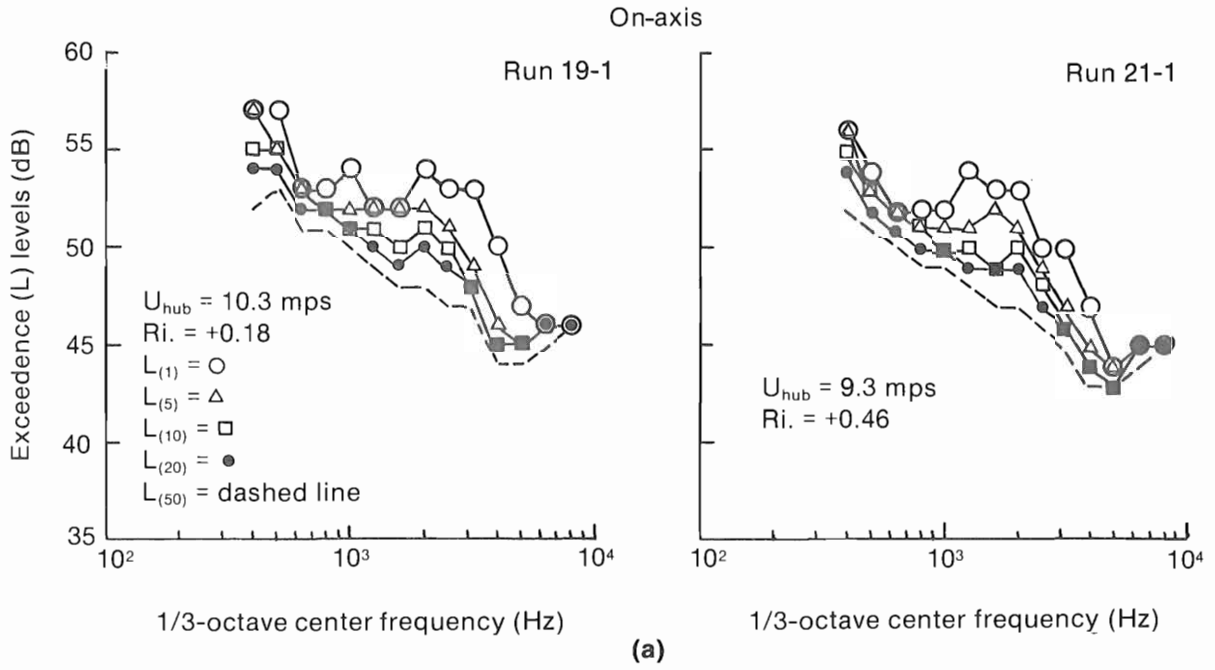


**Figure 4-15. Comparison of Mean 1/3-Octave BPL Spectra for Mean Wind Speeds of 9.3 and 10.3 mps under Stable Conditions**

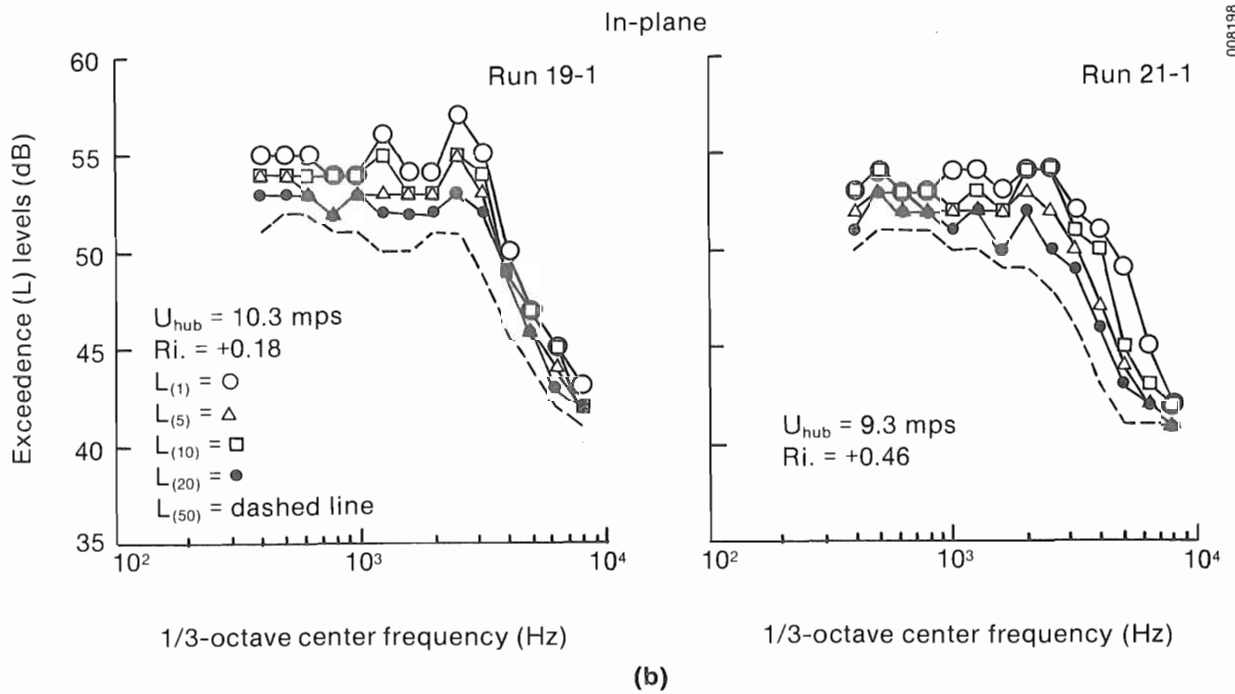
exceedence levels in Figure 4-16. It is clear, under these conditions, that there is essentially a uniform BPL increase across the spectrum with the increase in wind speed and stability. Not much variation is evident in the on-axis exceedence plots, as shown in Figure 4-16a. There is a noticeable increase in peaking in the 1000-Hz and 2500-Hz BPLs of the in-plane measurement (Figure 4-16b) in the higher-wind, lower-stability case (run 19-1).

The increase in the peaking with exceedence or L-level noted above appears to be associated with some form of oscillatory behavior of the acoustic emissions in these bands. This peaking appears to be load-related and often more noticeable in the in-plane rather than in the on-axis measurements. This apparent load dependency is shown in Figures 4-15 and 4-16 at both measurement stations. The on-axis, 2500-Hz band L-levels seem to be less affected than the in-plane exceedences, indicating that the process responsible radiates more strongly in the rotor plane. The in-plane peaking behavior broadens to include lower frequency bands. The extent of this broadening appears to be associated with lower stabilities (Richardson numbers). This is most noticeable in Runs 27 and 25-1 in Figure 4-17. We know, for example, that during Run 25-1, the turbine exhibited a very unstable behavior and finally shut itself down because of excessive drive-train vibration. Very high levels of coherent, low-frequency emissions were also present during this run, which are discussed in Section 5.0.

A good example of the effect of wind speed or rotor loading for two runs under similar stability conditions is plotted in Figure 4-17. The mean hub wind speed for Run 27 was 13.3 mps and the Richardson number was 0.42; the wind speed for Run 21-1 was 9.3 mps with a Richardson number of 0.46. The on-axis station shows the typical upward shift in BPL at frequencies below 2500 Hz for



008197



008198

Figure 4-16. Comparison of  $L_1$ ,  $L_5$ ,  $L_{10}$ ,  $L_{20}$ , and  $L_{50}$  1/3-Octave Level Spectra at 1.5D at the On-Axis (a) and In-Plane (b) Measurement Stations

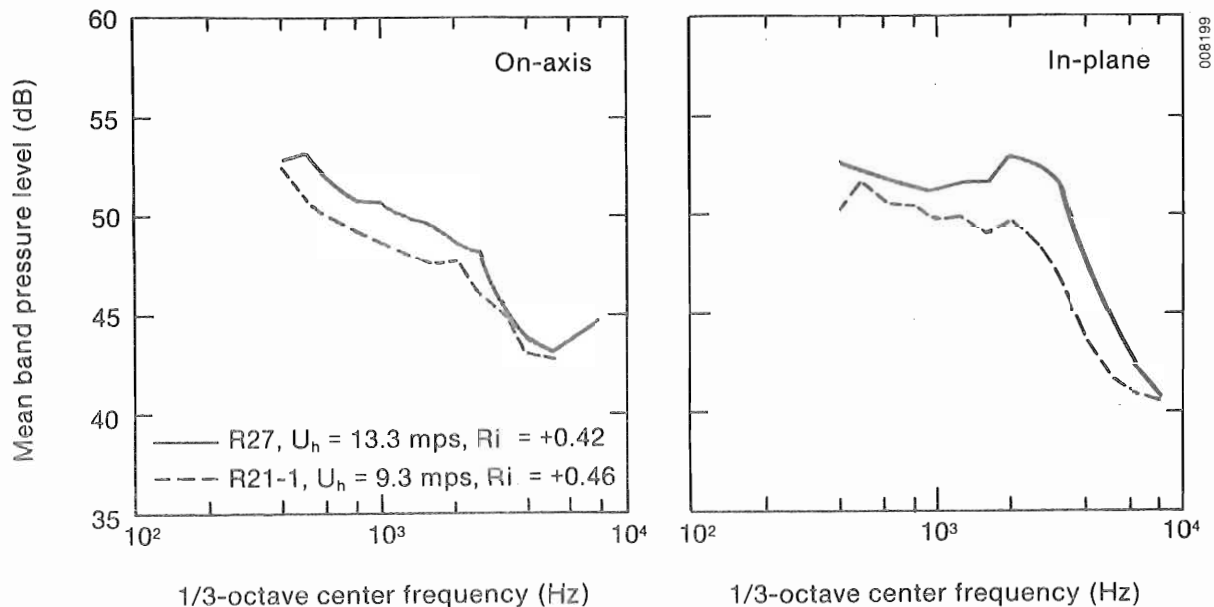


**Figure 4-17. Comparison of Mean 1/3-Octave BPL Spectra for High and Moderate Wind Speeds under Stable Inflow Conditions**

the higher wind speed, but above that frequency band the levels become similar. There is a more or less uniform upward BPL shift in the rotor plane, except for the peaking behavior in the 1600 to 4000-Hz bands in the run with the higher rotor loading. This difference is clearer in the peak BPL plots of Figure 4-18. To ascertain whether this fluctuating or oscillatory condition is related to the inflow stability, we looked at two high-wind runs (Run 25-1 at 14.5 mps and Run 27 at 13.3 mps) with Richardson numbers of -0.92 and 0.42. The mean BPL spectra associated with these two cases were plotted in Figure 4-19. While both the on-axis and in-plane mean BPL spectra are very similar, the peak BPLs shown in Figure 4-20 for each are quite different in the 2500-Hz region. The unstable case shows a greater tendency for peaking in the on-axis measurement (Figure 4-20a), and while the more stable one has the same tendency in the rotor plane measurement (Figure 4-20b). While it appears that rotor loading is the major factor determining whether or not high-frequency oscillatory behavior will occur, the stability (and therefore the turbulence structure) seems to influence the directivity of the acoustic radiation. We did not experience the degree of turbine operational instability under the stable atmospheric conditions of Run 27 that we observed during Run 25-1.

We attempted to compare the two available data runs of on-axis measurements taken in 1983 (with the modified turbine) with 1982 runs made under conditions as similar as possible. Run 27 (1982) and Run 11 (1983) had the same mean hub-height wind speed (mean rotor loading), but in the latter inflow was much more stable; i.e., 0.42 in 1982 and 6.68 in 1983. The closest corresponding 1982 run to 1983's Run 18 was Run 26-1. Run 26-1 had a mean wind speed of 12 mps and a Richardson number of 0.13, compared with 12.7 mps and 1.26, respectively, for Run 18. Figures 4-21 and 4-22 plot the ensemble mean BPL and  $\langle L_{20} \rangle$  spectra for these two cases. The mean and  $\langle L_{20} \rangle$  BPL spectra of

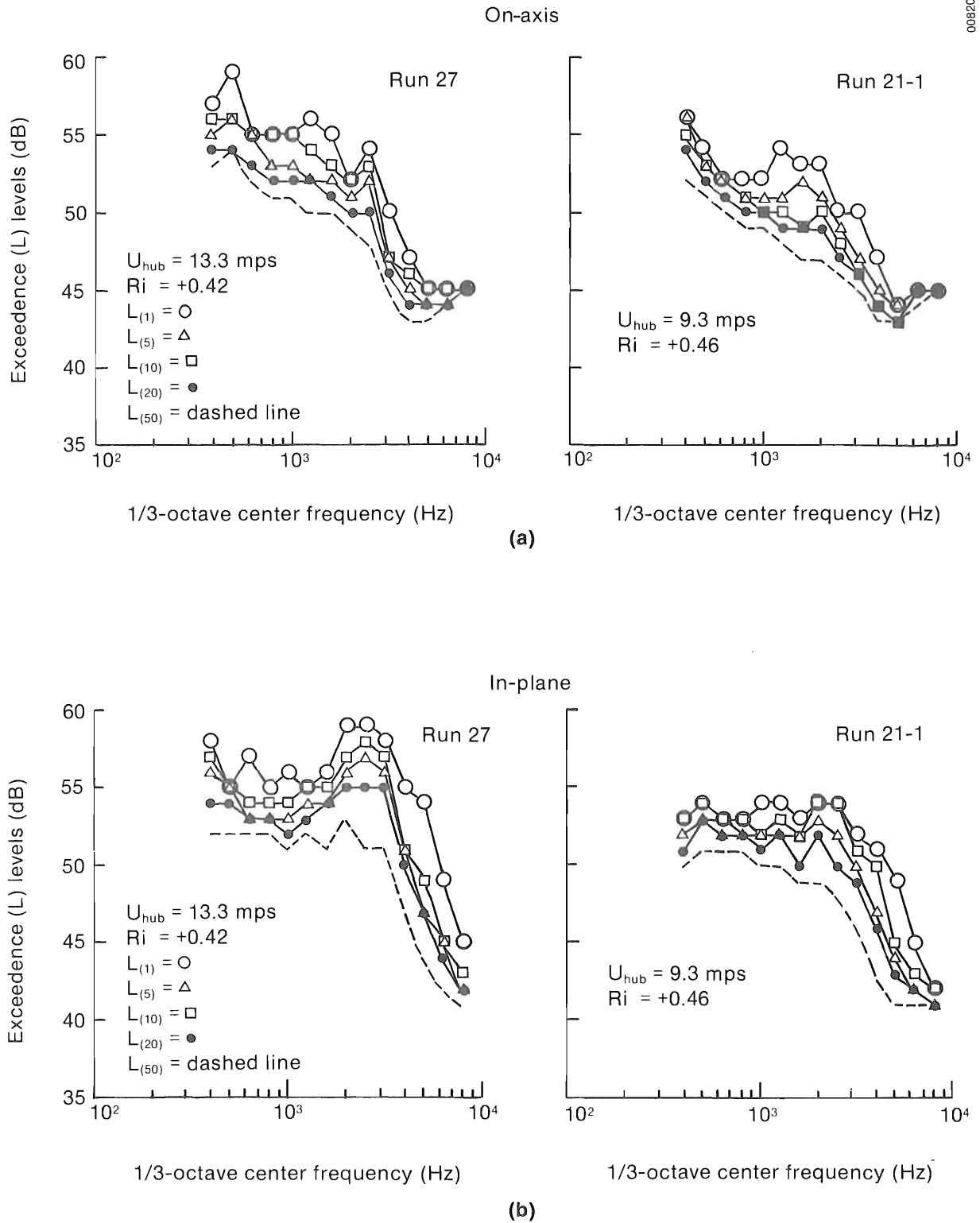


Figure 4-18. Comparison of  $L_1$ ,  $L_5$ ,  $L_{10}$ ,  $L_{20}$ , and  $L_{50}$  1/3-Octave Level Spectra for High and Moderate Wind Speeds under Stable Inflow Conditions. On-axis measurements are shown in (a) and in-plane measurements in (b).

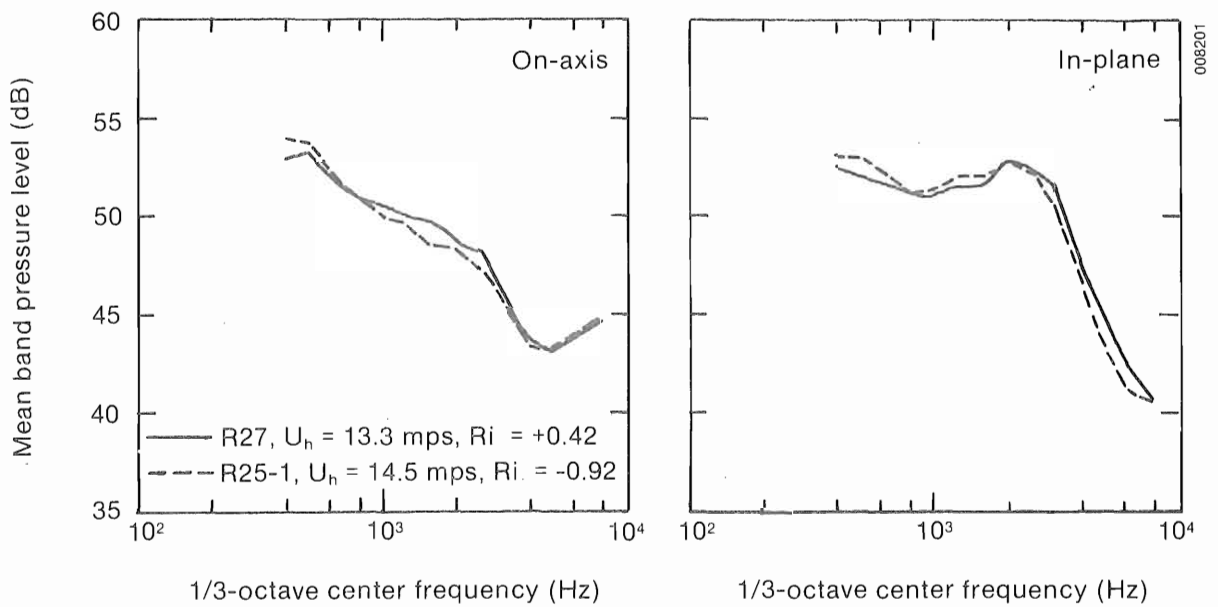
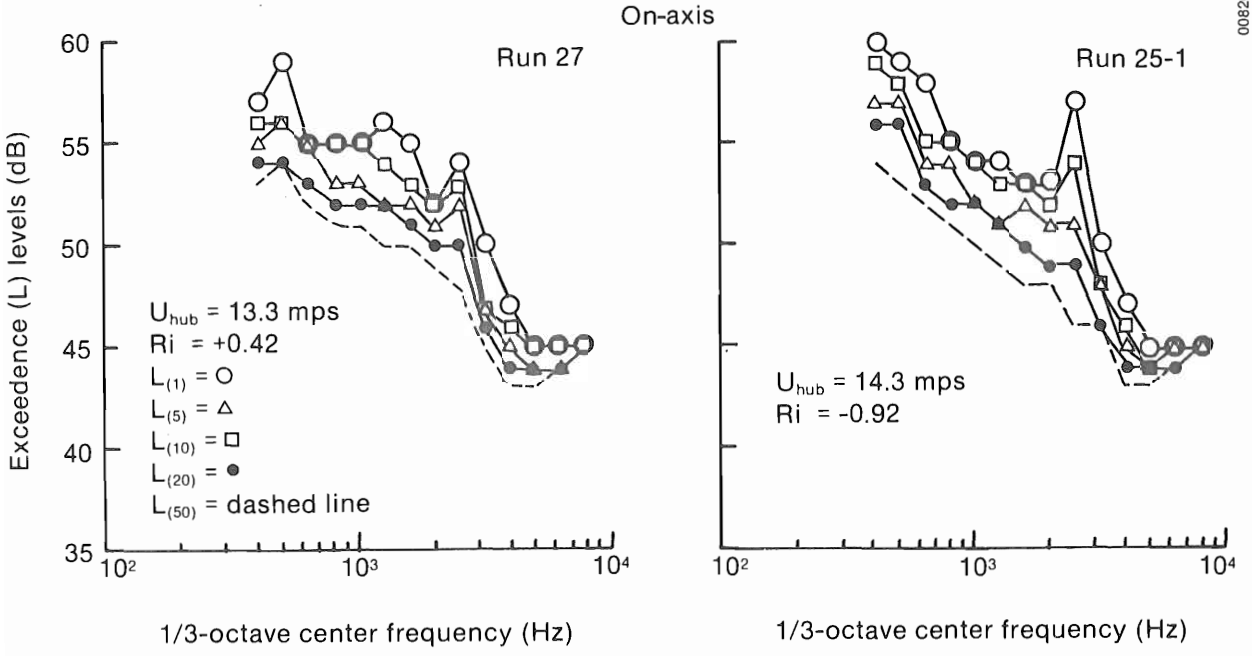
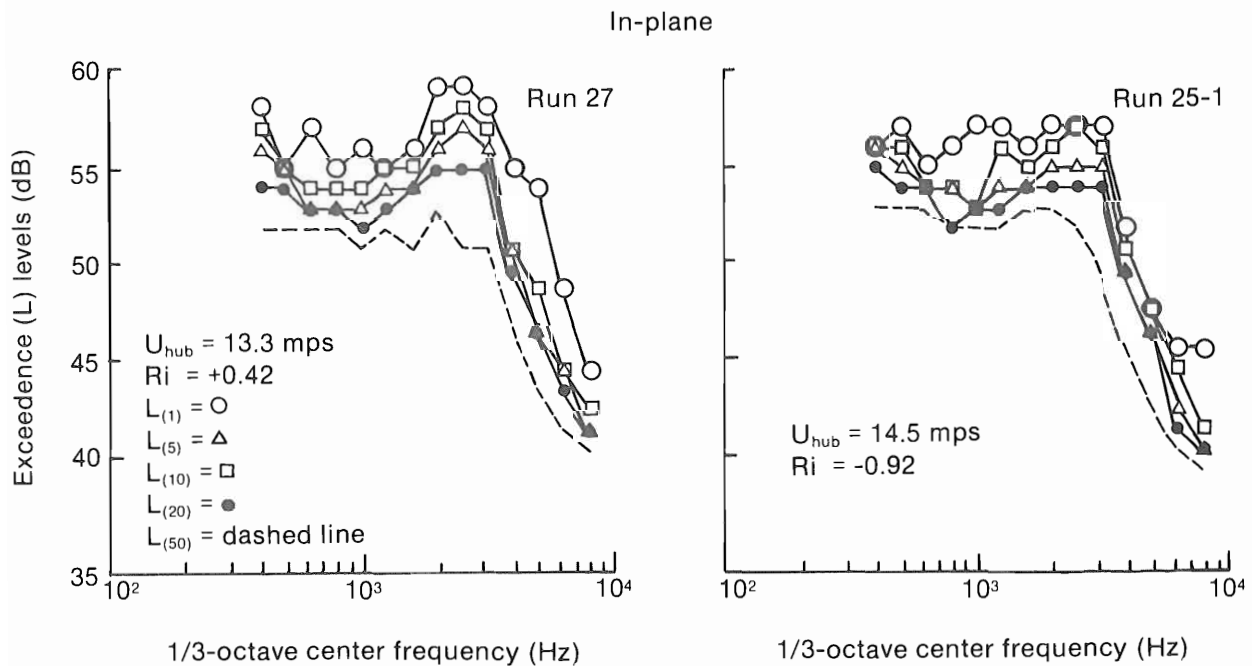


Figure 4-19. Comparison of Mean 1/3-Octave BPL Spectra for a Mean Wind Speed of 13.3 mps and Stable Conditions (Run 27) and a Mean Wind Speed of 14.5 mps and Unstable Conditions (Run 25-1)

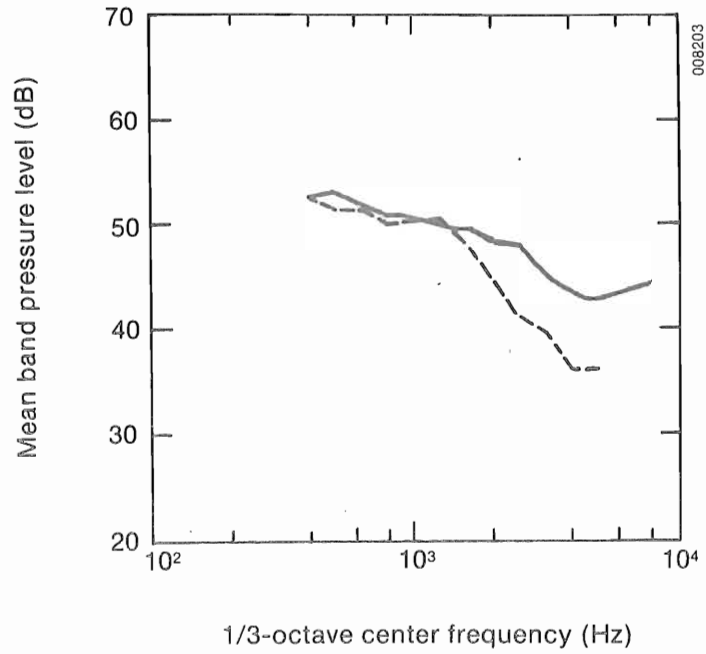


(a)

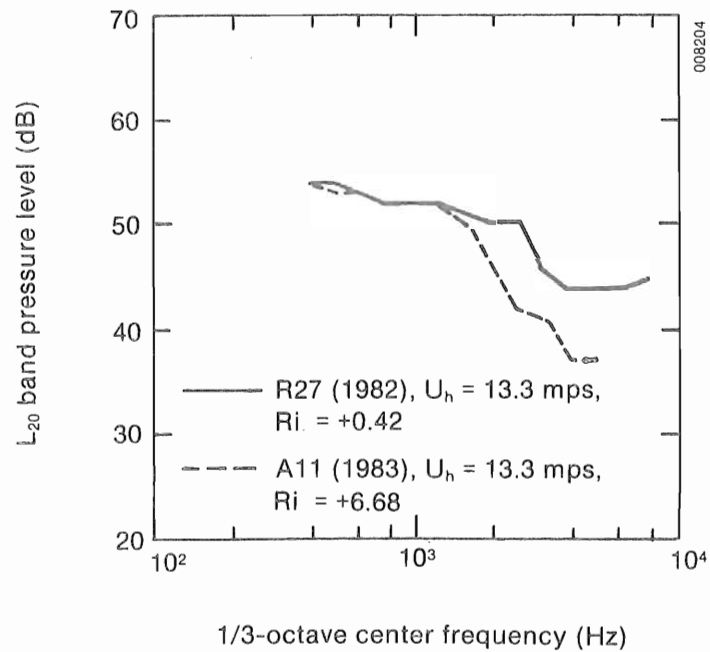


(b)

Figure 4-20. Comparison of  $L_1$ ,  $L_5$ ,  $L_{10}$ ,  $L_{20}$ , and  $L_{50}$  1/3-Octave Level Spectra for High-Wind, Stable vs. High-Wind, Unstable Inflow Conditions. On-axis measurements are shown in (a) and in-plane measurements in (b).

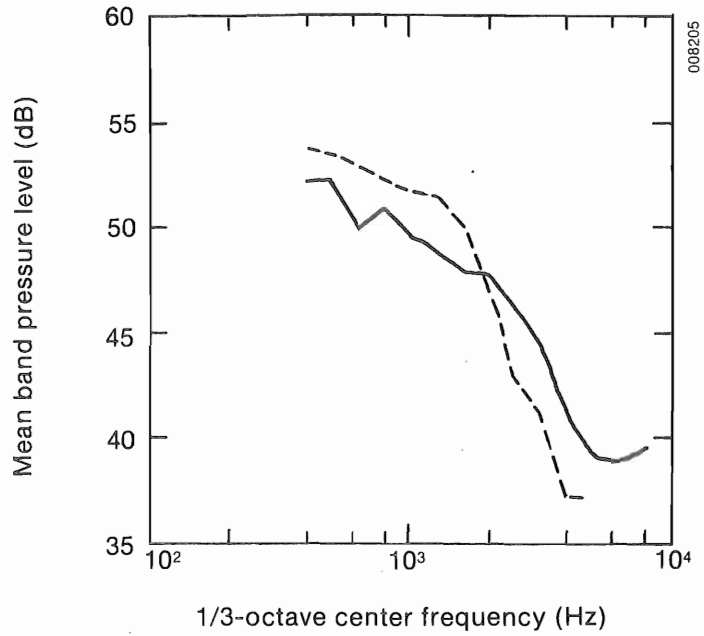


(a) mean 1/3-octave BPL spectra

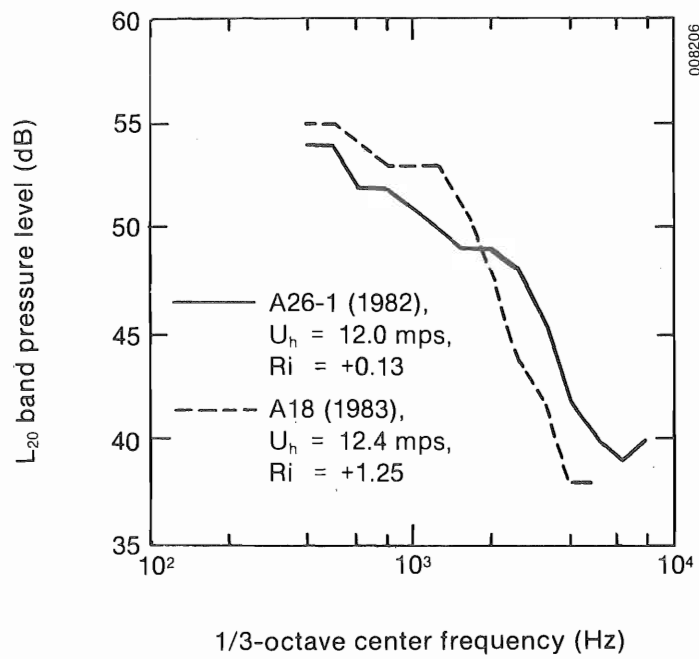


(b)  $L_{20}$  BPL spectra

Figure 4-21. Mean and  $L_{20}$  BPL Spectra for 1982 Run R27 and 1983 Run A-11



(a) mean 1/3-octave BPL spectra



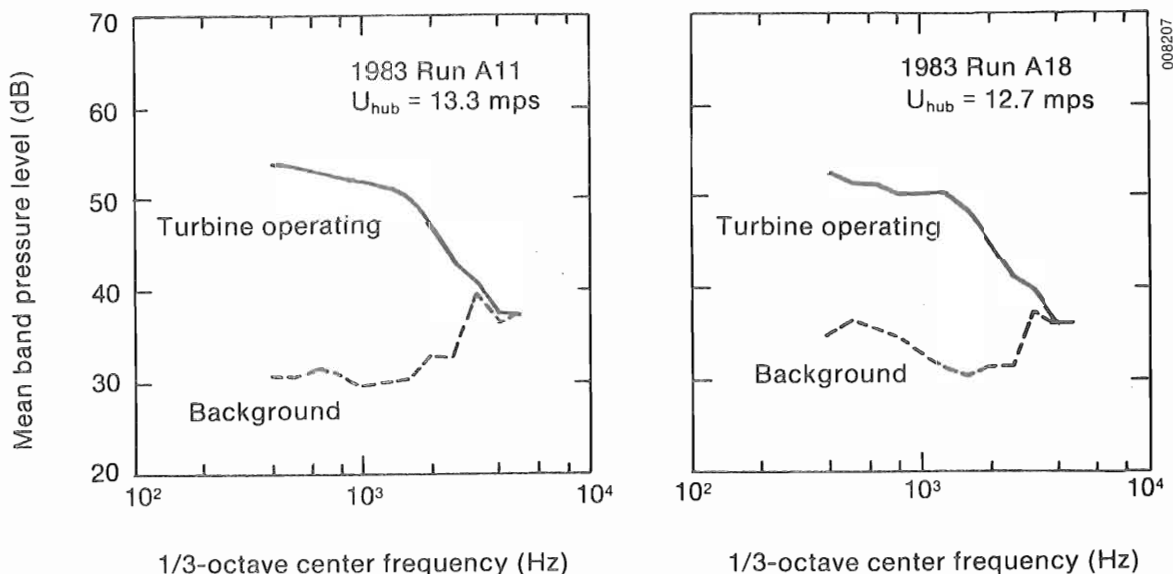
(b) L<sub>20</sub> BPL spectra

Figure 4-22. Mean and L<sub>20</sub> BPL Spectra for 1982 Run 26-1 and 1983 Run A18

Figure 4-21 show excellent agreement for the bands below 1600 Hz for the two years under the same mean loading conditions. Figure 4-22 shows the expected higher mean and  $\langle L_{20} \rangle$  levels for the 1983 run (since it has a higher wind speed) below the 1600 Hz band. What is different is the sharp spectral cutoff above the 1600-Hz band in both 1983 runs. There does seem to be a hint of the oscillatory peaking seen in the data for the 1982 higher wind-speed run, particularly for run 11, as shown in the L-level summaries of Figures 4-24 and 4-25. In the 1983 runs, there appears to have been a downward shift in the frequency band, in which the peaking occurs, from 2500 Hz in 1982 to 1000 Hz in 1983.

**4.4 Typical High-Frequency-Range Narrowband Spectra**

Averaged narrowband (25-Hz resolution) spectra were computed over a frequency range of 100 to 10,000 Hz for a 2-minute period located midway in each data run listed in Table 4-1. The purpose was to locate and identify the possible source(s) of any discrete tonal components found in the MOD-2 emissions. Figures 4-26, 4-27, and 4-28 present a sample of the resulting narrowband on-axis and in-plane spectra for Runs 23-1, 17-2, and 25-1 from the 1982 experiment (low, moderate, and high wind regimes). Figures 4-29 and 4-30 present the on-axis spectra from 1983 runs 11 and 18 in moderate to high winds. No significant, steady tone noise components were found. This indicates that the mechanical noise sources associated with the drive train are well controlled, and there appear to be no discrete aeroacoustic sources of consequence.



**Figure 4-23. Comparison of Acoustic Environment at 1.5D, On-Axis Measurement Location with and without the Turbine Operating under High Wind Conditions**

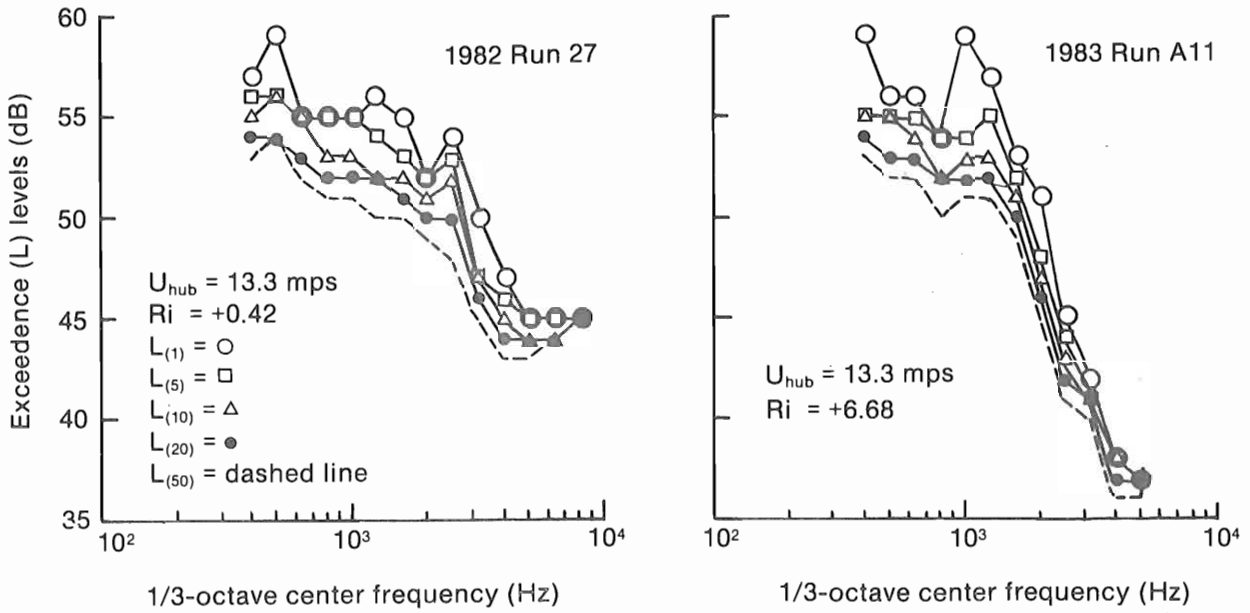


Figure 4-24. Comparison of  $L_1$ ,  $L_5$ ,  $L_{10}$ ,  $L_{20}$ , and  $L_{50}$  On-Axis 1/3-Octave Level Spectra for Identical Mean Wind Conditions during 1982 and 1983 Experiments

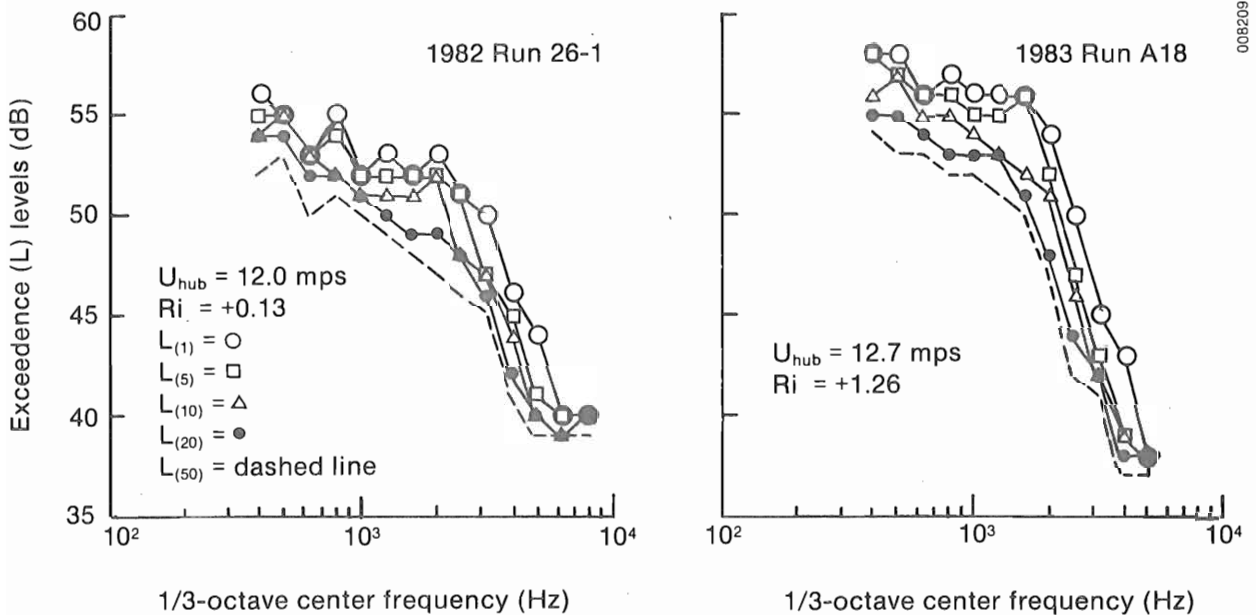


Figure 4-25. Comparison of  $L_1$ ,  $L_5$ ,  $L_{10}$ ,  $L_{20}$ , and  $L_{50}$  On-Axis 1/3-Octave Level Spectra for Similar Wind Speed Regimes in 1982 and 1983

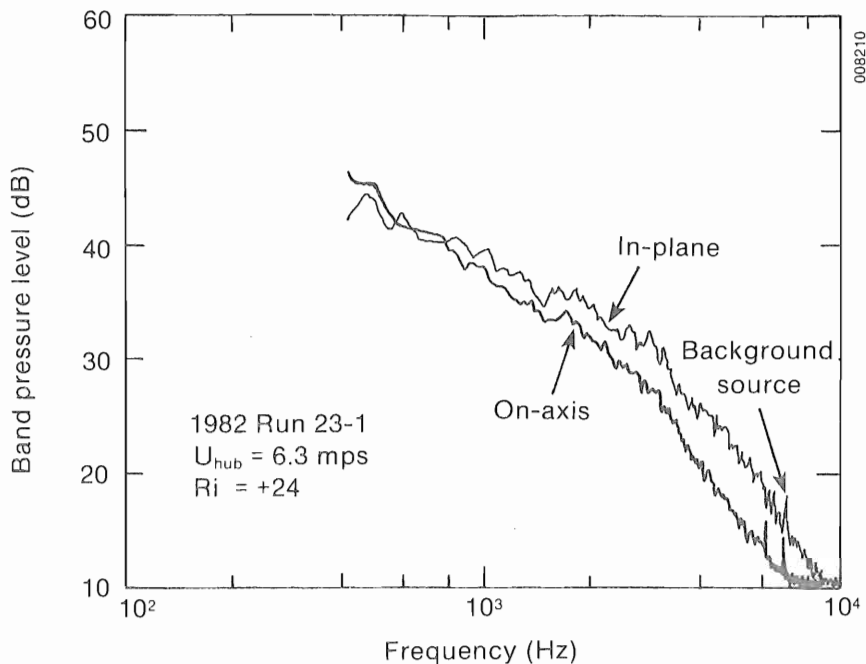


Figure 4-26. Representative 1982 HF-Range Narrowband ( $B_e = 12.5$  Hz) Spectra for Very Low Wind Conditions

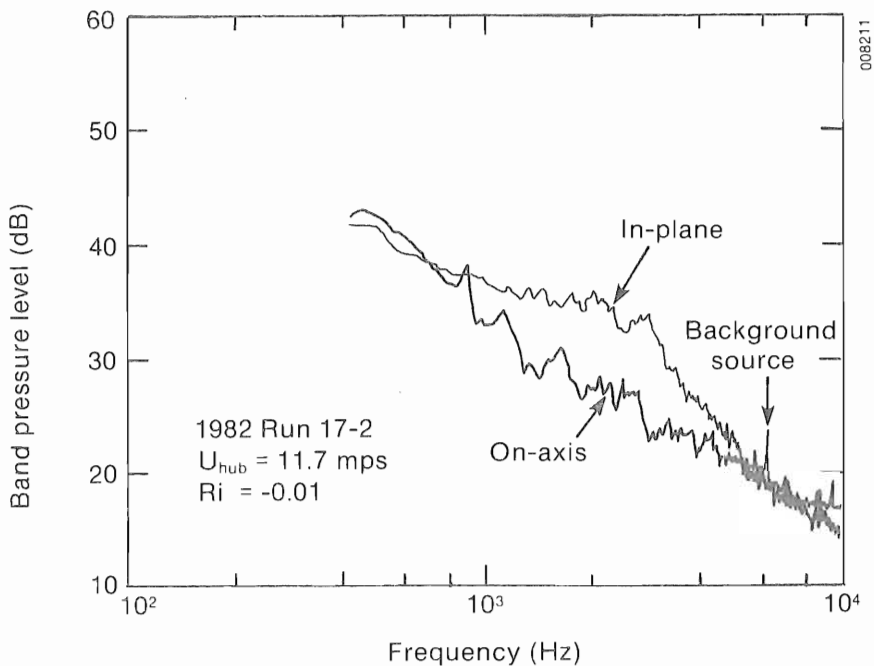


Figure 4-27. Representative 1982 HF-Range Narrowband Spectra for Moderate but Below-Rated Wind Conditions

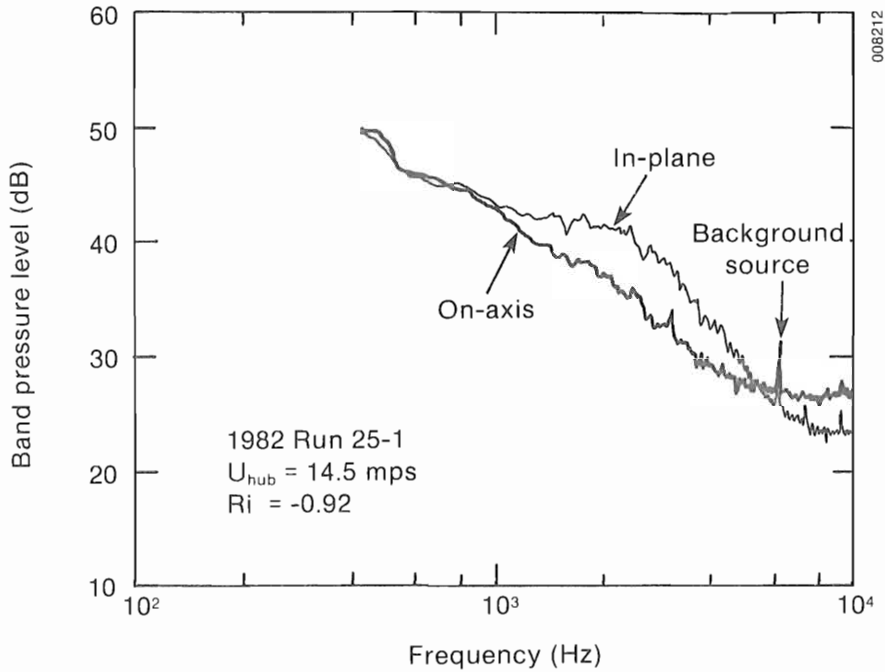


Figure 4-28. Representative 1982 HF-Range Narrowband Spectra for Above-Rated, Unstable Inflow Conditions

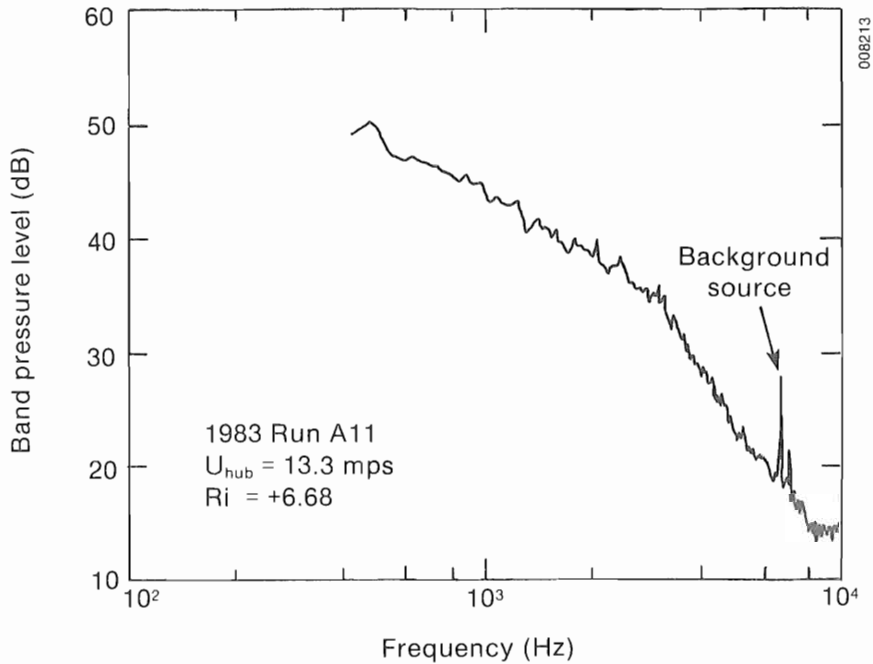


Figure 4-29. 1983 On-Axis HF-Range Narrowband Spectra for Above-Rated, Very Stable Inflow Conditions

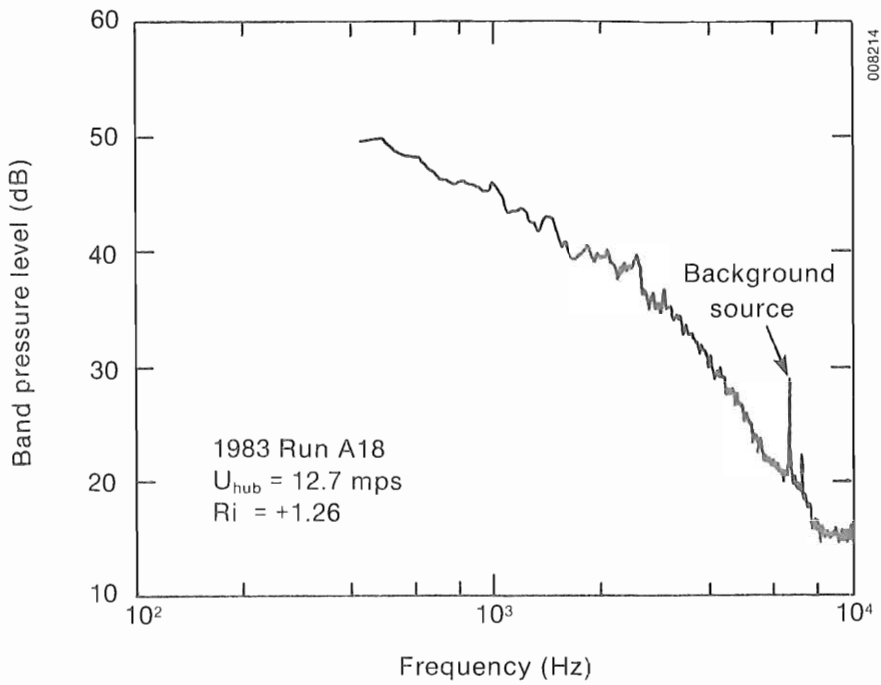


Figure 4-30. 1983 On-Axis HF-Range Narrowband Spectra for Near-Rated, Stable Inflow Conditions

## 5.0 CHARACTERISTICS OF LOW-FREQUENCY-RANGE EMISSIONS

In this section, we discuss the acoustic emissions characteristics of the MOD-2 design in the low-frequency-range (LF), nominally 5-100 Hz. Coherent or impulsive emissions in this frequency range were responsible for annoyance problems in several households within 3 km of the MOD-1 turbine near Boone, N.C., reported on in Refs. [1] and [19]. The acoustical loading of the homes affected by the MOD-2 LF emissions and subsequent internal acousto-mechanical interactions were responsible for the annoyance of the residents. Therefore, it is quite important not only to assess the MOD-2 emissions under a range of inflow conditions to determine the degree, if any, of similar characteristics, but also to identify the inflow properties responsible. In the MOD-1 case, the inflow was responsible for exciting Strouhal-type vortex shedding from the support tower legs, the ultimate cause of the coherent radiation. Since the MOD-2 rotor is upwind of its support tower, one would expect the source of coherent LF noise radiation to reside in the inflow structure itself. The question then arises of whether or not combinations of inflow structure and coupled rotor aerodynamic response could be responsible for coherent noise levels similar to that of the MOD-1.

In this section, we use both direct and ensemble statistical approaches to identify efficient inflow predictors for correlating the radiated 1/3-octave-band spectrum levels. We also apply a number of statistical measures of coherent noise radiation developed for characterizing the MOD-1 to the MOD-2 data and compare the results. Finally, we use available blade surface pressures, aeroelastic measurements, and radiated acoustic pressure fields to define the physical space scales in the inflow responsible for LF noise produced by the MOD-2 rotor.

### 5.1 Influence of Rotor Inflow Structure on LF Noise Spectra

#### 5.1.1 MOD-2 Aeroacoustic Response Function

An objective of this study was to determine, by experimental methods, the observed aeroacoustical response function of a MOD-2 turbine. This, of course, assumes that the turbulent inflow structure is the sole excitation and that it can be quantified in some manner in order to be successfully related to the radiated acoustic pressure spectrum. We have taken two approaches to this task. One, the direct approach, was based on taking the power spectra ratio of simultaneously measured inflow turbulence and radiated acoustic signals. In the other approach, we used the statistics of randomly sampled ensembles of the 1/3-octave acoustic spectra as the dependent variables and five bulk or characteristic properties of the inflow as the independent variables in a multivariate regression model. Both approaches are discussed below.

##### 5.1.1.1 Direct Measurement Approach

During our 1983 data Run No. A05, the tethered balloon instrument package, with the hot-film anemometer installed, was flown in the Turbine No. 2 inflow at approximately hub height. The orientation of the hot-film sensor (a 0.15-mm diameter, quartz-coated wire) in the flow was such that the electrical output was proportional to the vector sum of the local longitudinal and vertical (upwash) components of the turbulent wind. The nonlinear electrical

signal was transmitted via a digital FM radio telemetry link to a ground receiver, where the signal was re-converted to an analog voltage, linearized, and recorded on FM magnetic tape. The dynamic range of the radio telemetry link was better than 70 dB with a data bandwidth of 125 Hz. The bandwidth of the final FM tape recording was limited to 100 Hz, however.

Because of the nonstationary nature of the inflow, the 30-minute data run was divided into six 5-minute segments. The particular 5-minute period discussed here was chosen because it exhibited minimal variation in height of the anemometer (a standard deviation of  $\pm 6$  m) and contained substantial levels of high-frequency turbulence. Table 5-1 summarizes the pertinent operational and inflow characteristics associated with this run segment.

We chose a vertical window of  $\pm 10$  m from the mean hot-film anemometer height as the region of the rotor disk from which we would correlate the acoustic output at the 1.5D measuring station. This choice resulted in defining the two disk segments pictured in Figure 5-1. By delaying the data conversion and Fourier transformation a fixed amount from the time the rotor blade was parallel to the tower base, we could start the 0.5-second conversion period to coincide with the windows shown in Figure 5-1. The inflow turbulence signal was delayed in time equivalent the mean convection speed, 7.4 mps. The acoustic spectra were delayed an additional 0.5-second with respect to the turbulence signal to allow for the sound propagation (retarded) time from the disk segment to the microphone array. The resulting averaged spectra were calculated from ten 4-second records containing 80 blade passages and 81,920 data points.

The measured LF acoustic response (spectral ratio) in Pa/mps is plotted in Figure 5-2 over a frequency range of 2-100 Hz with an effective bandwidth (resolution) of 2 Hz. The abscissa has also been scaled in units of the reduced frequency parameter  $k$  defined by  $k = \pi cf/U$ , where  $c$  is the chord length and  $U$  the relative blade speed at 80% span. An interesting result is achieved if the response spectrum of Figure 5-2 is plotted against the turbulent wavelength (assuming the frozen turbulence hypothesis) as in Figure 5-3, in which the location of the integral scale is also shown. Since one interpretation of the integral scale is that it represents the largest

**Table 5-1. Summary of Important Turbulence Excitation and Turbine Operation Flow Angles for the Analyzed Segment of Run A05**

---

Turbulent Layer Structure Parameters

---

Mean measurement height (above the tower base)	78 $\pm$ 6 m
Mean horizontal wind speed	7.39 mps
Turbulence intensity	8.0%
Layer turbulence integral scale length	2.89 m

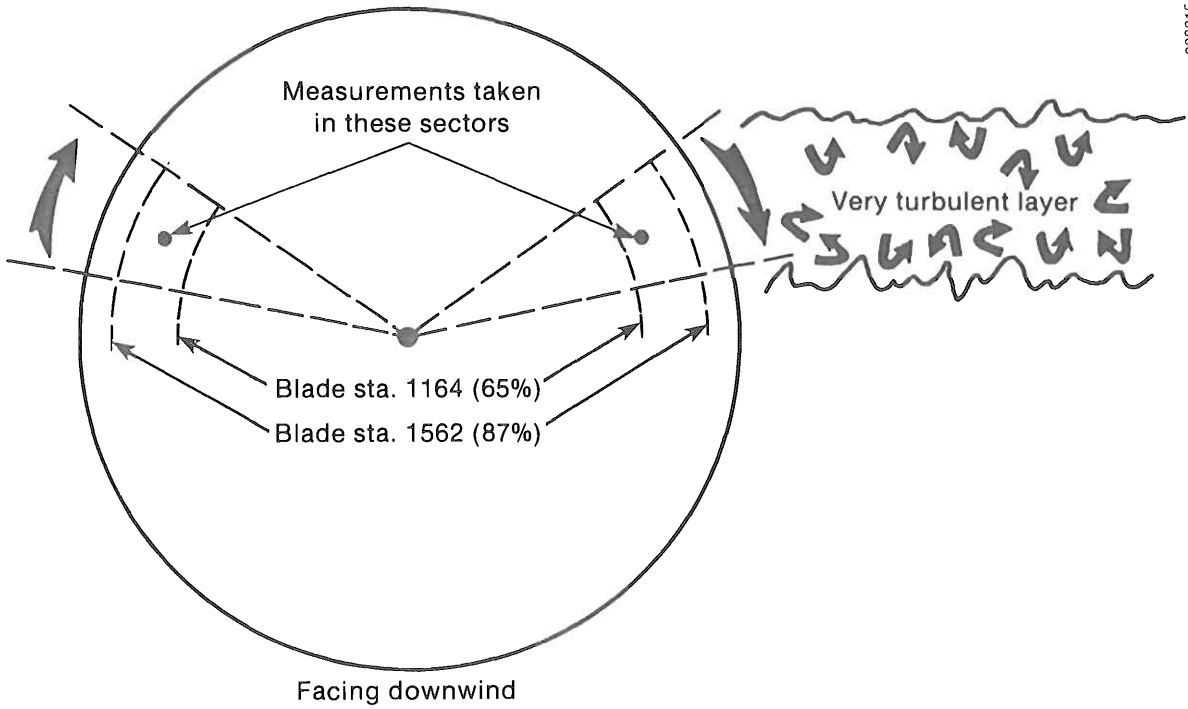
---

Turbine Operating Angles

---

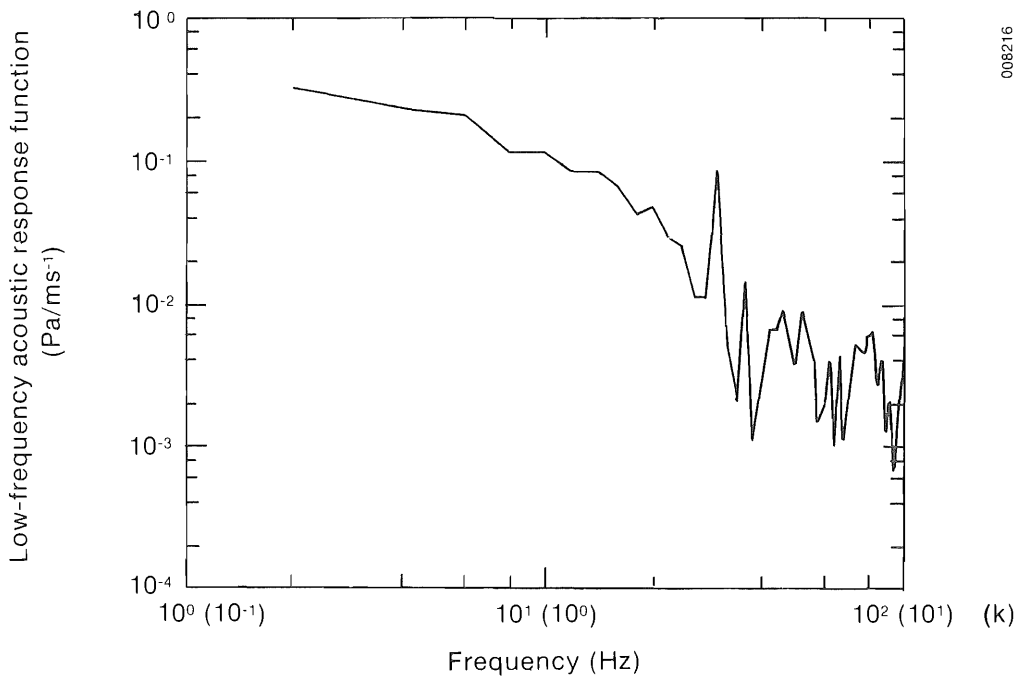
Indicated mean blade angle (ref. at Sta. 1260)	+0.62°
Calculated mean angle of attack (Sta. 1164)	11.6°
Calculated mean angle of attack (Sta. 1562)	9.6°

---



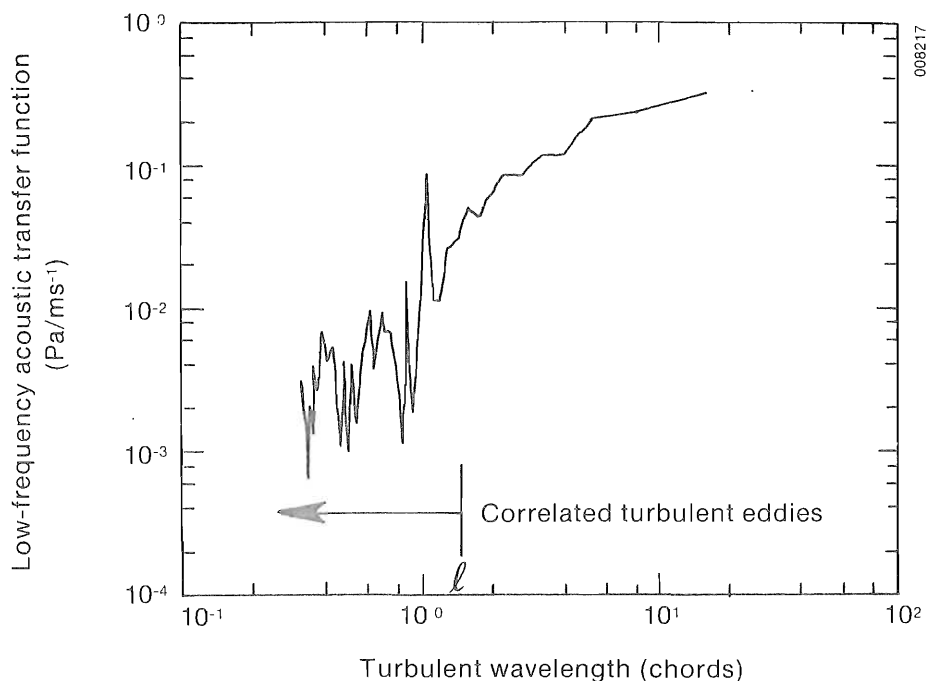
008215

Figure 5-1. Relationship of Location of Measurements on Blade No. 1, Rotor Disk Geometry, and Height of Elevated Turbulent Layer



008216

Figure 5-2. Measured Low-Frequency Acoustic Response Function



**Figure 5-3. Measured Low-Frequency Acoustic Response as a Function of Turbulent Space Scale**

correlated eddy size in the flow, it is clear from Figure 5-3 that the characteristics of the radiated spectrum appear to change at that boundary.

#### 5.1.1.2 Inflow Bulk Scaling Parameter/Multivariate Modeling Approach

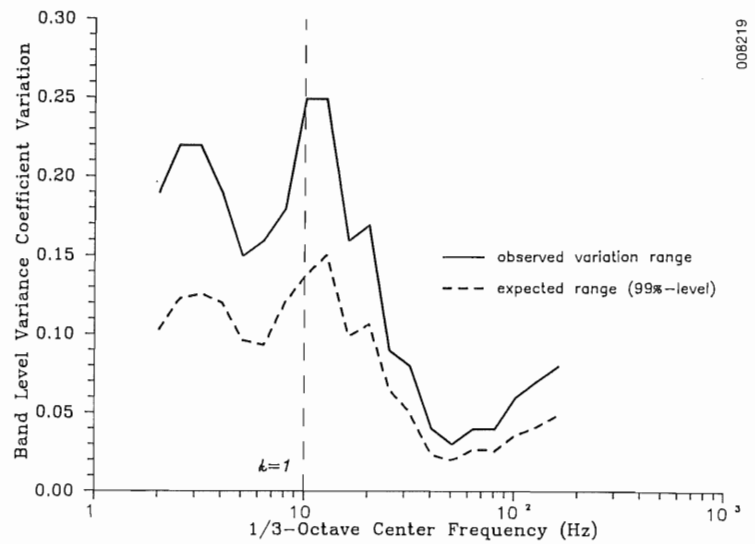
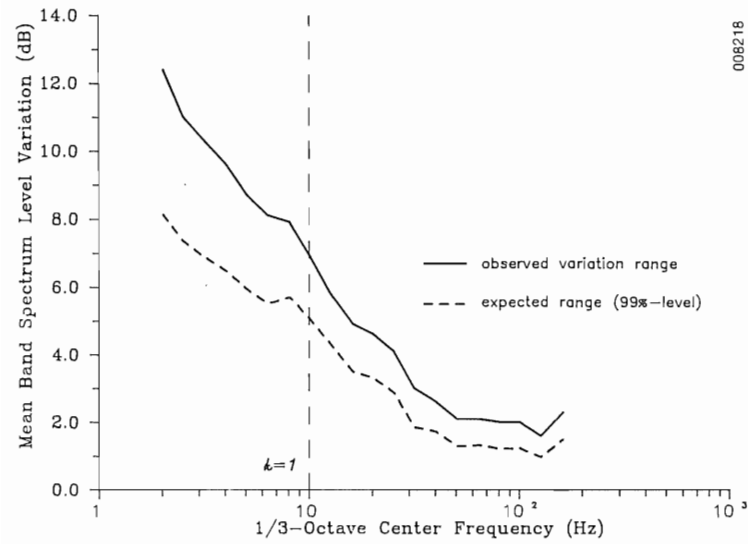
As explained in Section 2.4, ensemble statistics (up through and including the 4th moments) of the LF emissions spectra in 1/3- and octave-band resolution listed in Table 2-2 were compiled from 100 random samples of the MOD-2 far-field acoustic signals for each of the three, 10-minute segments of each data run. The resulting statistics were then averaged together to form the aggregate statistical record for the run. A similar approach was used for background measurements, but it was only 10 minutes in length and no averaging was necessary. Measures of the inflow bulk or characteristic scaling parameters (e.g., a reference-height mean horizontal wind speed  $U_H$ , the rotor disk gradient Richardson number  $Ri$ , and various turbulence length scales measured at a reference height) were compiled as discussed in Section 2.4.2.

#### Statistical Significance of Observed Run-to-Run Variations

Before attempting to correlate the observed run-to-run variations in the measured far-field acoustic emissions spectral statistics with inflow characteristics, we compared the observed variations to what would be expected for completely random fluctuations. Figures 5-4a, b, c, and d plot the observed run-to-run variations for the 1/3 octave band means and variance, skewness, and kurtosis coefficients. Also included in these figures are the variations which would be expected from a purely random noise process at the

mbal-range-comp

bi-covar-range-comp

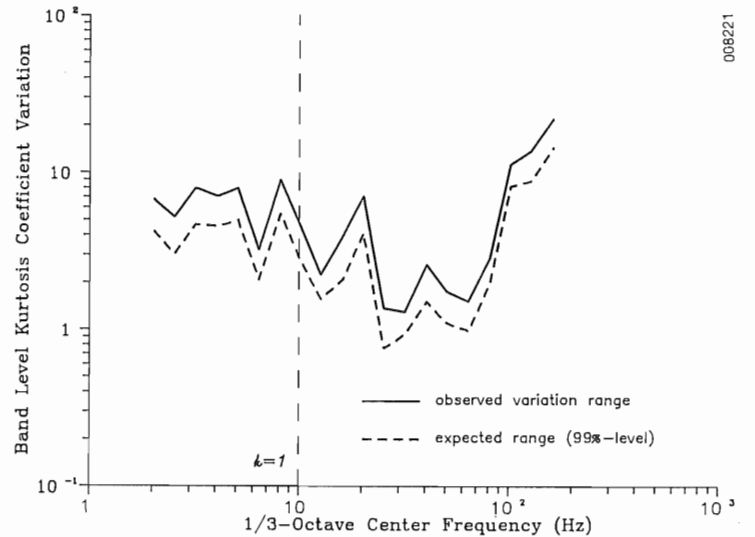
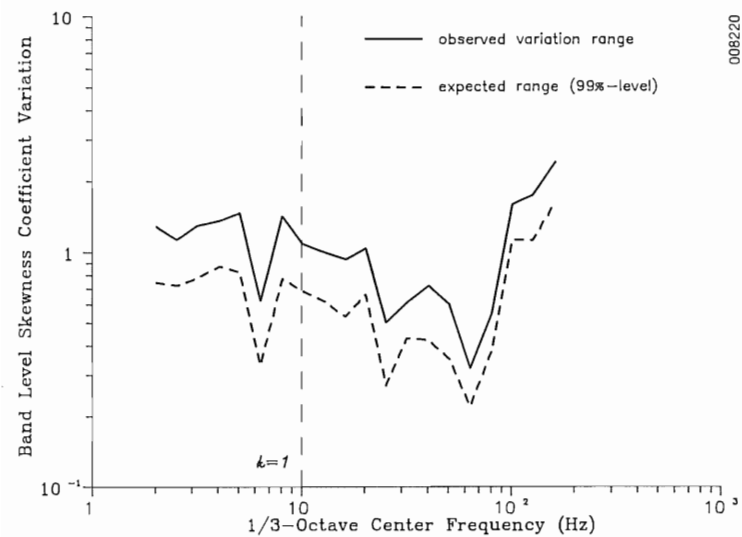


(a) mean BSL comparison

(b) variance coefficient comparison

bi-skew-range-comp

bi-kurt-range-comp



(c) skewness coefficient comparison

(d) kurtosis coefficient comparison

**Figure 5-4. Comparisons of the Observed Run-to-Run Variations of the BSL Mean and First Three Statistical Moments and the Variations Expected from a Purely Random Process.**

99% confidence level. These plots show that significant run-to-run variations did occur in the four statistical moment distributions. The  $k = 1$  line, shown in these figures, represents the acoustic (cyclic) frequency corresponding to an aerodynamic reduced frequency,  $k$ , of unity where  $k = n_c/V_c$  ( $c$  is the chord length and  $V_c$  the convection velocity at an effective spanwise radius of 75%.

### Choosing Multivariate Model Characteristic Inflow Predictors

In the specification of a multivariate regression model, one strives to choose independent variable predictors. While being sensitive to the predicted quantity, these variables are uncorrelated with one another; i.e., to minimize the degree of multicollinearity present. Unfortunately, in dealing with atmospheric inflow variables, this is often an impossible task. Under homogeneous flow conditions, the Monin-Obukov similarity theory gives us an independent set of turbulence predictors. However, for inhomogeneous flows, like those at the Goodnoe Hills site, the degree of collinearity between predictor variables can be minimized but not eliminated entirely.

Ideally, we would like to arrive at a set of independent variables which would adequately describe the inflow state in order to predict the ensemble statistical behavior of the observed spectral characteristics of the far-field acoustic emissions. We know from the work of Homicz and George (see Section 3.1) that these predictors should be representative of a mean axial convection velocity,  $V_c$ , and the accompanying turbulence scales and intensities. Coupling this requirement with the influence of surface layer similarity (see Section 3.2), we saw that the hydrodynamic stability has a strong influence on these parameters. Thus, a set of inflow state predictors should include parameters which serve as a representative measure of the

- mean inflow velocity;
- disk layer hydrodynamic stability;
- turbulence intensities; and
- characteristic turbulence scales.

From Table 2-5, available measures of mean inflow (axial convection velocity) included observations near the hub-height (59 m) and at the hot-film anemometer, located at a 45-m elevation on the BPA Met Tower. The variation of mean wind speed with height was shown in Section 3.2.2. This parameter varies as a function of the surface shear-stress or friction velocity,  $u_*$ , and roughness (fetch) or  $z_0$  and stability. Measures of the inflow stability included the disk gradient Richardson number,  $Ri$ , the Monin-Obukov length,  $L$ , and the  $z/L$  parameters. The vertical variation of turbulence intensity was shown in Section 3.2.3. It varies as a function of stability, mean wind speed, and  $u_*$ . Observations of the amount of small-scale turbulence present at the 45-m height are available as the 1-10 Hz-band mean square values for the longitudinal and vertical components. Available characteristic turbulence length scale measures include 45-m elevation observations of

- the  $I_{u,x}$ ,  $I_{w,x}$ , and  $I_{w,z}$  integral scales; and
- the longitudinal and vertical reduced frequency spectral peaks,  $f_{mu}$  and  $f_{mw}$ .

The degree of bivariate correlation for the turbulence intensities and scales versus the representative mean velocity, stability, and roughness parameters are shown in Table 5-2. The cross-correlation matrix for the stability,

velocity, and roughness scales is shown in Table 5-3. As is apparent by the content of these tables, there are few inflow characteristic scales which are completely independent of one another, thus, raising the degree of multicollinearity in multivariate models where they are used as independent variables.

### Inflow Stability

Because of the lack of independence in most of the available inflow characteristics scales, we have more thoroughly examined the inter-relationships between these parameters. For example, using one-way analysis of variance (ANOVA) techniques, we examined the percentage of observed variation in the longitudinal and vertical 45-m level turbulence components ( $u'$ ,  $w'$ ), explained by a multivariate model consisting of the

**Table 5-2. Bivariate Correlation Coefficients for Inflow Turbulence Scales and Intensities versus Stability, Velocity, and Roughness**

	$I_{u^x}$	$I_{w^x}$	$I_{wz}$	$f_{\mu}$	$f_{mw}$	$\overline{\langle S_u \rangle^2}$	$\overline{\langle S_w \rangle^2}^a$
<u>Stability</u>							
Ri	.332	-.277	-.492	-.455	.170	-.249	-.604
z/L	-.200	-.848	-.932	.132	-.207	-.217	-.791
L	-.225	-.248	-.134	.267	.342	.639	.937
<u>Velocity</u>							
$U_{45}$	.586	-.538	-.428	-.609	.202	.598	-.222
$U_H$	.593	-.541	-.365	-.502	.317	.697	-.084
$u_*$	.562	-.263	-.044	-.604	-.617	.733	.269
<u>Roughness</u>							
$z_o$	.397	-.577	-.732	-.648	.116	-.191	-.710

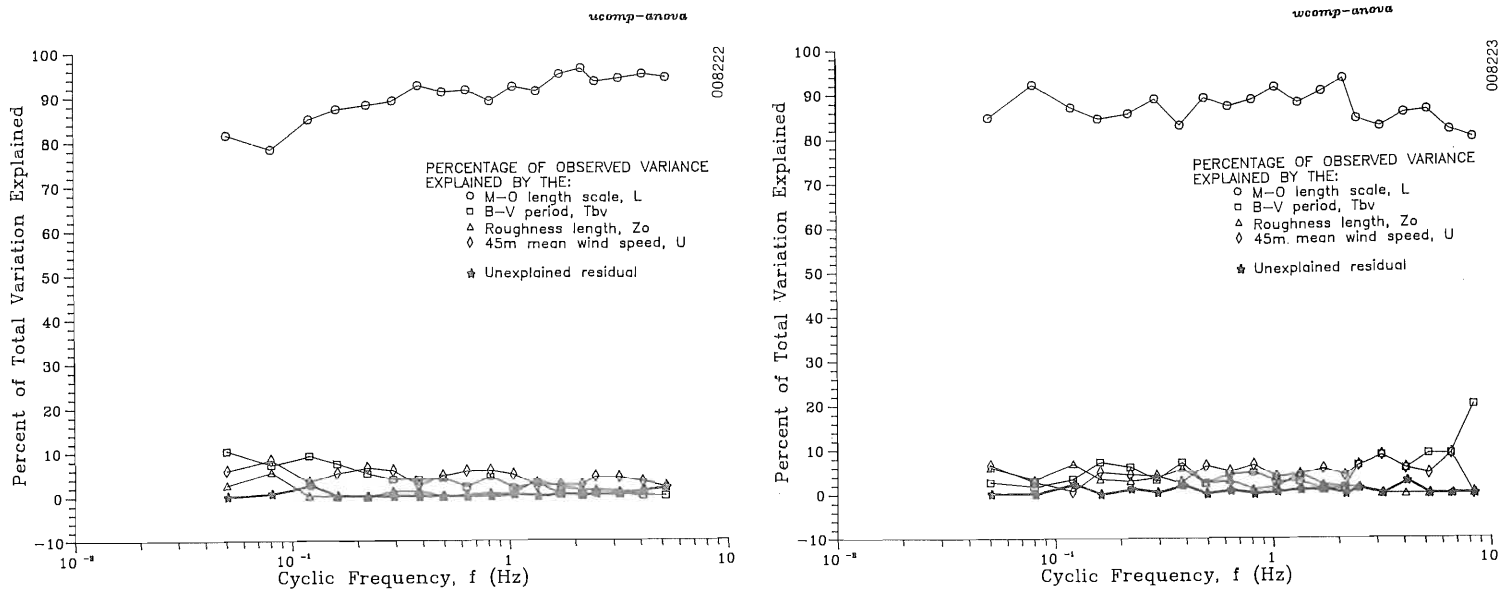
<sup>a</sup> $\langle S_{u,w} \rangle = 1-10$  Hz band mean square value.

**Table 5-3. Cross-Correlation Matrix for Stability, Velocity, and Roughness Predictors**

	Ri	z/L	L	$U_{45}$	$U_H$	$u_*$	$z_o$
Ri	-	.374	-.121	.118	-.017	.097	.517
z/L	.374	-	.443	.297	.319	.103	.523
L	-.121	.443	-	.175	.239	.475	.266
$U_{45}$	.118	.297	.175	-	.981	.814	.460
$U_H$	-.017	.319	.239	.981	-	.816	.403
$u_*$	.097	.103	.475	.814	.816	-	.576
$z_o$	.517	.523	.266	.460	.403	.576	-

- o M-O length scale,  $L$ ;
- o disk Brunt-Väisälä period,  $T_{BV}$ ;
- o roughness length,  $z_0$ ; and the
- o 45-m mean wind speed,  $U_{45}$ .

Figures 5-5a and b demonstrate that, on average, 90% of the observed spectral variance in these turbulence components is related to changes in the inflow stability. We have found that the hydrodynamic stability of the rotor disk layer, as expressed by the Richardson number parameter, strongly varies with the time-of-day at the Goodnoe Hills site. This can be seen for the period of 1600-2400 h local standard time (LST) in Figure 5-6. In the figure, the 30-minute disk Richardson number is plotted for 25 data runs from both the 1982 and 1983 experimental periods. The shift from unstable to stable inflow conditions is seen to take place rather abruptly in the vicinity of 1630 hours. The 1983 data set contained much more stable runs than those of 1982. These runs are depicted as a function of time in Figure 5-7 with the most stable conditions occurring after 1930 h LST.



(a) longitudinal component

(b) vertical or in-plane component

Figure 5-5. Spectral Run-to-Run Variation ANOVA Results for the 45-m Longitudinal (u) and Vertical or In-Plane (w) Turbulence Components

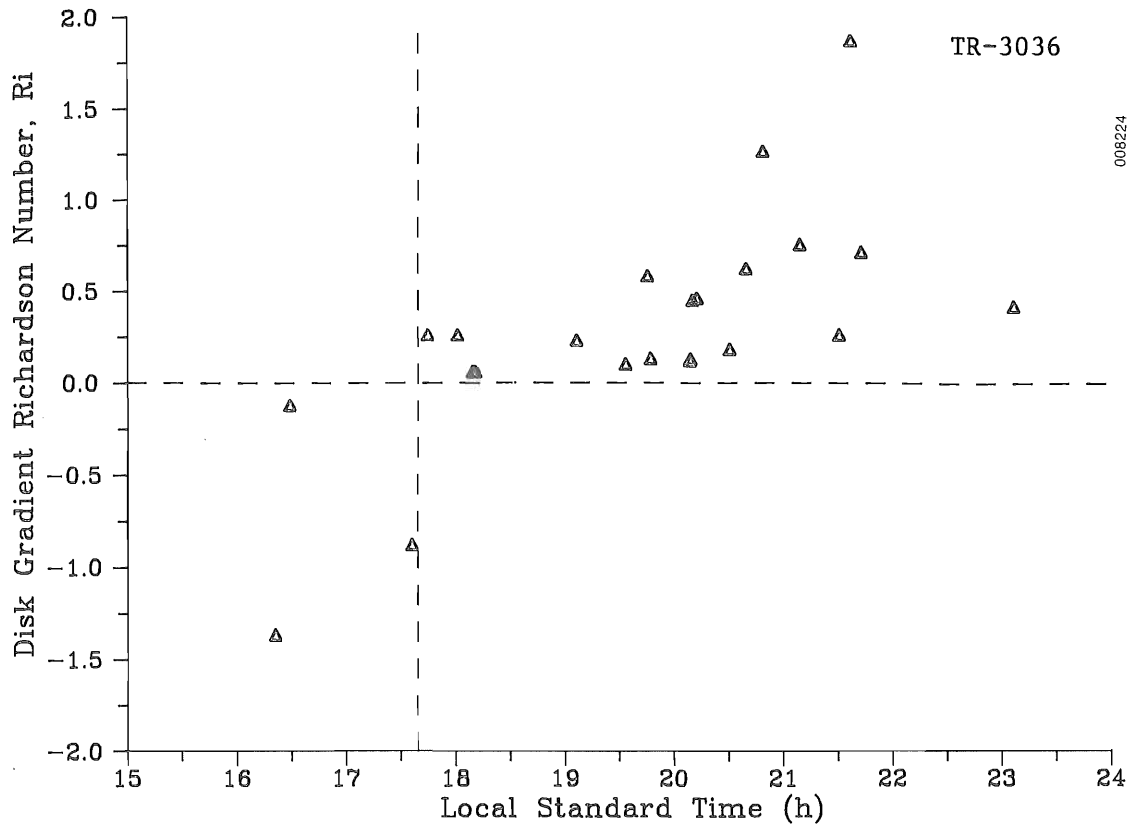


Figure 5-6. Observed Variation of the Disk Gradient Richardson Number as a Function of the Time-of-Day for the Combined 1982/83 Experimental Periods

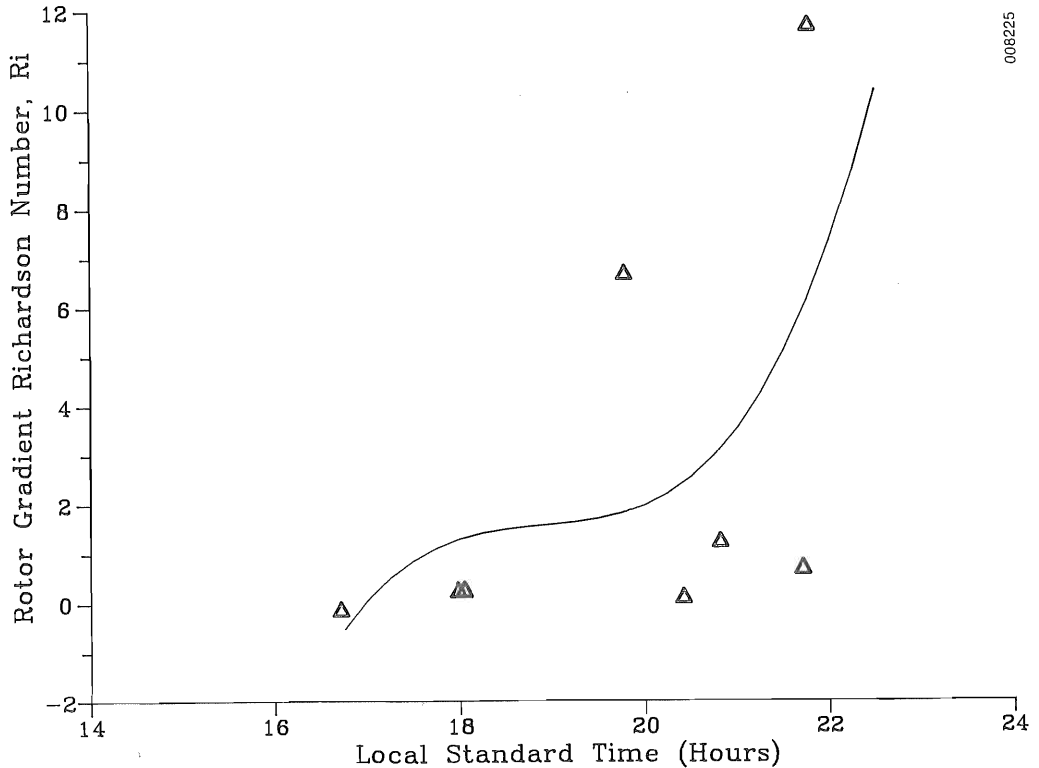


Figure 5-7. Observed Variation of the Rotor Gradient Richardson Number for the Combined 1982/83 Experimental Periods

### Influence of Stability on Mean Wind Speed

The change from unstable to stable inflow conditions was found to have a pronounced effect on the character of the mean wind speed profile. Figure 5-8 plots the combined 1982/83 hub-height mean wind speed values ( $U_H$ ) as a function of the disk,  $Ri$ , between -1 and +2. The tendency for a step-up in speed under stable flow conditions is apparent. One reason why there are not many data points in the unstable region is that prior to about 1600 h the winds were generally below the turbine cut-in speed ( $\sim 6$  m/s). Figure 5-9 shows the 1982/83 variation of  $U_H$  with the time span corresponding to our data collection period. While at first glance there appears to be considerable scatter, a closer inspection reveals the tendency for a dual grouping of points into high- and low-speed sets in the stable flow, present after about 1900 h. The least-squares trend line reveals the tendency towards maximum  $U_H$  values in the vicinity of 2000 h and a trend towards another maximum after 2230 h. The high mean wind point in the unstable region prior to 1630 h was related to a 1982 case in which a passing upper atmosphere disturbance was influencing the normal diurnal wind speed variation.

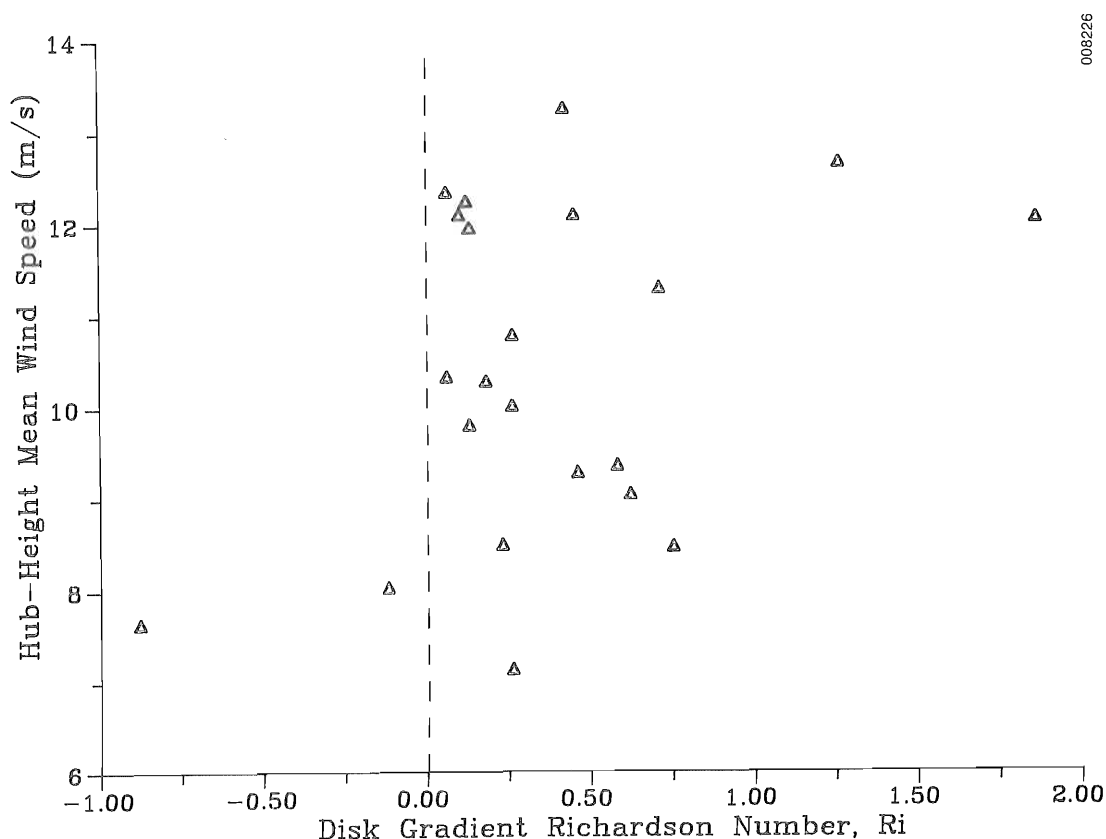


Figure 5-8. Observed Variation of the Mean Hub-Height Wind Speed as a Function of the Disk Gradient Richardson Number for the Combined 1982/83 Experimental Periods

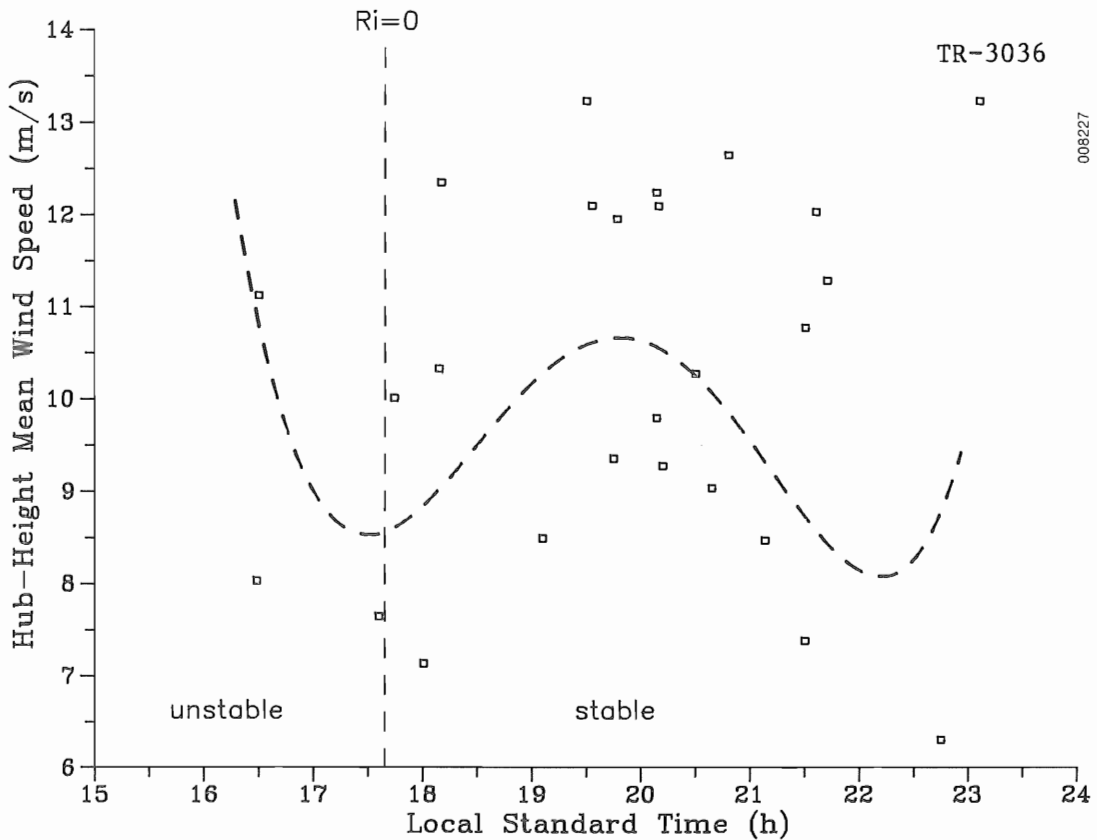


Figure 5-9. Observed Variation of the Mean Hub-Height Wind Speed as a Function of the Time-of-Day for the Combined 1982/83 Experimental Periods

The 1983 variation of the observed height of the PNL Tower peak mean wind speed is plotted as a function of the disk Richardson number in Figure 5-10. The amplitude at this height and time of occurrence are shown in Figures 5-11 and 5-12, respectively. The horizontal dashed lines in the latter two figures correspond to the turbine cut-in (6 m/s) and cut-out (20 m/s) velocities. The variation of the mean wind speed vertical profile,  $U(z)$ , as a function of the Richardson number is displayed in Figure 5-13.

Influence of Stability on Characteristic Turbulence Scales

The relative sensitivity of the 45-m mean wind speed ( $U_{45}$ ) and the characteristic turbulence scales to the disk Richardson number are shown in Figures 5-14 and 5-15. The relationship between  $U_{45}$  and the 45-m level longitudinal and vertical turbulence integral scales  $I_{u,x}$  and  $I_{w,z}$  are plotted in Figure 5-14. Figure 5-15 plots the relationship for  $U_{45}$  and the reduced frequency peaks associated with the longitudinal and vertical component spectral peaks,  $f_{mu}$  and  $f_{mw}$ . The observed relationship between the component integral scale lengths ( $I_{u,x}$  and  $I_{w,z}$ ) and the spectral peak reduced frequencies are plotted in Figures 5-16a and b. While the expected inverse relationship between the longitudinal characteristic scales seems to exist, the scatter in the vertical component scales resists specific classification for this small sample.

Influence of Stably-Stratified Inflow on Turbulent Energy Distribution

The inflow structure at the Goodnoe Hills site follows a pronounced diurnal cycle, particularly in the summer month's when the peak energy production was achieved. Figure 5-17 plots the hourly mean wind speed normalized by the

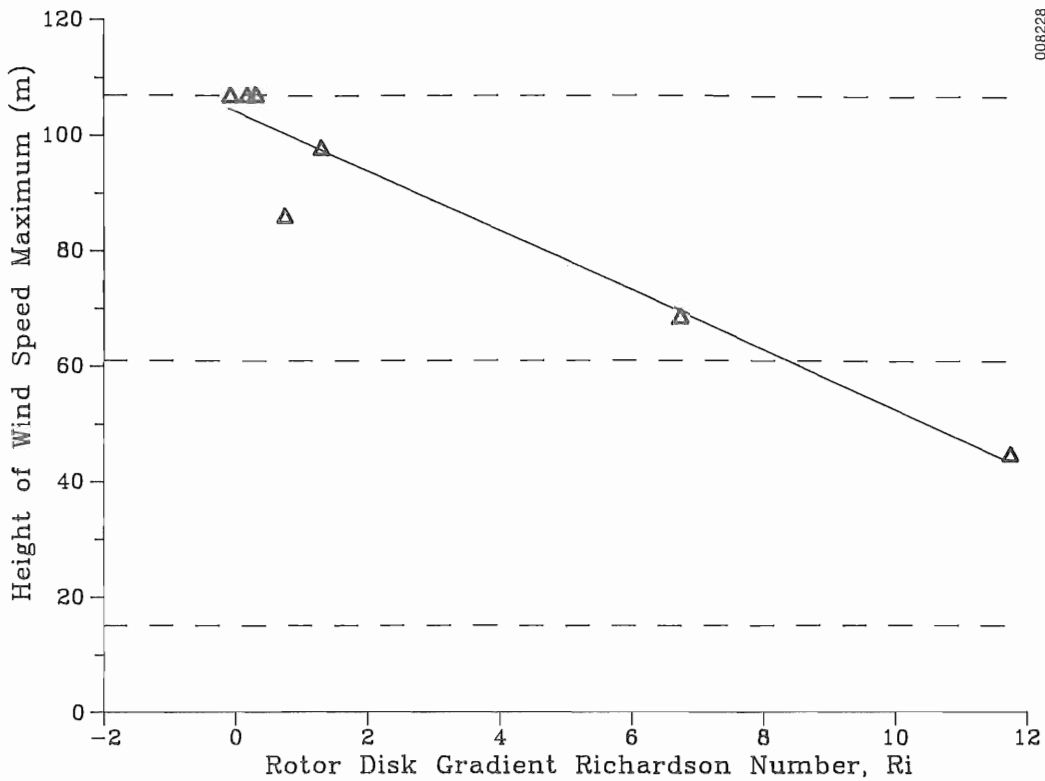


Figure 5-10. Observed Variation of the Height of the Mean Wind Speed Maximum as a Function of the Gradient Richardson Number for the 1983 Experimental Period

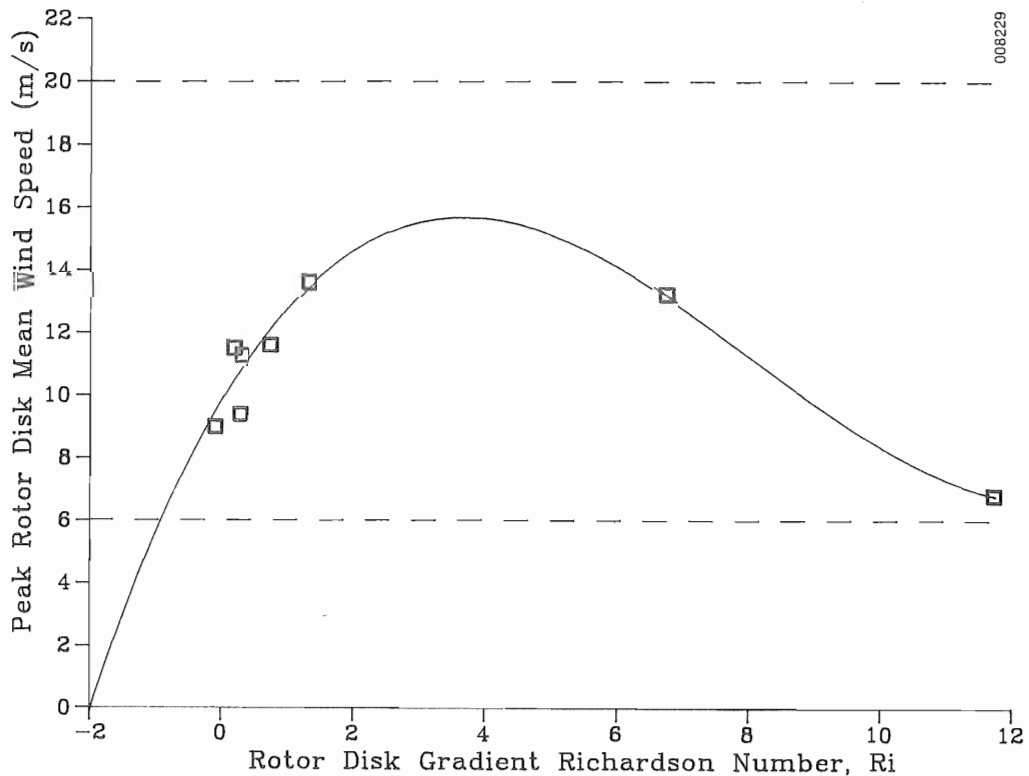
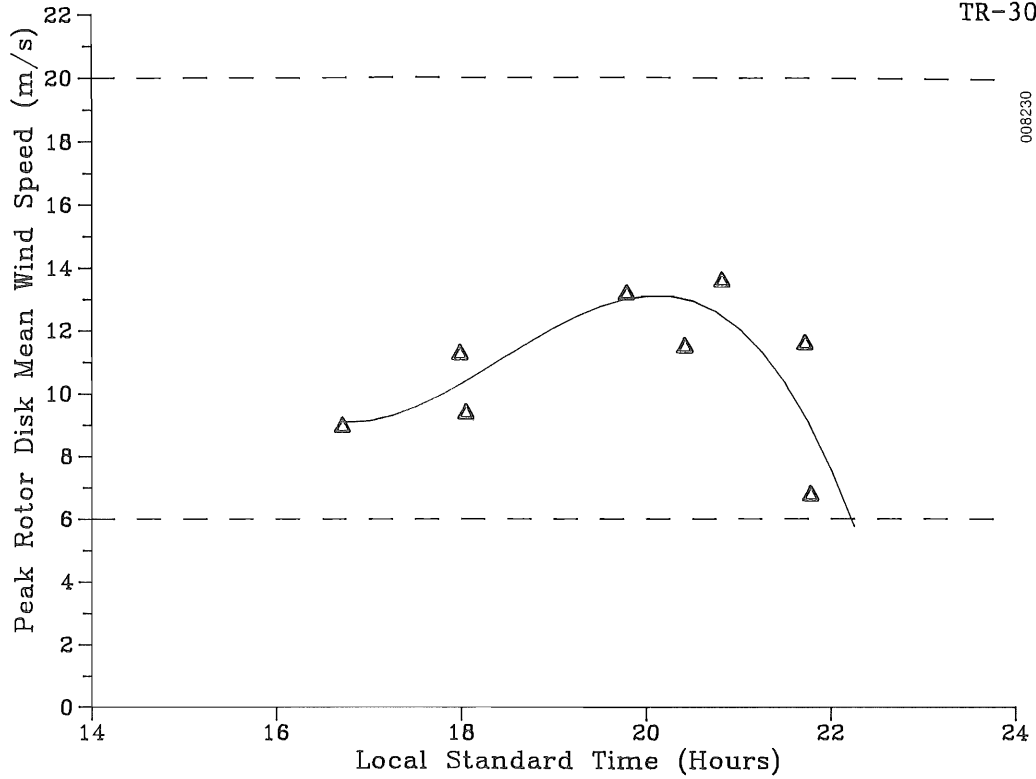
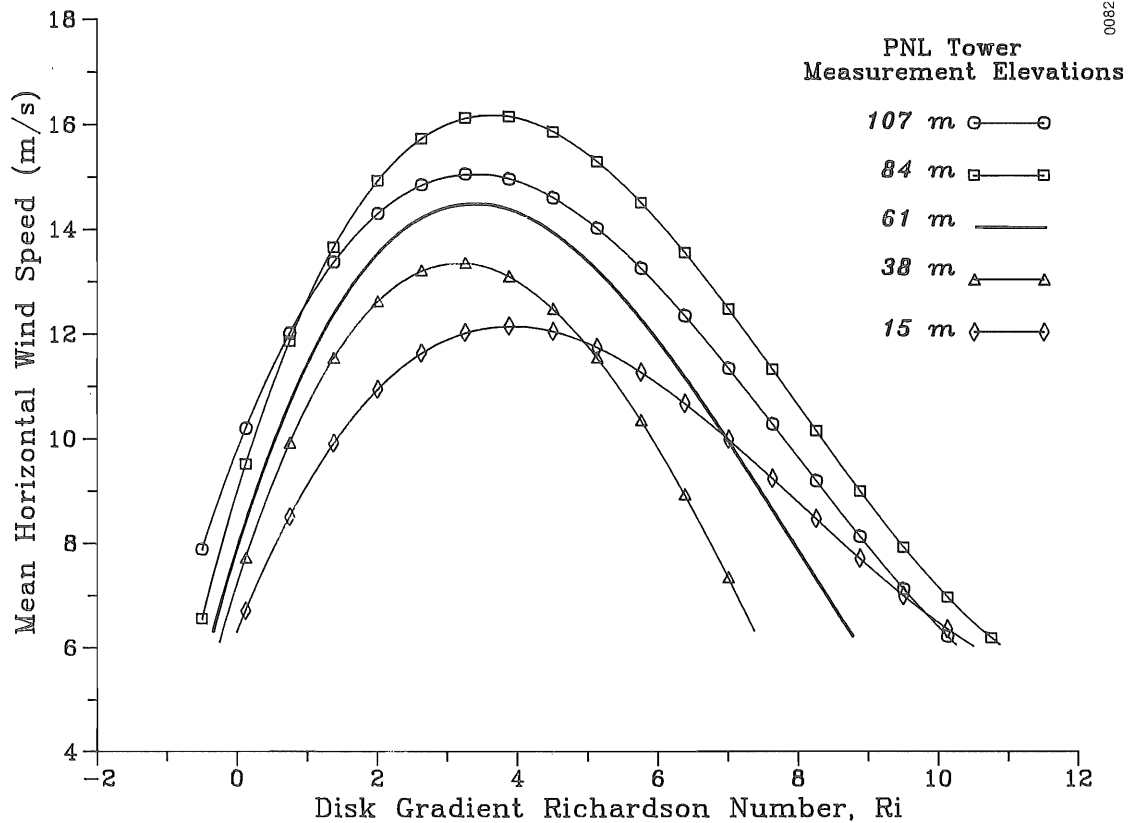


Figure 5-11. Observed Rotor Disk Maximum Mean Wind Speed as a Function of the Richardson Number for the 1983 Experimental Period



008230

Figure 5-12. Observed Rotor Disk Maximum Mean Wind Speed as a Function of the Time-of-Day for the 1983 Experimental Period



008231

Figure 5-13. Observed Variation in the Mean Wind Speed at the Five Levels of the PNL Tower as a Function of the Gradient Richardson Number for the 1983 Experimental Period

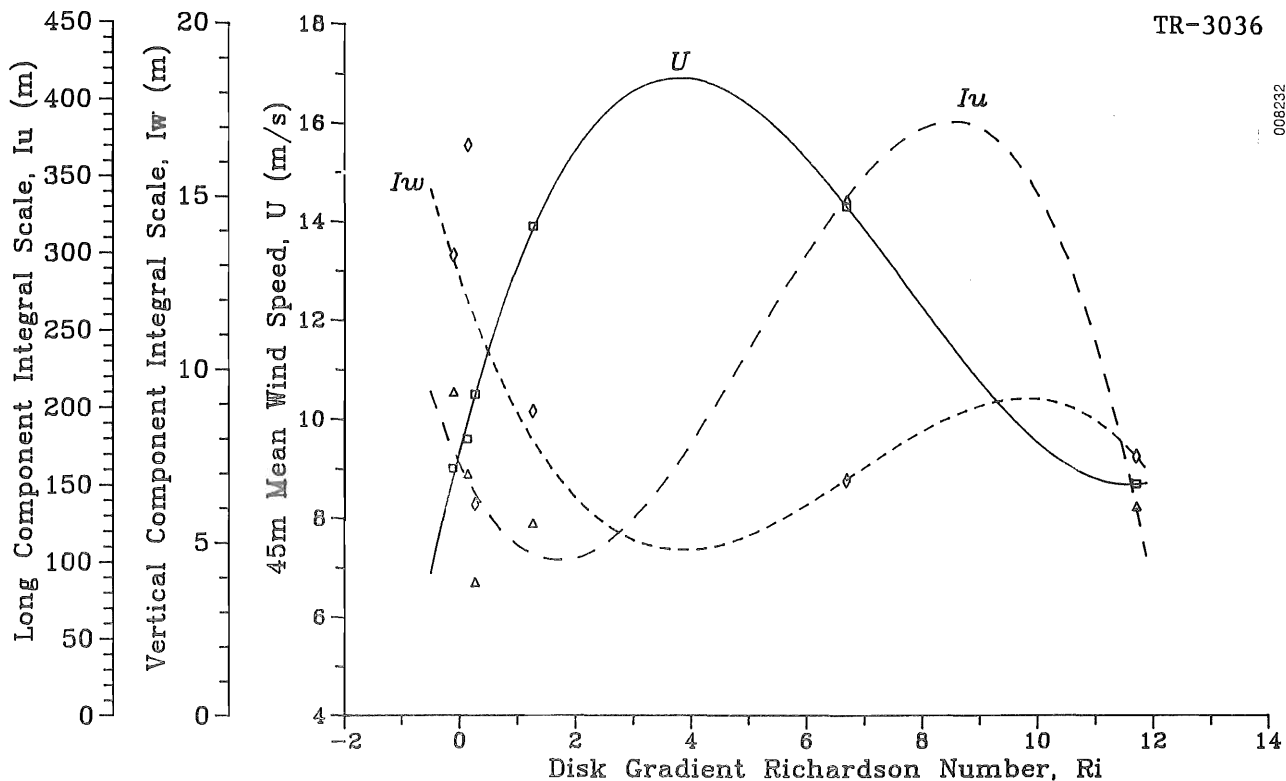


Figure 5-14. Observed Variation of the Mean 45-m Horizontal Wind ( $U$ ) and the Horizontal ( $I_{u,x}$ ) and Vertical ( $I_{w,z}$ ) Length Scales as a Function of the Richardson Number

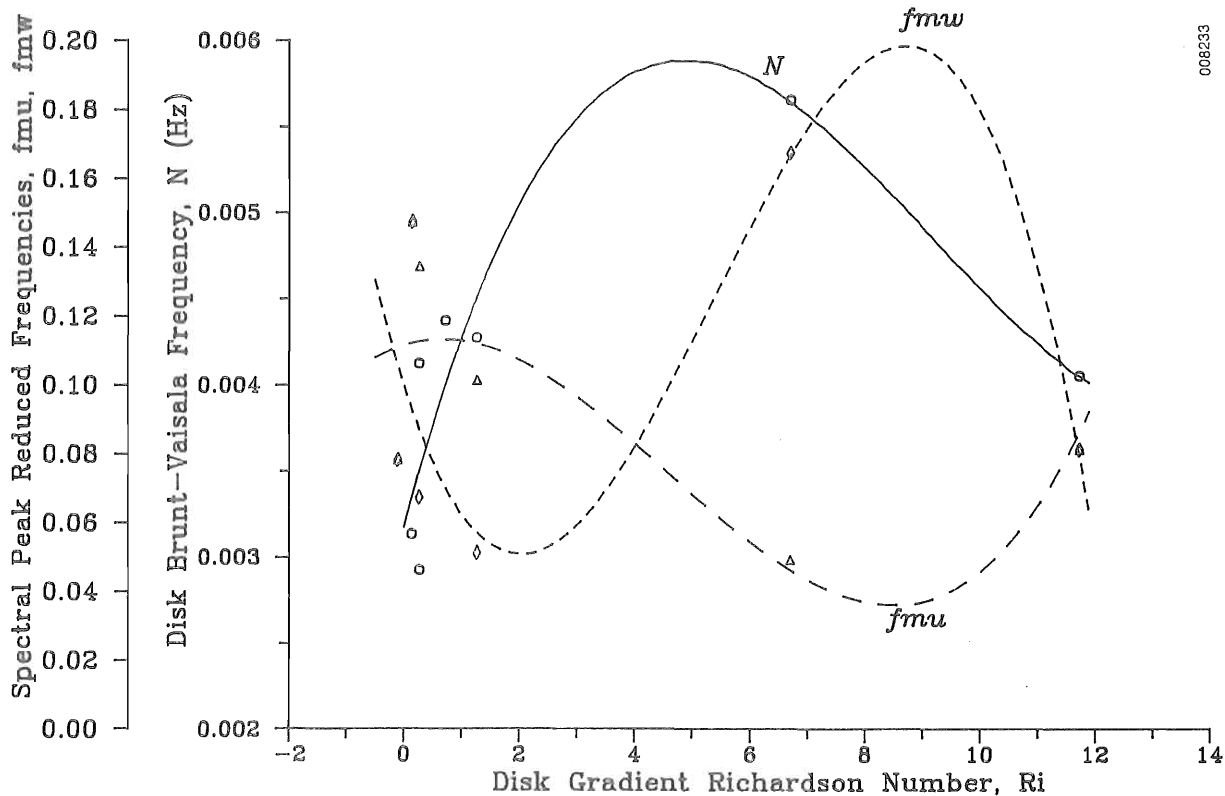
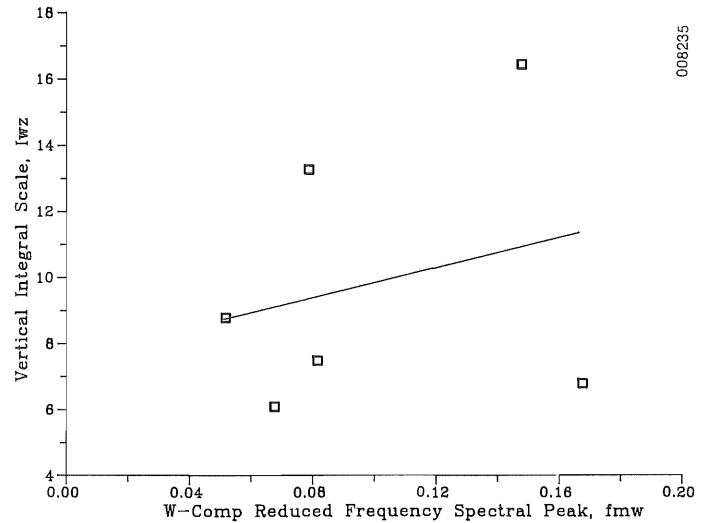
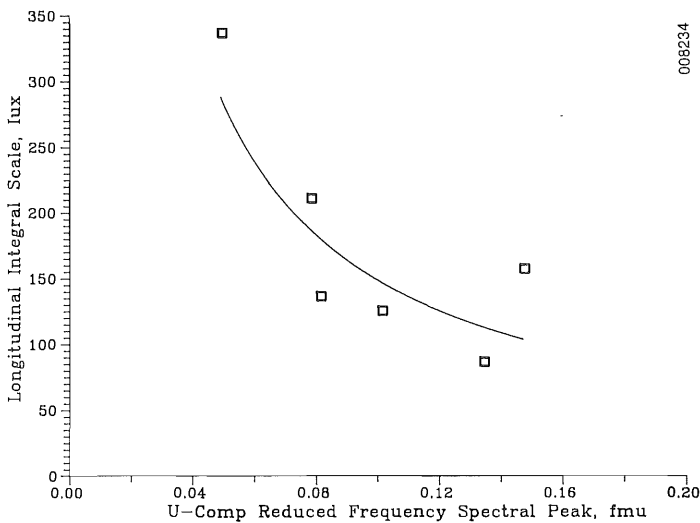


Figure 5-15. Observed Variation of the Mean 45-m Horizontal Wind Speed ( $U$ ) and Horizontal ( $f_{\mu}$ ) and Vertical ( $f_{mw}$ ) Spectral Peak Reduced Frequencies as a Function of the Richardson Number



(a) Variation of  $I_{u,x}$  Versus  $f_{\mu}$

(b) Variation of  $I_{w,z}$  Versus  $f_{mw}$

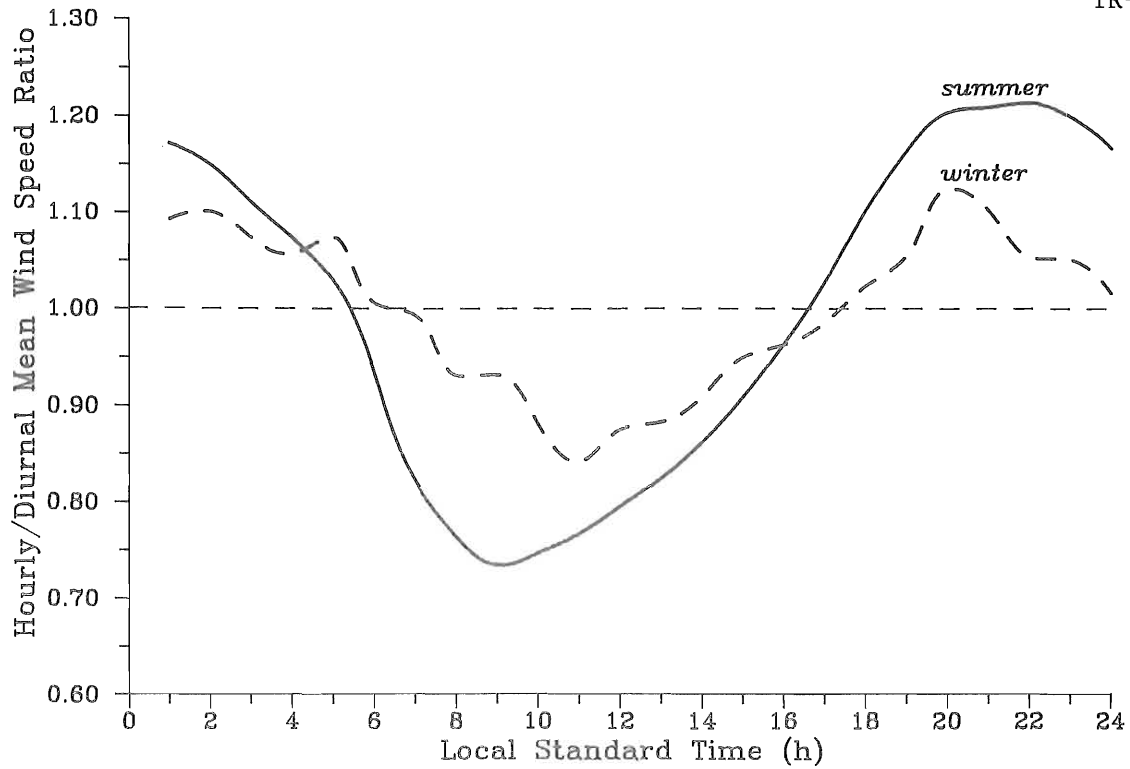
**Figure 5-16. Observed variations of the 45-m Horizontal and Vertical Length Scales as Functions of the Spectral Frequency Reduced Frequencies**

daily or diurnal mean for the summer or peak wind period (May through August) and winter or minimum wind period (November through January) of the 1985/86 wind season. The same data is plotted in absolute units in Figure 5-18 to show the relationship to the turbine cut-in speed.

The above figures clearly demonstrate that the maximum energy availability occurs between the hours of 1700-0600 LST, during non-disturbed conditions. Even in winter, with its short days and low sun angle, the thermally-driven cycle is clearly discernible in Figure 5-17. From Figures 5-6 and 5-7, it is obvious that the period of maximum energy availability also coincides with a disk-layer inflow, which is stable and becomes increasingly so as the night progresses. Peak energy availability (at the hub elevation) typically occurs between 2000 and 2100 LST or 3-4 hours after sunset. From Figures 5-6 and 5-7, the corresponding disk Richardson number ranges from about +0.5 to +7.0 for a geometric mean located between +3.0 and +4.0.

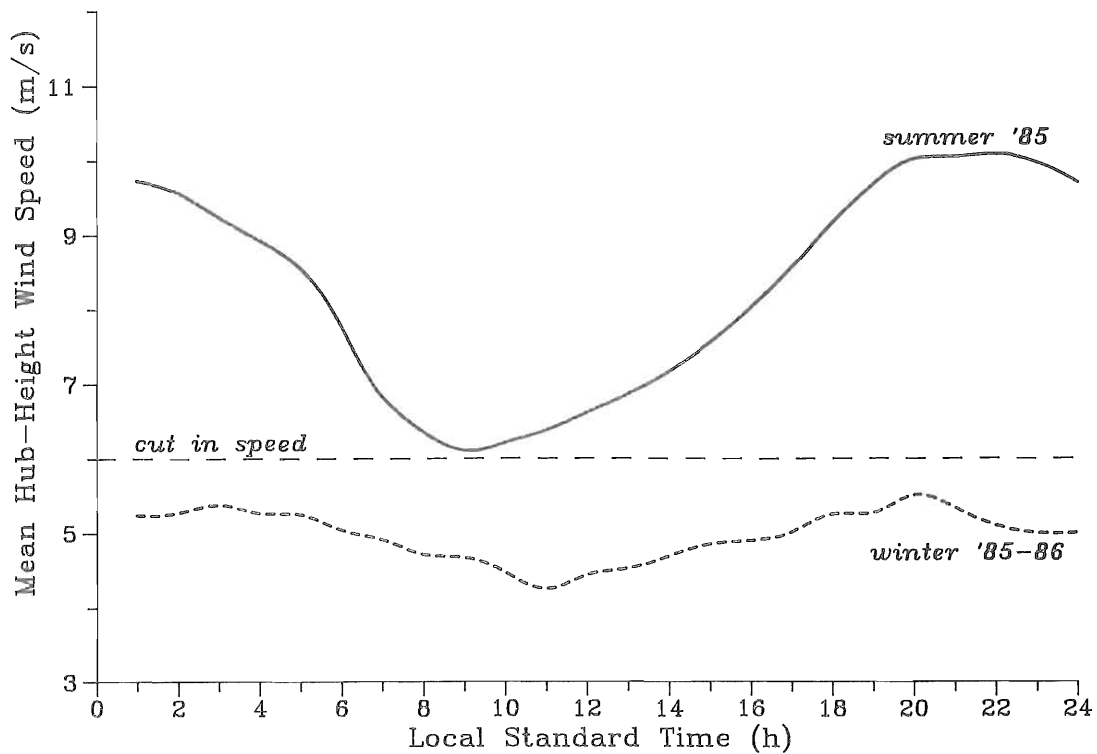
The thermal and kinematic fields are nearly in phase, indicated by the plots of the Brunt-Väisälä frequency ( $N$ ) and the 45-m mean wind speed, as a function of the disk Richardson number in Figure 5-19. The phase relationship between the Brunt-Väisälä frequency and the characteristic turbulent scales ( $I_{u,x}$ ,  $I_{w,z}$ ,  $f_{\mu}$ , and  $f_{mw}$ ) in terms of the Richardson number are shown in Figures 5-20 and 5-21.

From the foregoing series of graphs, it is clear that the structure of the stably-stratified inflow at Goodnoe Hills responds or tracks the disk gradient Richardson number. As the stability increases, an internal boundary layer



008236

Figure 5-17. Ratio of Hourly-to-Diurnal Mean Hub-Height Wind Speed as a Function of Time-of-Day for Summer and Winter of 1985/86 Wind Season



008237

Figure 5-18. Observed Diurnal Variation of Actual Hub-Height Mean Wind Speed for Summer and Winter of the 1985/86 Wind Season

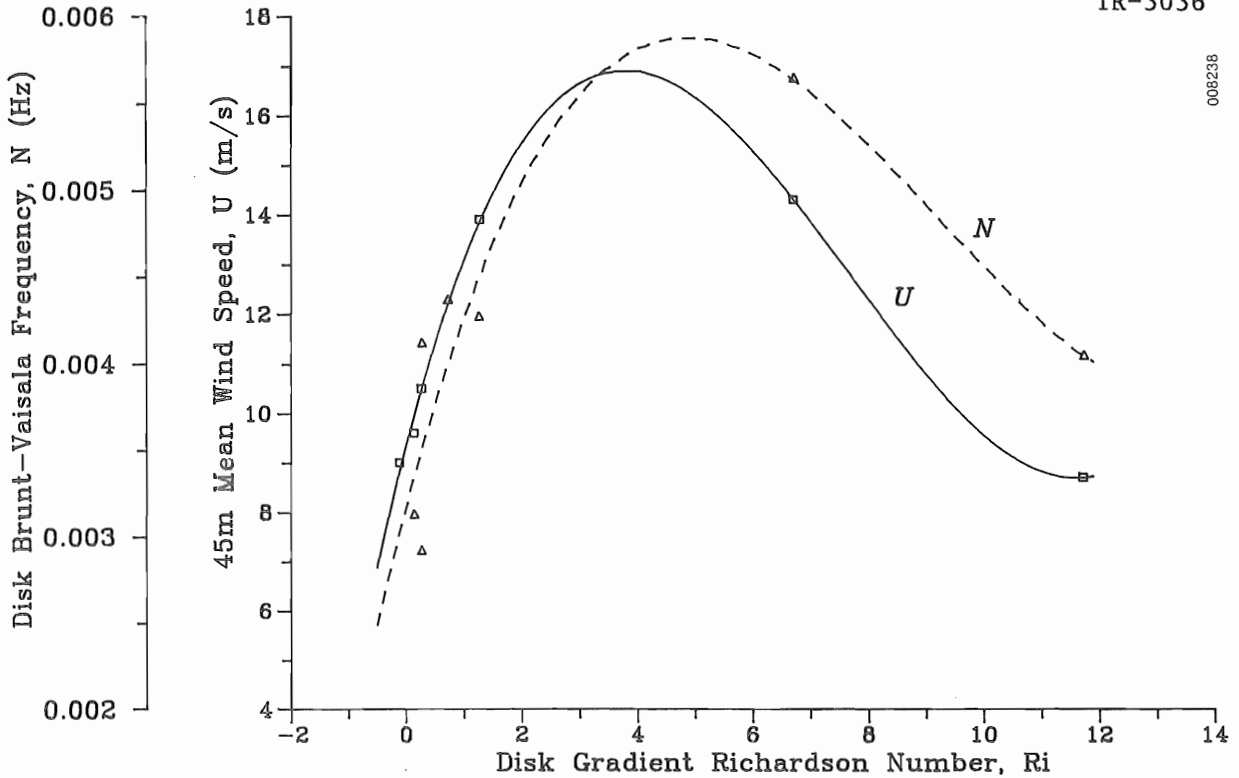


Figure 5-19. Observed Variation of the 45-m Mean Wind Speed ( $U$ ) and the Brunt-Väisälä Frequency ( $N$ ) as a Function of the Disk Richardson Number

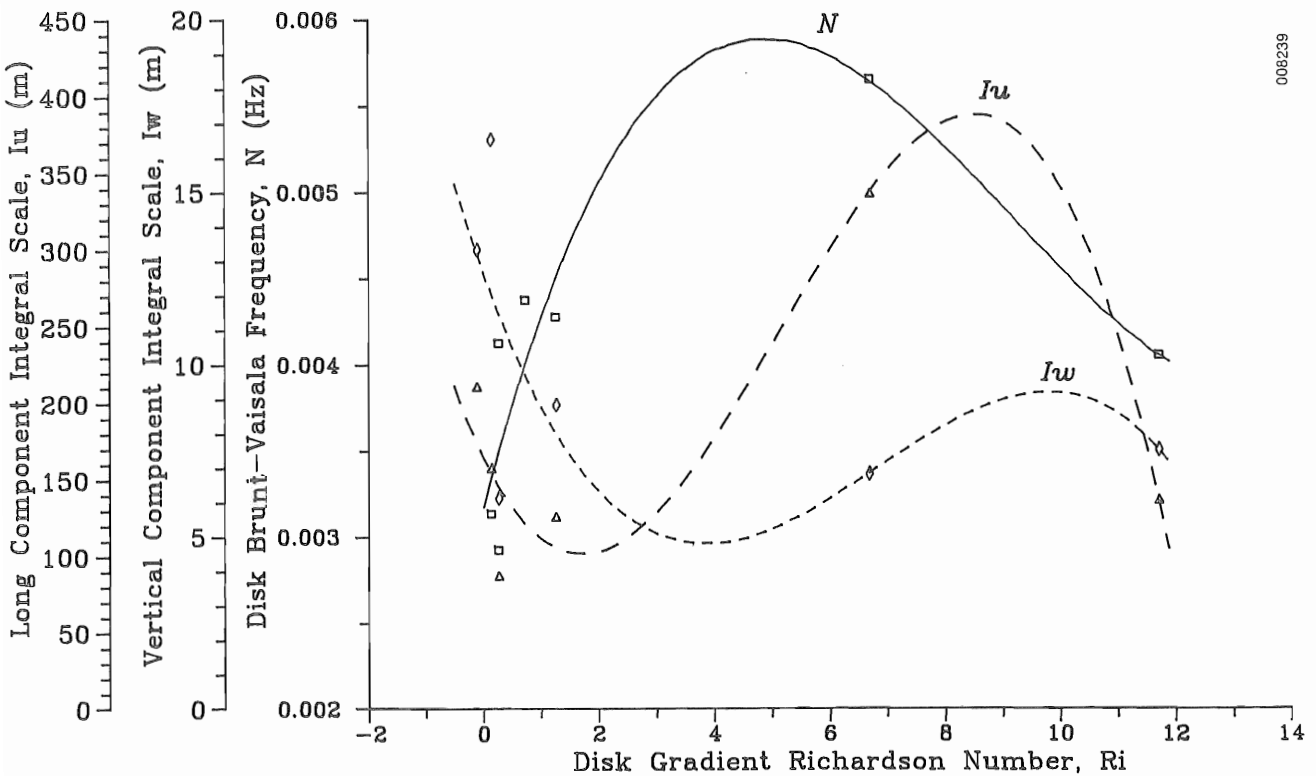


Figure 5-20. Observed Variation of the Brunt-Väisälä Frequency ( $N$ ) and the Horizontal ( $I_u$ ) and Vertical ( $I_w$ ) length Scales as a Function of the Disk Richardson Number

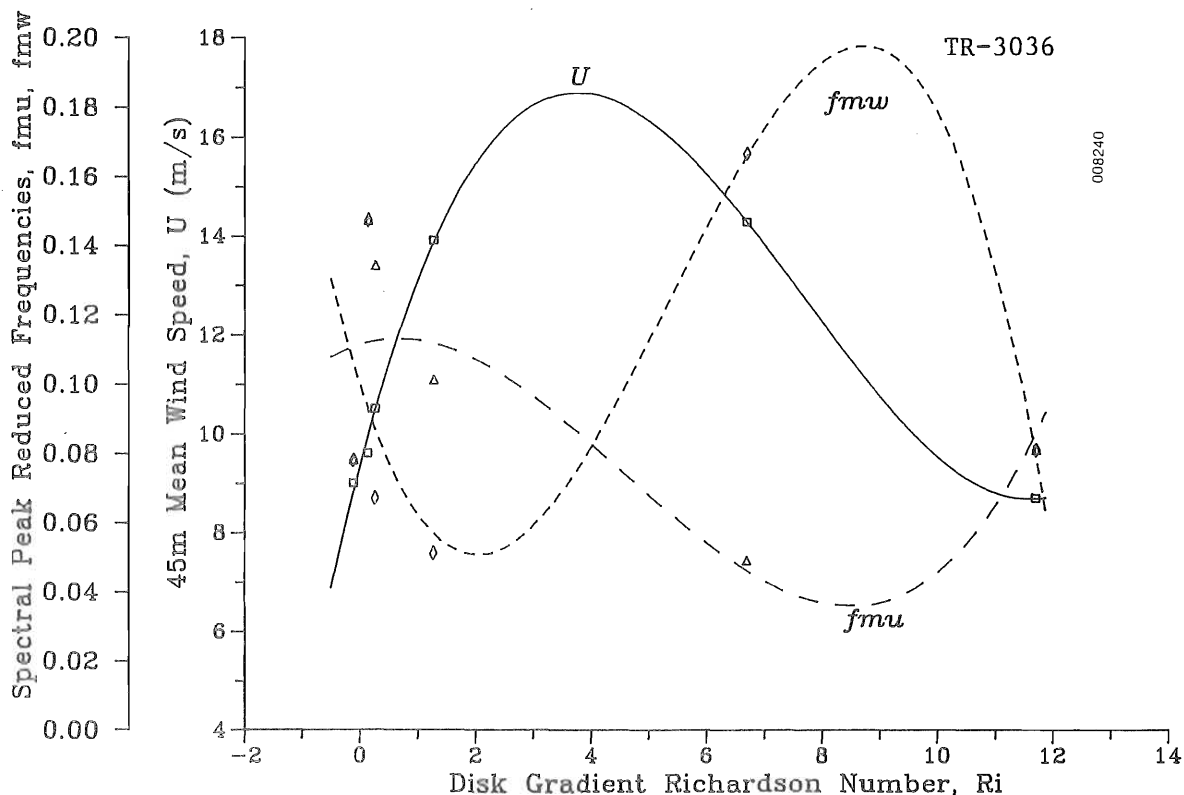


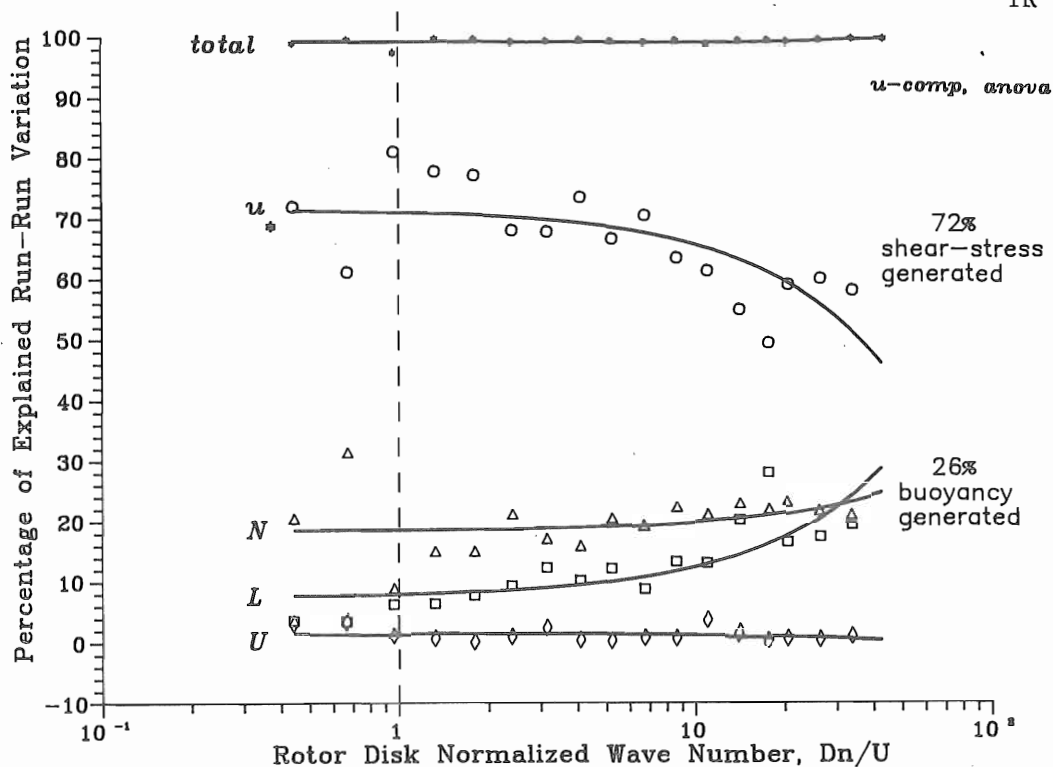
Figure 5-21. Same as Figure 5-20 Except for Spectral Peak Reduced Frequencies  $f_{\mu}$  (Horizontal Component) and  $f_{mw}$  (vertical Component)

forms within the rotor disk, accompanied by a wind speed maximum and increased vertical mean shear. Under these conditions, as indicated by the peak in the Brunt-Väisälä frequency near an Ri of +4.0, shear flow instabilities become well developed, including the possibility of breaking waves (Kelvin-Helmholtz instability). Figures 5-22 and 5-23 present an ANOVA analysis of the observed run-to-run variation of the longitudinal and vertical 45-m elevation turbulence components. These figures provide a crude presentation of the turbulent energy generation balance for each component. Roughly two-thirds of the observed run-to-run changes in the turbulent energy spectrum (at space scales of the rotor disk and smaller) can be explained from variations in the shear-stress (local shear generation). The bulk of the remainder are due to variations in flow stability (buoyancy).

#### Establishing Inflow Predictors for Far-Field Acoustic Emission Statistical Quantities

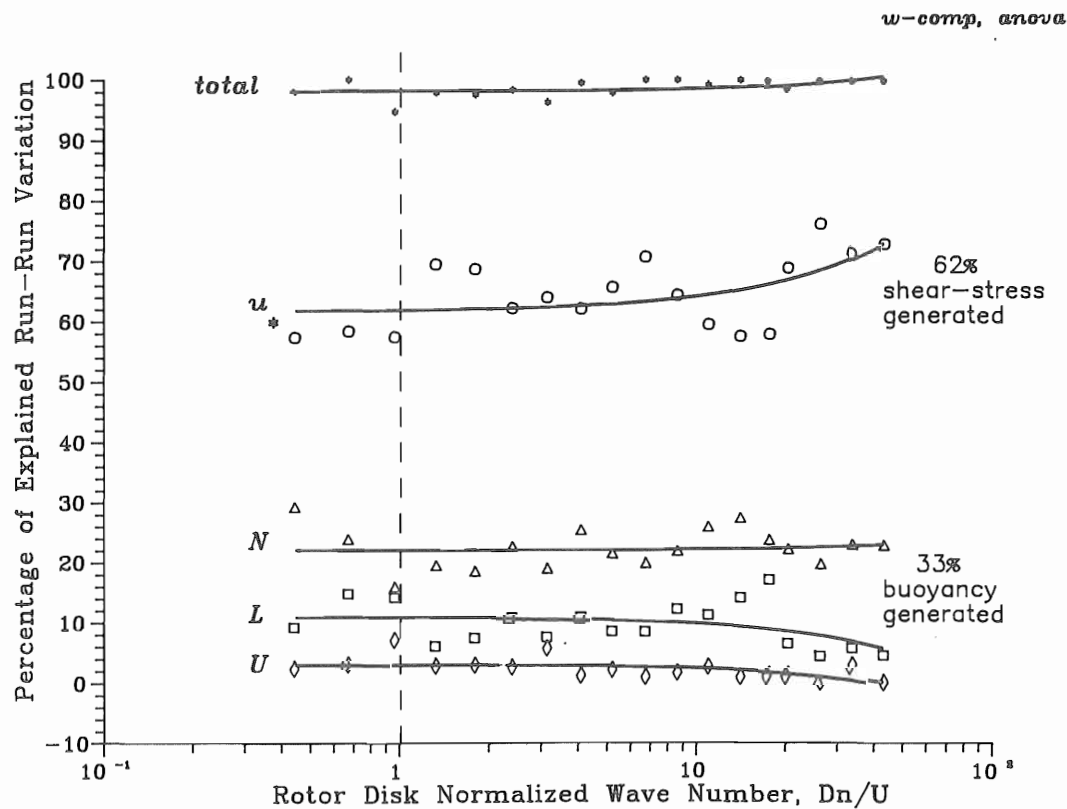
A series of inflow characteristic scales, which would serve as independent variables for predicting the MOD-2 turbine far-field acoustic spectral response via a linear multivariate model, were evaluated using ANOVA techniques. Three predictor (characteristic) scales, which exhibited maximum independence in Tables 5-2 and 5-3, were identified for evaluation. These included

- M-0 scaling length, L  
disk gradient Richardson number, Ri  
45-m mean wind speed,  $U_{45}$
- Vertical turbulence scale length,  $I_{w,z}$   
Richardson number, Ri  
45-m mean wind speed,  $U_{45}$



008241

Figure 5-22. ANOVA Analysis of the Observed Run-to-Run Variation in the Longitudinal or Axial ( $u$ ) Turbulence Component



008242

Figure 5-23. Same as Figure 5-22 but for the Vertical or In-Plane ( $w$ ) Turbulence Component

- M-O scaling length,  $L$
- Richardson number,  $Ri$
- Vertical turbulence scale length,  $I_w z$
- 45-m mean wind speed,  $U_{45}$ .

The ANOVA results are presented in Figures 5-24 and 5-25 for the multivariate model predicting the far-field, mean 1/3-octave band spectrum levels or  $\langle m(n)^1 \rangle$  where  $\langle m^1 \rangle$  is the ensemble mean. It is clear from Figure 5-24, the addition of a measure of the turbulent scale  $I_w z$  explains the variation in mean acoustic output above 10-Hz or  $k = 1$  (referenced at 75% span). A slightly better prediction is achieved if both the  $L$  and  $Ri$  parameters are included in addition to  $U_{45}$  and the  $I_w z$  scales. The relative contribution to the total variation explained by each of the predictors is shown in Figure 5-25. Below the 10-Hz band, changes in mean wind speed explain more than 90% of the observed MBSL variation. Above 10-Hz, all four predictors help explain the variation, the vertical length scale  $I_w z$  becoming dominate in the 50-Hz band and above.

The performance of the three models in explaining the observed run-to-run variation in the MBSL second moment,  $\langle b_2(n) \rangle = \langle m(n)^2 / m(n) \rangle$ , or variance coefficient is plotted in Figure 5-26. The ensemble variance is denoted  $\langle m(n)^2 \rangle$ . While not explaining 100% of the observed variation, the four-predictor model does much better than the other two across the frequency band

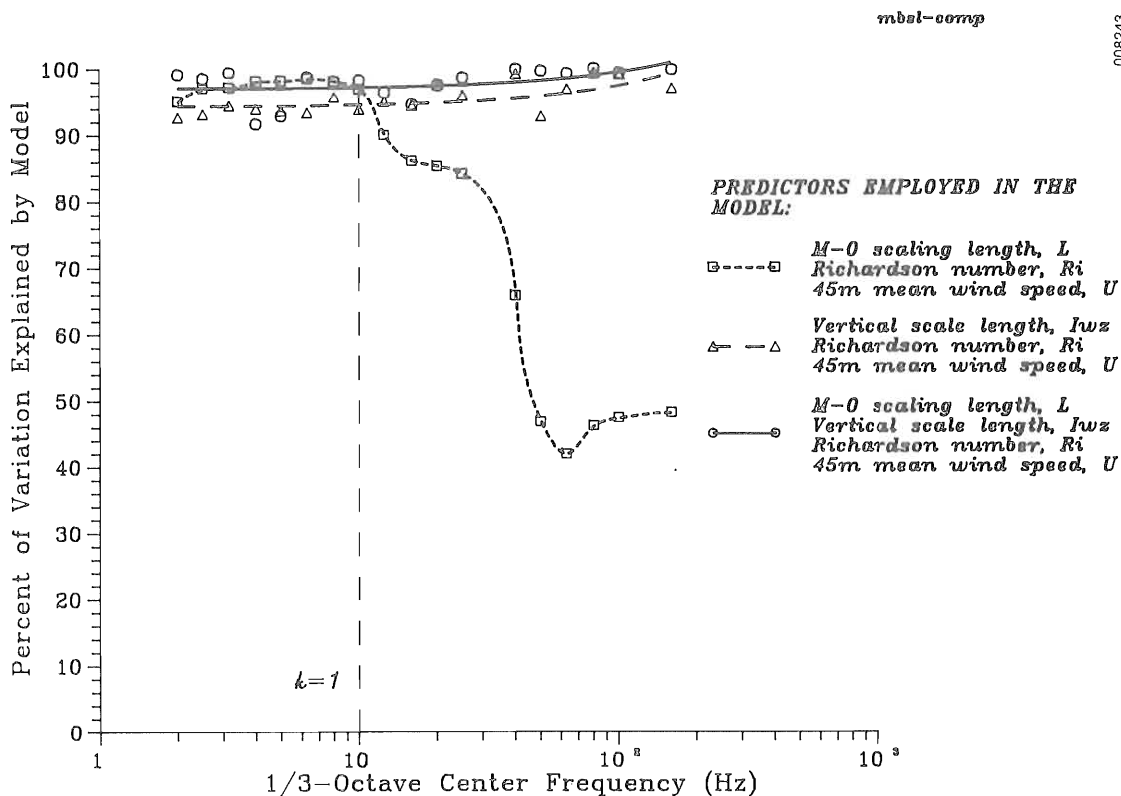
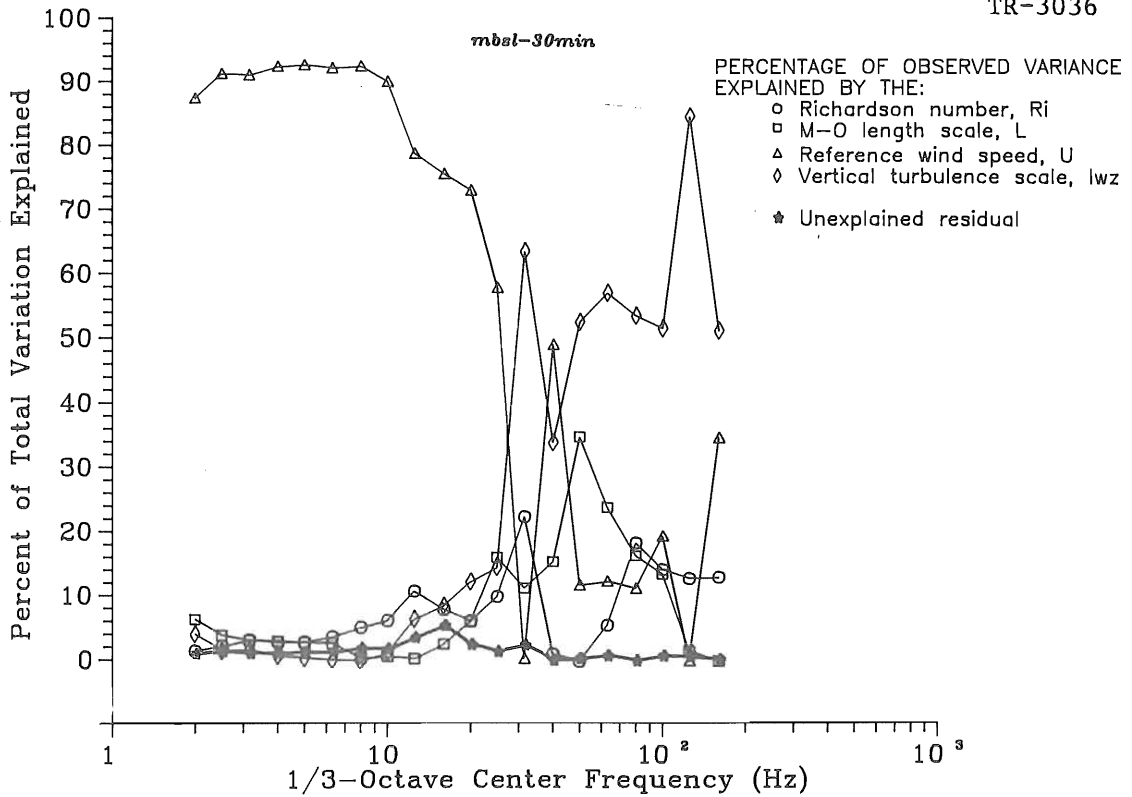
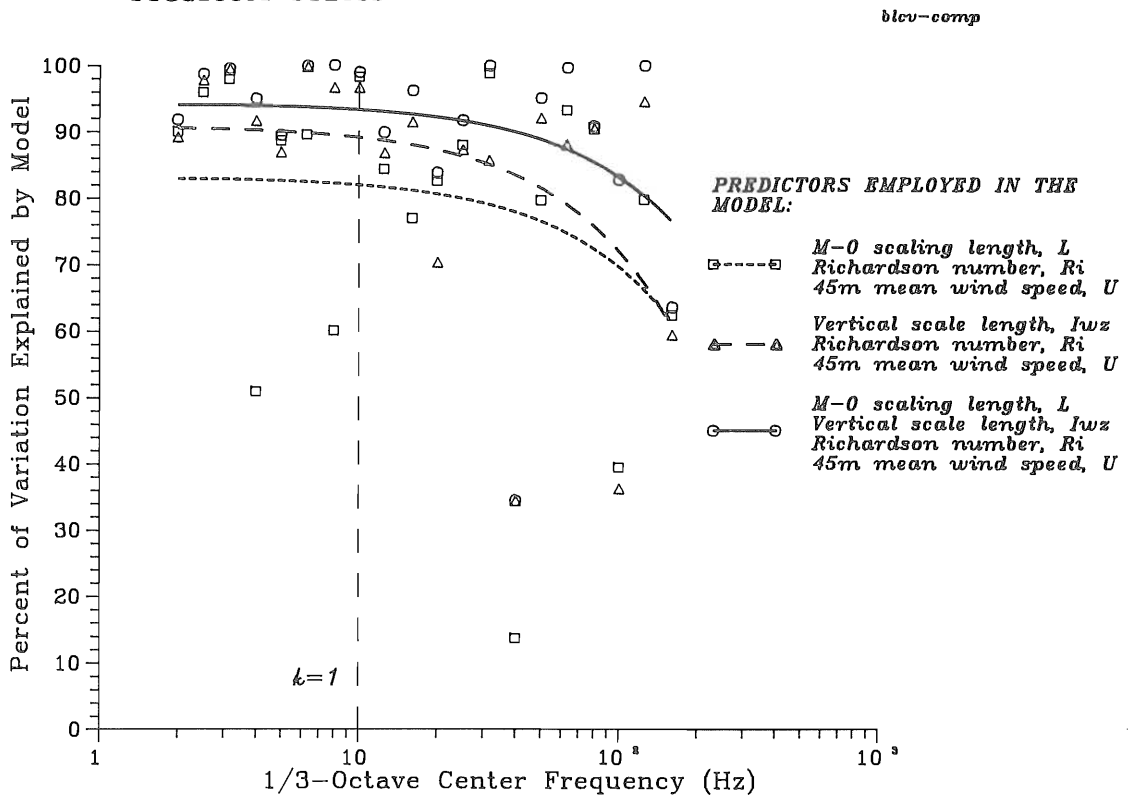


Figure 5-24. ANOVA Analysis of the Efficiency of Multivariate Models Using a Series of Predictors for the Observed Run-to-Run Variation of the Acoustic MBSL Spectra



008244

Figure 5-25. ANOVA Analysis of the Observed Run-to-Run Variation of the Acoustic MBSL Spectra as a Function of Four Inflow Predictor Scales



008245

Figure 5-26. Same as Figure 5-24 but for the Observed Variation in the Acoustic BSL Variance Coefficient  $\langle b_2 \rangle$  Spectra

of interest. The performance of all three models tends to drift downward above  $k = 1$ . The relative variation explained by each of the four predictors is shown in Figure 5-27. In contrast to the MBSL situation, in which changes in the mean wind speed explained the bulk of the observed variation at 10 Hz and below, all four predictors are necessary to cover the entire 2-160 Hz band range for the MBSL second moment.

Figures 5-28 and 5-30 present the performance of the three models in explaining the observed run-to-run variations in the MBSL third and fourth statistical moments (skewness and kurtosis coefficients), or  $\langle b_3(n) \rangle = \langle m(n)^3 \rangle / (\langle m(n)^2 \rangle)^{3/2}$  and  $\langle b_4(n) \rangle = \langle m(n)^4 \rangle / (\langle m(n)^2 \rangle)^2$ . Again, the four-predictor model performs better than the other two, particularly in explaining the spectral variation of the MBSL fourth moment or kurtosis coefficient. Figures 5-29 and 5-31 display the relative variation explained by each of the four predictors for the skewness and kurtosis coefficients, respectively. Again, all four predictors are necessary to explain the bulk of the run-to-run variation in the 1/3-octave bands of interest.

Spectral Sensitivity to Inflow Characteristic Scales

The four predictors evaluated above were employed as independent variables in a linear, multivariate spectral regression model. In this model the response or dependent variables were the four statistical moments (mean and variance, skewness, and kurtosis coefficients) of the mean 1/3- and octave-band spectral levels (MBSL) for each data run. The model for the BSL mean is of the form

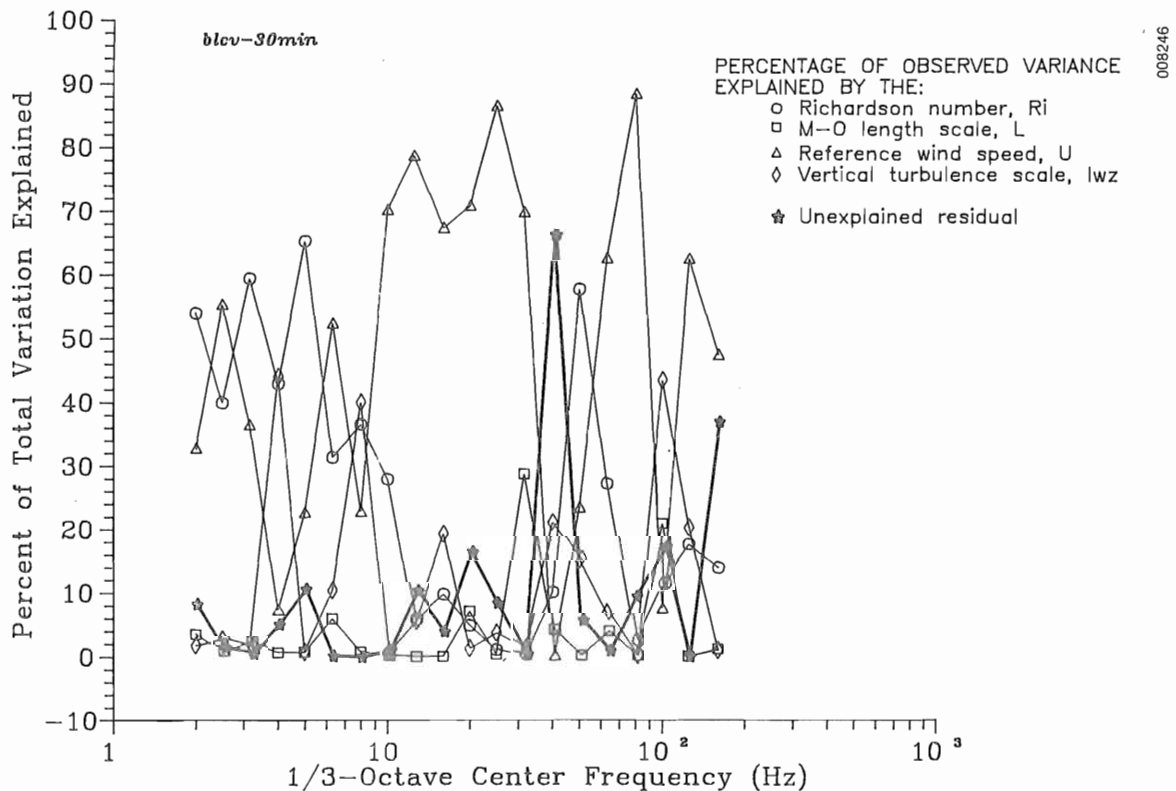


Figure 5-27. Same as Figure 5-25 but for the Observed Variation in the Acoustic BSL Variance Coefficient  $\langle b_2 \rangle$  Spectra

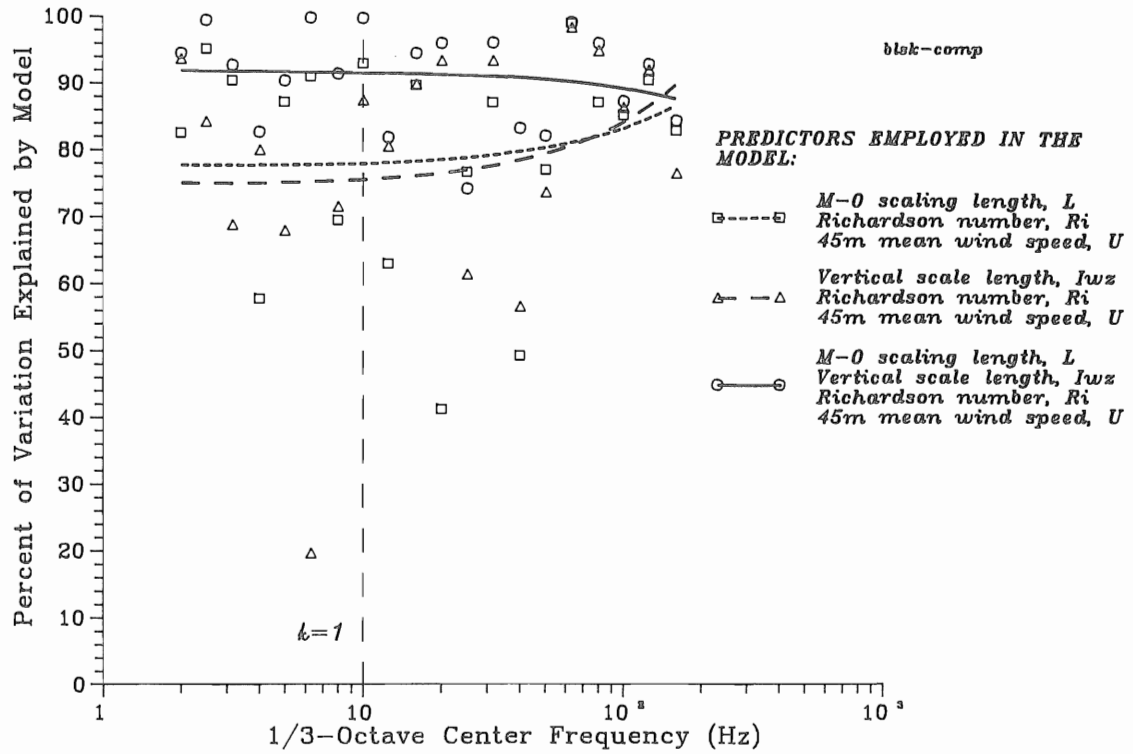


Figure 5-28. Same as Figure 5-24 but for the Observed Variation in the Acoustic BSL Skewness Coefficient  $\langle b_3 \rangle$  Spectra

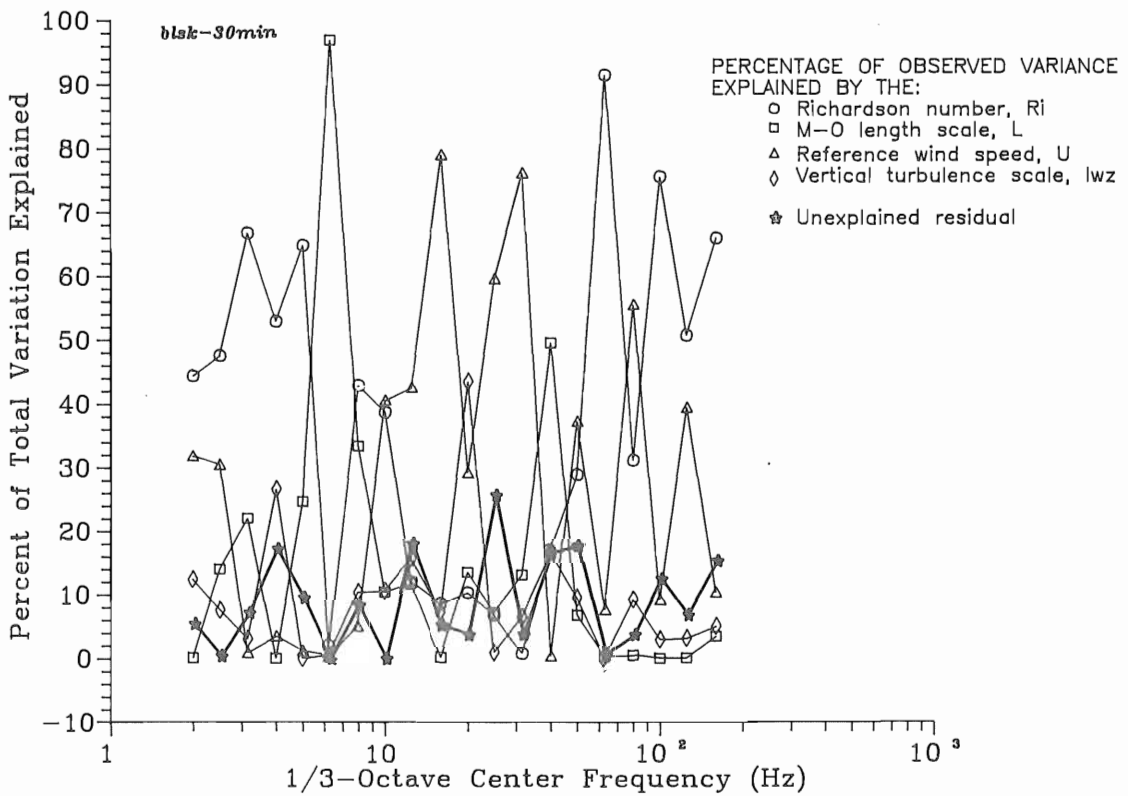


Figure 5-29. Same as Figure 5-25 but for the Observed Variation in the Acoustic BSL Skewness Coefficient  $\langle b_3 \rangle$  Spectra

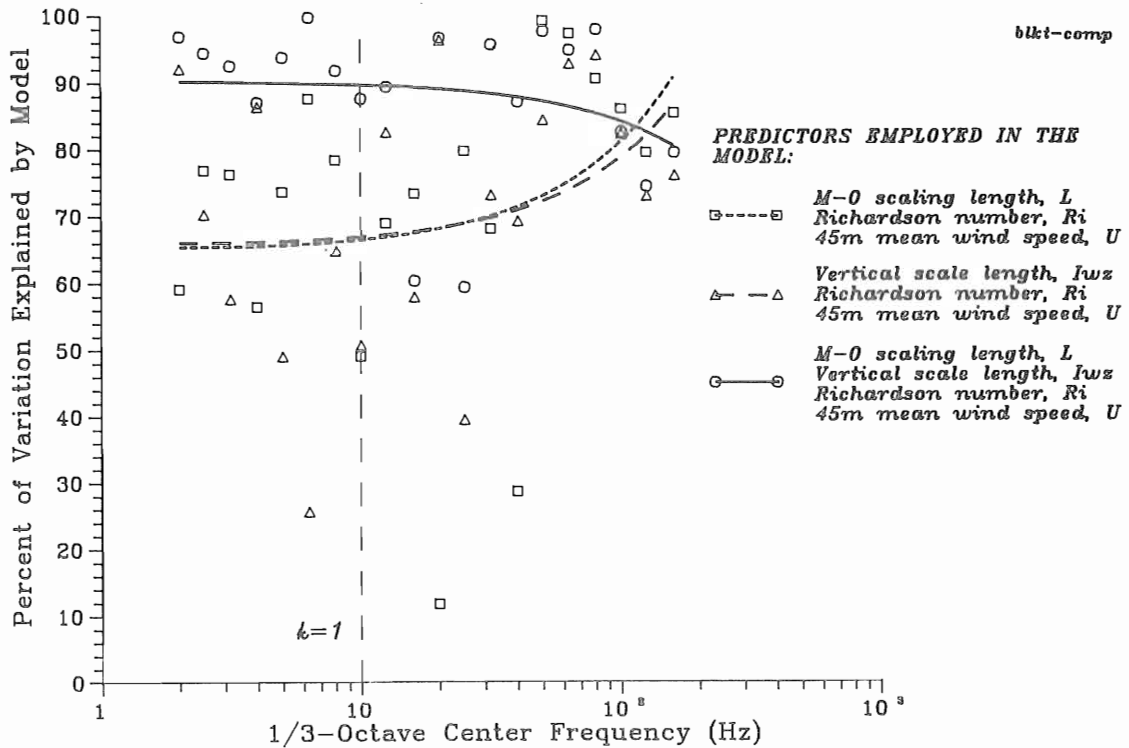


Figure 5-30. Same as Figure 5-24 but for the Observed Variation in the Acoustic BSL Kurtosis Coefficient  $\langle b_4 \rangle$  Spectra

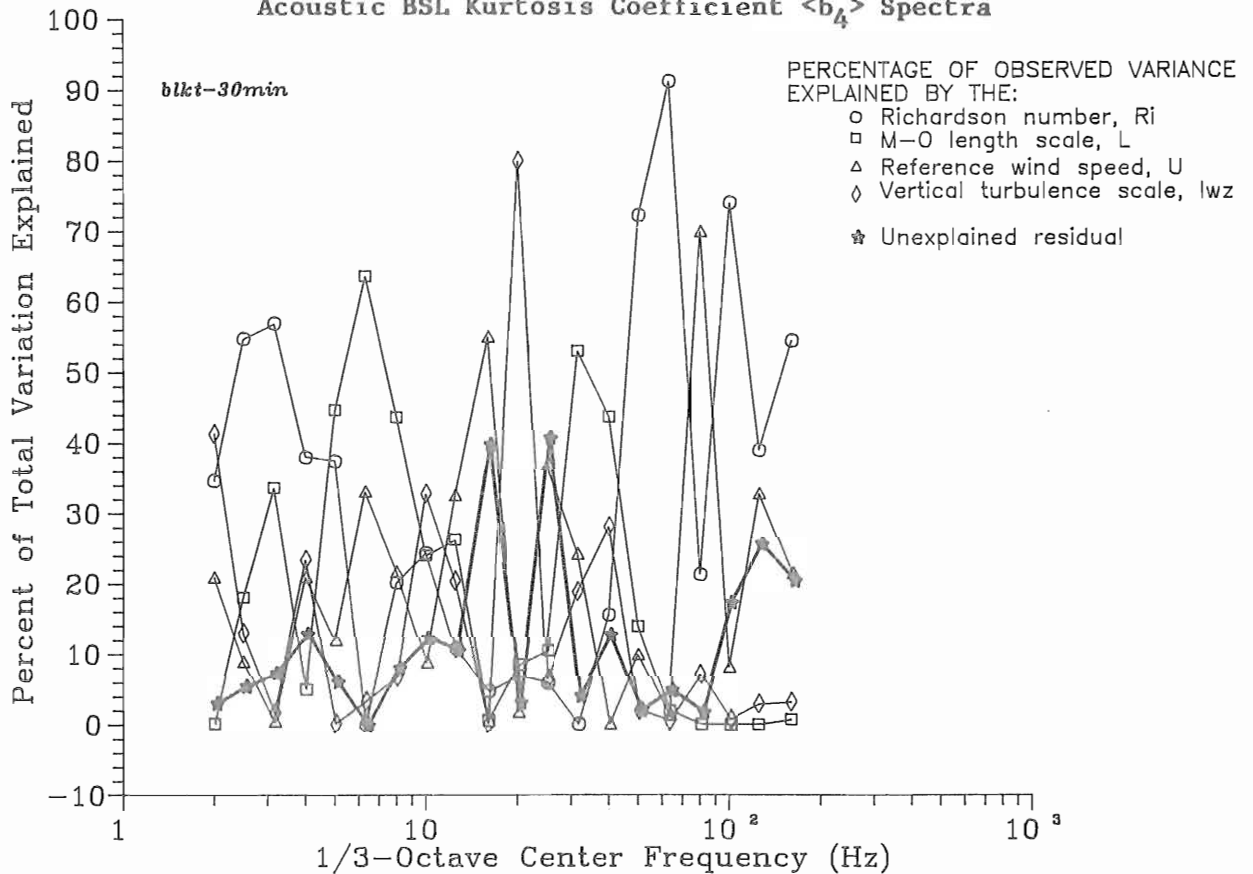


Figure 5-31. Same as Figure 5-25 but for the Observed Variation in the Acoustic BSL Kurtosis Coefficient  $\langle b_4 \rangle$  Spectra

$$\overline{\langle S_{1/3}(n) \rangle} = a_1(n)Ri + a_2(n)L + a_3(n)U_{45} + a_4(n)I_w^z + a_0(n) + E(n), \quad (5-1)$$

where  $n$  is the band center frequency and  $E(n)$  is the residual error between the observed and predicted values. The relationship for the second, third, and fourth statistical moments [ $b_2(n)$ ,  $b_3(n)$ , and  $b_4(n)$ ] would be similar but with a different coefficient vector [ $a_0, \dots, a_4$ ] for each.

### 5.1.1.3 Model Interpretation

The models discussed above allow us to examine not only the relationship of the mean acoustic spectral response to changing inflow conditions, but the variations of that response (the higher-order statistical moments) as well. The elements of the model coefficient vector [ $a_1, \dots, a_4$ ] for each 1/3-octave frequency band listed in Table 2-2 reflect the change in the mean response per unit increase in the associated predictor variable, with the remainder of the predictors held constant or

$$\frac{\partial \langle S_{1/3}(n) \rangle}{\partial R_i} = a_{1j} \frac{\partial \langle S_{1/3}(n) \rangle}{\partial L} = a_{2j}, \text{ etc.} \quad (5-2)$$

If each coefficient is normalized by the predictor population mean or

$$[a_1/\overline{Ri}; a_2/\overline{L}; a_3/\overline{U_{45}}; a_4/\overline{I_w^z}],$$

then the relative spectral sensitivity of each inflow predictor scale can be measured on each frequency band response and the results compared. Thus, we can use these models to identify the characteristic scales or predictors which have the most influence over the statistical distributions of the MOD-2 LF emissions spectra. Those predictor scales, having substantial slopes relative to the remainder, can be considered indicative of the dominant physical processes responsible for acoustic radiation in a particular frequency band.

Mean Acoustic Band Spectrum Level. A plot of the normalized coefficients (response slopes) for the expected or mean BSL  $\langle S_{1/3}(n) \rangle$  model is shown in Figure 5-32. In this diagram the reference wind speed ( $U_{45}$ ) and disk gradient Richardson number ( $Ri$ ) have the most influence on the average spectral far-field acoustic radiation below 10 Hz ( $k = 1$ ). Above that frequency, the vertical turbulent length scale,  $I_w^z$ , gradually becomes more important. It is also interesting to note the change in sign for this parameter; i.e., band output increased with decreasing scale length below 10 Hz ( $k = 1$ ) and the inverse occurred above 10 Hz.

BSL Variance Coefficient. The influence of the four inflow characteristic scales on the second moment (variance coefficient  $\langle b_2 \rangle$ ) of the observed BSL distributions is shown in Figure 5-33. The  $\langle b_2 \rangle$  statistic is a measure of the width or range of levels observed in a particular 1/3-octave band, relative to the band mean or expected level. Large values of  $\langle b_2 \rangle$  correspond to a very wide probability distribution, indicating the associated processes may be wideband random. Similarly, small  $\langle b_2 \rangle$ s may indicate that some form of a narrowband random process (or processes) is responsible for the observed variation. A large run-to-run range of  $\langle b_2 \rangle$  values are noted in the 3.15, 10, and 12.5-Hz bands, as is indicated Figure 5-4b. The sensitivity plot of

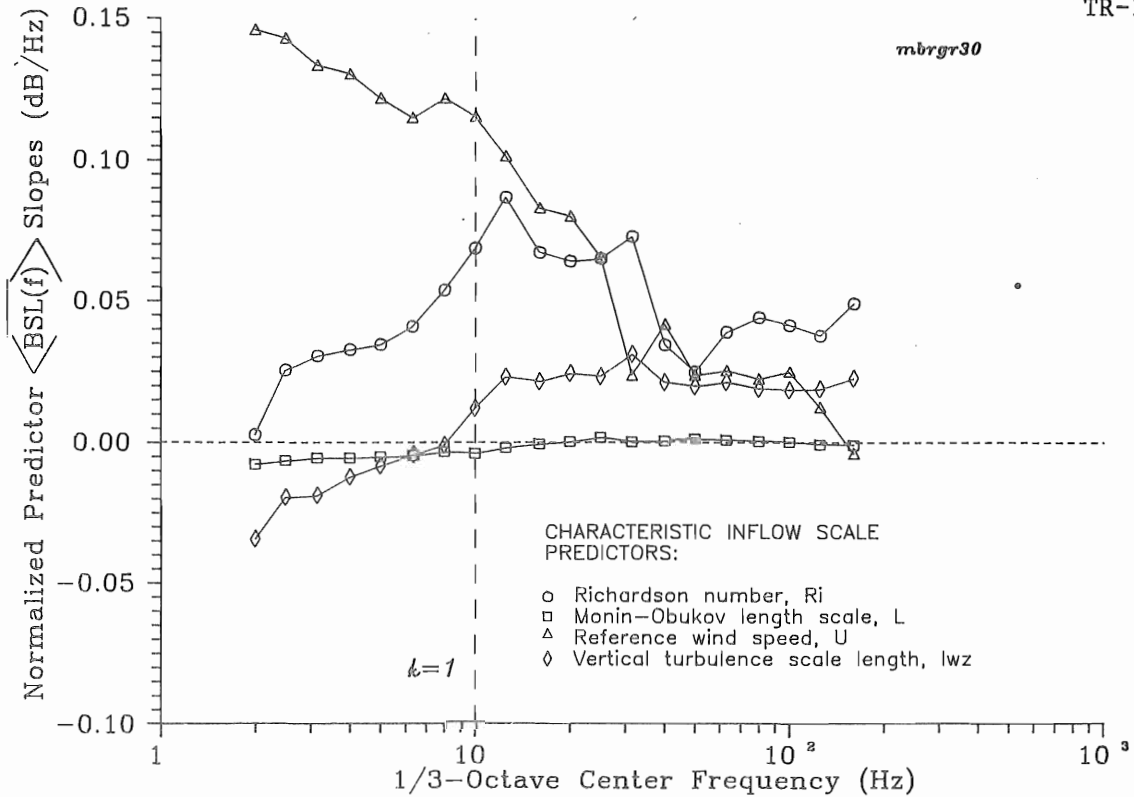


Figure 5-32. Characteristic Scaling Sensitivities for Mean Band Spectrum Levels

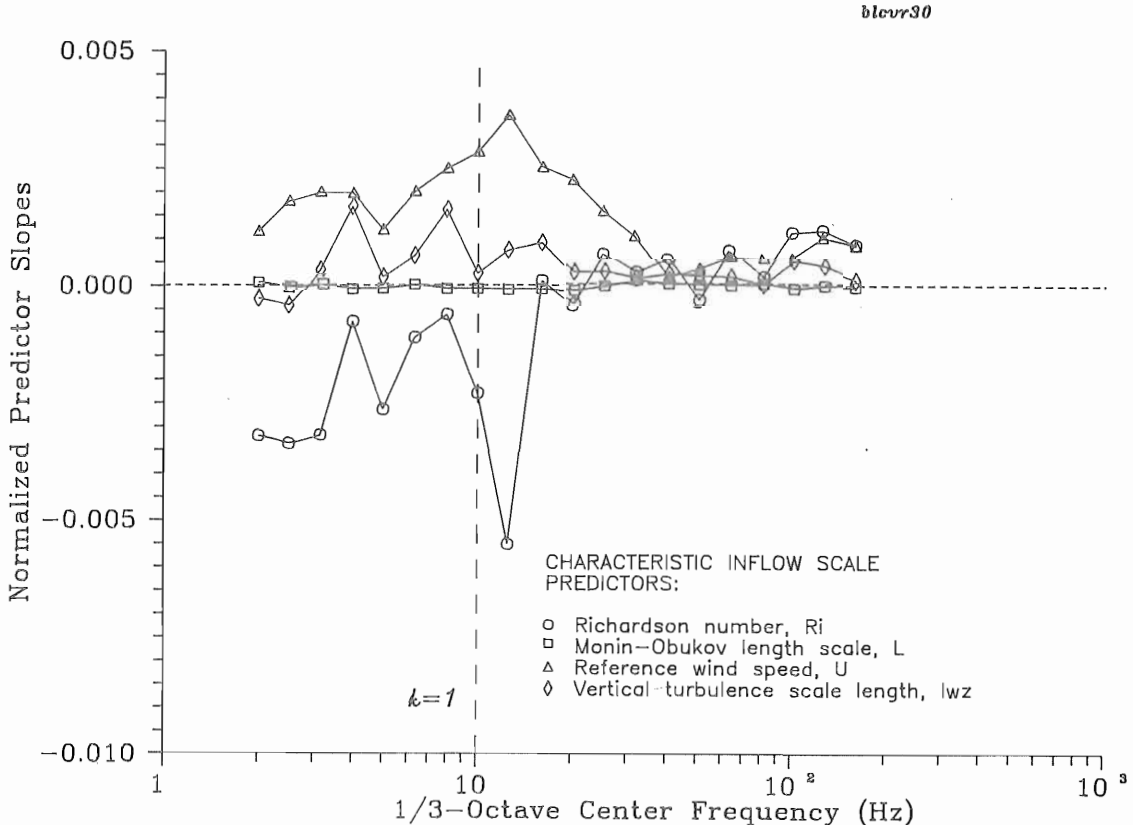


Figure 5-33. Characteristic Scaling Sensitivities for BSL Variance Coefficients

Figure 5-33 indicates the  $U_{45}$  and  $Ri$  (atmospheric structure) have the most influence in these bands with a moderate contribution from the vertical scale length  $I_{wz}$ . This time the  $\langle b_2 \rangle$  sensitivity to the vertical turbulent scale remains inverse below 12.5 Hz and becomes essentially zero until it achieves dominant influence and positive correlation with and above the 80-Hz band.

**BSL Acoustic Skewness Coefficient.** The relative spectral sensitivity of the characteristic inflow scaling parameters on the BSL distribution third moment, or skewness coefficient  $\langle b_3 \rangle$ , is plotted in Figure 5-34. The skewness coefficient is a measure of the lack of symmetry in the sample probability density function. A normal or Gaussian distribution is symmetrical about the mean; therefore, the skewness is zero. A positive skewness coefficient in a particular frequency band reflects a predominance of large BSL values (peaks) over smaller ones; therefore, the distribution is "positively skewed." The run-to-run variation plot of  $\langle b_3 \rangle$  in Figure 5-4c indicates a multi-band structure, with large variations in the 2-5, 8-20, 40, and 80-160 Hz bands. Figure 5-34 indicates parameter sensitivities similar to those that were found for the variance coefficient  $\langle b_2 \rangle$ .

**BSL Acoustic Kurtosis Coefficient.** The normalized BSL sensitivity of the fourth moment  $\langle b_4 \rangle$ , or kurtosis coefficient, to the set of four inflow characteristic scales is shown in Figure 5-35. The kurtosis coefficient, or "flatness factor," is a relative measure of the magnitude of the BSL values in

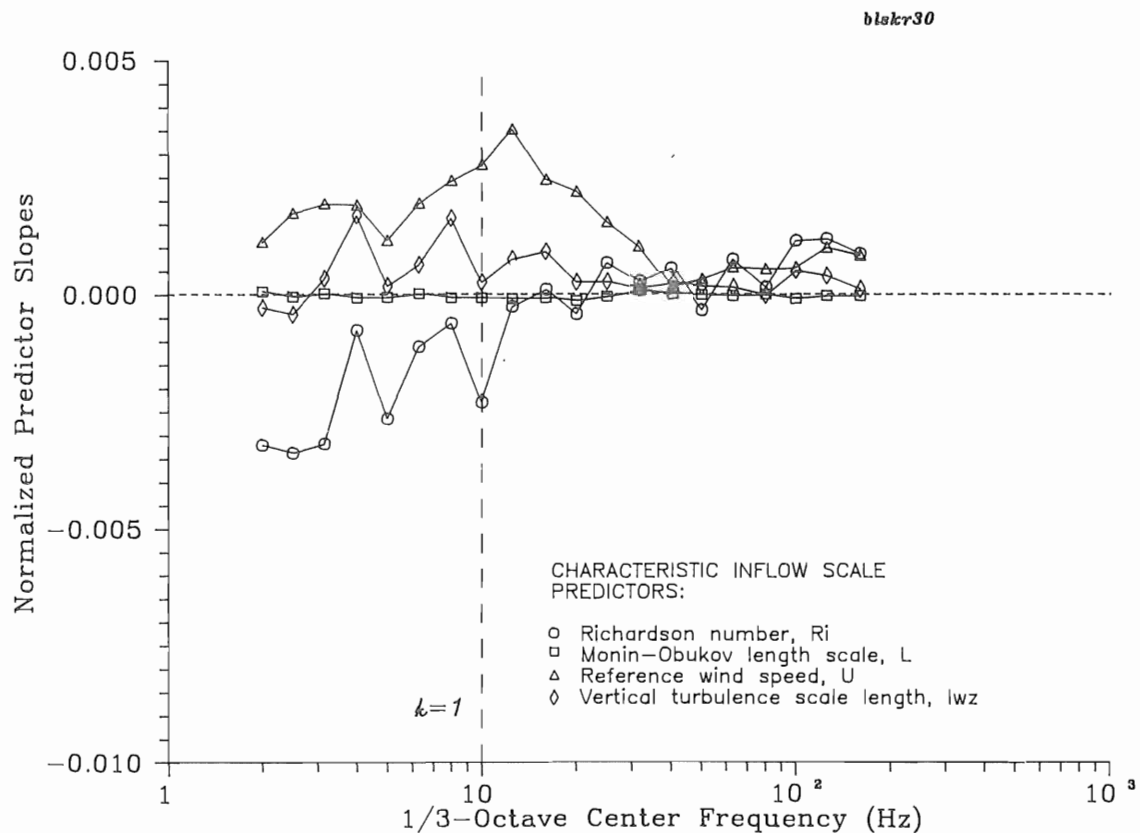


Figure 5-34. Characteristic Scaling Sensitivities for BSL Skewness Coefficients

the observed band probability distribution. The kurtosis coefficient for a normal distribution is 3. An observed BSL distribution void of sharp peaks will have a kurtosis of 3 or will possibly be negative (flat). A high value of  $\langle b_4 \rangle$  in a particular frequency band indicates a substantial percentage of large values (peaks) relative to the mean band level and a distribution peaked at the mean. The band structure noted in Figure 5-4c of the  $\langle b_3 \rangle$  statistic has become more discrete in the plot of  $\langle b_4 \rangle$  in Figure 5-4d. The largest variations of  $\langle b_4 \rangle$  occur in the 3.15-5, 8, 20, 40, and 100-160 Hz bands. The parametric sensitivity plots of Figure 5-35 indicate that atmospheric structure, as indicated by the Richardson number, is the dominant influence on  $\langle b_4 \rangle$  below 10 Hz and inversely correlated (low stability). High values of  $\langle b_4 \rangle$  in the 100-160 Hz bands are positively correlated with very stable flows.

Empirical Agreement with the Theory of Homicz and George. In general, there is excellent agreement between the theories of Homicz and George [10,11] and our measurement of the MOD-2 wind turbine. They identified the axial convection velocity,  $V_c$ , the upwash or in-plane turbulence component intensity, and scale  $I_{wz}$  as the primary inflow properties that influence the mean band spectrum  $\langle S_{ap}(n) \rangle$  level emissions. We found that the dominant characteristic inflow scales were axial wind component,  $U$ , the upwash or vertical turbulent scale,  $I_{wz}$ , measured within the rotor disk, and the gradient Richardson number stability parameter measured across the vertical extent of the rotor disk. We agree with the axial flow component, since the axial and convection velocity

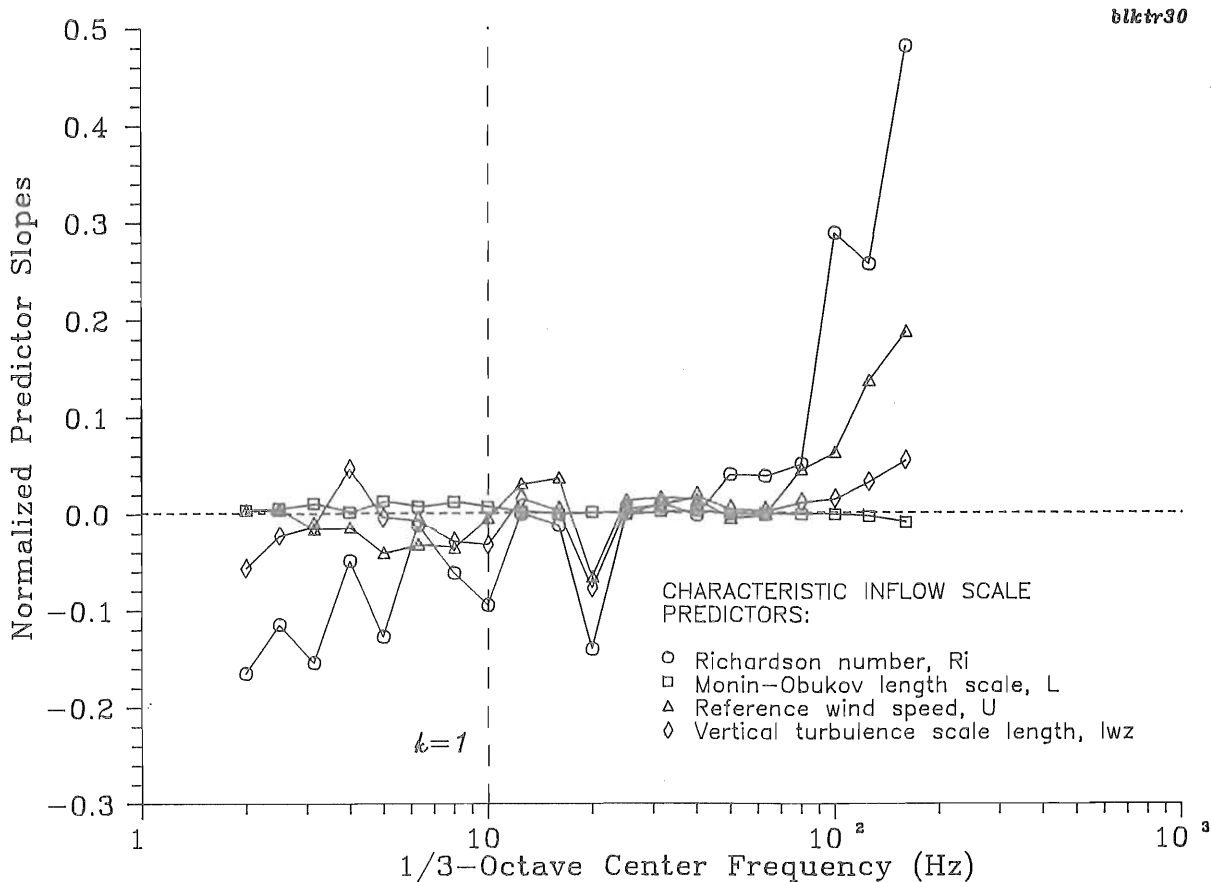


Figure 5-35. Characteristic Scaling Sensitivities for BSL Kurtosis Coefficients

are approximately related by  $V_c = 0.8U$ . And, since  $I_{wz}$  is proportional to  $S_w(n)$ , as well as to the mean-square value of the integrated value of  $S_w(n)$  or  $w^2$ , again there is agreement. Including the Richardson number parameter is necessary to account for the seemingly unique, stratified flow structure present at the Goodnoe Hills site. We must also include the M-O length scale,  $L$ , to provide the diabatic surface-layer scaling in the rotor disk discussed in Section 3.2. These adjustments would not, however, be necessary in the homogeneous isotropic inflow turbulence assumed by Homicz and George in their models. Thus, including them is a concession to the real atmosphere.

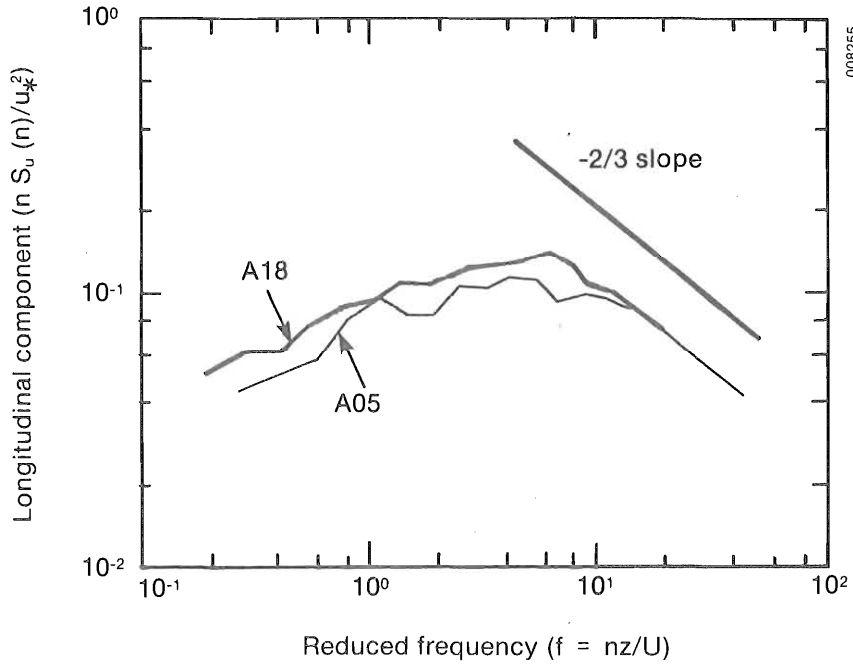
#### 5.1.1.4 Case Studies of the Role of Inflow Structure on Radiated Spectral Characteristics

A series of case-study comparisons were made among the six usable data runs of 1983. Tables 3-3a, b, and c show that four inflow regimes were available for comparison: (1) low wind speed, low stability (LWLS); (2) low-to-moderate wind speed, low-to-moderate stability (LMWLS); (3) low wind, high stability (LWHS); and (4) high wind, high stability (HWHS). These cross-comparison run combinations and associated run data are listed in Table 5-4.

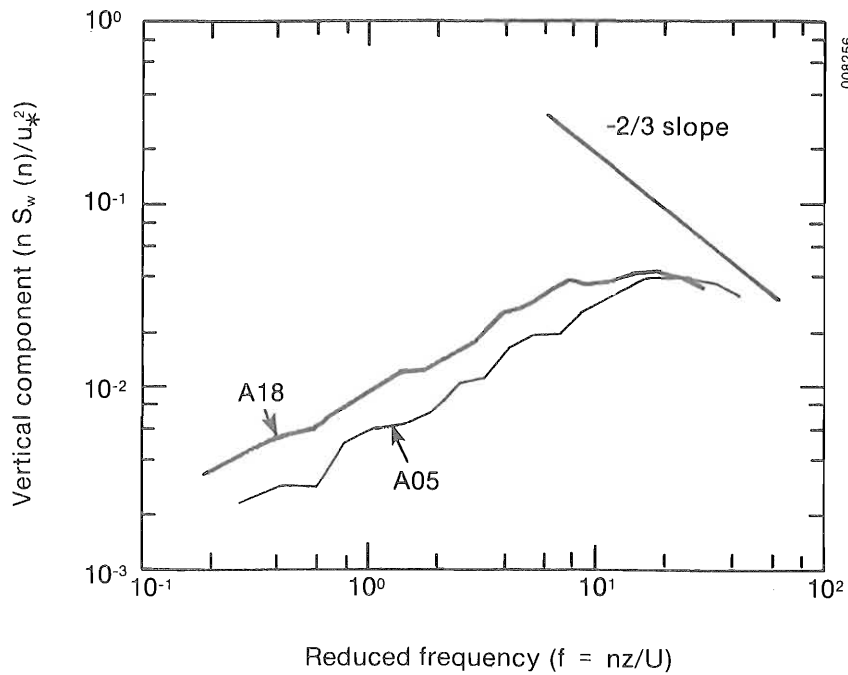
Low Wind, High Stability versus High Wind, High Stability Inflow Conditions. The normalized, longitudinal (axial) and vertical (upwash) 45-m level turbulence spectra for Runs A05 and A18 are plotted in Figure 5-36. The corresponding mean BSL  $\langle S_{1/3}(f) \rangle$ ,  $\langle b_2(f) \rangle$ ,  $\langle b_3(f) \rangle$ , and  $\langle b_4(f) \rangle$  acoustic spectra are shown in Figures 5-37a, b, c, and d. The lower abscissa is scaled in terms of the convection wave number, normalized by the rotor disk dimension,

Table 5-4. Inflow Structure Comparisons Data

Comparison Category	Run Numbers	$U_H$ (mps)	Ri	L (m)	$I_u^x$ (m)	$I_w^z$ (m)
LWHS (3)	A05	7.3	11.7	10.7	136	7.5
HWHS (4)	A18	12.4	1.25	10.7	125	8.8
LMWLS (2)	A14-1	9.2	0.13	183	157	16.5
HWHS (4)	A18	12.4	1.25	10.7	125	8.8
LMWLS (2)	A14-2	9.9	0.26	10.7	86.5	6.1
HWHS (4)	A11	13.6	6.68	10.7	336	6.8
LWLS (1)	A03	8.1	-0.12	-508	210	13.3
LMWLS (2)	A14-1	9.2	0.13	183	157	16.5
LWLS (1)	A03	8.1	-0.12	-508	210	13.3
LWHS (3)	A05	7.3	11.7	10.7	136	7.5
HWHS (4)	A18	12.4	1.25	10.7	125	8.8
HWHS (4)	A11	13.6	6.68	10.7	336	6.8
LMWLS (2)	A14-1	9.2	0.13	183	157	16.5
LMWLS (2)	A14-2	9.9	0.26	10.7	86.5	6.1

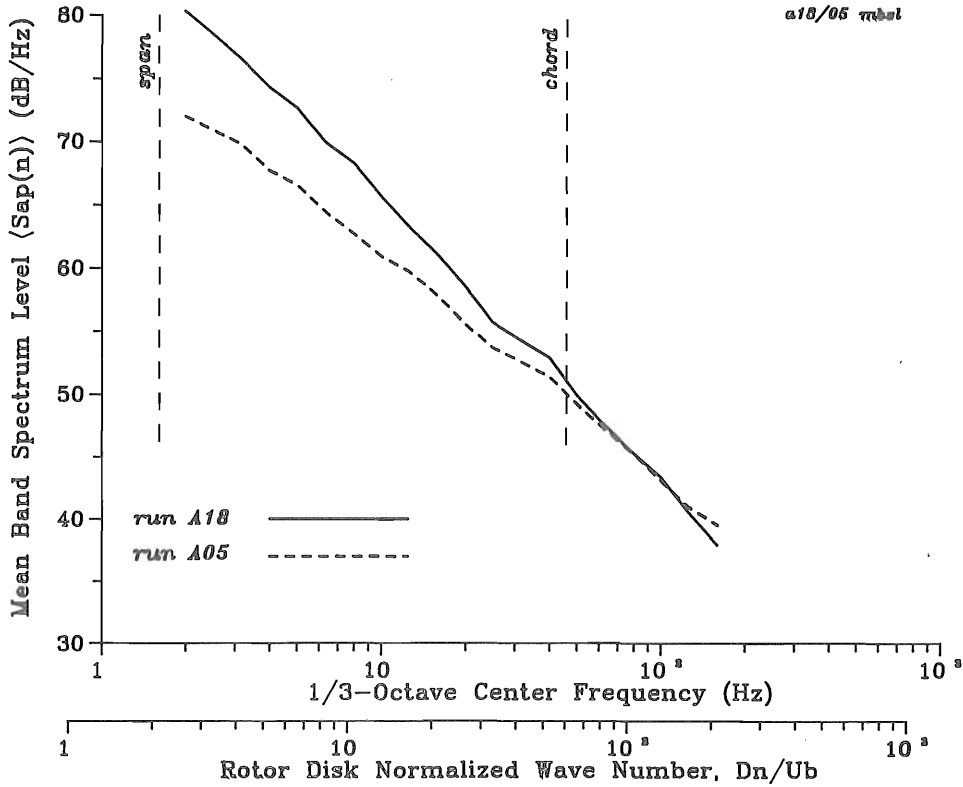


(a) longitudinal (axial) turbulence component normalized spectra

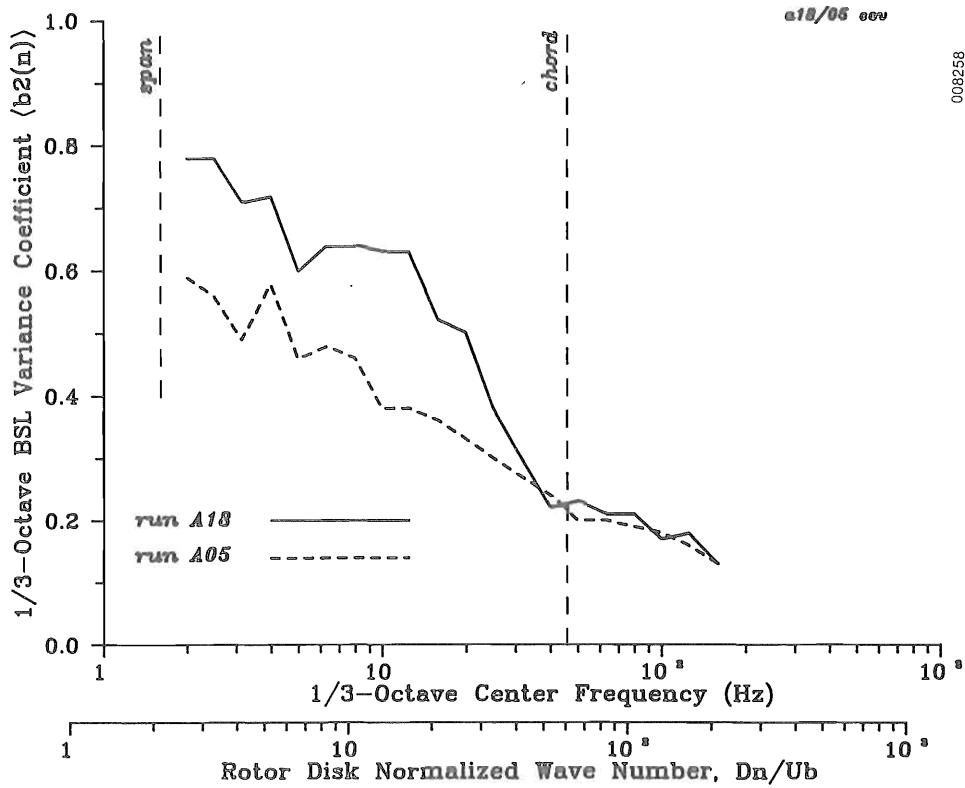


(b) vertical (upwash) turbulence component normalized spectra

Figure 5-36. Normalized 45-m Turbulence Spectra for Runs A18 and A05

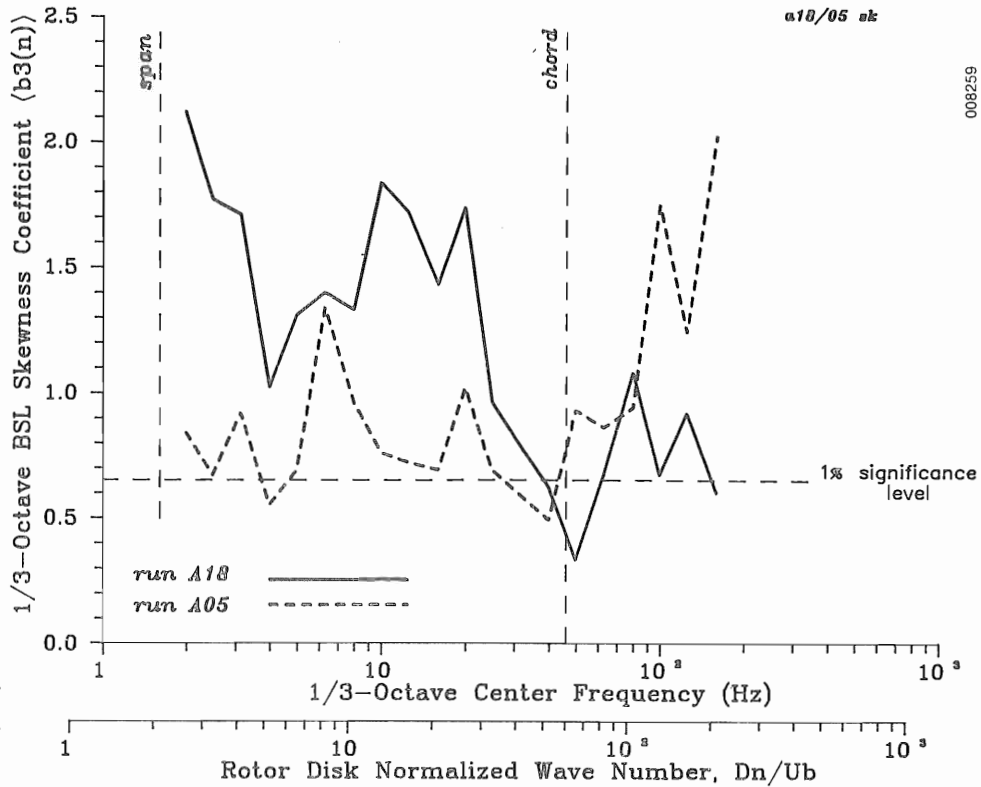


(a) mean band spectrum levels

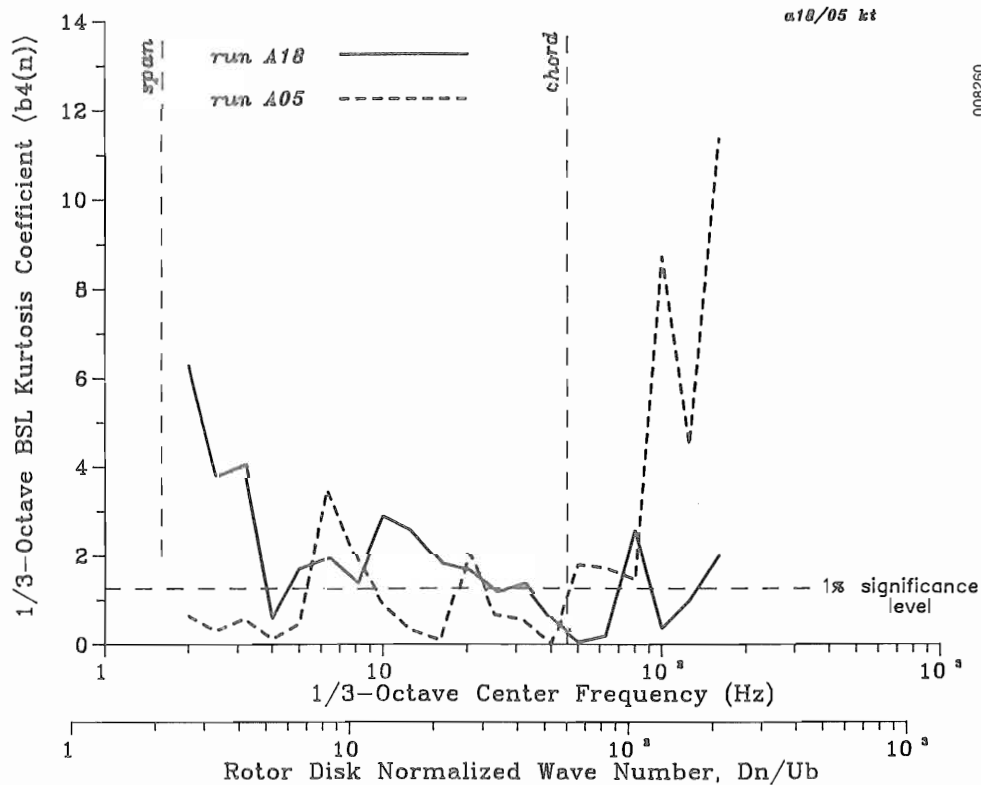


(b) band spectrum level variance coefficient

Figure 5-37. Ensemble Statistical Moments of 1/3-Octave Acoustic Band Spectral Levels for Runs A18 and A05



(c) band spectrum level skewness coefficient



(d) band spectrum level relative kurtosis coefficient

Figure 5-37. Ensemble Statistical Moments for 1/3-Octave Acoustic Band Spectral Levels for Runs A18 and A05

or  $Dn/U_b$ , where  $U_b$  is the relative rotor velocity at the effective radius of 75% span. The span and chord dimensions, in terms of the wave number, are indicated on the plots. The mean BSL plot of Figure 5-37a shows the influence of the higher axial wind speed below 20 Hz, but above that the two spectra are essentially the same. A similar situation exists for the  $\langle b_2(f) \rangle$  spectra of Figure 5-37b, though the lower wind run becomes more discrete below 20 Hz. The plots of the  $\langle b_3(f) \rangle$  and  $\langle b_4(f) \rangle$  spectra in Figures 5-37c and d indicate some spectral shifts in the bands for the two runs. The clear difference, however, is the strong peaking behavior being exhibited at 80 Hz and above in the A05 run data. We believe this to be associated with the intense vertical stratification present during this run as indicated by the detailed profiles measured by the tethered balloon shown in Figure 5-38.

Low-to-Moderate Wind, Low Stability versus High Wind, High Stability Inflow Conditions. The 45-m axial and upwash spectra are shown in Figure 5-39 for Runs A14-1 and A18. The mean BSL spectra of Figure 5-40a show a much sharper difference in the spectral slopes below 20 Hz than was true for the previous comparison, even though the lower wind run here has a higher mean velocity. Above 20 Hz, the curves again nearly overlap. The variance coefficient spectra of Figure 5-40b indicate less variation in the lower speed run in the bands between 6.3 and 25 Hz. The skewness and kurtosis spectra in Figures 5-40c and d indicate a much more discrete behavior in the bands below 10 Hz for the lower speed, lower stability run, though a harmonic relationship in the A18 run does seem to exist.

The A14-2 and A11 runs each fall into similar classifications in Table 5-4, but the inflow conditions are quite different from those of the previous pair. For example, both the axial and upwash turbulence spectra of run A11 exhibit a discrete feature near  $f = 0.6$ . This can indicate that atmospheric wave motions are present at the anemometer height. Even though the hub-height mean wind speed of the A11 run is almost 50% higher than that for run A14-2, there is more turbulent energy in the inflow of the latter, as indicated in Figure 5-41. This seems to be reflected in the steeper slope of the mean BSL curve in Figure 5-42a and the variance coefficient spectra in Figure 5-42b. The skewness and kurtosis coefficient spectra shown in Figures 5-42c and d are also quite different from those of the A18 and A14-1 runs. There is much more evidence of spectral peaking in the more turbulent A14-2 run below 20 Hz. The A11 run, however, shows evidence of peaks occurring often in the bands above 63 Hz, probably as a result of the discrete peak in the inflow spectra in Figure 5-41.

Low Wind, Slightly Unstable versus Low Wind, Slightly Stable Inflow Conditions. The axial (longitudinal) and upwash (vertical) reduced-frequency spectra for Runs A03 and A14-1 are compared in Figure 5-43. Again, even though the A14-1 run has a higher associated mean wind speed, there is more turbulent energy in the A03 run's unstable inflow. This underscores the need to consider the stability characteristics of the inflow as well as the velocity magnitudes. As before, this excess turbulent energy is reflected in the mean BSL spectra in Figure 5-44a as larger low-frequency emission levels and a steeper slope with increasing frequency. Above the 10-Hz band, however, the slightly stable A14-1 run emits slightly higher levels. The variance coefficient or  $\langle b_2 \rangle$  spectra of Figure 5-44b show essentially the same behavior for this pair of runs. The effects of increased stability and a slightly greater mean wind speed in Run A14-1 are demonstrated in the  $\langle b_3 \rangle$  and  $\langle b_4 \rangle$

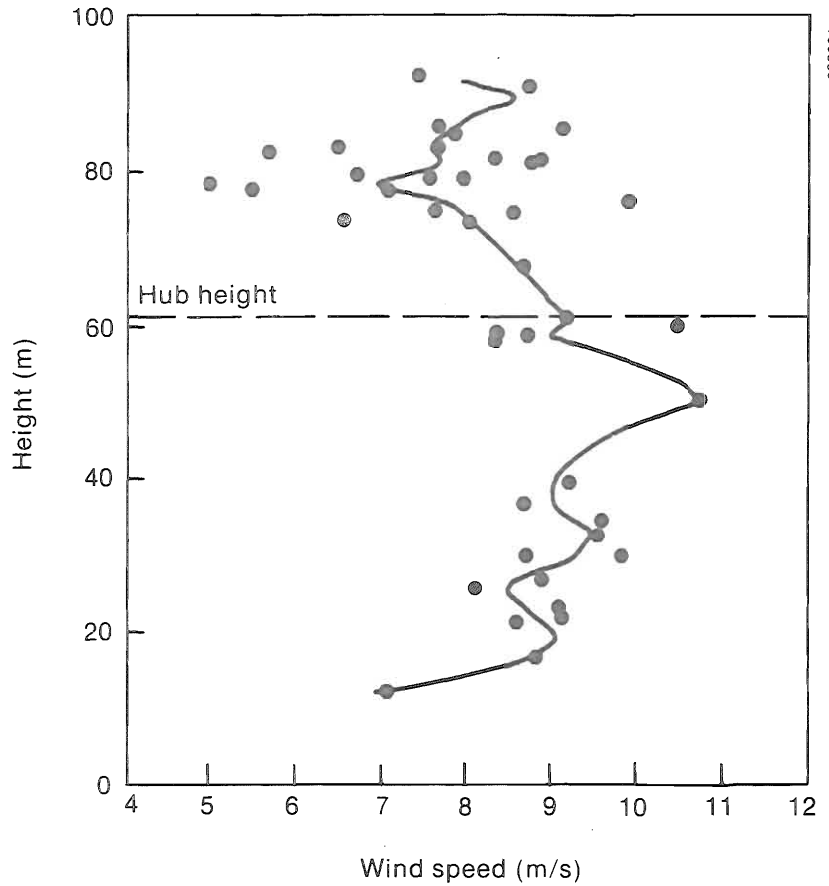
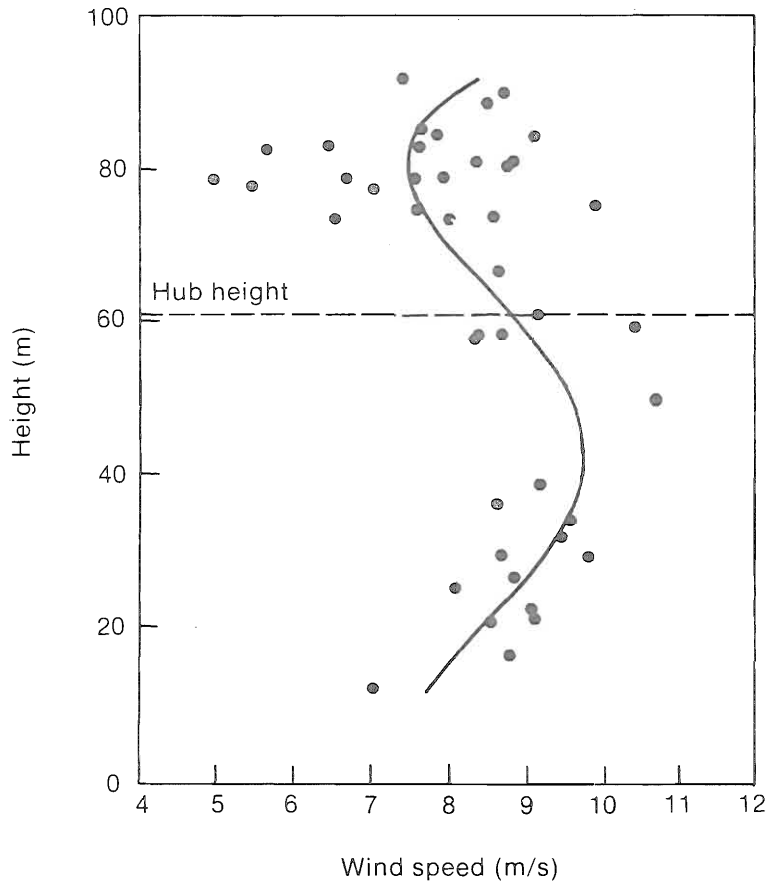


Figure 5-38a. Smoothed (a) and High-Resolution (b) Vertical Profiles of Wind Speed for Run A05

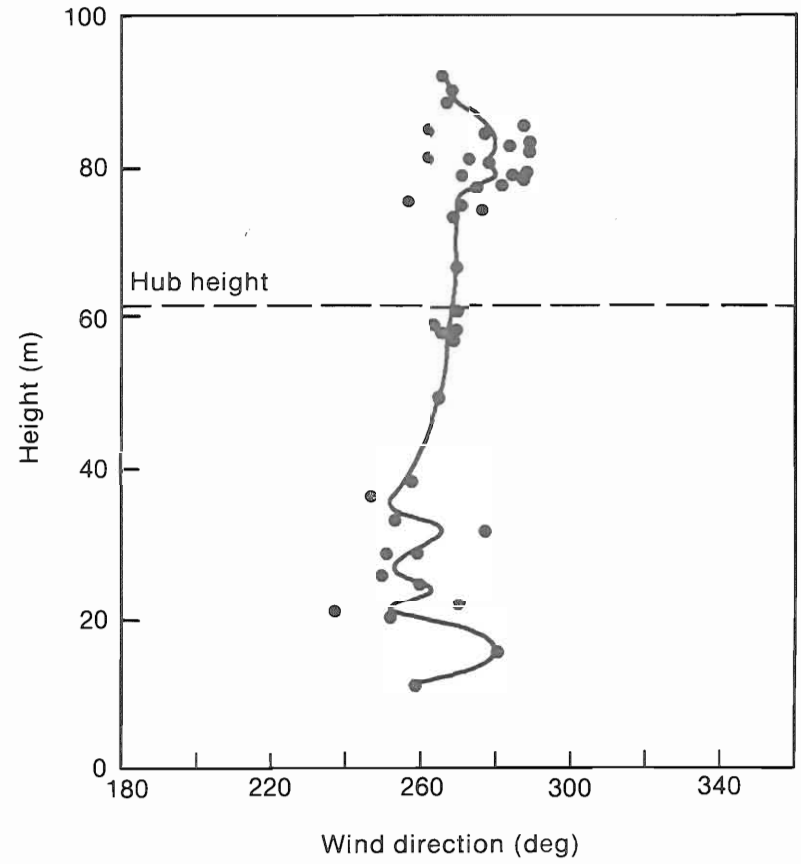
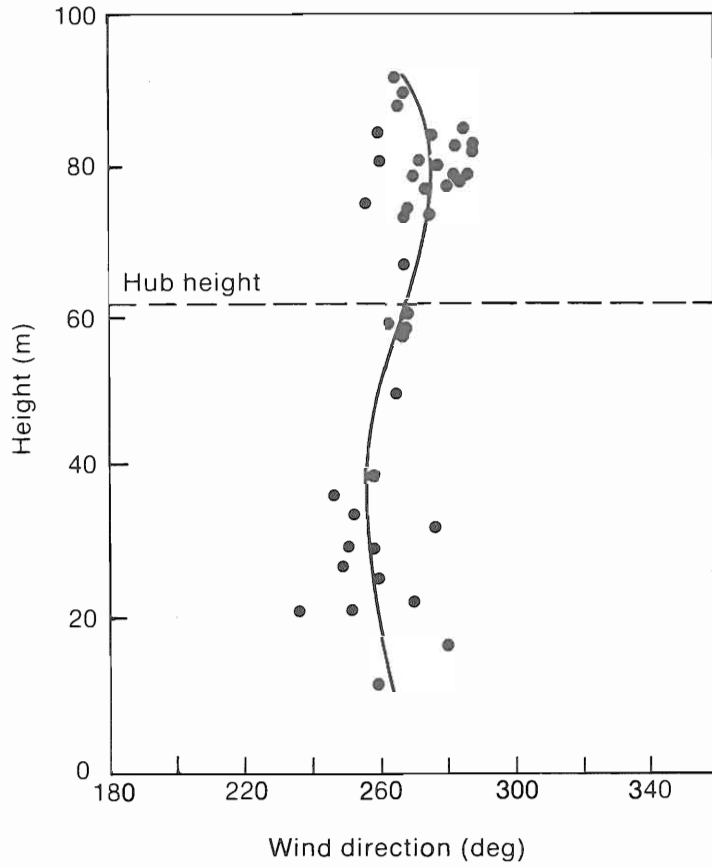


Figure 5-38b. Smoothed (a) and High-Resolution (b) Vertical Profiles of Wind Direction for Run A05

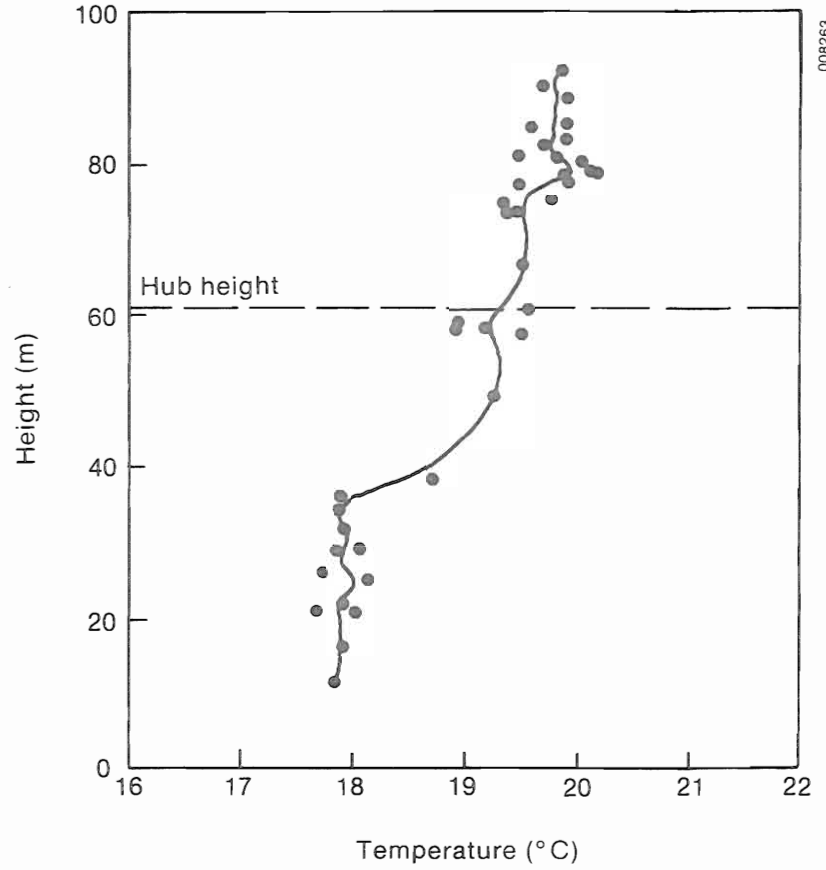
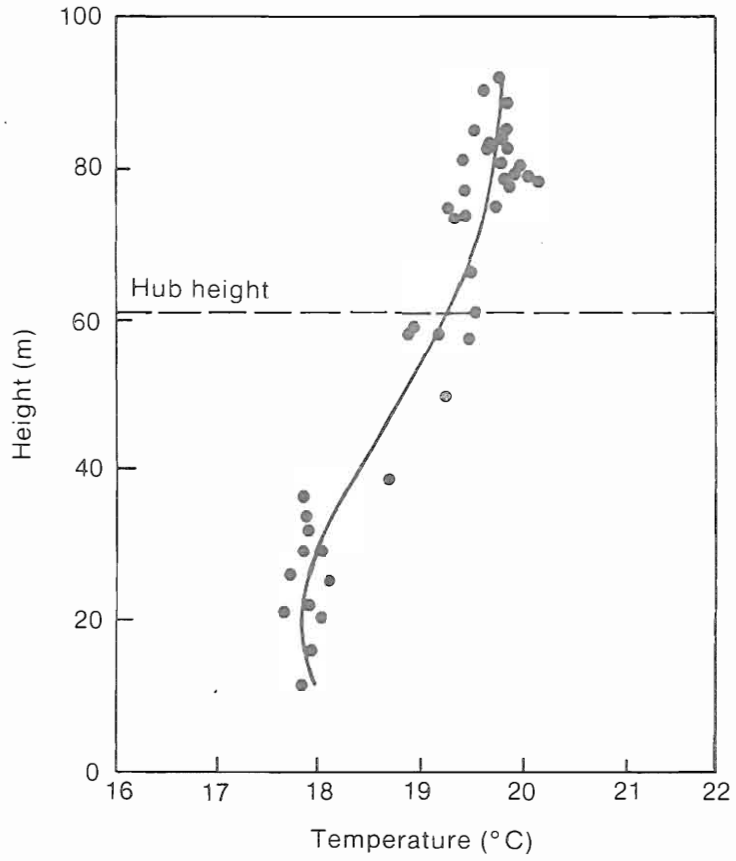
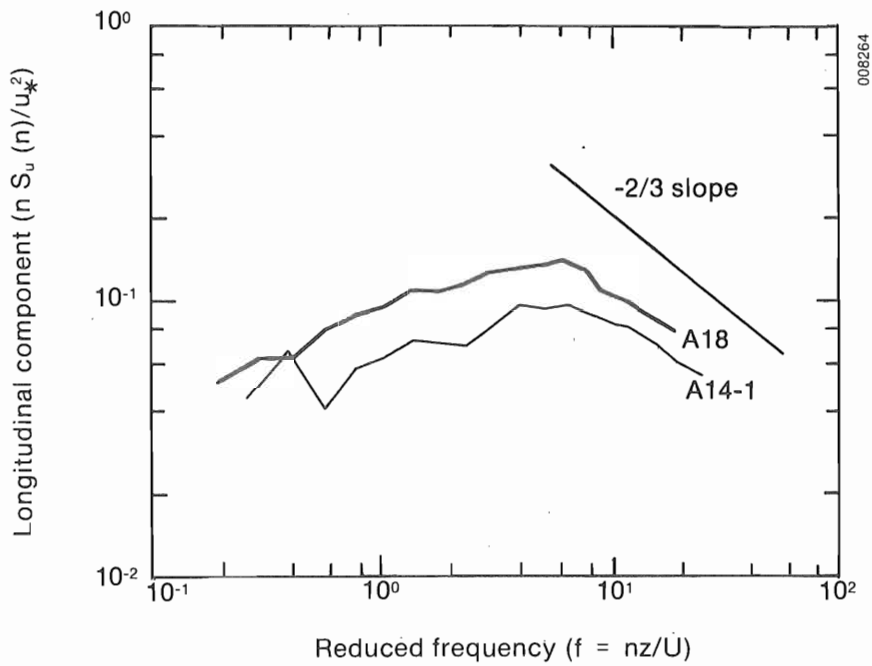
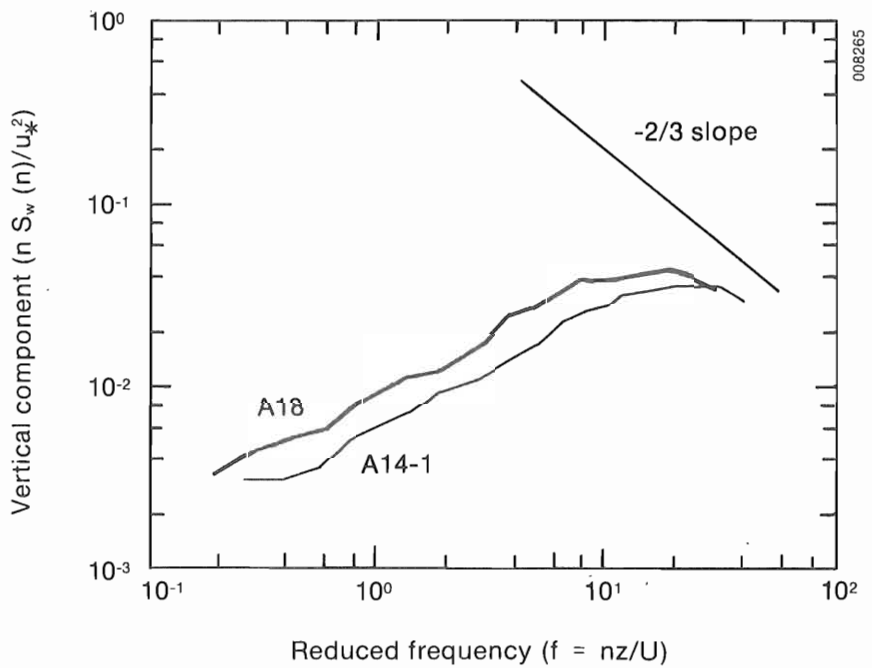


Figure 5-38c. Smoothed (a) and High-Resolution (b) Vertical Profiles of Sensible Temperature for Run A05

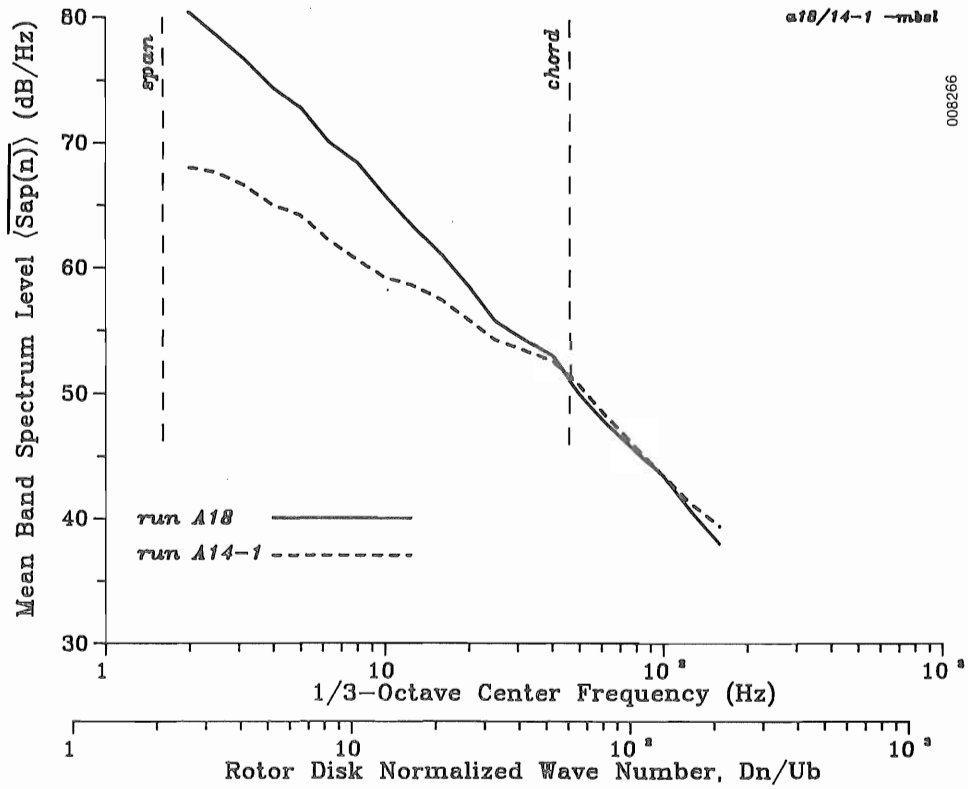


(a) longitudinal (axial) turbulence component normalized spectra

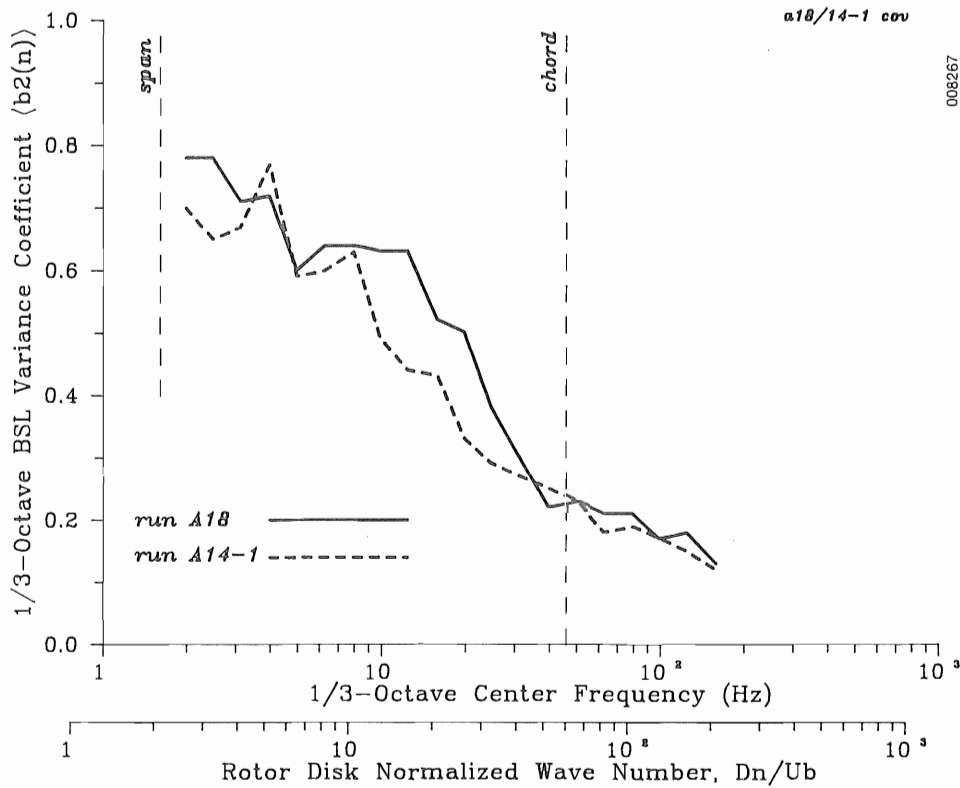


(b) vertical (upwash) turbulence component normalized spectra

Figure 5-39. Normalized 45-m Turbulence Spectra for Runs A18 and A14-1

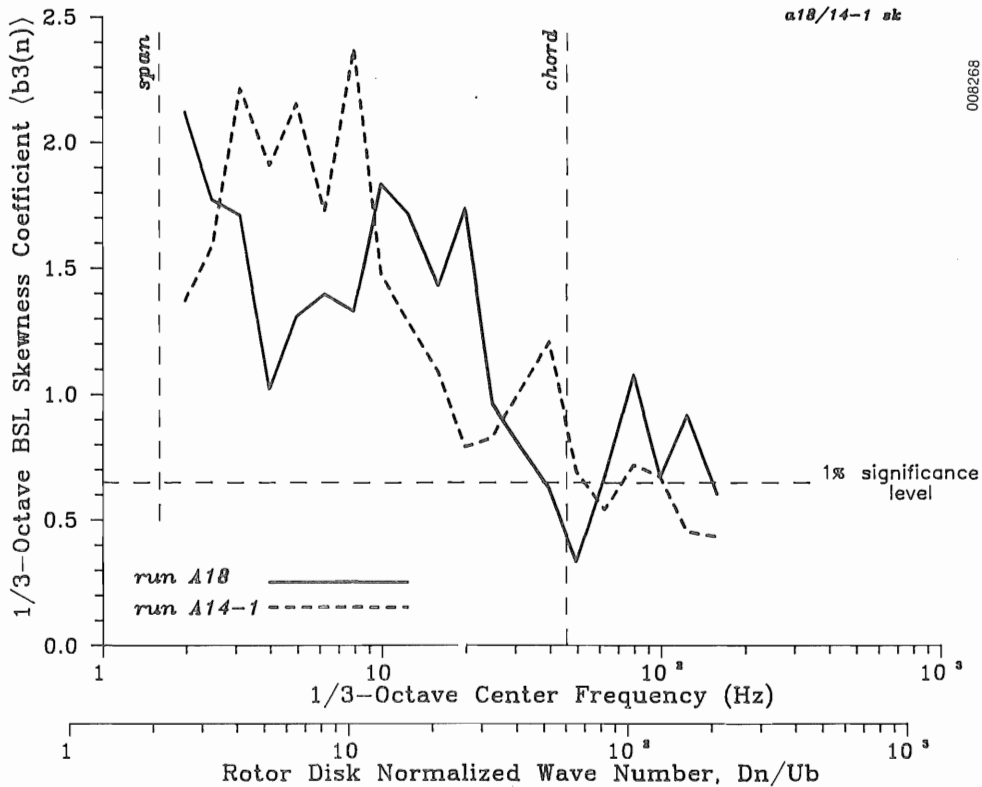


(a) mean band spectrum levels

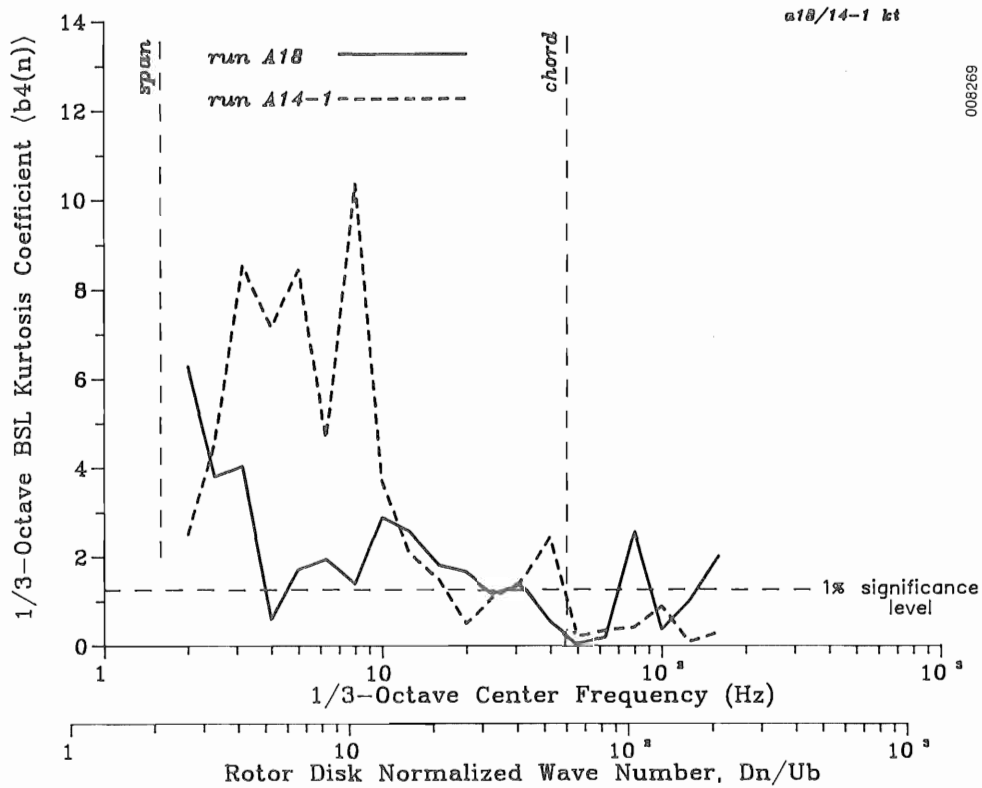


(b) band spectrum level variance coefficient

Figure 5-40. Ensemble Statistical Moments of 1/3-Octave Acoustical Band Spectrum Levels for Runs A18 and A14-1

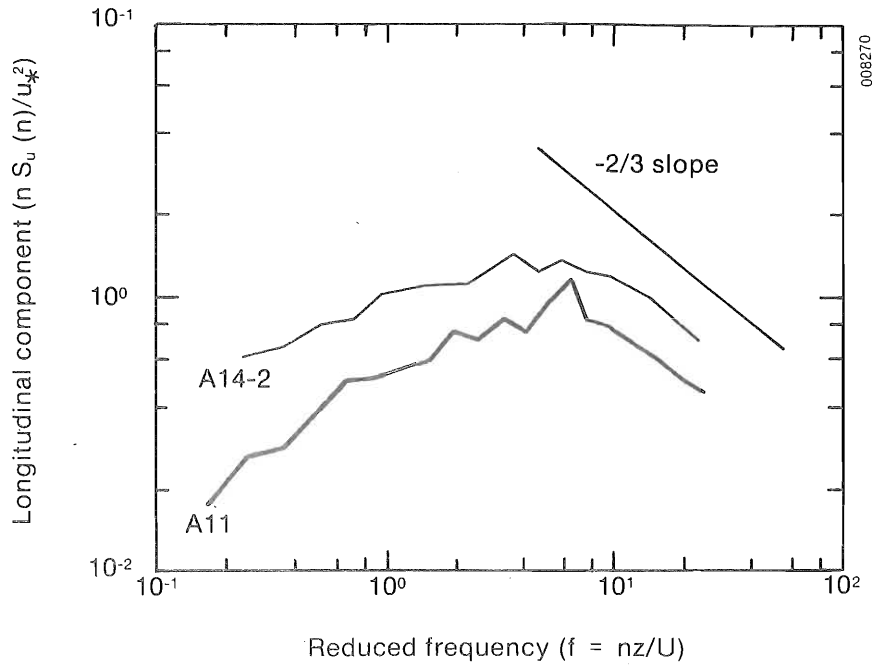


(c) band spectrum level skewness coefficient

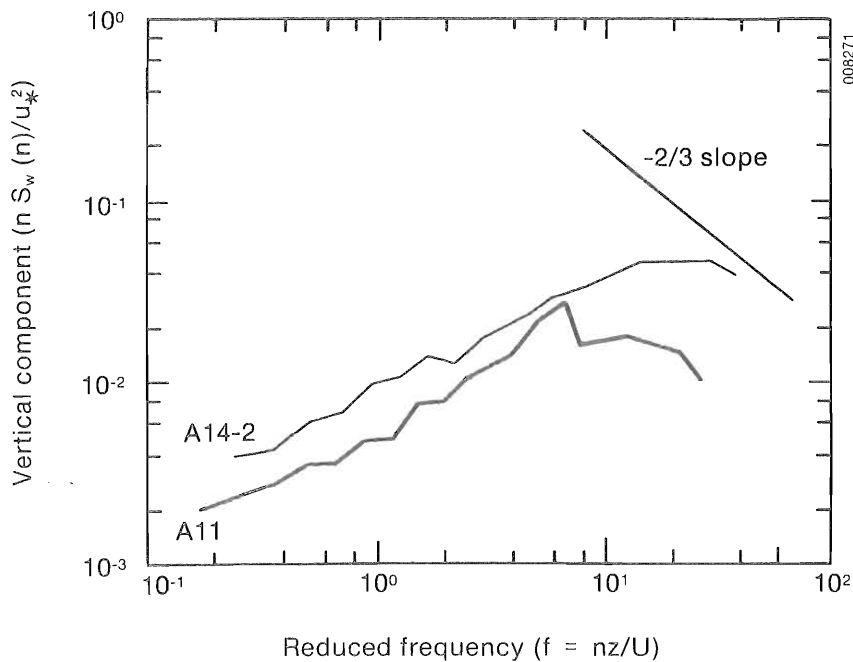


(d) band spectrum level relative kurtosis coefficient

Figure 5-40. Ensemble Statistical Moments of 1/3-Octave Acoustical Band Spectrum Levels for Runs A18 and A14-1

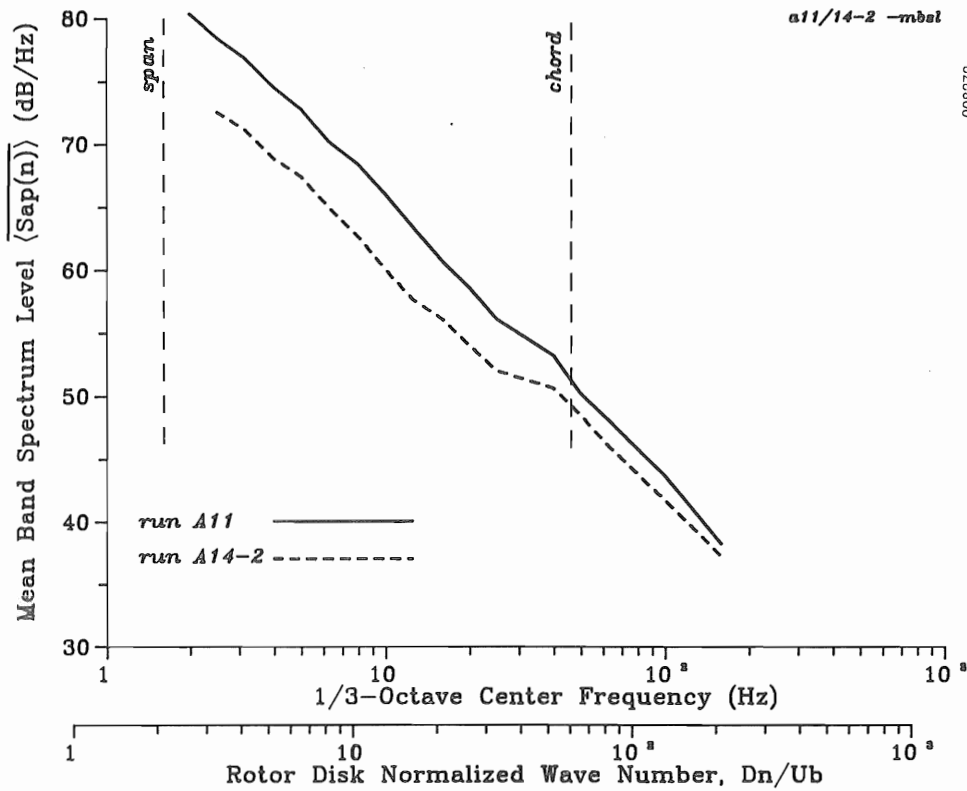


(a) longitudinal (axial) turbulence component normalized spectra

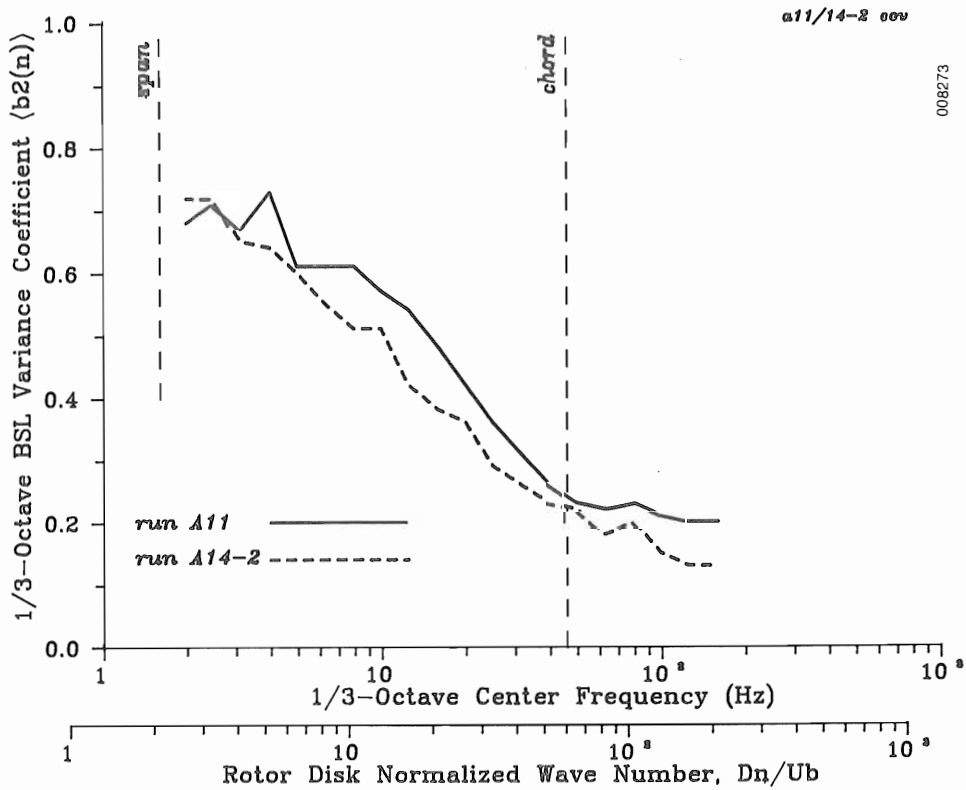


(b) vertical (upwash) turbulence component normalized spectra

Figure 5-41. Normalized 45-m Turbulence Spectra for Runs A14-2 and A11

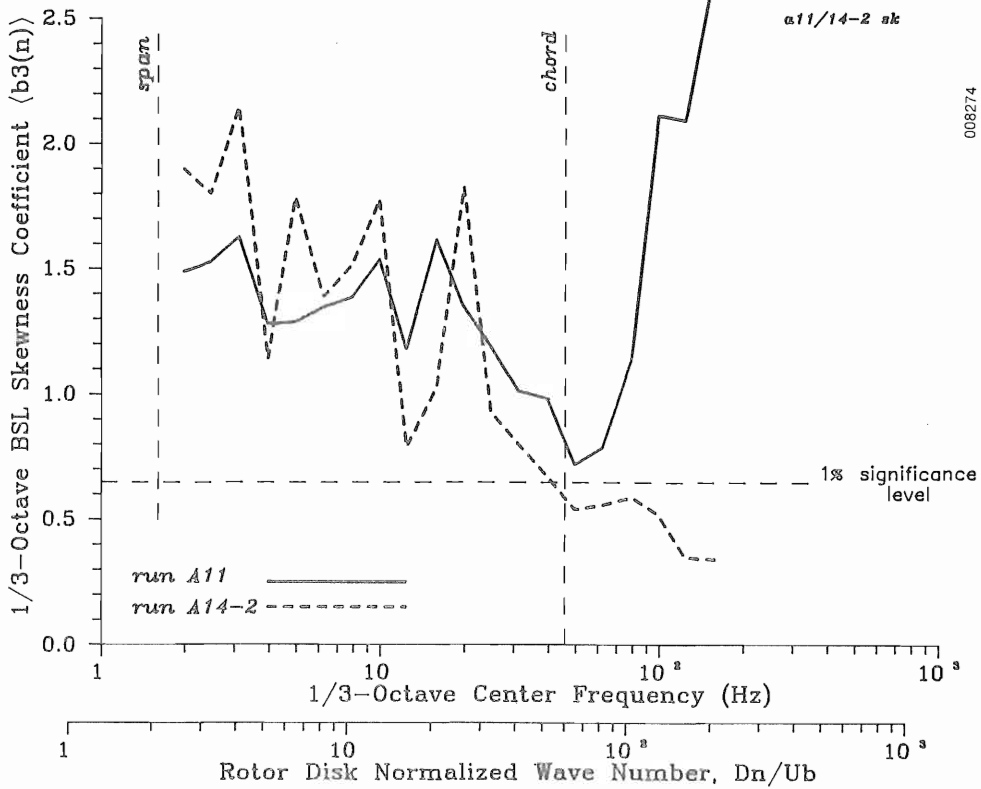


(a) mean band spectrum levels

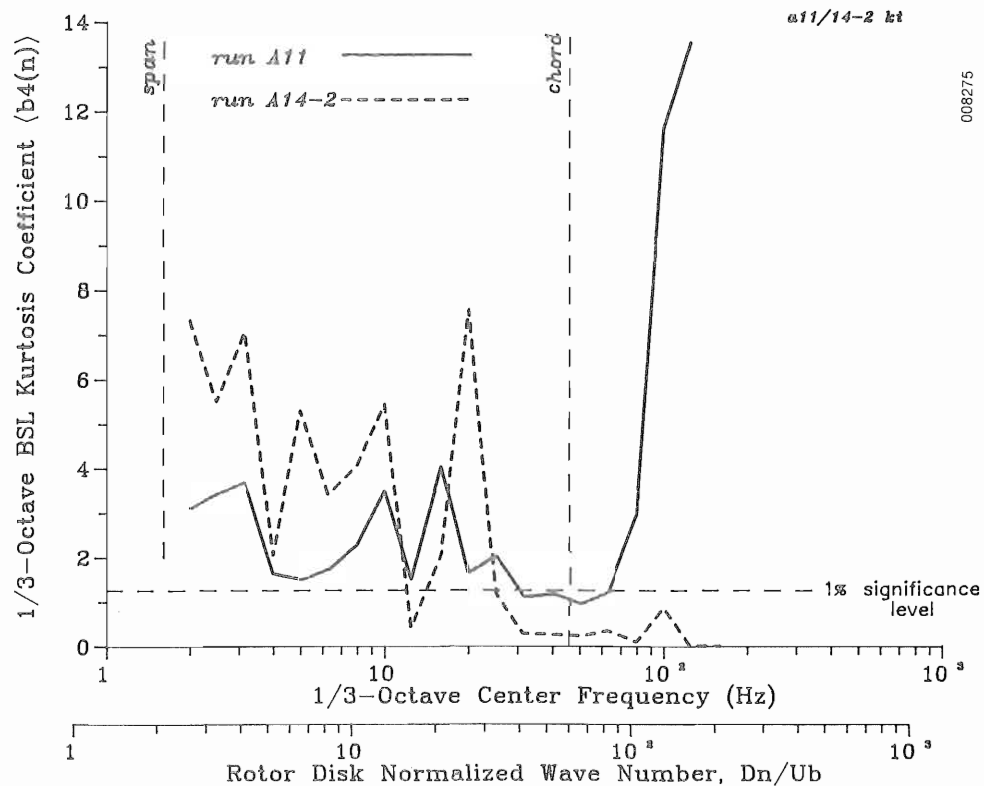


(b) band spectral level variance coefficients

Figure 5-42. Ensemble Statistical Moments of 1/3-Octave Acoustical Band Spectrum Levels for Runs A14-2 and A11

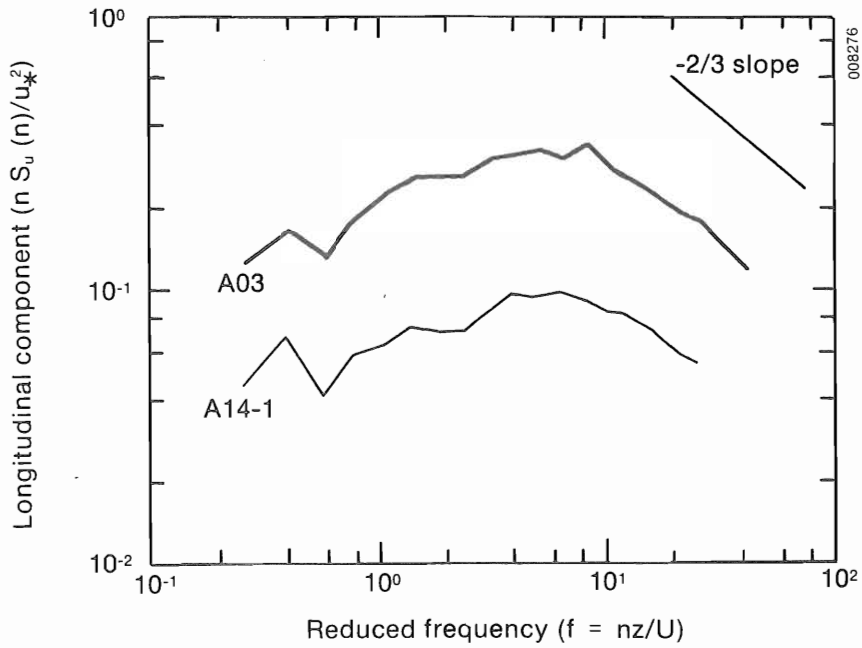


(c) band spectral level skewness coefficients

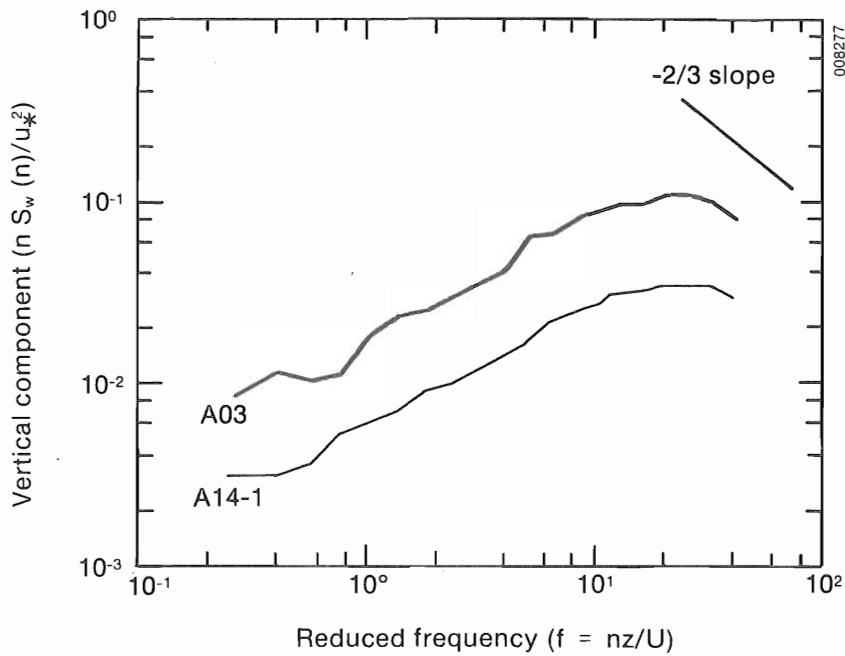


(d) band spectral level relative kurtosis coefficients

Figure 5-42. Ensemble Statistical Moments of 1/3-Octave Acoustical Band Spectrum Levels for Runs A14-2 and A11



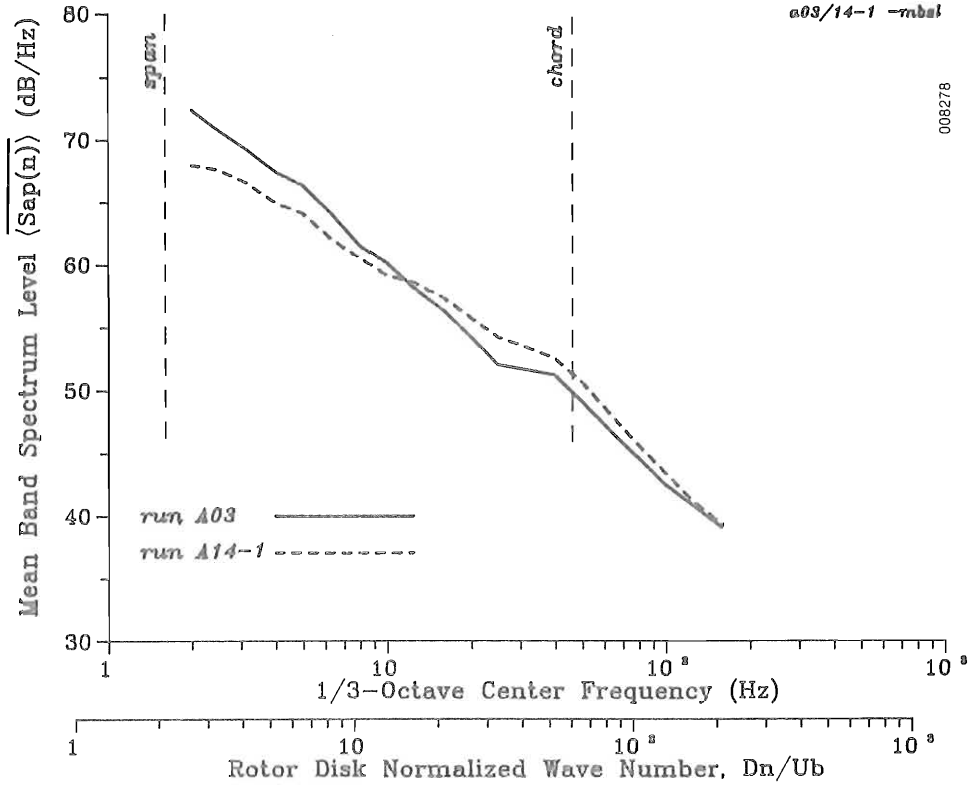
(a) longitudinal (axial) turbulence component normalized spectra



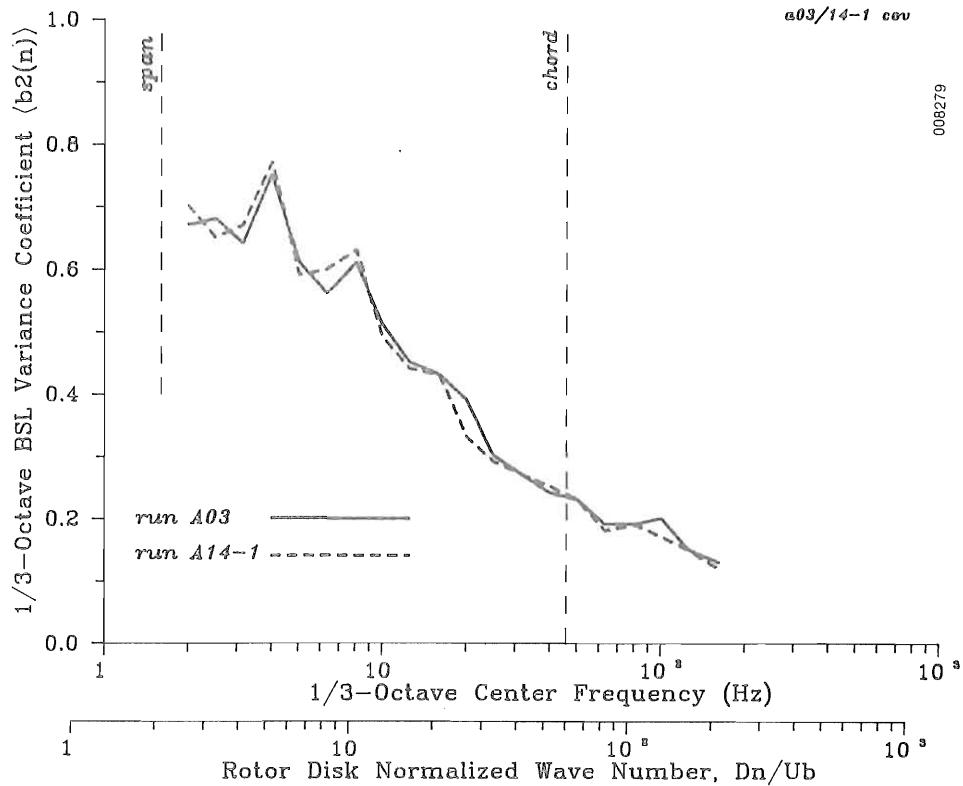
(b) vertical (upwash) turbulence component normalized spectra

Figure 5-43. Normalized 45-m Turbulence Spectra for Runs A03 and A14-1

008278

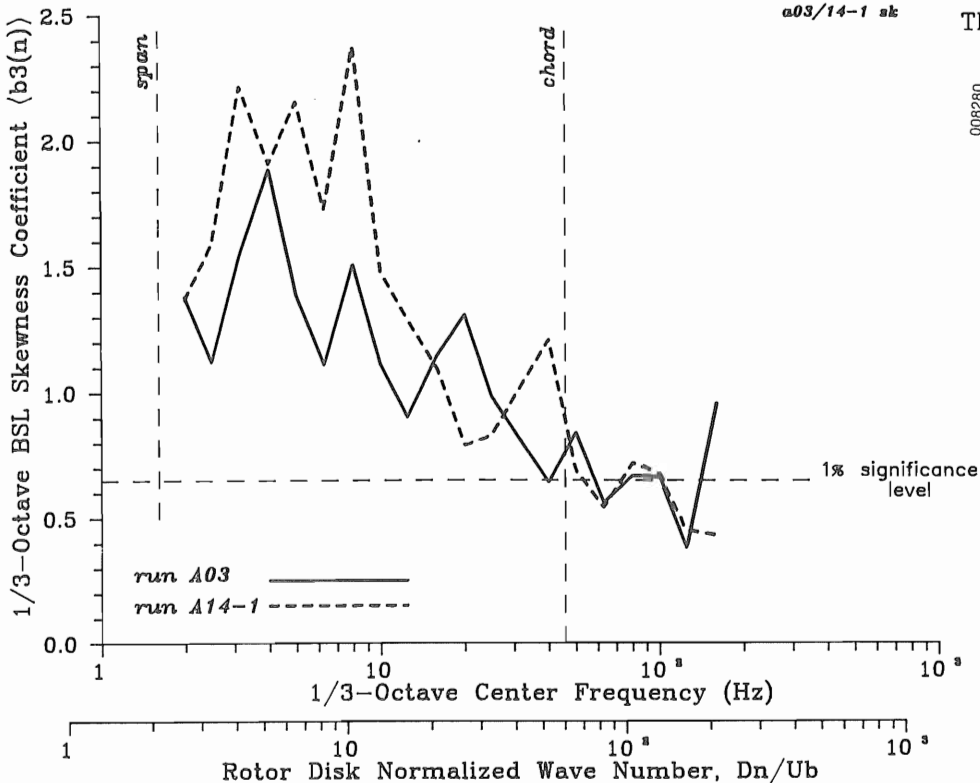


(a) mean band spectrum levels

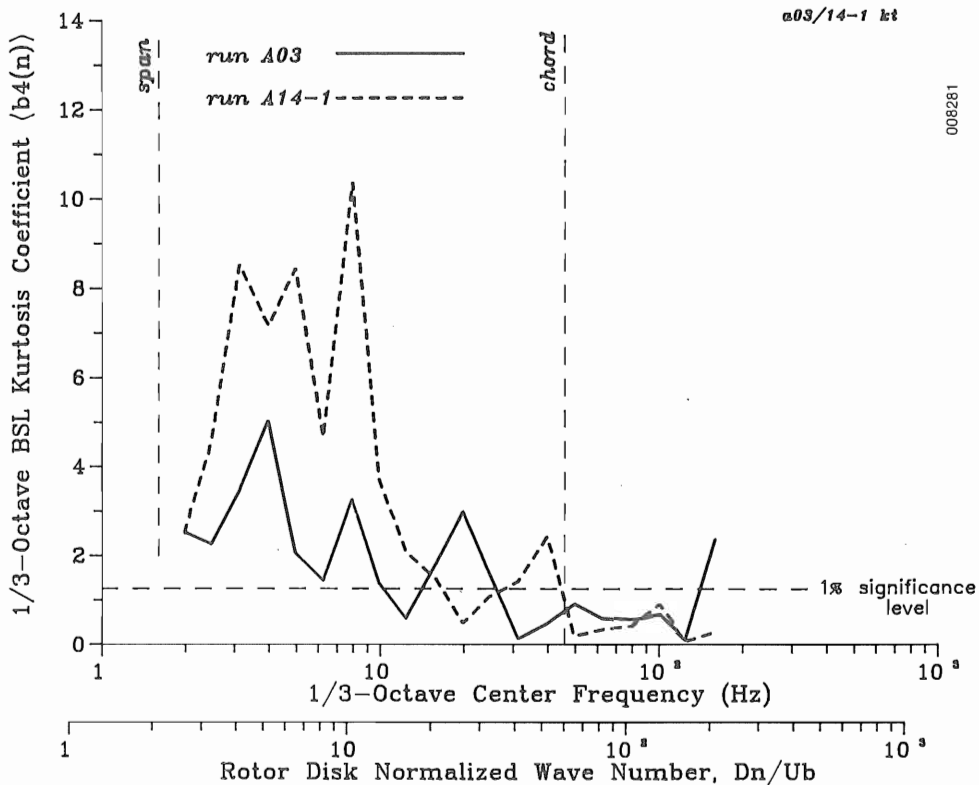


(b) band spectrum level variance coefficients

Figure 5-44. Ensemble Statistical Moments of 1/3-Octave Acoustic Band Spectrum Levels for Runs A03 and A14-1



(c) band spectrum level skewness coefficients



(d) band spectrum level relative kurtosis coefficients

Figure 5-44. Ensemble Statistical Moments of 1/3-Octave Acoustic Band Spectrum Levels for Runs A03 and A14-1

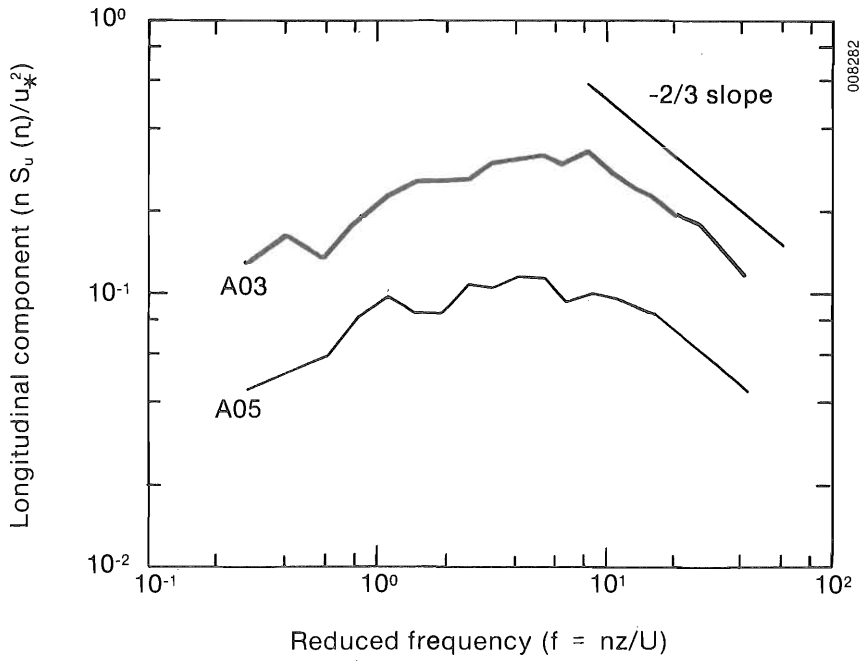
spectra of Figures 5-44c and d. The frequency shift and characteristics are very noticeable. The distinct harmonic nature of the bands in which peaking occurs in the unstable A03 run gives way to very strong, but much more band-limited behavior in the slightly stable A14-1 run.

Low Wind, Unstable Inflow versus Low Wind, Very Stable Inflow Conditions. The normalized spectra associated with the two inflow components are shown in Figure 5-45. A  $-2/3$  spectral slope at high frequencies is indicative of the turbulent inertial subrange. As one would expect, there is much less turbulent energy present in the very stable inflow. The slight discreteness in the band between  $f = 0.06$  and  $0.6$  in the axial spectra of Run A05 hints that waves may be present. The plot of the mean BSL spectra in Figure 5-46a is surprising, however. Even though Run A05 has a lower mean wind speed and less energy in the turbulent inflow, its mean LF radiated acoustic levels are essentially identical to those of Run A03.

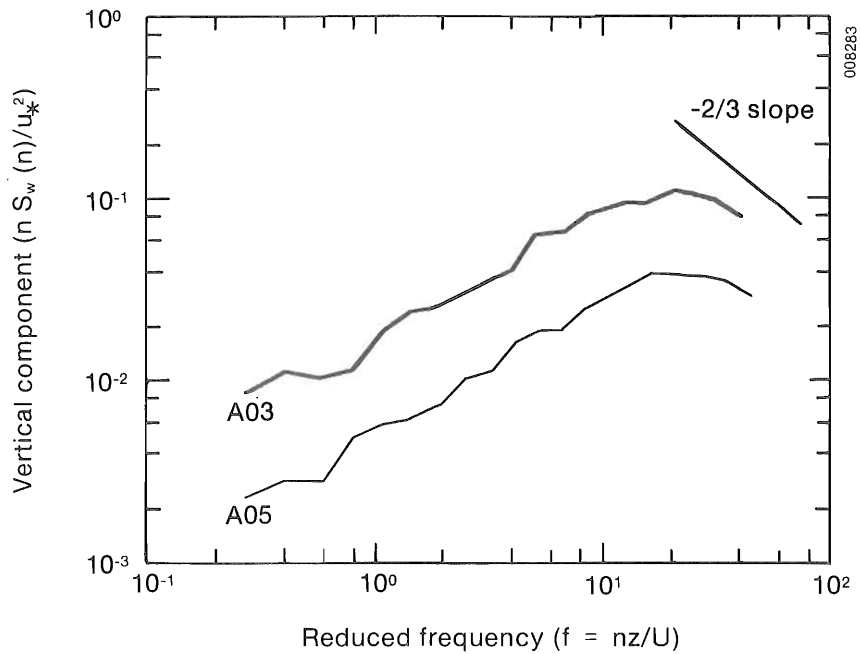
The reason for this behavior becomes apparent when we compare the detailed inflow structure. The first hint is that the upwash scale length  $I_w^z$  is  $7.5$  m for Run A05, versus  $13.3$  m for run A03. The transfer function plot of Figure 5-4 shows a strong, negative slope (almost  $2$  dB/Hz/m in the  $2$ -Hz  $1/3$ -octave band) with  $I_w^z$  below  $12.5$  Hz; i.e., the smaller the  $I_w^z$ , the greater the mean BSL below  $12.5$  Hz. Second, the peak wind speed occurs at a height of  $45$  m (as listed in Table 3-3c) with its attendant strong shears and just below the hub of the turbine. Finally, these features are clearly illustrated in the detailed tethered balloon profiles of Figure 5-47. The strong shear layer near  $45$  m is distinctly evident. It is the A05 run we discussed in connection with the direct measurement of the MOD-2 acoustical response function in Section 5.1.1.

The  $\langle b_2 \rangle$  spectra of Figure 5-46b shows that the acoustic levels of Run A05 are related to a more narrowband random process than those of Run A03 below about  $20$  Hz. While some frequency shifting has taken place in the  $\langle b_3 \rangle$  and  $\langle b_4 \rangle$  spectra of Figures 5-46c and d, the low-stability run exhibits the distinct harmonic structure while the high-frequency peaking is characteristic of the very stable case. Again, these two runs underscore the role of vertical stability in determining the aeroacoustic response of a large wind turbine.

High Wind, Moderate-to-High Stability vs. High Wind, Very-High-Stability Inflow Conditions. Here we compare the effects of increased stability under high wind conditions. Figure 5-48 plots the normalized axial and upwash turbulence spectra for Runs A11 and A18. The discrete peak in the A11 spectra is evident and not present in the A18 run data. The mean BSL spectra of Figure 5-49a for both runs are almost linear in log acoustic pressure (dB) versus log cyclic frequency. Furthermore, only the effect of the increased wind speed for the A11 run appears to be responsible for the slightly higher levels associated with it. The variance coefficient spectra in Figure 5-49b are essentially the same, indicating that the processes operating are dynamically similar. The skewness and kurtosis spectra of Figures 5-49c and d below about the  $31.5$ -Hz band are very similar. We believe the peaking activity in the A11 data is a result of the high-frequency discreteness of the turbulence inflow spectra in Figures 5-48. This is reflected somewhat in the smaller upwash length scale for the A11 run.



(a) longitudinal (axial) turbulence component normalized spectra



(b) vertical (upwash) turbulence component normalized spectra

Figure 5-45. Normalized 45-m Turbulence Spectra for Runs A03 and A05

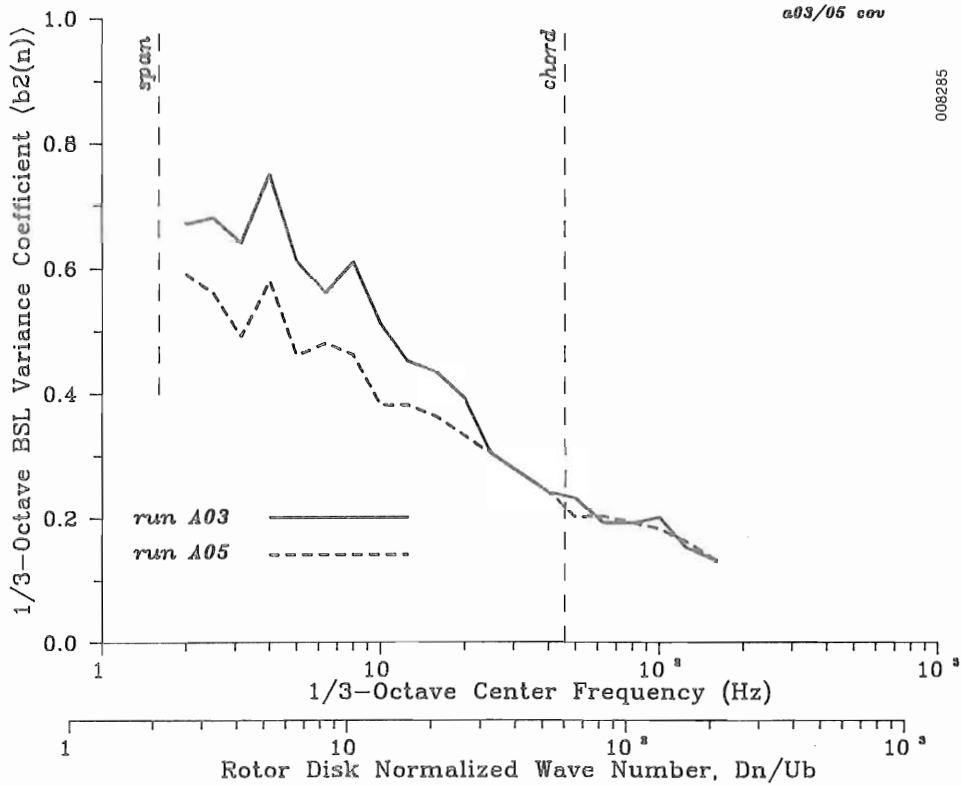
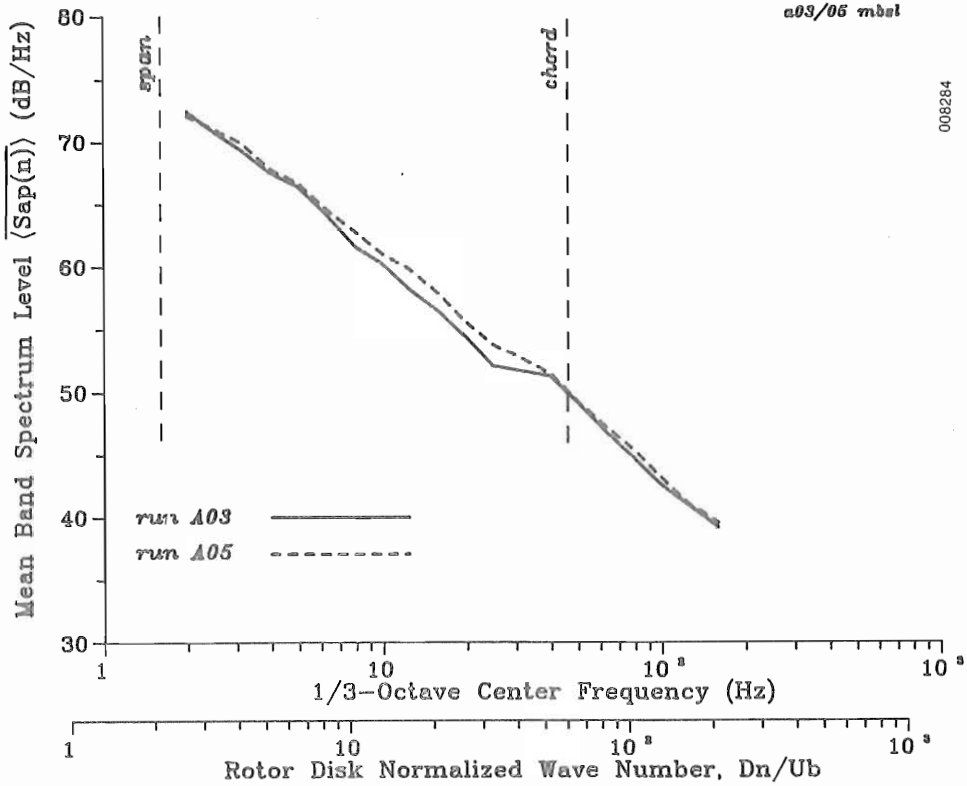
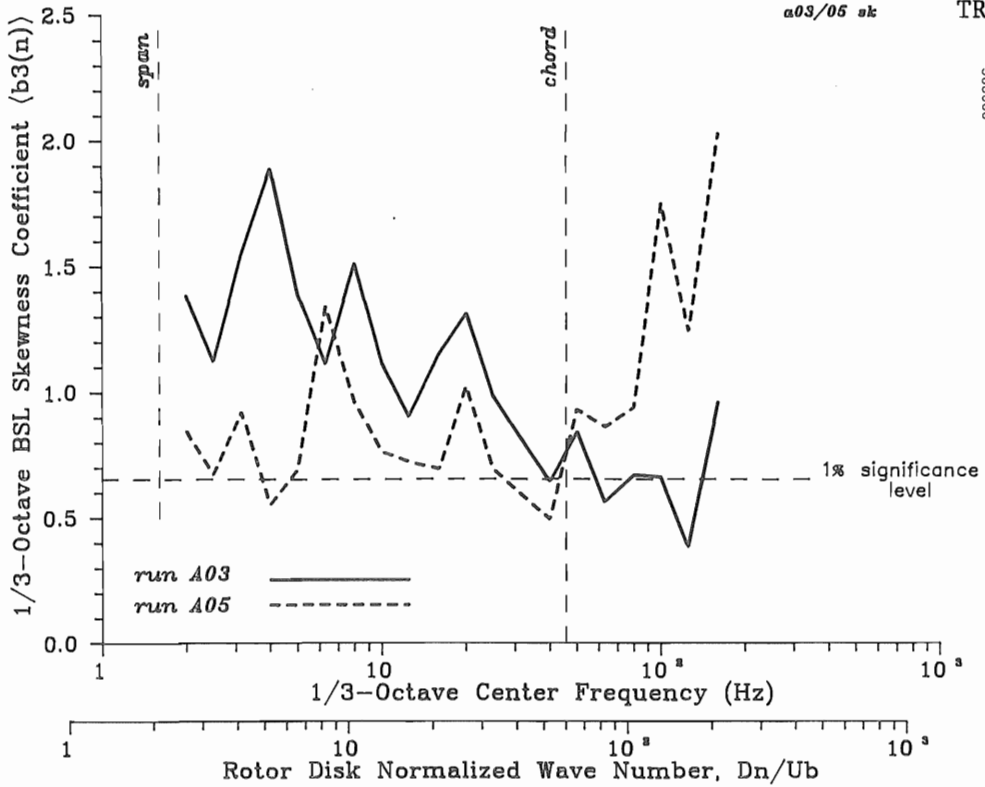
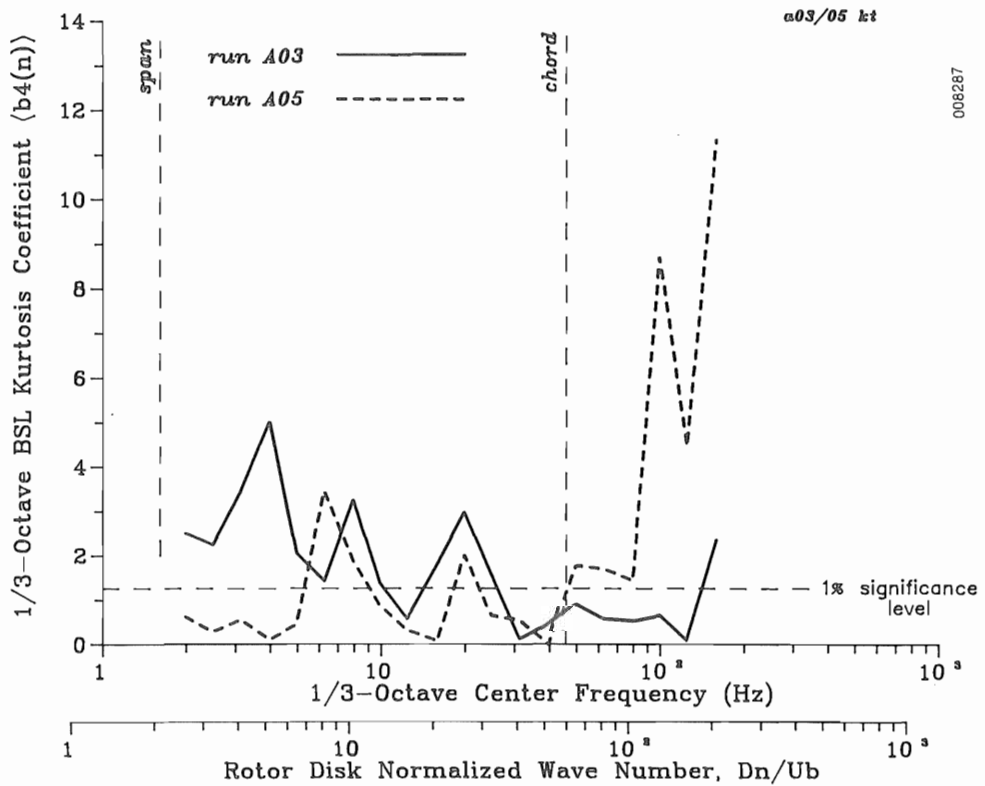


Figure 5-46. Ensemble Statistical Moments of Acoustic 1/3-Octave Band Spectral Levels for Runs A03 and A05



(c) band spectrum level skewness coefficients



(d) band spectrum level relative kurtosis coefficients

Figure 5-46. Ensemble Statistical Moments of Acoustic 1/3-Octave Band Spectral Levels for Runs A03 and A05

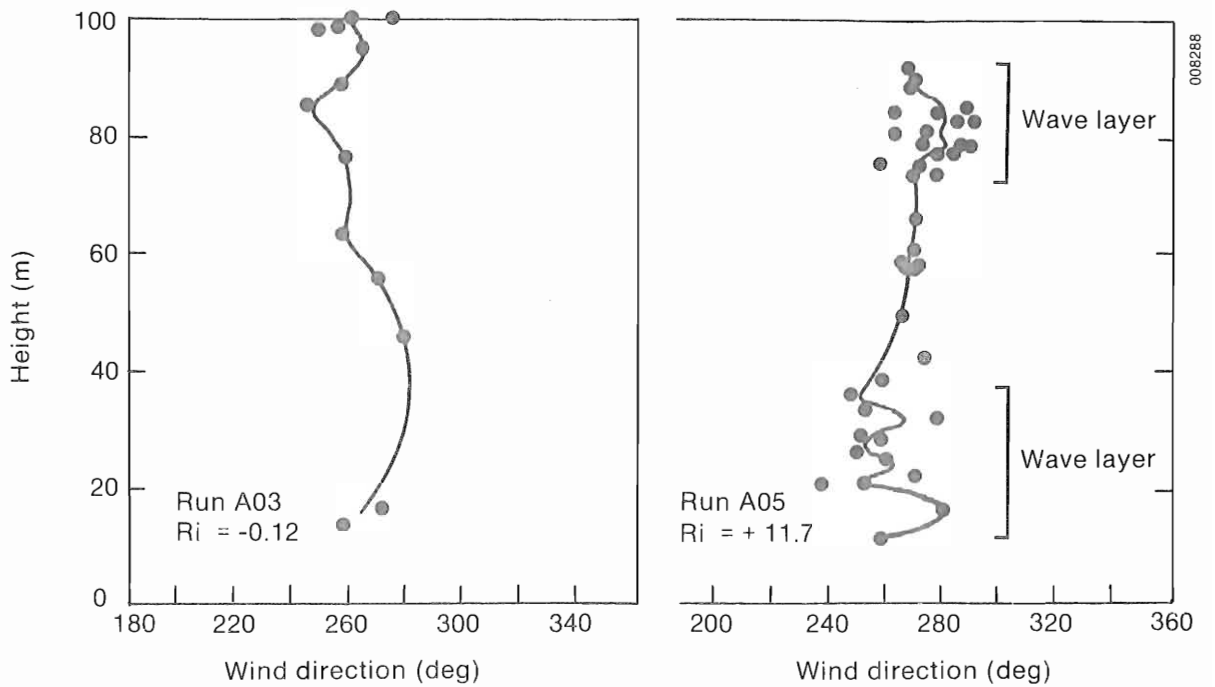


Figure 5-47a. Detailed Vertical Profiles (3-m resolution) of Wind Direction for Runs A03 and A05

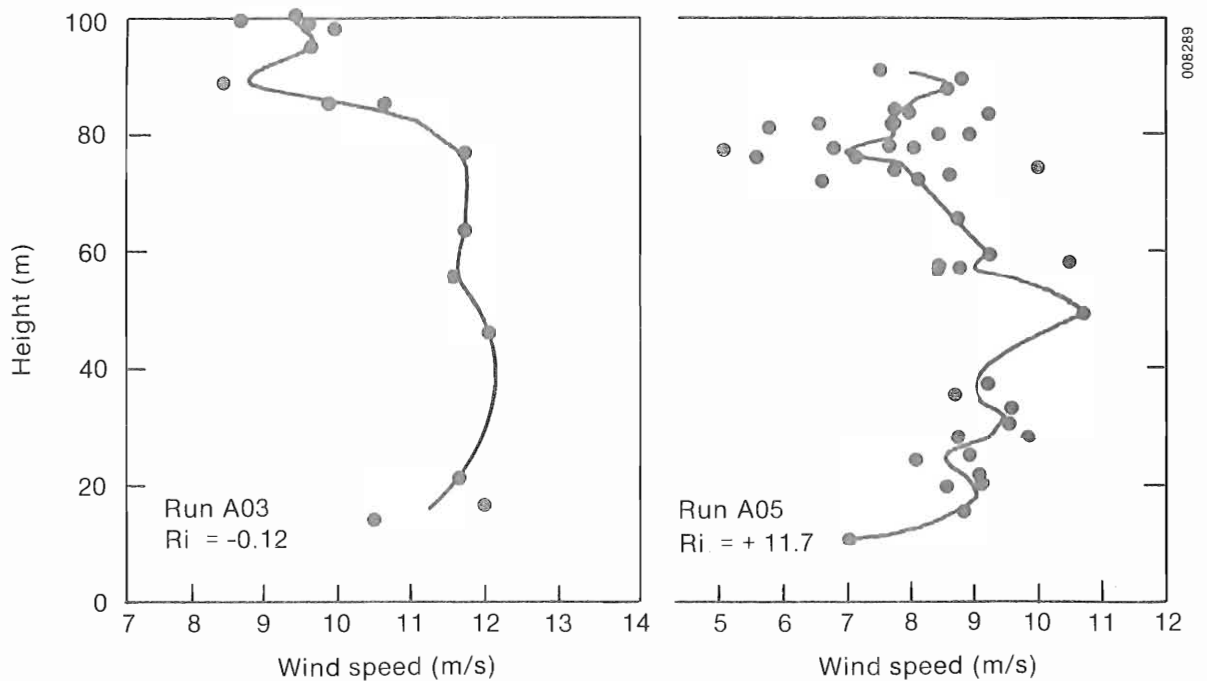
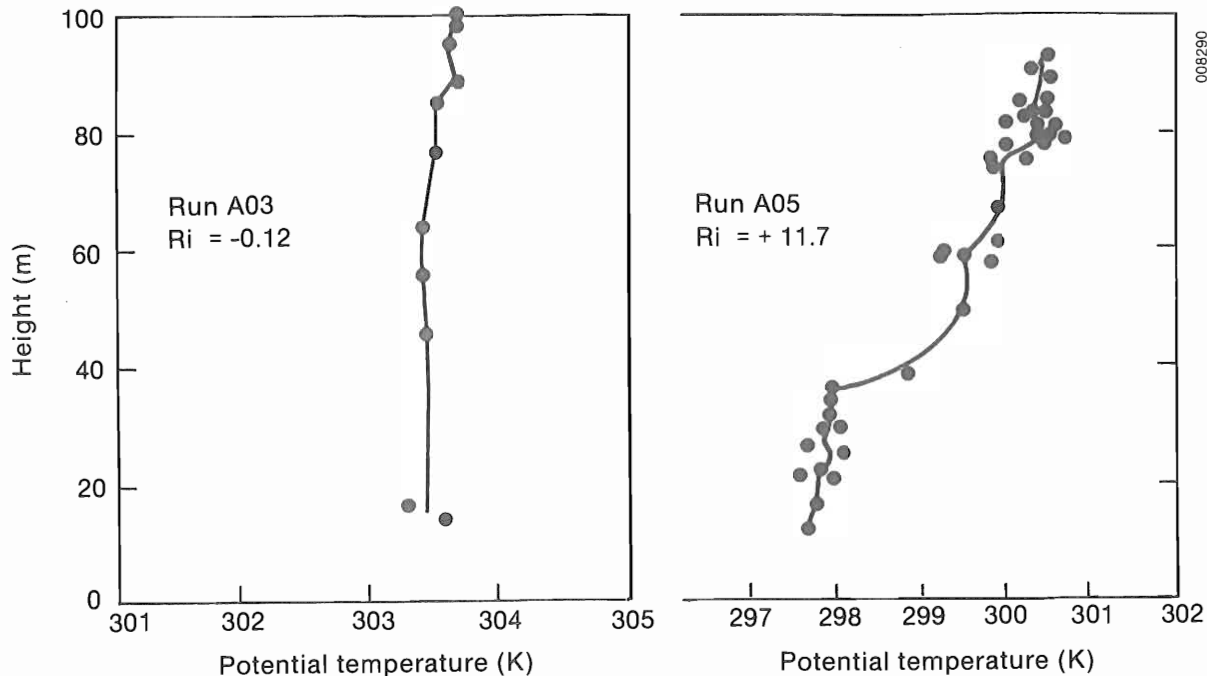


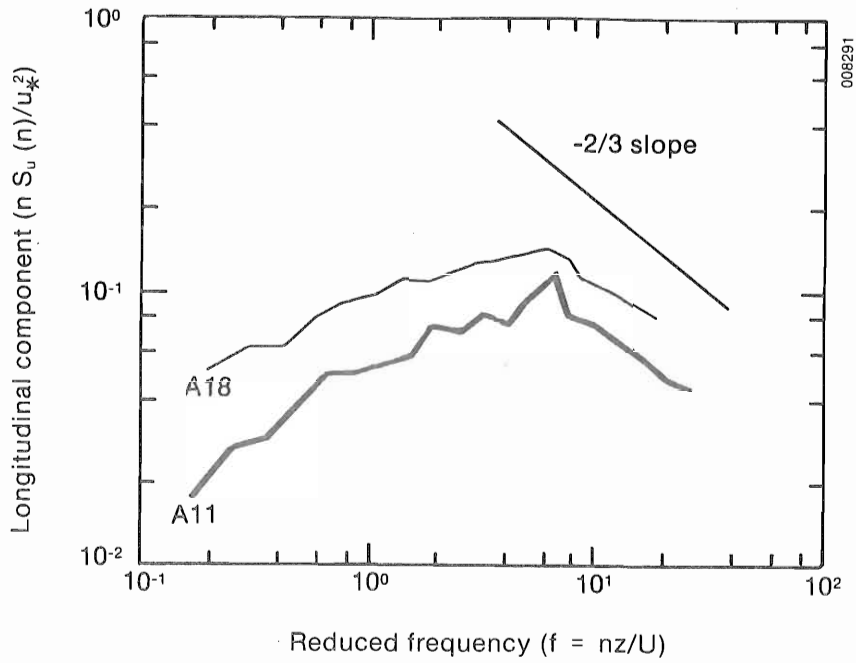
Figure 5-47b. Detailed Vertical Profiles of Wind Speed for Runs A03 and A05



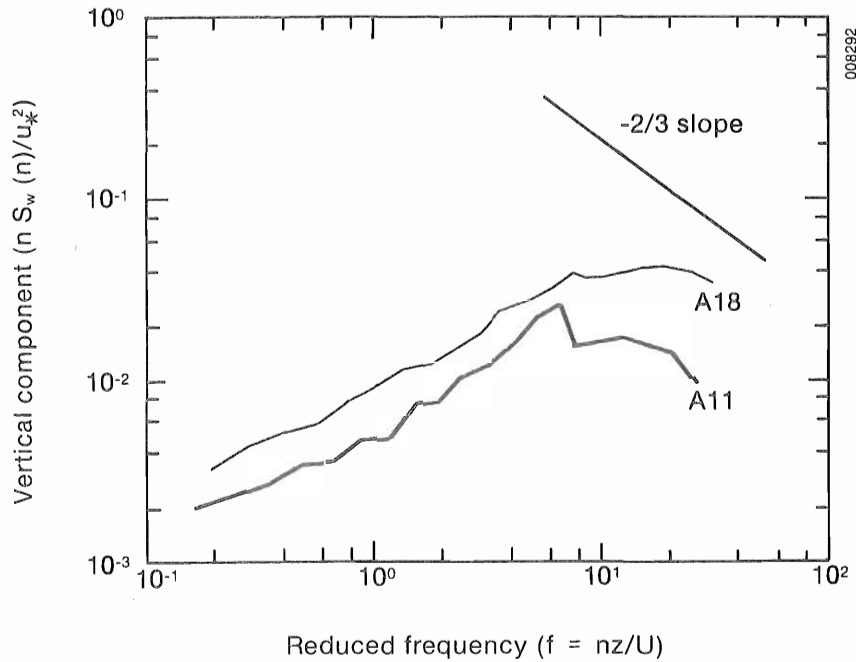
**Figure 5-47c. Detailed Vertical Profile of Thermal Structure (Potential Temperature) for Runs A03 and A05**

Low-to-Moderate Wind, Slightly Stable versus Low-to-Moderate Wind, Slightly More Stable Inflow Conditions. Finally, Runs A14-1 and A14-2 give us the opportunity to examine the acoustic effects of inflows with similar wind speeds but with subcritical ( $Ri < 0.25$ ) and above-critical stabilities. The normalized axial and upwash spectra are shown in Figure 5-50. The mean BSL spectra of Figure 5-51a shows what may be described as a rotation about the 10-Hz band; i.e., the A14-2 run emits higher levels below 10 Hz but less than the A14-1 run above 10 Hz. The characteristic inflow length scales ( $I_u^x$ ,  $I_w^x$ , and  $I_w^z$ ) listed in Table 5-4 indicate that the lengths associated with the more stable run (A14-2) are approximately half those of the less stable run. In particular, the in-plane scale length  $I_w^z$  is only 6.1 versus 16.5 m, respectively. Thus, this demonstrates that the effect of increasing the stability above the critical is to decrease the characteristic turbulence scales. This has the effect of increasing the LF acoustic output below 10 Hz while decreasing it above 10 Hz.

The  $\langle b_2 \rangle$  spectra, plotted in Figure 5-51b, indicate that some form of a wide-band dynamic process is present at the lower stability which produces harmonic aeroacoustic excitation. The frequency shifts in the  $\langle b_3 \rangle$  and  $\langle b_4 \rangle$  spectra in Figures 5-51c and d are quite evident. The shift toward smaller turbulence scales appears to be illustrated by the growth of the peak in the 20-Hz band and the decrease in those below 10 Hz for the more stable run. A comparison of these two runs has given clear evidence of the role of varying stability conditions under similar mean loads.

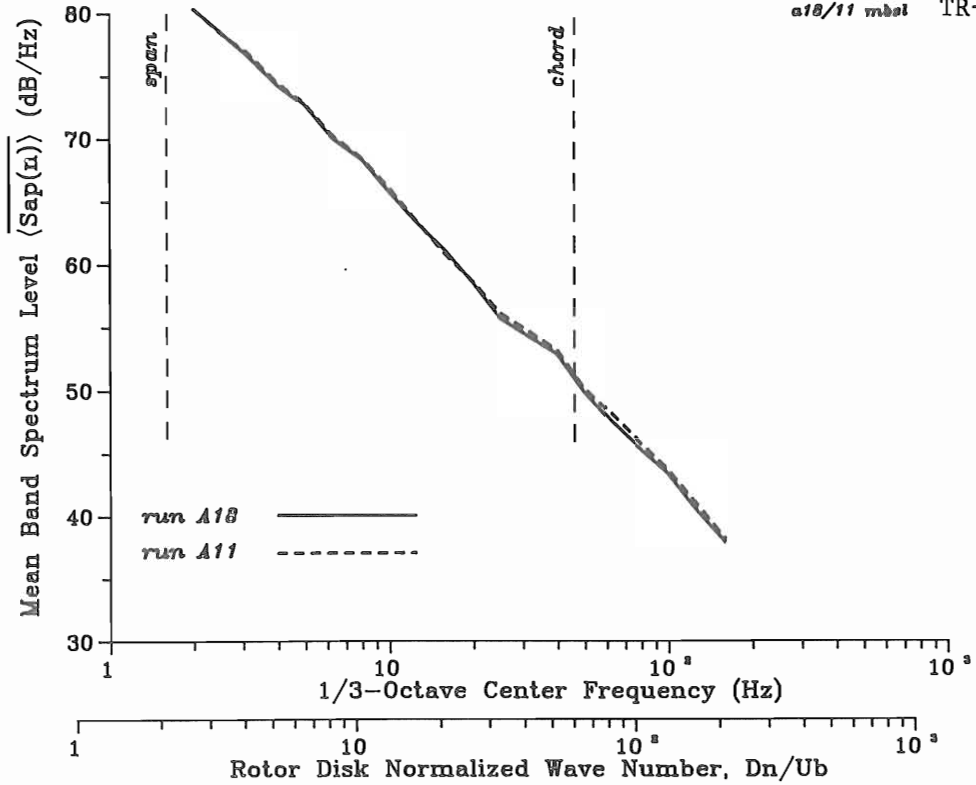


(a) longitudinal (axial) turbulence component normalized spectra

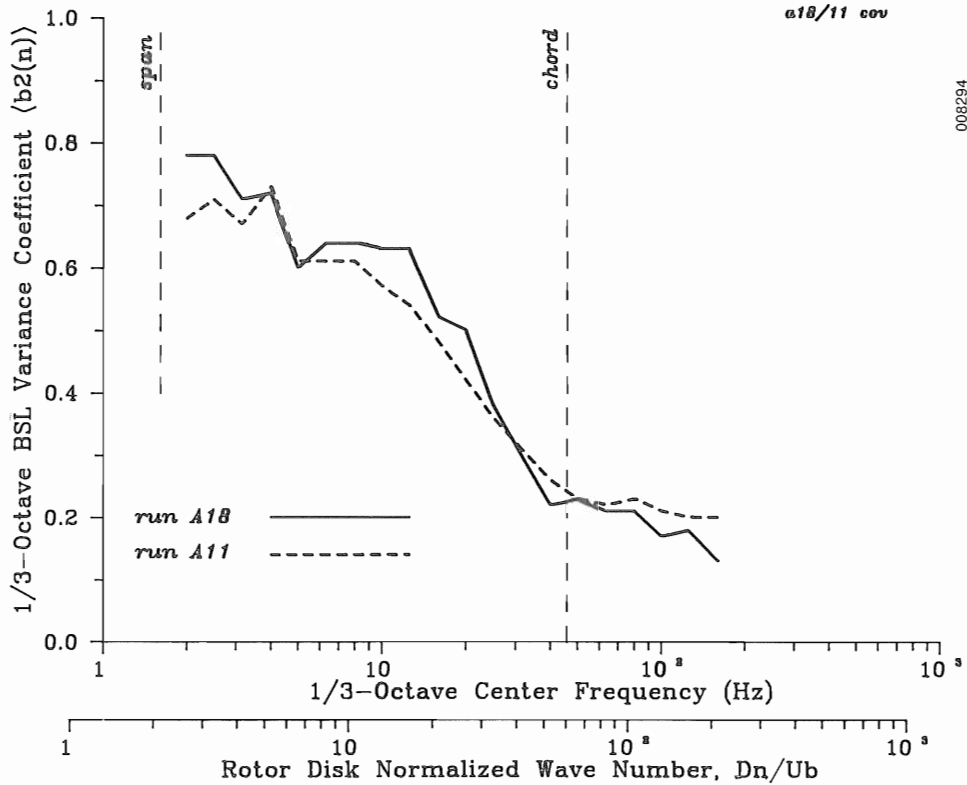


(b) vertical (upwash) turbulence component normalized spectra

Figure 5-48. Normalized 45-m Turbulence Spectra for Runs A11 and A18

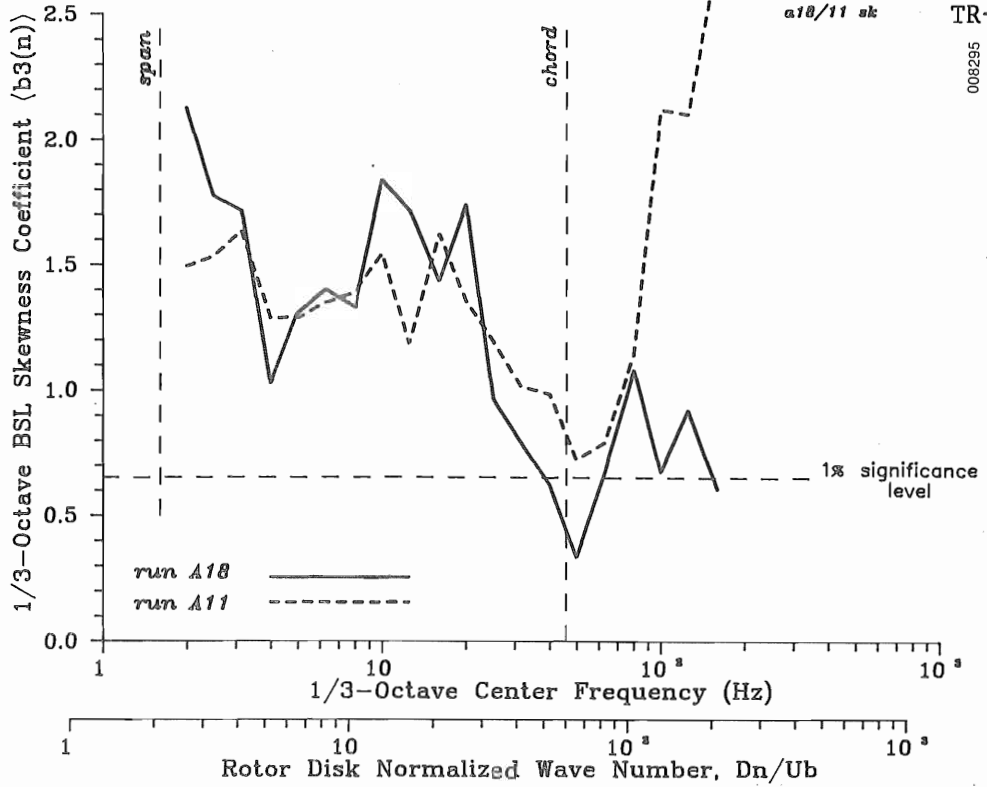


(a) mean band spectrum levels

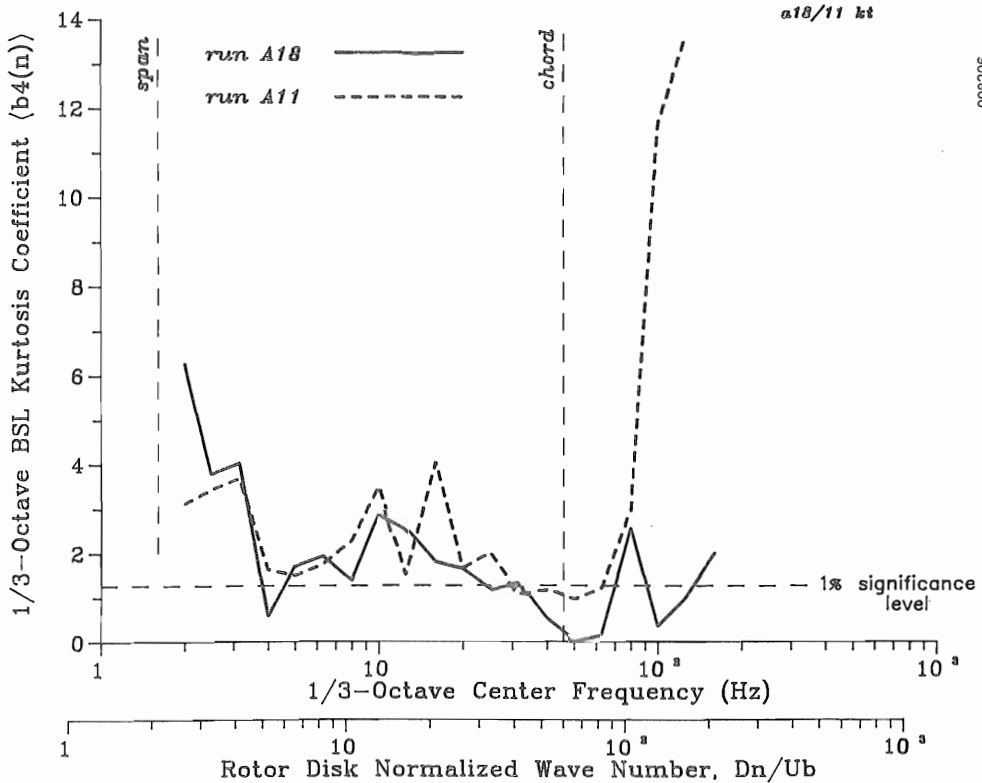


(b) band spectrum level variance coefficients

Figure 5-49. Ensemble Statistical Moments of Acoustic 1/3-Octave Band Spectrum Levels for Runs A11 and A18

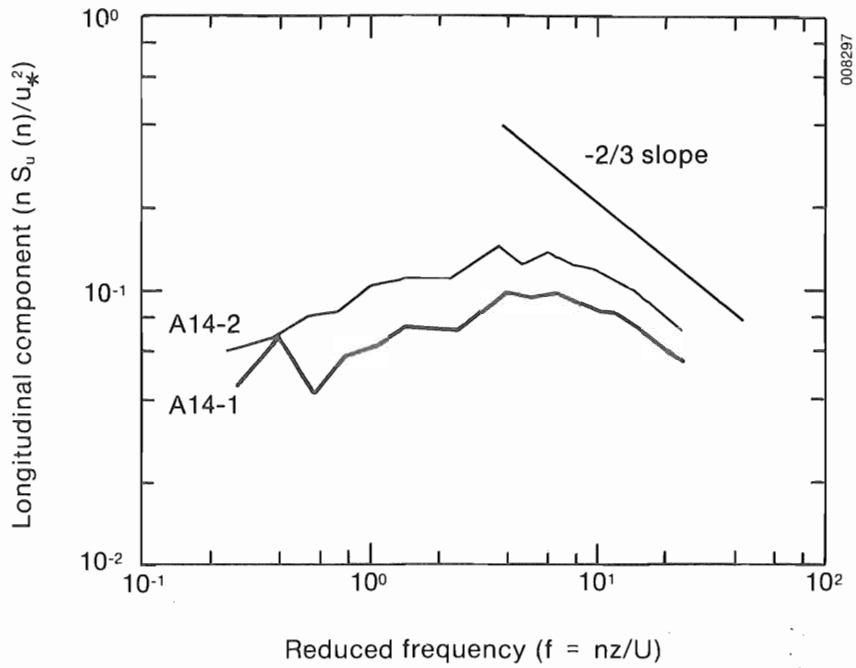


(c) band spectrum level skewness coefficient

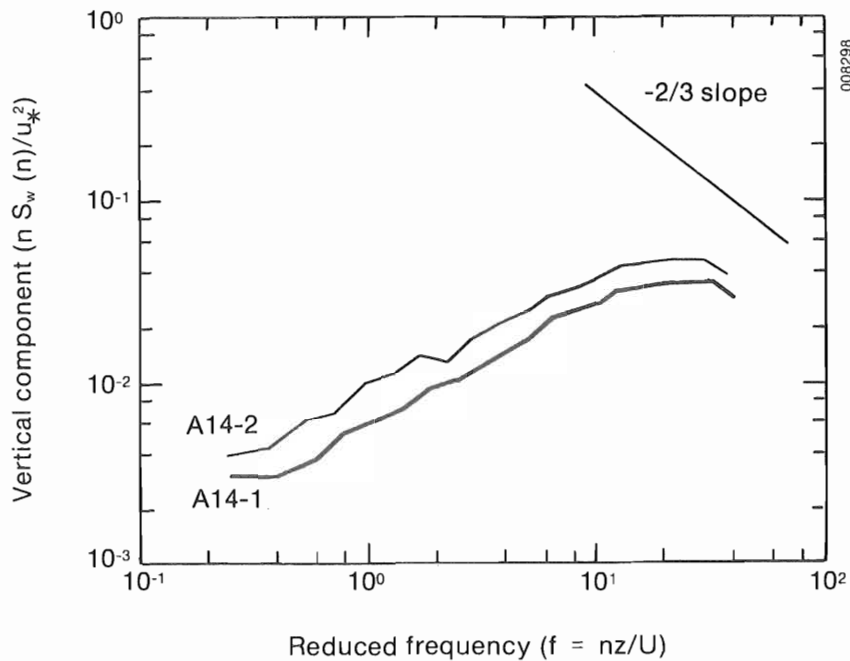


(d) band spectrum level relative kurtosis coefficients

Figure 5-49. Ensemble Statistical Moments of Acoustic 1/3-Octave Band Spectrum Levels for Runs A11 and A18

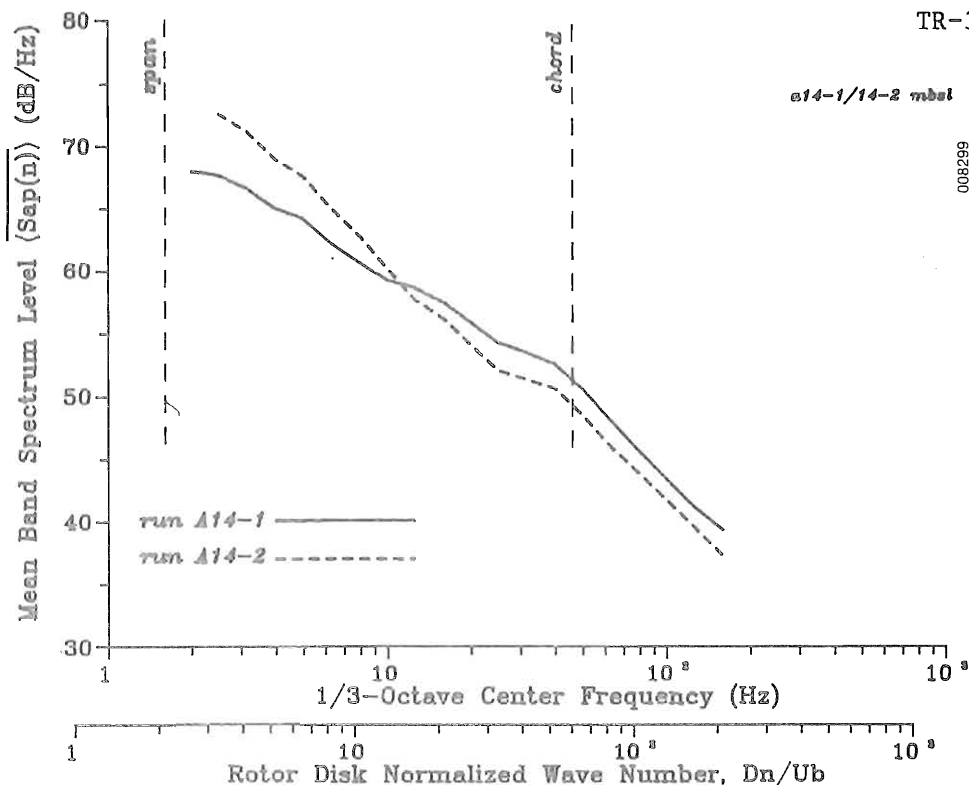


(a) longitudinal (axial) turbulence component normalized spectra

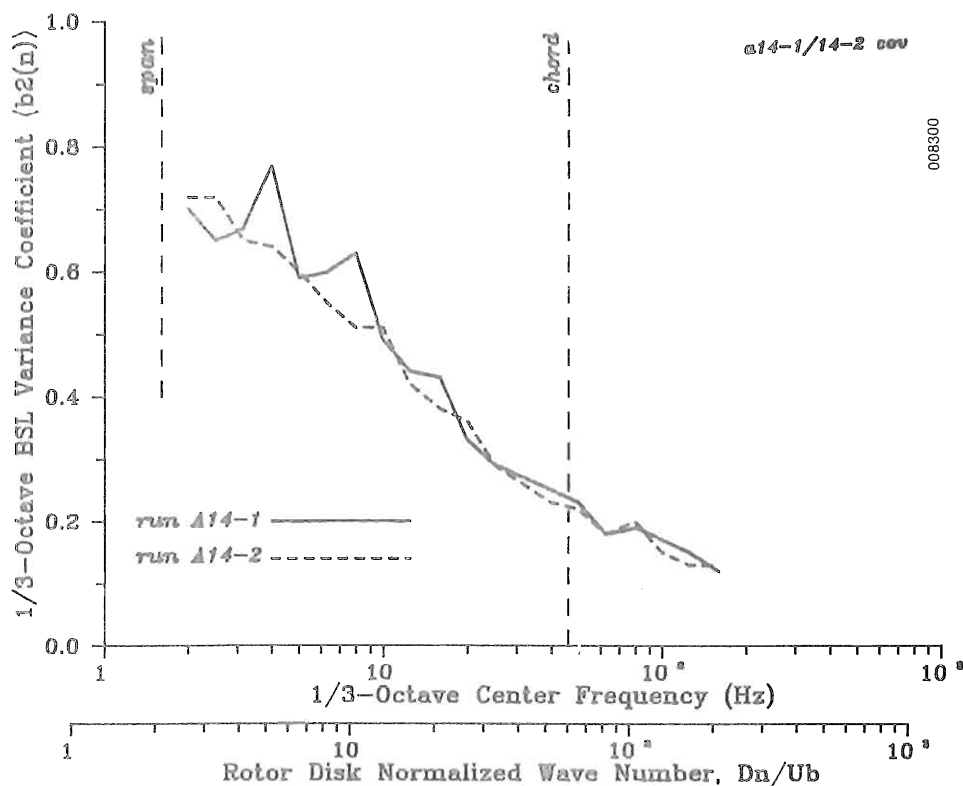


(b) vertical (upwash) turbulence component normalized spectra

Figure 5-50. Normalized 45-m Turbulence Spectra for Runs A14-1 and A14-2

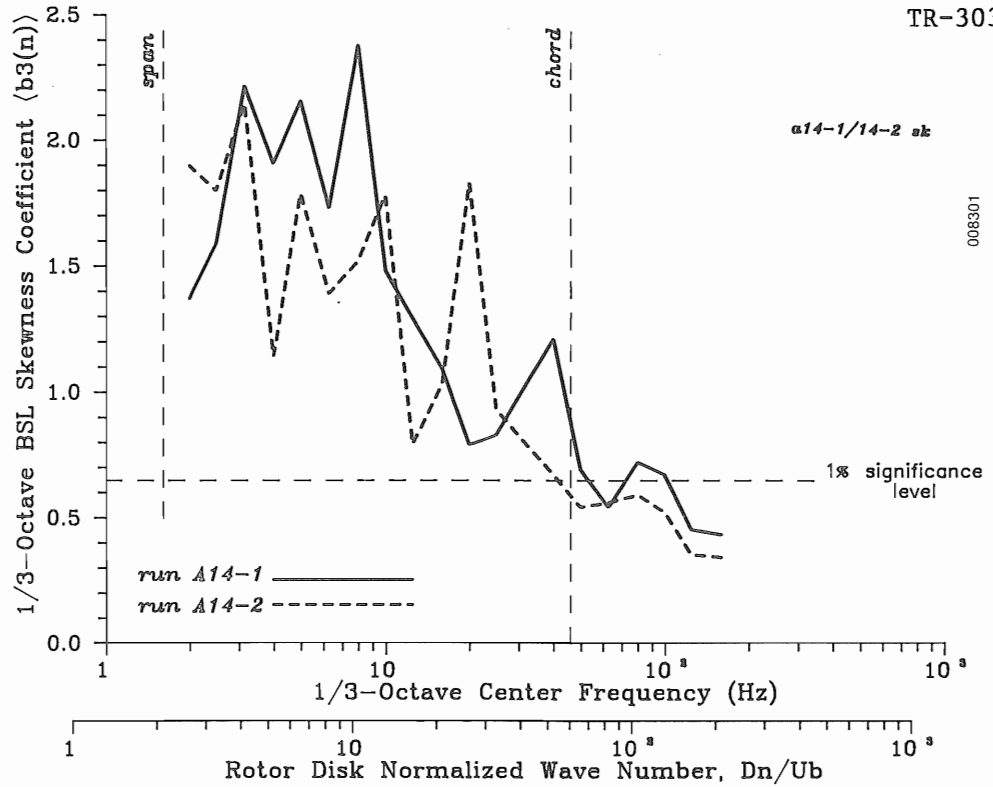


(a) mean band spectrum levels

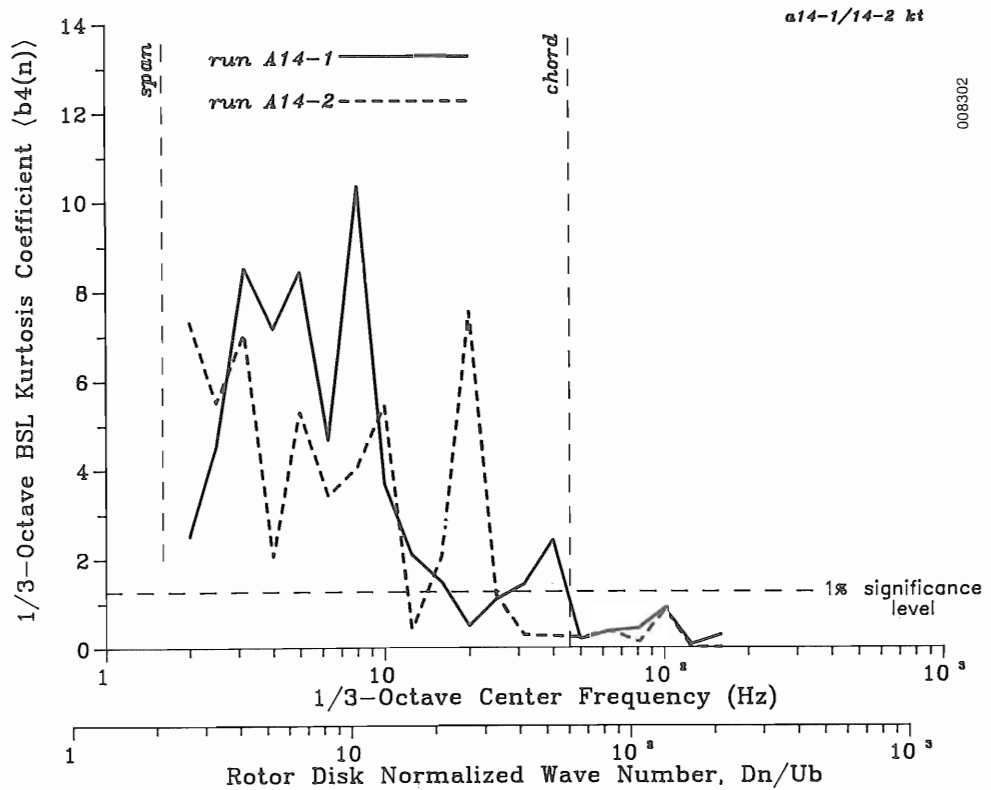


(b) band spectrum level variance coefficients

Figure 5-51. Ensemble Statistical Moments of Acoustic 1/3-Octave Band Spectrum Levels for Runs A14-1 and A14-2



(c) band spectrum level skewness coefficients



(d) band spectrum level relative kurtosis coefficients

Figure 5-51. Ensemble Statistical Moments of Acoustic 1/3-Octave Band Spectrum Levels for Runs A14-1 and A14-2

### 5.1.1.5 Relationship of Inflow Spectral Characteristics to the Mean LF Acoustic Spectrum

We attempted to relate the spectral characteristics of the reference level (45-m) axial (longitudinal) and upwash (vertical) turbulence to the shape of the acoustic mean BSL curves. One immediate problem confronting such a comparison is that the acoustic sources, while perhaps generated by a linear dynamic process, are rotating within the surface boundary layer. The turbulence measurements, on the other hand, have been made at a fixed location, although within the rotor disk layer. What is needed is to provide a scaling quantity to allow conversion from the fixed position to the rotating plane. We suggest the following fixed-to-rotating space-frequency transformation:

$$n' = n(2 \Omega R_o / I_w^z), \quad (5-3)$$

where  $n'$  is the estimated cyclic frequency in rotating space (as seen by the rotor),  $n$  is the frequency in fixed space coordinates,  $\Omega$  is the rotor rotation rate,  $R_o$  is the effective radius (75% span), and  $I_w^z$  is the vertical or upwash turbulence characteristic scale length. Equation 5-3 adjusts the fixed-position cyclic frequency to the rotating one by increasing the former by the equivalent of the time it takes the rotor (at 75% span and quasi-horizontal) to traverse the characteristic vertical turbulent scale. This transformation factor averages about 6.4 for a mean  $I_w^z$  of 9.8 m for the 1983 experimental data set. Thus, a spectral feature occurring at a cyclic frequency of 1 Hz in fixed coordinates would be estimated at 6.4 Hz at 75% span in the rotating frame for  $I_w^z$  of 9.8 m.

The approximation of Equation 5-3 allows us to plot the far-field acoustic pressure and inflow turbulence spectra on the same graph with abscissa values of  $n$  (acoustic) and  $n'$  (transformed turbulent). Figures 5-52 through 5-57 plot each of the six mean, far-field acoustic spectral densities observed in 1983,  $\langle S_{ap}(n) \rangle$ , with the corresponding 45-m axial,  $S_u(n')$ , and upwash or in-plane,  $S_w(n')$ , mean turbulence spectra in logarithmic coordinates. A second abscissa is also provided which is scaled in terms of the rotor convection wave number normalized by the disk dimension of  $Dn/U_b$ , where  $D$  is the rotor diameter and  $U_b$  the rotor relative velocity at the 75% span station (63 mps). The wave number corresponding to the chord dimension at this span location is indicated on the plots. A line with a  $-5/3$  slope is also included in these plots as a reference to the spectral slope associated with the turbulent inertial subrange. A turbulence spectrum with a  $-5/3$  slope is necessary, but not sufficient to guarantee the isotropy of the inertial range. An examination of these six figures reveals, in general, that

- (1) There is a small positive slope change in the mean acoustic pressure spectra in the vicinity of the rotor effective chord length which also seems to coincide with the isotropic turbulence region (indicated by the two turbulence component spectra becoming parallel); and
- (2) The roll-off of the mean acoustic pressure spectrum approximates a  $-5/3$  slope for reference wind speeds below about 10 mps.

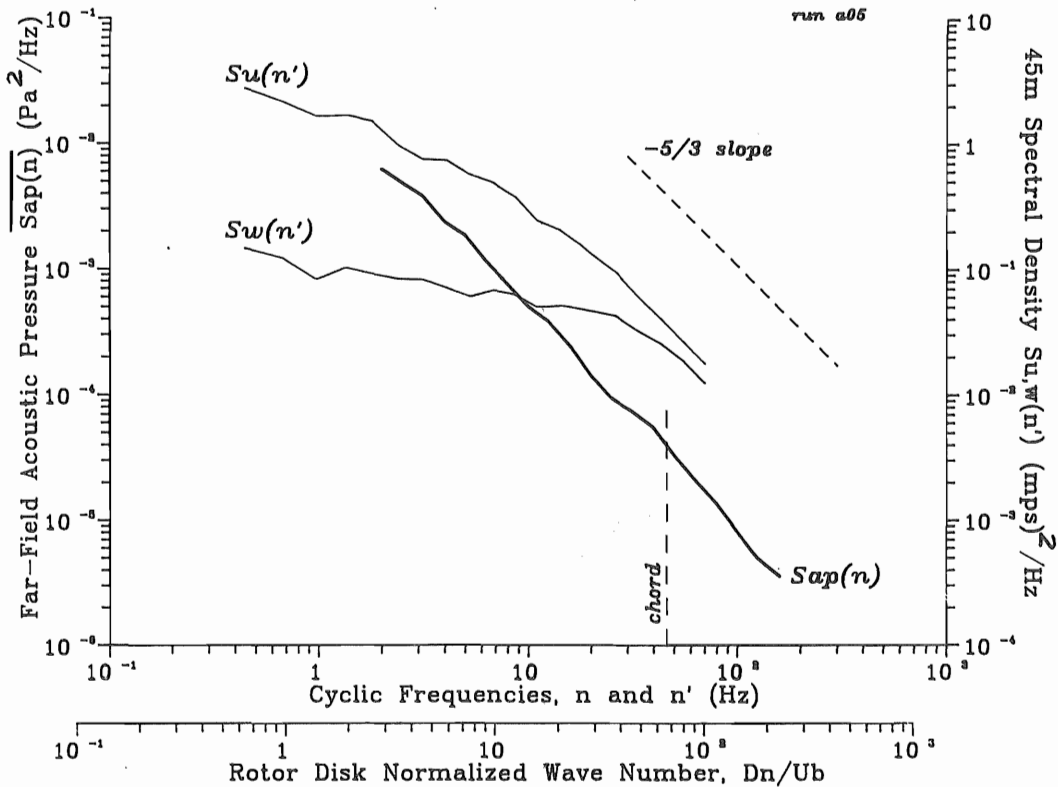


Figure 5-52. Relationship of Mean Acoustic Pressure Spectral Distribution  $S_{ap}(f)$  to 45-m Axial  $S_u(f')$  and Upwash  $S_w(f')$  Turbulence Components for Run A05

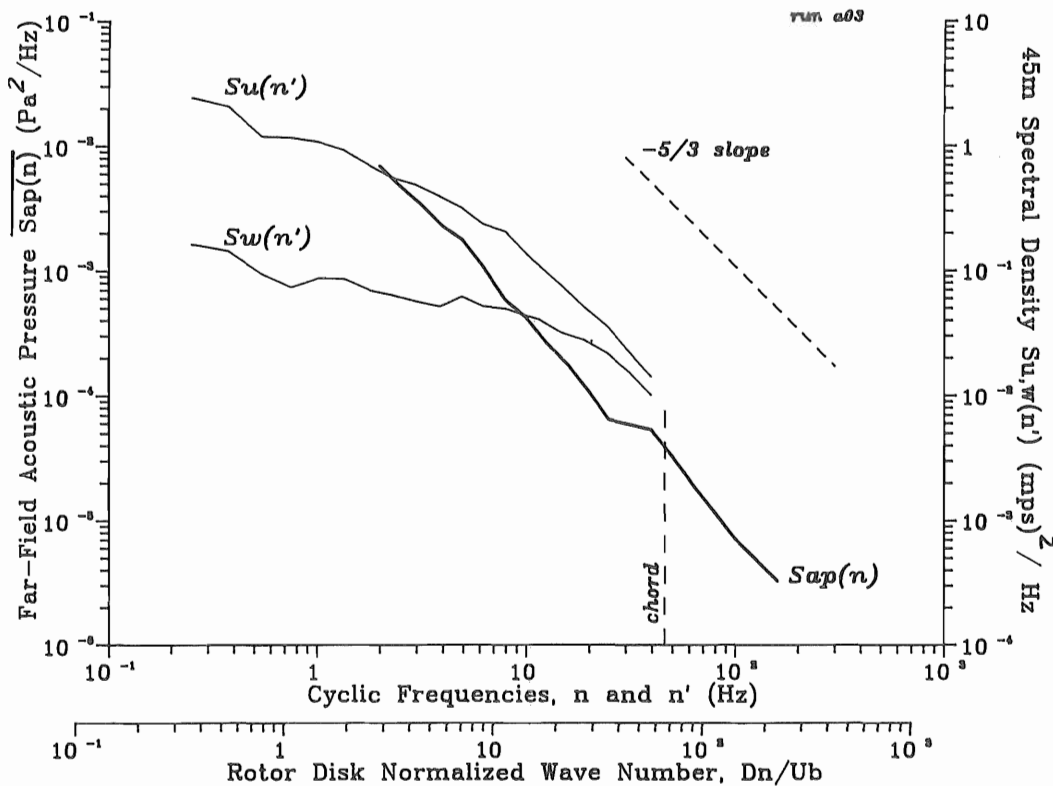


Figure 5-53. Relationship of Mean Acoustic Pressure Spectral Distribution  $S_{ap}(f)$  to 45-m Axial  $S_u(f')$  and Upwash  $S_w(f')$  Turbulence Components for Run A03

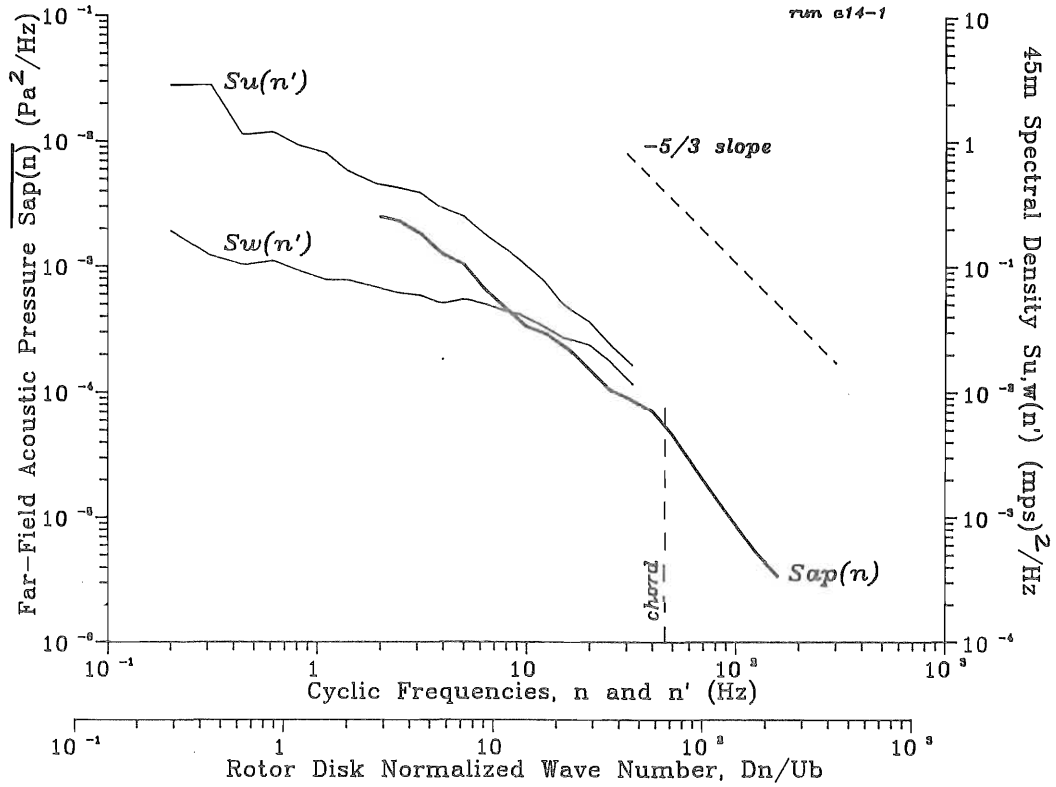


Figure 5-54. Relationship of Mean Acoustic Pressure Spectral Distribution  $S_{ap}(f)$  to 45-m Axial  $S_u(f')$  and Upwash  $S_w(f')$  Turbulence Components for Run A14-1

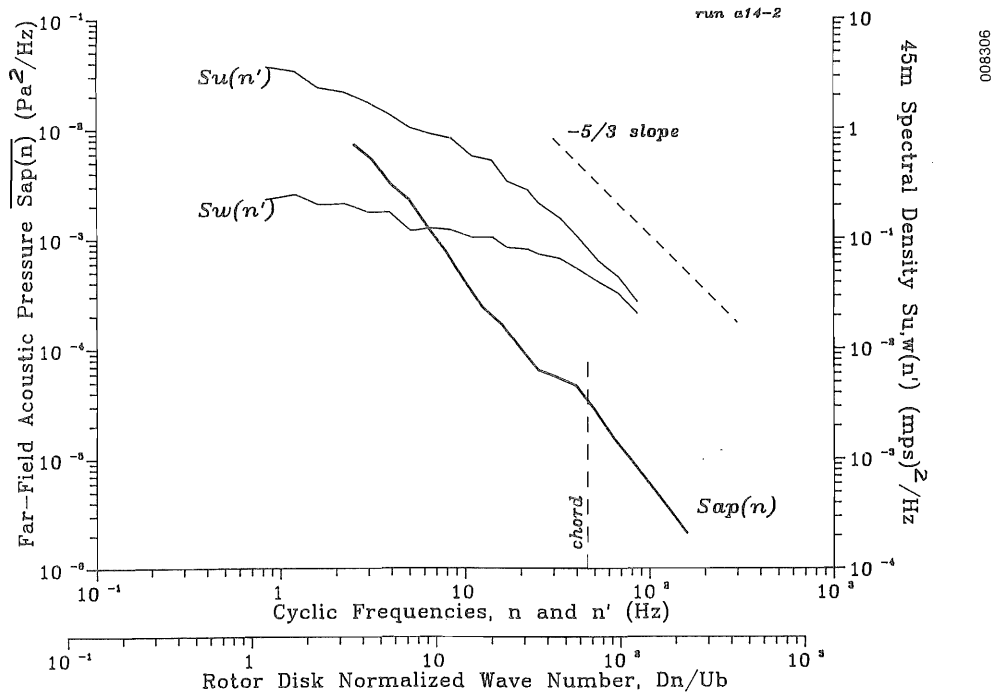


Figure 5-55. Relationship of Mean Acoustic Pressure Spectral Distribution  $S_{ap}(f)$  to 45-m Axial  $S_u(f')$  and Upwash  $S_w(f')$  Turbulence Components for Run A14-2

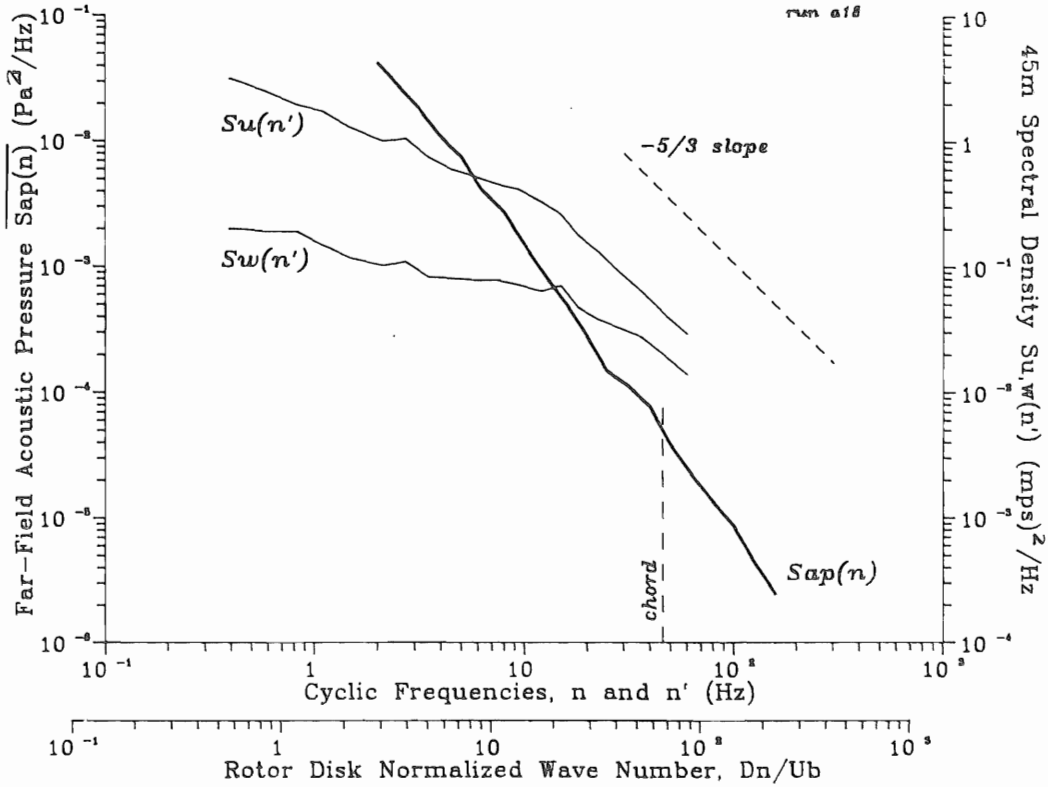


Figure 5-56. Relationship of Mean Acoustic Pressure Spectral Distribution  $S_{ap}(f)$  to 45-m Axial  $S_u(f')$  and Upwash  $S_w(f')$  Turbulence Components for Run A18

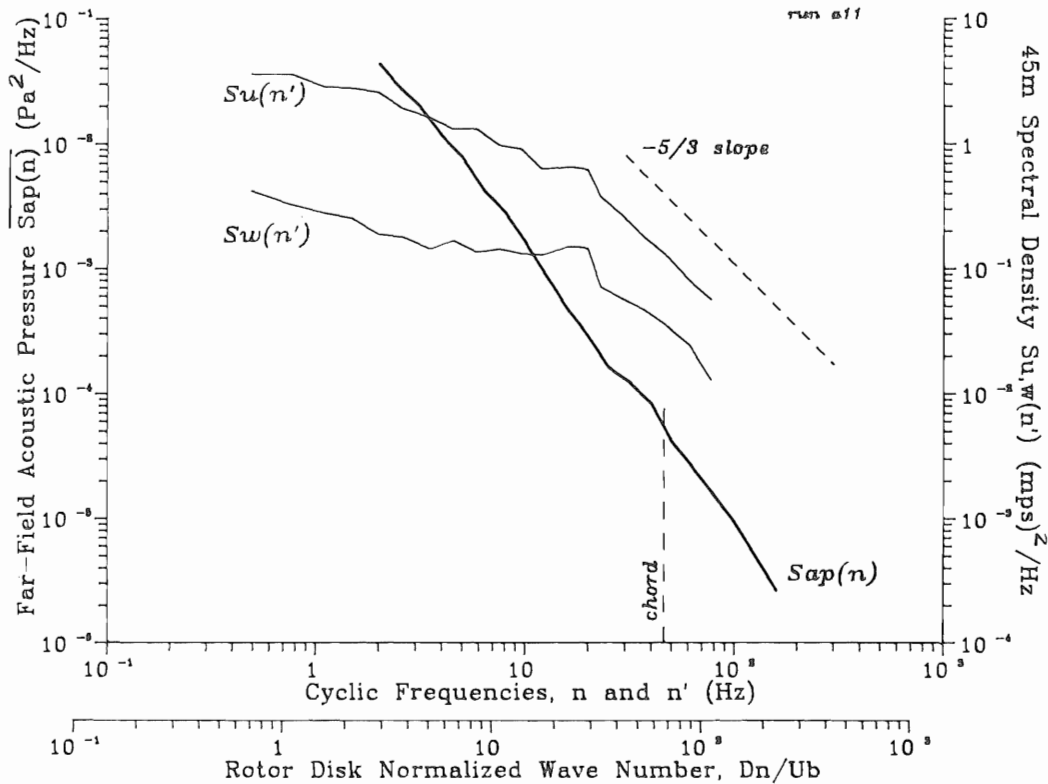


Figure 5-57. Relationship of Mean Acoustic Pressure Spectral Distribution  $S_{ap}(f)$  to 45-m Axial  $S_u(f')$  and Upwash  $S_w(f')$  Turbulence Components for Run A11

## 5.2 Comparison of 1982 and 1983 Results

As previously stated, we attempted to compare the characteristics of the MOD-2 LF emissions before and after major modifications were installed. The changes that occurred between our 1982 data collection and that done in 1983 included modifying the pitch-angle schedule and installing vortex generators near the leading edge and along 70% of the rotor span. The primary objective of both modifications was to improve stability under turbulent loads. Unfortunately, we did not have the high-frequency, hot-film anemometer data available to us in 1982, though the remainder of the instrumentation was the same for both years. Furthermore, inflow conditions during the April/May 1982 runs tended to be more windy and less stable than those encountered in August 1983, as documented in Table 3-1. This reduced the region of overlap we needed to compare the turbine response.

The lack of the dual-axis, hot-film anemometer data required us to identify a new set of inflow scaling predictors from the available 1982 information. From our 1983 results, we knew we needed measures of the stability, reference wind speed, and turbulence. The first two were available, but only the variance from the slow-responding propeller anemometer could be used as a measure of the turbulence input. This meant that we had no information about the high-frequency (small-scale) portion of the axial wind component and no information at all about the upwash or in-plane component. Because the overlap in inflow conditions between the two years was limited, we were able to identify only six 1982 runs and four 1983 runs for comparison. Table 3-2 lists the mean for the available predictors, including the hub-height mean wind speed, its variance and turbulence intensity, and the mean Richardson number and the Monin-Obukov  $z/L$  parameter derived from it. Table 5-5 lists the ranges of the parameters used for the comparisons. Only the hub-height wind speed variance did not overlap completely. Table 5-6 lists the mean BSL values observed, and the differences between them for the two years, under the conditions listed in Table 5-5. These mean differences are also plotted in Figure 5-58, with a least-squares trend line added. As the graph and table show, there appears to be a trend to higher mean emission levels above 10 Hz (in 1983) with the modified turbine.

### 5.2.1 Multivariate Modeling of the 1982/1983 Data

We applied the same technique as that described in Section 5.1.1.2 to the reduced 1982 and 1983 acoustic data sets, using the parameters listed in Table 5-5 as scaling predictors. Figures 5-59a, and b present the results of an ANOVA analysis for the 1982 and 1983 MBSL run-to-run variations using the Richardson number,  $Ri$ , mean hub-height wind speed,  $U_H$ , and variance,  $u'$ , as inflow predictors. It is clear from these two figures that the LF acoustics emission response was considerably different in 1982 than it was 1983. In 1982 the run-to-run variations in the expected MBSL spectra, over the entire band of interest, were explained by variations in the inflow structure ( $Ri$ ). A different picture appears in Figure 5-59b for 1983. Below a frequency of 10 Hz ( $k = 1$ ), the run-to-run variation in the expected MBSL is explained by changes in the mean wind speed (mean angle of attack). Above 10 Hz, the variations are spectral functions of all three predictors with the variance,  $u'$  and the mean wind speed,  $U_H$ , dominant.

**Table 5-5. Overlap Ranges of Reduced 1982/83 Inflow Data Sets**

Parameter	1982 Ranges	1983 Ranges
Richardson number	-0.01 to +0.75	-0.12 to +0.71
z/L parameter	-0.01 to 5.62	-0.12 to 5.62
Hub-height wind speed ( $\text{ms}^{-1}$ )	8.1 to 11.9	8.1 to 11.1
Hub-height variance ( $\text{ms}^{-1}$ ) <sup>2</sup>	0.24 to 3.45	0.5 to 1.31
M-O length L (m)	9.5 to 638	-444 to 160

The relative spectral sensitivities to these three predictors for 1982 and 1983 are shown in normalized form in Figures 5-60a and b. The coefficients of multiple determination, or  $r_2$ , are also plotted as an indication of the applicability of the models in explaining the observed variation. It is quite clear from both figures that, at least for this choice of predictors, the vertical structure of the atmospheric inflow has the greatest influence on the spectral characteristics of the expected LF acoustic emission levels. The 1983 MOD-2 configuration, with the incorporated pitch schedule and vortex generator modifications, displays a pronounced emissions level sensitivity to

**Table 5-6. Comparison of Mean 1/3-Octave Band Spectral Levels for the Conditions in Tables 3-2 and 5-9 for 1982 and 1983 Runs**

Band Center Frequency (Hz)	1982 $\langle S(f) \rangle$ (dB)	1983 $\langle S(f) \rangle$ (dB)	1983-1982 Difference (dB)
2.00	74.2	73.8	-1.4
2.50	72.4	72.2	-0.2
3.15	70.9	70.8	-0.1
4.00	69.0	68.8	-0.2
5.00	67.7	67.6	-0.1
6.30	65.2	65.2	0
8.00	63.4	63.0	-0.4
10.0	61.4	61.1	-0.4
12.5	59.0	59.2	0.2
16.0	56.9	57.6	0.7
20.0	54.8	55.6	0.8
25.0	53.2	53.7	0.5
31.5	55.2	54.5	-0.7
40.0	52.1	52.4	0.3
50.0	49.7	50.2	0.5
63.0	47.2	47.7	0.5
80.0	43.6	45.4	1.8
100	41.7	43.3	1.6
125	39.1	41.3	2.2
160	37.9	39.2	1.3
		Mean:	0.4

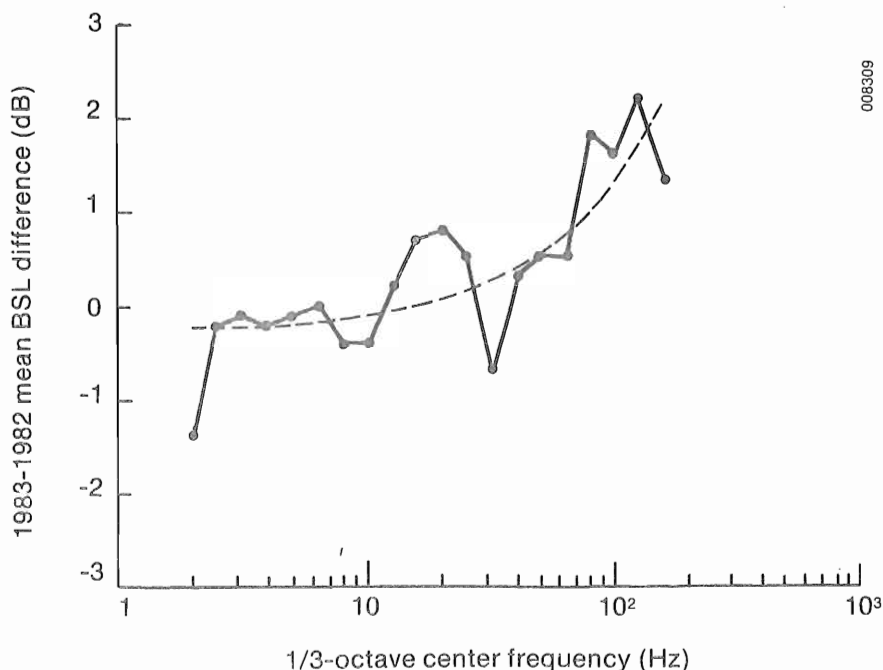


Figure 5-58. Difference in Mean Band Spectrum Levels for 1982 and 1983

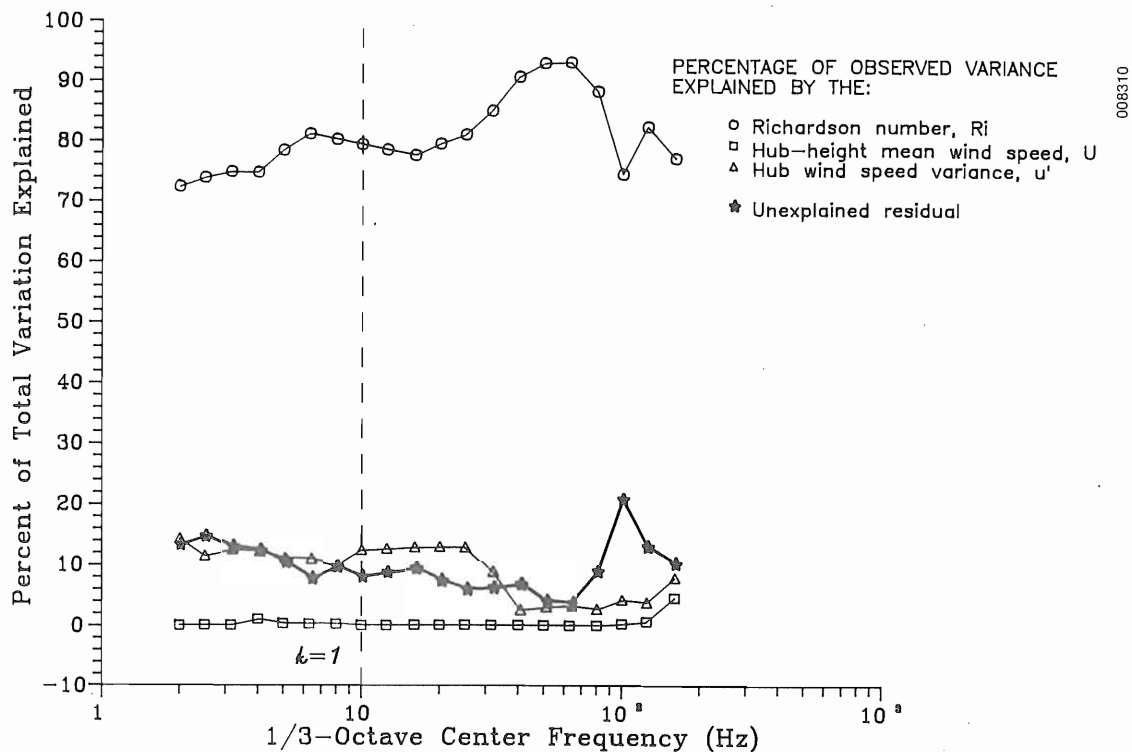
less stable flows below 10 Hz ( $k = 1$ ) and just the opposite above that frequency to increasingly stable flows. The 1982 configuration, on the other hand, showed a lower overall stability sensitivity. In this case higher mean emission levels were associated with less stable flows, reaching a peak in the 8-Hz frequency band.

The relative 1982/1983 normalized spectral sensitivities to the  $R_i$ ,  $U_H$ , and  $u'$  predictors are presented in Figures 5-61, 5-62, and 5-63, respectively. The much increased LF acoustic sensitivity to the  $R_i$  (atmospheric structure) in 1983 over that in 1982 is quite obvious in the presentation of Figure 5-61, suggesting a dramatic change in the responsible aeroacoustic mechanisms. The spectral sensitivities to the mean axial wind component, shown in Figure 6-62, supports the statement that the 1983 turbine was acoustically more sensitive to the mean attack angle below 10 Hz and less sensitive above that range. The plot of the variance sensitivities ( $k = 1$ ) in Figure 6-63 seems to suggest that the 1983 rotor experienced a more stable boundary layer. This is indicated by the low turbulence sensitivity resulting in increased lift and higher radiated mean acoustic levels below 10 Hz over the 1982 data for the same inflow conditions.

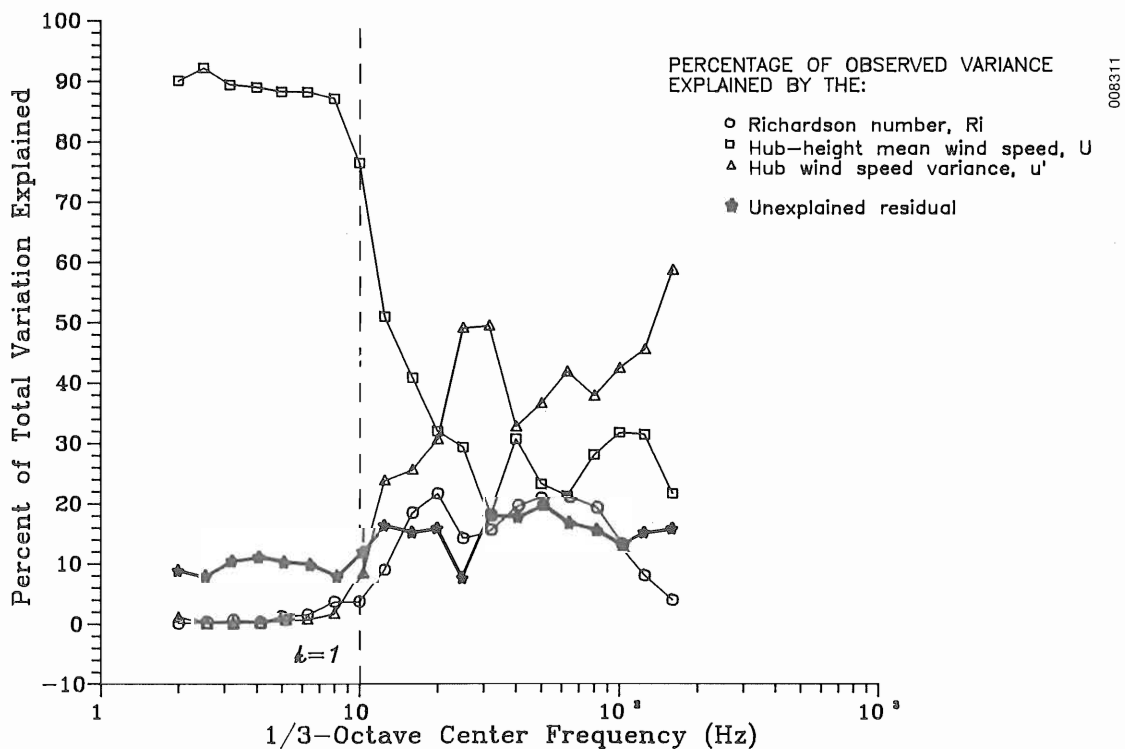
5.3 Comparison of MOD-2 with MOD-1 LF Emissions

The most dominant (and annoying) characteristic of the MOD-2 LF emissions was their coherence or impulsiveness. We have developed several measures of the degree of coherence in wind turbine radiated emissions [1], including

- The root-mean-square (rms) correlated 8- and 16-, 16- and 31.5-, and 31.5- and 63-Hz octave spectrum levels (CBSL) and corresponding correlation coefficient (Ccoef)

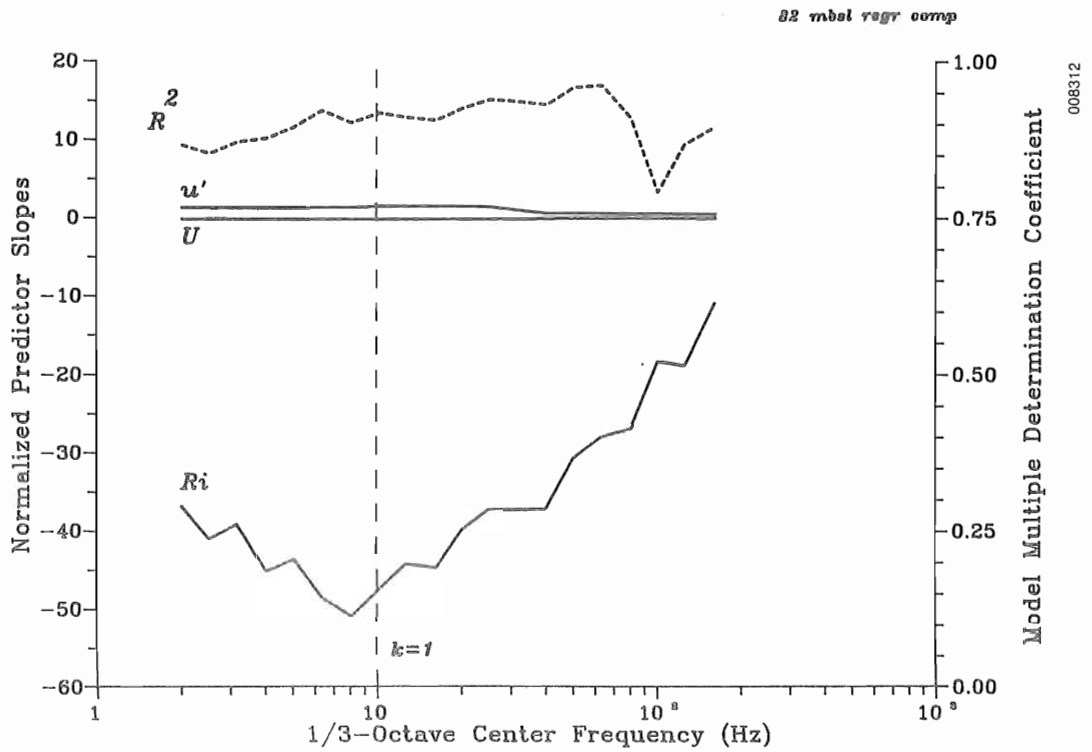


(a) 1982 turbine configuration

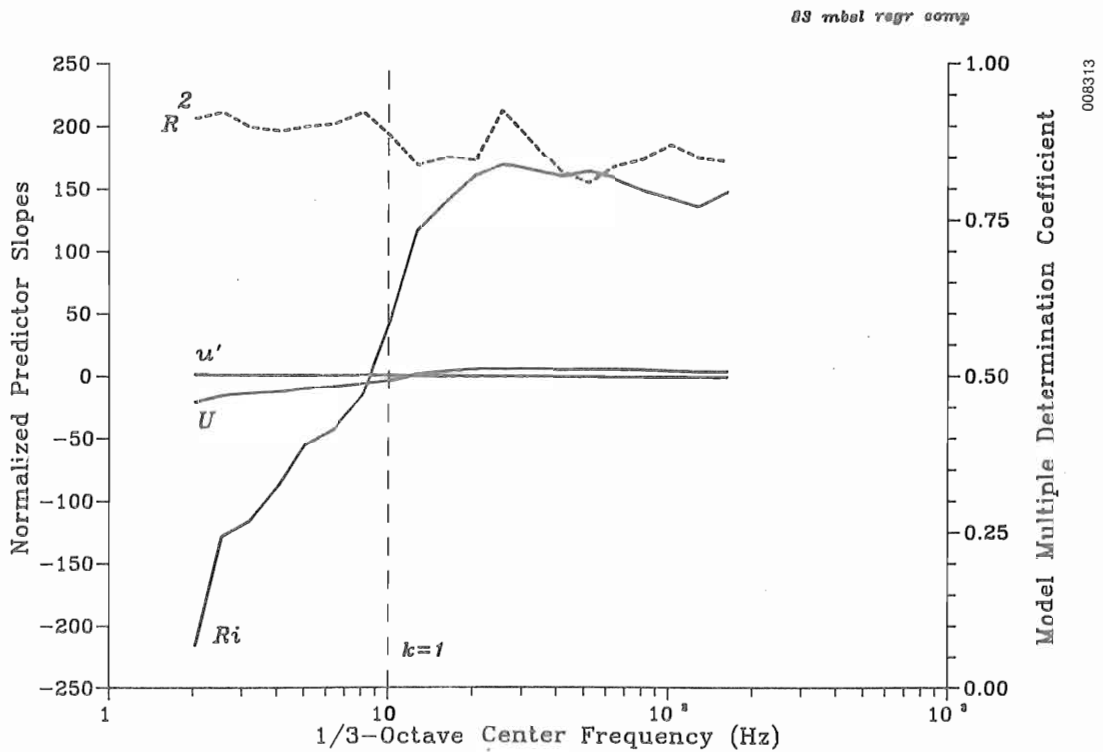


(b) 1983 turbine configuration

Figure 5-59. Results of ANOVA Analysis for Mean Bard Spectrum Level Inflow Parameter Sensitivities



(a) 1982



(b) 1983

Figure 5-60. Normalized Inflow Parameter Predictor Slopes for Observed Mean Band Spectrum Levels

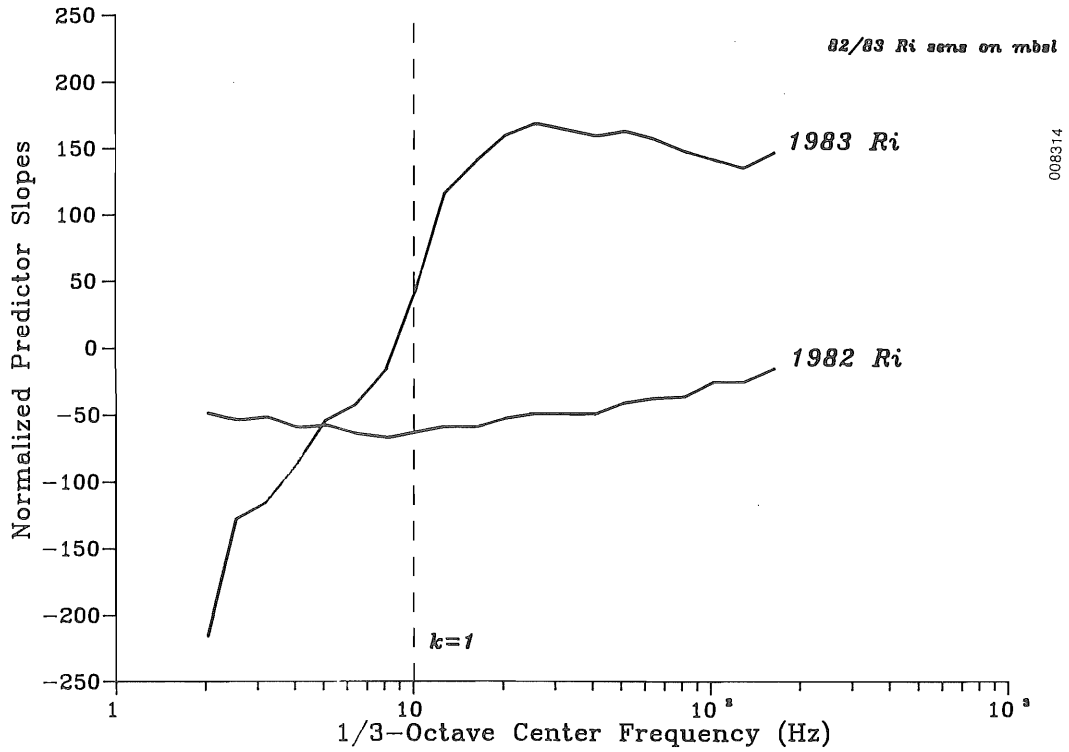


Figure 5-61. Relative MBSL Spectral Sensitivity to Inflow Stability (Richardson Number) for 1982 and 1983 Configurations

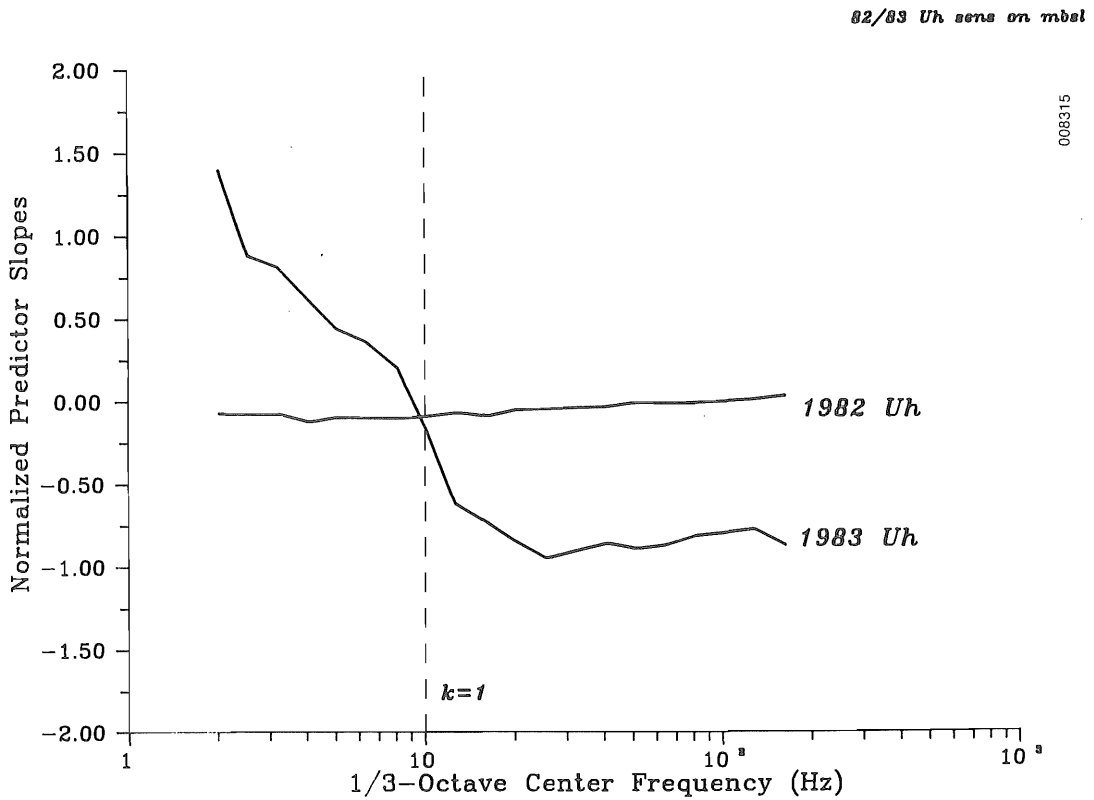


Figure 6-62. Relative MBSL Spectral Sensitivity to Inflow Stability for Mean Hub-Height ( $U_H$ ) Wind Speed

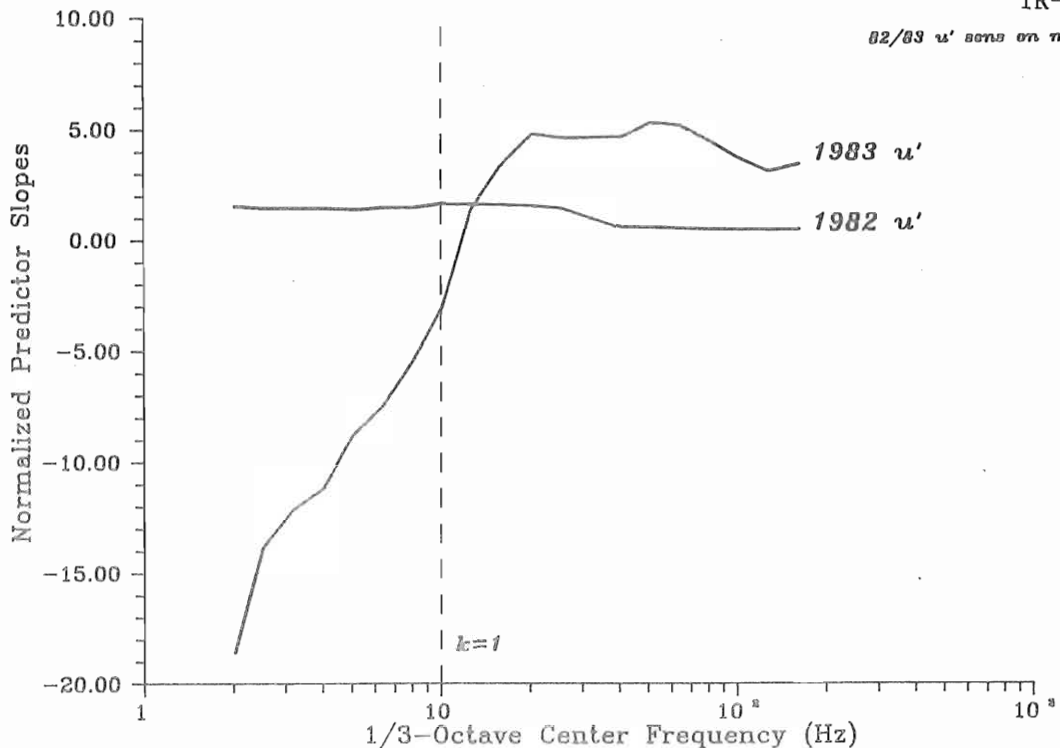


Figure 5-63. Relative MBSL Spectral Sensitivity to Inflow Stability for Hub-Height Wind Speed Variance ( $u'$ )

- Plots of observed joint and triple frequency distributions of the three octave BSL pairs listed above
- The observed conditional octave BSL statistical exceedences for the 8-, 16-, and 31.5-Hz bands.

We observed in Ref. [1] that as the degree of impulsiveness or coherence increased in the MOD-1 emissions, the degree of correlation of the adjacent octave band pressure levels also increased. This indicated that a specific phase relationship exists in the radiated acoustic pressure field. The band-to-band correlation or phase coherency was in part responsible for the degree of annoyance of the affected residents, since it acoustically loaded the structures simultaneously at several resonant modes. Therefore, we performed the same analysis on the MOD-2 emissions over the available range of inflow conditions in order to compare them with those of the MOD-1 and their known consequences.

### 5.3.1 Statistical Measures of Impulsiveness or Coherency

#### 5.3.1.1 Adjacent Band Correlated Spectral Levels

Table 5-7 summarizes the adjacent octave band correlations for the available data from the 1982 and 1983 MOD-2 experiments and the reference 23- and 35-RPM MOD-1 runs. As we can see, the correlated band spectrum levels (CBSL) for the MOD-1 running at 35 RPM tend to be very high in all three adjacent band pairs. The associated correlation coefficient (Ccoef), however, is not particularly large, indicating a large blade-to-blade passage variation in the coherency of the radiated emissions. In the 23-RPM case, on the other hand, we see the consequences of shifting the impulsive spectrum lower in frequency with the decrease in the blade speed (tower passage frequency). The coherency

**Table 5-7. Statistical Summary of Correlated or Coherent Octave Band Spectrum Levels Measured On-Axis at 1.5D for 1982/83 MOD-2 Data Runs Compared with the MOD-1 Turbine at 35 and 23 RPM**

Run	Correlated Octave Band Spectrum Level			Hub Wind Speed (mps)	Richardson Number
	8/16Hz CBSL <sup>a</sup> /Ccoef <sup>b</sup> (dB/Hz)	16/31.5-Hz CBSL/Ccoef (dB/Hz)	31.5/63-Hz CBSL/Ccoef (dB/Hz)		
<u>MOD-2, 1982</u>					
ST23-1	44.1/0.645	39.1/0.768	33.4/0.865	6.3	24
ST21-1	57.7/0.464	53.4/0.564	47.0/0.525	9.3	0.46
ST19-1	59.6/0.705	48.9/0.258	43.5/0.292	10.3	0.18
ST17-2	74.7/0.871	69.4/0.869	59.9/0.733	11.7	-0.01
ST26-1	65.8/0.768	56.1/0.412	49.3/0.469	12.0	0.13
ST27	67.8/0.776	60.9/0.677	50.4/0.375	13.3	0.42
ST25-1	75.2/0.813	70.4/0.735	61.8/0.751	14.2	-0.92
<u>MOD-2, 1983</u>					
A05	55.1/0.358	51.3/0.407	40.5/0.097	7.3	11.7
A03	58.9/0.712	47.6/0.270	41.6/0.194	8.1	-0.12
A14-1	52.3/0.330	46.8/0.174	46.1/0.352	9.0	0.13
A14-2	54.3/0.466	46.3/0.260	41.7/0.273	9.9	0.26
A18	65.6/0.780	57.3/0.631	47.6/0.347	12.4	1.25
A11	66.7/0.776	59.2/0.723	49.0/0.409	13.6	6.68
<u>MOD-1</u>					
35 RPM <sup>c</sup>	70.8/0.540	72.9/0.663	67.7/0.571	17.0	Stable
23 RPM <sup>d</sup>	71.2/0.825	66.2/0.773	58.1/0.809	13.9	Stable

<sup>a</sup>Correlated band spectrum level.

<sup>b</sup>Band pair correlation coefficient.

<sup>c</sup>Extreme level of interior annoyance in homes at 1 km.

<sup>d</sup>Moderate level of interior annoyance at 1 km.

actually exceeds (as indicated by the much greater correlation coefficients) that of the 35-RPM case, with slightly more correlated energy in the 8/16-Hz band pair than for the higher rotation rate. We believe this is the reason that slowing down the rotor did not give the affected residents complete relief from the impulsive annoyance.

We found that the annoyance threshold was reached when the impulse, measured outside an affected home, in the 8/16-, 16/31.5-, and 31.5/63-Hz CBSL simultaneously exceeded 52, 47, and 35 dB/Hz, respectively, with associated correlation coefficients of 0.200 or greater [1]. These figures correspond to CBSLs of 73, 68, and 56 dB/Hz at the reference distance of 1.5D (91.5 m) from the turbine, assuming only geometric spreading for propagation. We know that sometimes the combination of terrain and atmospheric focusing raised the level at one or more of the homes as much as 25 dB above the equivalent value that

would be expected from divergence alone [1]. Thus, we can use the documented MOD-1 experience to gauge the low-frequency annoyance factor of the MOD-2 and other subsequent turbine designs.

5.3.1.2 Statistical BSL Exceedence Values

While not a direct measure of the degree of impulsiveness or coherency, the use of exceedence BSL statistics can also be useful for comparative purposes. There are two approaches to expressing exceedence statistics: (1) the percentage of time a given level is exceeded or (2) levels expressed in terms of percentiles of the observed distribution. The percentage-of-time criterion is useful in determining the persistence of observed levels. The percentile or "L-level" criterion is useful in examining peak-to-mean values to identify impulsiveness. Typical criteria are the  $L_{10}$ ,  $L_{20}$ , and  $L_{eq}$  values, which represent the 90th and 80th percentiles and the temporal mean. Thus, the  $L_{10}$  value represents the BSL which is exceeded 10% or more of the time. The differences between the  $L_{10}$  and  $L_{eq}$  values are a measure of the impulsiveness or the degree to which loud levels of short duration contribute to the noise environment.

5.3.2 Degree of 1982/83 MOD-2 versus MOD-1 Emissions Coherency

The ensemble correlated or coherent BSL (CBSL) for the seven 1982 and six 1983 MOD-2 data runs are compared with the 23 and 35 RPM MOD-1 high annoyance-level cases in Table 5-7. Plots of the CBSL for the MOD-2 in 1982 and 1983 as a function of hub-height mean wind speed for each of the three adjacent octave band pairs are shown in Figures 5-64, 5-65, and 5-66. The corresponding MOD-1

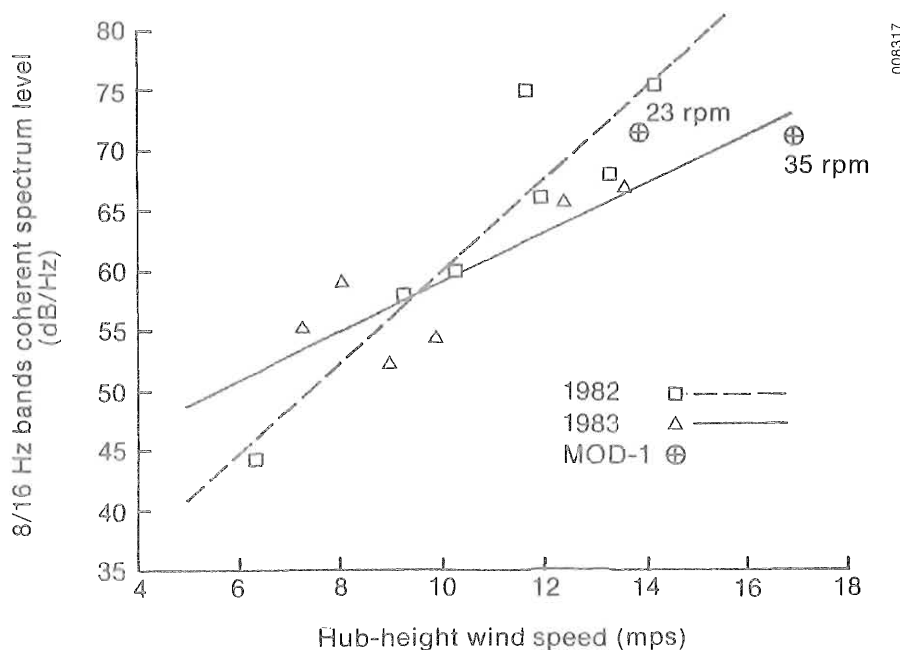


Figure 5-64. Comparison of 8/16-Hz CBSLs vs. Hub-Height Wind Speed for 1982 and 1983 MOD-2 Configurations and the MOD-1 Turbine

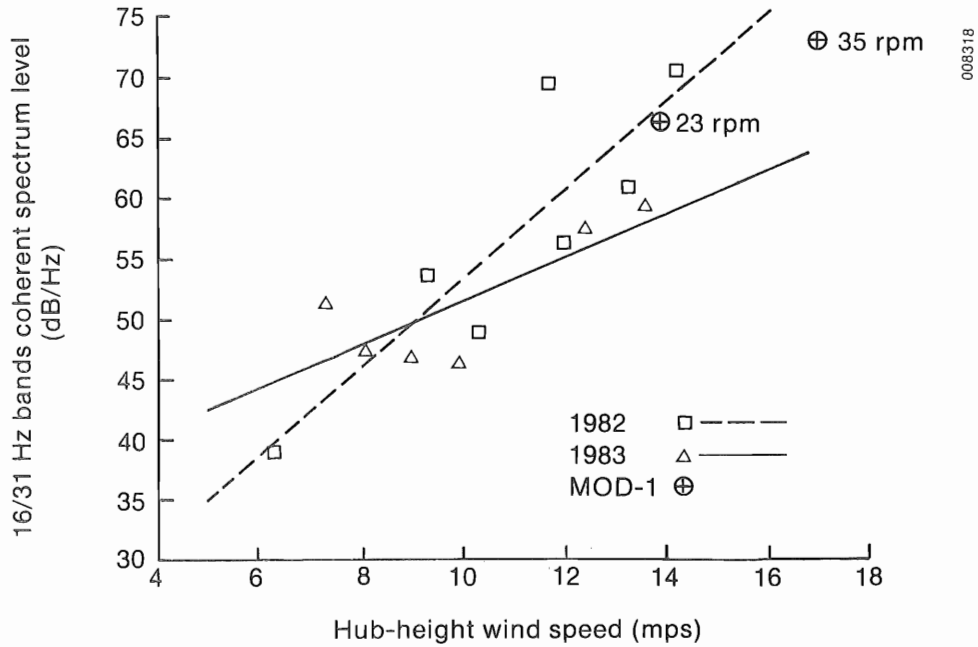


Figure 5-65. Comparison of 16/31.5-Hz CBSLs vs. Hub-Height Wind Speed for 1982 and 1983 MOD-2 Configurations and MOD-1 Turbine

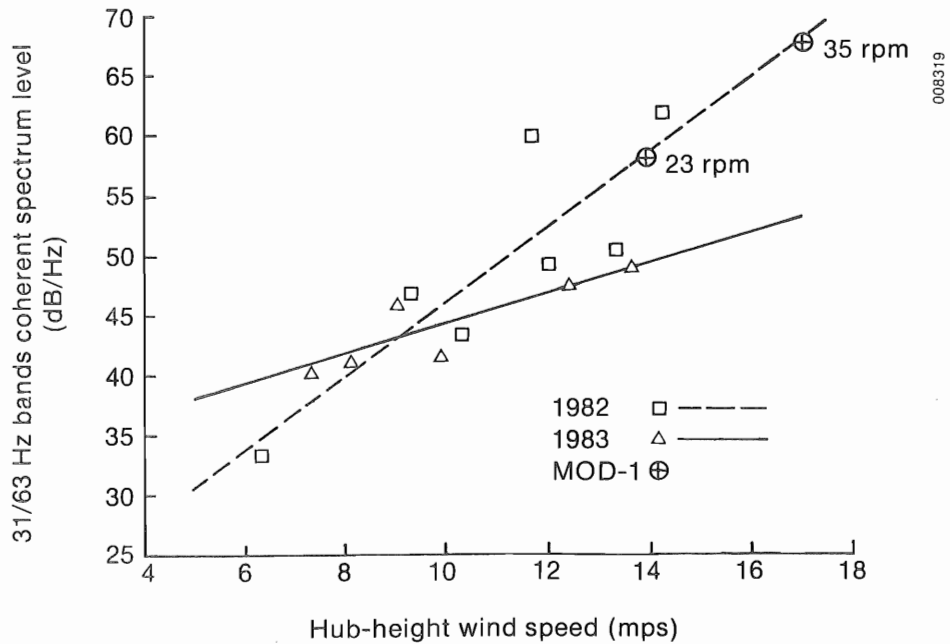


Figure 5-66. Comparison of 31.5/63-Hz CBSLs vs. Hub-Height Wind Speed for 1982 and 1983 MOD-2 Configurations and MOD-1 Turbine

values for 23- and 35-RPM operating conditions are also included in each plot. We believe that the difference in the slope of the two trend lines reflects changes in the rotor's unsteady aerodynamic response caused by the vortex generators and the pitch schedule modifications. It is clear that the 1983 emissions are less coherent above about 9-10 mps and slightly more coherent below that. It is also clear that, because of whatever instabilities were present, the 1982 turbine operating configuration appeared to be much more like that of its predecessor, the MOD-1. Thus, a definite improvement was achieved in the degree of coherence in the radiated LF emissions by adding the vortex generators and the pitch schedule changes.

Figure 5-67 plots the sensitivity of the four predictor parameters (the Richardson number, the M-O z/L parameter, and the hub-height wind speed and variance) for the 1982 and 1983 octave band coherent pressures and correlation coefficients of the reduced data defined in Table 3-2. Again, there is a marked difference in the coherency characteristic sensitivities of the radiated acoustic pressure fields before and after the modifications. Table 5-8 summarizes the aggregate CBSL statistics for the two years and compares them with those of the MOD-1 running at 23 RPM. The sensitivity of the 1983 coherent emissions to the inflow scaling parameters of the Richardson number, reference wind speed, and the three characteristic length scales are shown in Figure 5-68. The plots indicate that the degree of radiated coherency is a strong function of the Richardson number and its relationship to the vertical atmospheric structure and vertical or upwash velocity scale length,  $I_w^z$ , and the blade loading, as indicated by the mean axial velocity.

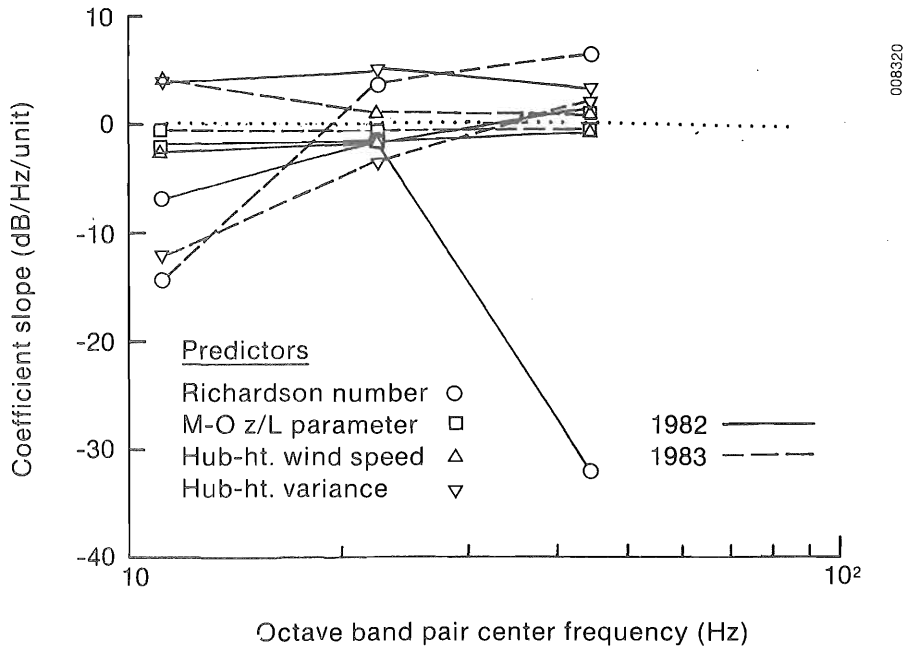
### 5.3.3 Comparison of 1982/1983 MOD-2 Exceedence Analysis

The exceedence analysis criteria results (percent-of-time and percentile or L levels) are summarized in Table 5-9 for the 1982/83 MOD-2 for the cases in Table 3-2 and for the 23-RPM MOD-1 at the 1.5D location. It is clear why there was a greater potential for interior annoyance, even with the MOD-1 operating at 23 RPM, over the MOD-2. The sharp impulsiveness associated with the MOD-1's emissions shows up in the differences between the  $L_{10}$  and  $L_{eq}$  values. This did not carry over to either the 1982 or 1983 MOD-2 results.

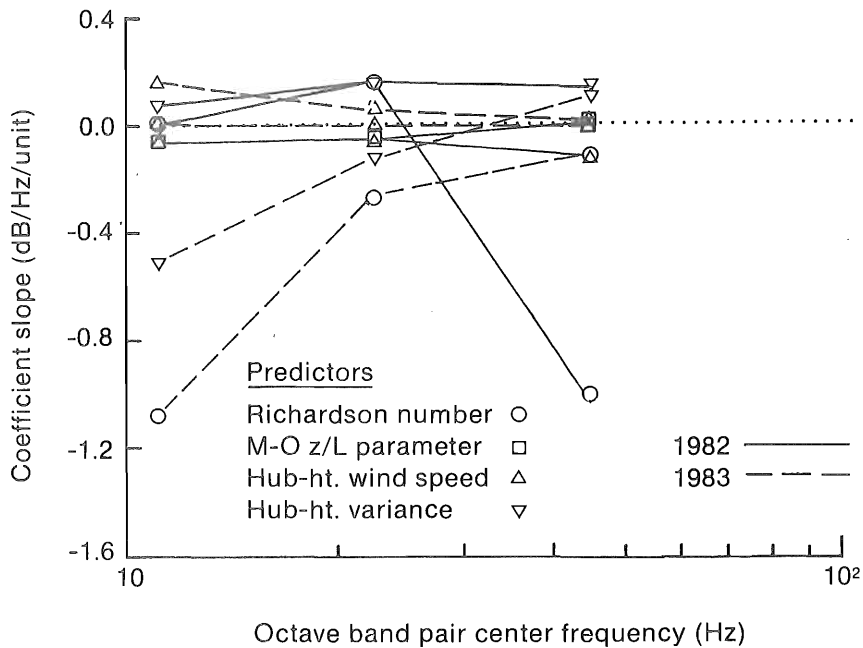
Table 5-10 summarizes the 1983 MOD-2 percent-of-time exceedence results. Somewhat surprising are the values for the lowest-wind-speed run (A05), which are comparable to the two highest-speed runs (A11 and A18) between 60 and 65 dB/Hz. The A05 exceedences are also significantly higher than those of runs A03, A14-1, and A14-2, which all have higher rotor loadings. We believe this to be a consequence of the complex, vertical turbulent structure present during this run.

### 5.4 Observed Physical Scales of MOD-2 LF Noise Generation

In order to understand better the physical processes responsible for aero-acoustic noise generation and its relationship to the accompanying structural response, we performed a space-time correlation analysis using three parameters measured on the blade itself and the far-field acoustic pressure in the 8-Hz octave band at 1.5D. The rotor parameters included the chord and flapwise moments and the 15% chord normal force (pressure taps) measured on the movable pitch portion of the rotor at Blade Station 1562 (87% span). The autocorrelation coefficient  $R(x,0,0)$  was computed for each appropriate time



(a) comparison of inflow predictors on CBSL



(b) comparison of inflow predictors on the adjacent octave band Ccoef

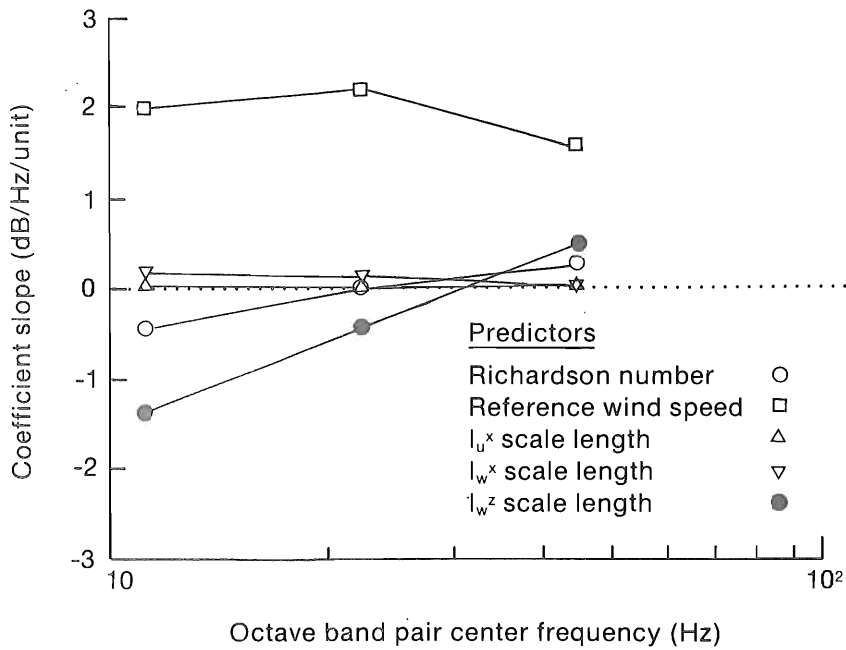
Figure 5-67. Comparison of Inflow Predictor Sensitivities on Adjacent CBSLs and Ccoefs for 1982 and 1983 Turbine Configurations

**Table 5-8. Comparison Summary of 1982/83 Adjacent-Band Correlated Spectrum Levels for Reduced Meteorological Data Set of Table 3-2 and the 23-RPM Operation of the MOD-1**

Octave Band Pairs (Hz)	MOD-2		MOD-1
	1982 CBSL/Ccoef (dB/Hz)	1983 CBSL/Ccoef (dB/Hz)	23 RPM CBSL/Ccoef (dB/Hz)
8/16	59.8/0.632	58.8/0.570	71.2/0.825
16/31.5	52.4/0.474	50.7/0.355	66.2/0.773
31.5/63	44.2/0.327	43.6/0.225	58.1/0.809

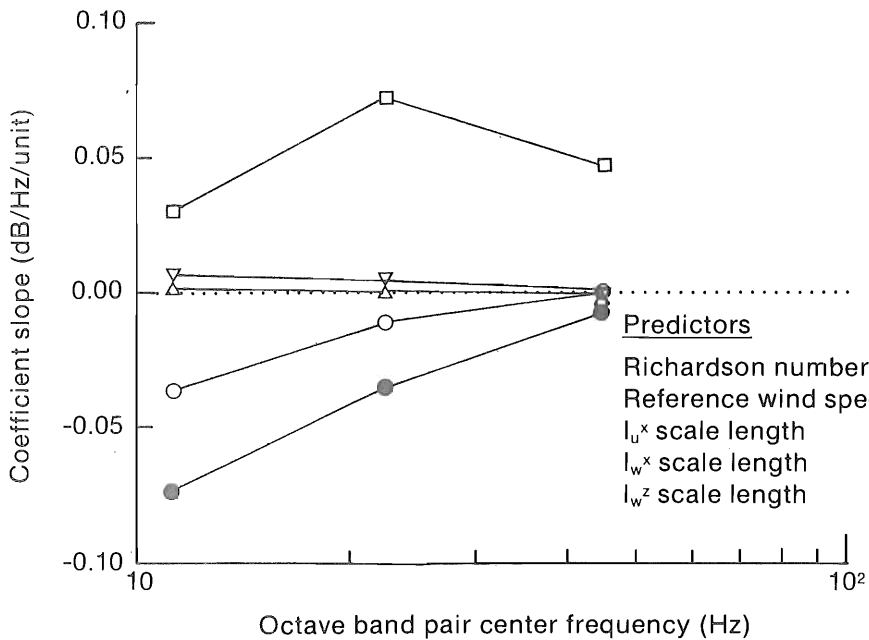
series and the correlation time was defined as the lag associated with the first zero crossing. This time correlation was converted to space coordinates by multiplying it by the relative blade speed at the 87% span station. Table 5-11 lists the resulting time ( $t_c$ ) and space ( $l_c$ ) correlations found for each of the four parameters of the eight available 1983 data runs.

It is clear from Table 5-11 that, at least at the 87% span station, the processes responsible for the observed flap and chordwise moments, normal and radiated acoustic pressures, are correlated over time periods of 65-75 ms, which translates to the rotor moving through about 5 meters in space. Thus, one interpretation is that inflow structures that have characteristic spatial dimensions of 5 meters or less will have a pronounced effect on the unsteady rotor response and radiated LF acoustic pressure field.



008322

(a) sensitivity of inflow predictors on adjacent CBSL



008323

(b) sensitivity of inflow predictors on adjacent band Ccoef

Figure 5-68. Sensitivity of Inflow Predictors on Adjacent CBSLs and Correlation Coefficients for 1983 MOD-2 Configurations

**Table 5-9. Comparison Summary of 1982/83 LF-Range Octave Band Exceedence Levels for Reduced Meteorological Data Set of Table 3-2 and the 23-RPM Operation of the MOD-1**

Octave Band Exceedence Levels  
(conditional on 8-Hz band level)

Octave Band and Criteria	1982 (Percent of time BSL exceeded)	1983 (Percent of time BSL exceeded)	MOD-1 (Percent of time BSL exceeded)
8-Hz BSL	>60 dB/Hz	81	88
	>65 dB/Hz	47	50
	>70 dB/Hz	21	13
16-Hz BSL	>50 dB/Hz	80	88
	>55 dB/Hz	71	85
	>60 dB/Hz	37	44
	>65 dB/Hz	14	7
31.5Hz BSL	>40 dB/Hz	81	88
	>45 dB/Hz	81	88
	>50 dB/Hz	81	88
	>55 dB/Hz	60	58

L-Criteria Exceedence Levels

Octave Bands (Hz)	BSL (dB/Hz)	BSL (dB/Hz)	BSL (dB/Hz)
8-Hz	L <sub>10</sub>	68	68
	L <sub>20</sub>	66	66
	L <sub>eq</sub>	64	63
16-Hz	L <sub>10</sub>	61	61
	L <sub>20</sub>	59	60
	L <sub>eq</sub>	57	58
31.5-Hz	L <sub>10</sub>	56	56
	L <sub>20</sub>	55	55
	L <sub>eq</sub>	54	54
63-Hz	L <sub>10</sub>	49	50
	L <sub>20</sub>	48	49
	L <sub>eq</sub>	47	48

**Table 5-10. Exceedence Level Summary for 1983 LF-Range Octave BSL Values**

Run Number	Percent of Time Exceeded		
	8-Hz Band		
	BSL > 60 dB/Hz	BSL > 65 dB/Hz	BSL > 70 dB/Hz
A05	97	54	4
A03	83	40	8
A14-1	77	24	3
A14-2	94	48	7
A18	99	84	46
A11	99	87	51
	16-Hz Band		
	BSL > 55 dB/Hz	BSL > 60 dB/Hz	BSL > 65 dB/Hz
A05	95	54	1
A03	76	32	1
A14-1	76	36	3
A14-2	87	24	1
A18	98	75	28
A11	99	80	27
	31.5-Hz Band		
	BSL > 45 dB/Hz	BSL > 50 dB/Hz	BSL > 55 dB/Hz
A05	97	97	73
A03	83	83	43
A14-1	77	77	63
A14-2	94	94	27
A18	99	99	77
A11	99	99	84

**Table 5-11. MOD-2 Rotor Space-Time Correlation Scales for Four Aeroacoustic/Aeroelastic Parameters**

Run No.	Chord Moment		Flap Moment		Normal Force		Acoustic Pressure <sup>a</sup>		Ri No.	U <sub>H</sub> (mps)
	l <sub>c</sub> (m)	t <sub>c</sub> (ms)	l <sub>c</sub> (m)	t <sub>c</sub> (ms)	l <sub>c</sub> (m)	t <sub>c</sub> (ms)	l <sub>c</sub> (m)	t <sub>c</sub> (ms)		
A03-1	5.1	69.5	5.2	71.0	4.4	59.6	4.4	60.5	0.26	6.9
A05	5.3	72.3	5.6	77.0	5.0	68.0	4.6	63.3	12	7.3
A03	4.6 <sup>b</sup>	62.9 <sup>b</sup>	5.3	73.0	4.7	64.8	5.0	68.4	-0.12	7.9
A14-1	4.8	65.6	5.4	74.6	4.7	64.5	4.6	62.9	0.13	8.2
A14-2	4.7	64.1	5.3	72.7	5.5	75.0	4.8	65.2	0.26	9.9
A15-1	4.4	59.8	5.3	73.0	4.5	61.7	4.8	66.0	0.71	10.3
A18	4.7	64.1	5.2	71.5	5.1	70.3	4.7	64.5	1.26	12.9
A11	4.8	66.0	5.5	75.8	5.8	80.0	4.5	62.5	6.68	13.6
Mean	4.8	65.5	5.4	73.6	5.4	73.6	4.7	64.2		
S.D. <sup>c</sup>	0.28	3.9	0.15	2.1	0.74	10.2	0.18	2.4		

<sup>a</sup>8-Hz octave band acoustic pressure (Pa).

<sup>b</sup>Oscillatory behavior (36.7 Hz).

<sup>c</sup>Standard deviation.

## 6.0 MEASURING THE ANNOYANCE POTENTIAL OF A SINGLE MOD-2 TURBINE

Given our experience with the MOD-1 downwind turbine near Boone, N. C., summarized in Ref. [1], the desirability of assessing the potential of MOD-2 emissions for interior, low-frequency annoyance problems in nearby homes is very important. Several approaches to assessing this annoyance potential are available to us and include

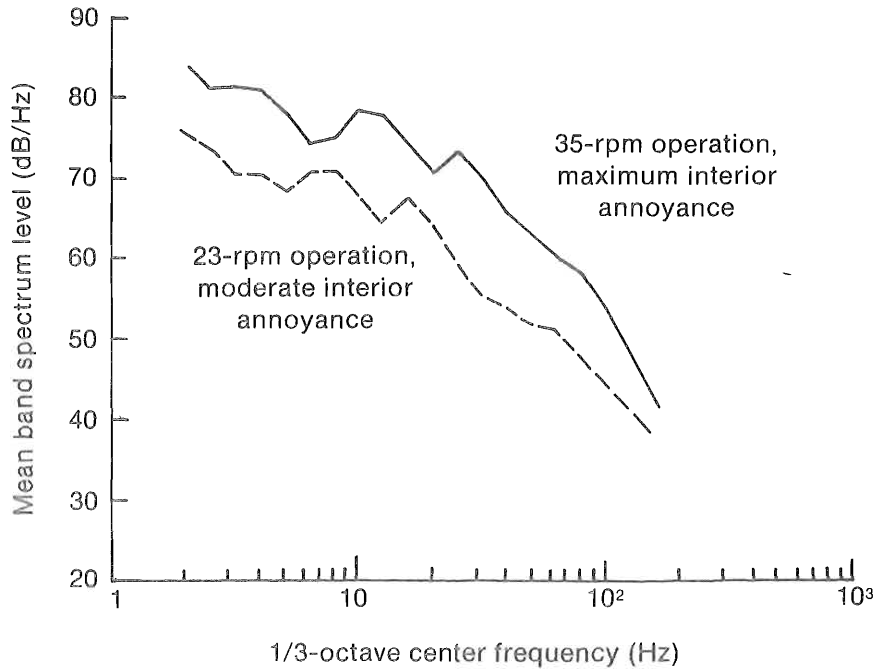
- (1) Comparing the known physical properties of the radiated acoustic pressure fields at a specified reference distance from the turbines
- (2) Assessing the interior annoyance potential from measurements of the MOD-2 emissions and comparing them with documented low-frequency annoyance situations.

The first of these was addressed to some extent in Section 5.3 and is expanded a bit more in this section. The real crux of the matter, however, lies with item (2), since the human element (i.e., the ultimate receptor of any annoyance) must somehow be brought into the equation. On this latter point, though considerable study has been done around the world, we have only a meager scientific data base on exactly what constitutes interior low-frequency annoyance and what conditions must be present for it to occur. Human annoyance from low-frequency sound and associated stimuli is highly subjective by its very nature. However, at some point the human element must be considered, and we have attempted to do that in a companion study [7]. The results of that limited study have been applied to individual MOD-1 and MOD-2 turbine emission characteristics to estimate the potential for interior annoyance problems in homes near these machines.

### 6.1 Additional Comparisons of MOD-1 and MOD-2 Emissions Characteristics and Their Relationship to Interior Annoyance Potential

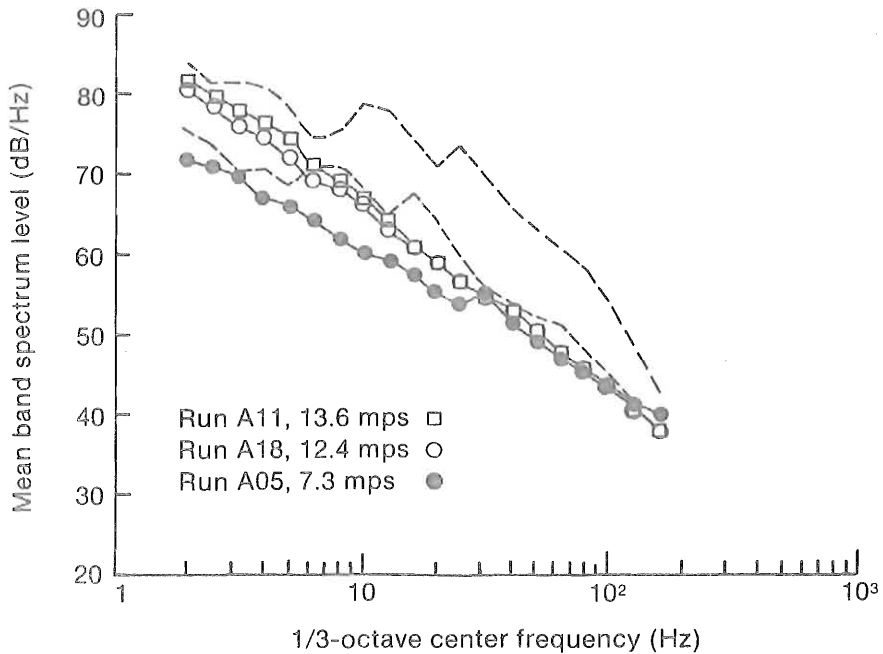
In the previous section, we pointed out that the degree of impulsiveness or coherence in the MOD-1 emissions was a major factor in the degree of annoyance described by occupants within 1-3 km (0.6-1.8 miles) of the turbine. This impulsiveness is manifested by a strong phase coherency in the radiated acoustic pressure field and can be measured by the degree of cross-correlation in the 8-, 16-, 31.5-, and 63-Hz octave band spectrum levels. These four octave bands cover the structural resonance region of most home construction in the United States. Tables 5-13 and 5-14 showed that, with one exception, the MOD-2 emissions were much less correlated or impulsive than those of the MOD-1 running at 23 or 35 RPM.

The mean band pressure spectra of Figure 6-1 show an approximate annoyance envelope for the MOD-1 at the reference distance of 1.5D. The upper curve (35 RPM) corresponds to the highest degree of interior annoyance at a far-field distance of 1 km and the lower one (23 RPM) to a moderate level. The six available MOD-2 MBSL spectra are plotted over this envelope in Figure 6-2. As indicated, above the 5-Hz band all fall below the lower MOD-1 curve. The fact that the two spectra associated with the highest winds do fall within the dotted area is insignificant, since this occurs below the lower structural resonance cut-off of 5 Hz. The 1982 MOD-2 case that we noted (Table 5-7) as having the potential to cause low-frequency annoyance is shown in Figure 6-3, overlaid on the MOD-1 envelope. In this case, the MBSL spectrum falls



008324

Figure 6-1. MOD-1 Mean 1/3-Octave Band Acoustic Spectra Associated with Numerous Complaints of Community Annoyance at 1 km from the Turbine



008325

Figure 6-2. Comparison of MOD-1 Acoustic Spectra of Figure 6-1 with Spectra from the 1983 MOD-2 under Lowest (Run A05) and Highest (Runs A11 and A18) Wind Conditions

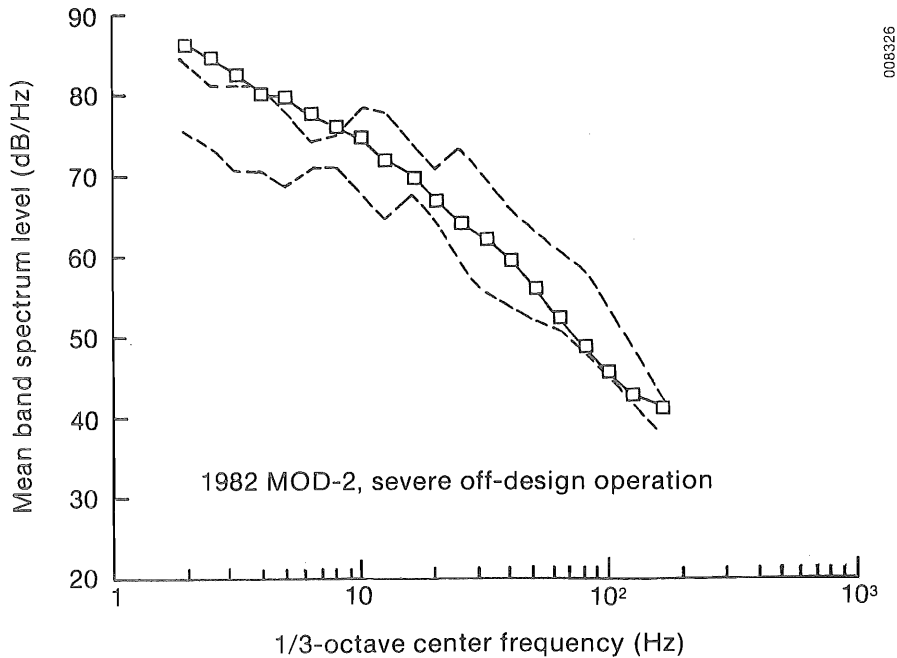


Figure 6-3. Comparison of MOD-1 Acoustic Spectra of Figure 6-1 with Spectra from the 1982 MOD-2 Operating in a Severe Off-Design Condition (Run 25-1)

between the two MOD-1 curves (between 5 and 100 Hz) and, under the right circumstances, we believe it could result in interior annoyance. This again demonstrates that even though the turbine's rotor is upwind of the support tower, there is the potential for acoustic emissions characteristics similar to a downwind turbine if the turbine is allowed to run severely off-design!

6.2 Use of the PLSL Metric in Assessing Potential Interior Annoyance

We found that the interior annoyance problem associated with the MOD-1 turbine was a complex interaction between a room's structural and acoustic resonances excited by the external impulsive acoustical loads being propagated from the turbine [1]. It has never been totally clear whether the occupants heard, felt, or experienced some combination of both stimuli as a result of this periodic loading. Many experts believe both that tactile (feeling) and aural (hearing) responses to these stimuli are involved. As a result, we used volunteer subjects to conduct a limited evaluation of simulated, interior low-frequency noise environments that could result from three wind turbine designs or installations. The details of the testing and the development of the proposed metric are given in Ref. [7].

6.2.1 Synopsis of Results of the Interior Low-Frequency Noise Evaluation Experiment

A limited evaluation of the degree of annoyance in four simulated interior noise environments related to wind turbine installations was performed with volunteer subjects. The interior noise environments were associated with (1) a single, large upwind turbine (a random periodic source); (2) the same source as (1) except with a 40-dBA pink noise masking; (3) a single, downwind turbine

operating at 30 RPM (a periodic impulsive source); and (4) multiple downwind turbines (a random impulsive source). The volunteers listened to these simulations, which were systematically varied in intensity, in an environment comparable to a small room in a typical home and provided written impressions of what they were experiencing.

#### 6.2.1.1 Identifying an Efficient Estimator of Interior LF Annoyance

The volunteers' responses were quantified by means of a five-level ranking in terms of loudness, the overall degree of annoyance and displeasure, any feelings of vibration or pressure, and the sensing of any pulsations. Table 6-1 lists the subjective ranking criteria. These ranked responses were then numerically correlated with a series of low-frequency noise descriptors or metrics. The metrics used have been suggested as measures of low-frequency annoyance by a number of investigators and included the following spectral weighting factors:

- o The ISO (International Organization for Standards) proposed "G<sub>1</sub>" weighting [22]
- o The ISO proposed "G<sub>2</sub>" weighting [21]
- o The "LSPL" weighting [22]
- o The "LSL" weighting [22]
- o The ISO/ANSI (American National Standards Institute) "C" weighting [23]
- o The ISO/ANSI "A" weighting [23].

Figure 6-4 plots the weighting windows in the frequency range under 100 Hz for the metrics above. The ISO "G<sub>1</sub>" and "G<sub>2</sub>-weighting" curves have been proposed for assessing subjective human responses to infrasonic-range (less than 20 Hz) acoustic stimuli. The ISO/ANSI "C-weighting" was originally developed to approximate the human ear loudness sensitivity for pure tones at a high sound pressure level (100 phons). As we see in Figure 6-4, the "C-weighting" spectral curve extends to much lower frequencies than the most common noise weighting metric, the "A-weighting" scale. Tokita et al. [22] proposed two new frequency weightings for residential interior environments, the LSPL (low-frequency sound pressure level) and LSL (low-frequency sound level). The LSL metric, according to Ref. [22], "reflects three low-frequency noise influences: structural, physiological, and psychological complaint stimuli." The LSL metric has been proposed as an appropriate descriptor for evaluating residential interior environments that contain both infra- and low-frequency-range audible acoustic components.

The ranked responses were correlated by regression; the results for the loudness and annoyance/displeasure categories are listed in Table 6-2. Immediately obvious is the superiority of the five metrics that contain significant low frequencies, in comparison with the A-weighted scale. The highest correlation occurs with the LSL metric, with a mean correlation coefficient of 0.936 for these two perception categories. We believe that the LSL weighting provides an efficient measure of the annoyance potential to persons exposed to low-frequency wind turbine noise in their homes.

Table 6-1. Low-Frequency Noise Environments Subjective Ranking Criteria

Rank	Stimuli Response Rating					
	0	1	2	3	4	5
	Perception					
<u>Noise Level</u> (loudness)	Can't Hear	Barely can hear	Weak, but definitely audible	Moderate loudness	High noise level, loud	Very high noise level, very loud
<u>Annoyance/Displeasure</u>	None	Barely aware of presence	Definitely aware of presence	Moderate distraction/some irritation	Very annoying, irritating	Extremely annoying, uncomfortable
<u>Vibration/Pressure</u>	None	Feel presence	Definitely feel vibration/pressure	Moderate vibration/pressure feeling	Very noticeable	Severe vibration
<u>Pulsations</u>	None	Barely feel pulses	Definite pulses or bumping	Moderate booming or thumping	Heavy booming or thumps	Very heavy pulses, booms, thumps
-----	Acceptable		????????????????		Clearly unacceptable	
-----	-----					

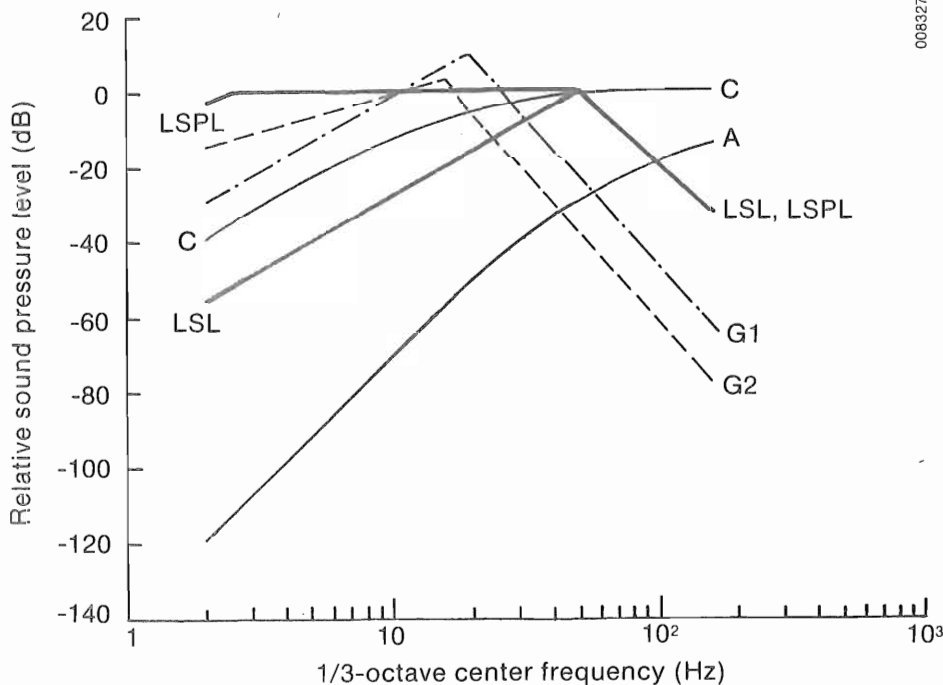


Figure 6-4. Low-Frequency Noise Metrics Spectral Weightings

**Table 6-2. Correlation Coefficients of Volunteer Ratings of Low-Frequency Noise Stimuli versus Six Noise Metrics**

Metric	Noise Level	Annoyance/ Displeasure	Mean
LSL	0.923	0.948	0.936
C	0.913	0.938	0.926
G <sub>1</sub>	0.891	0.920	0.906
LSPL	0.894	0.913	0.904
G <sub>2</sub>	0.868	0.887	0.878
A	0.307	0.270	0.289

#### 6.2.1.2 Establishing an LSL Annoyance Scale

The volunteer-comment rankings for each of the four stimuli were summarized, and three final levels were determined for each. The perception threshold has been defined as the corresponding LSL value for an evaluation ranking of 1. The annoyance threshold LSL was assigned a ranking of 2.5, and an unacceptable annoyance level assigned an LSL of 4 or above. The LSL values corresponding to these levels are listed in Table 6-3 for the four stimuli evaluated. As we can see in the upper portion of Table 6-3, three of the four stimuli have similar threshold LSL values. It is interesting to note that even though many individually impulsive sources may be present, the net effect of a random summing of these contributions invokes a response similar to that from a random periodic source. Thus, the threshold is considerably lower for a source consisting of an individual or a few impulsive sources. This is reflected by the two categories at the bottom of Table 6-3.

#### 6.2.2 A Methodology for Predicting Interior LSL Values

Often we must predict the low-frequency annoyance potential to a surrounding community from a new turbine or turbines before installation as part of the siting approval process. Since we will rarely have the opportunity to have actual measurements within nearby residences, we needed to find a way to estimate or predict interior LSL levels (predicted low-frequency sound level or PLSL), given the characteristic low-frequency acoustic emission statistics of a given wind turbine design.

##### 6.2.2.1 Predicting an Interior LSL Level

In order to predict interior LSL levels, given a representative external acoustic loading spectrum, we needed to determine a typical indoor/outdoor acoustic transfer function for housing construction in the United States. We identified a typical transfer function by using available data collected from two homes under MOD-1 impulsive excitation, from five homes in Oregon experiencing nonimpulsive, low-frequency acoustic loading (the exhaust stack from a gas turbine's peaking generator [24]), and from an experiment utilizing a standard-construction test home operated by SERI. We found that a different

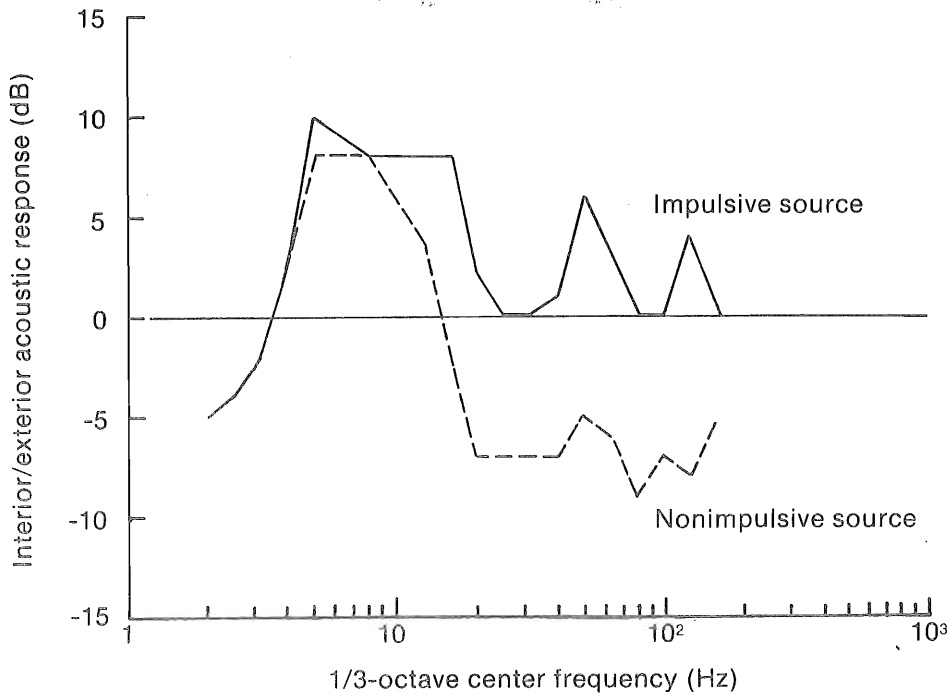
**Table 6-3. SERI Interior Low-Frequency Annoyance Criteria Employing the LSL Metric**

Stimuli	LSL Threshold Perception (dB)	LSL Annoyance Threshold (dB)	LSL Unacceptable Annoyance Level (dB)
Upwind turbines (random periodic)	58	65	68
Single or few downwind turbines (periodic impulsive)	53	57	60
Many downwind turbines (random impulsive)	59	68	70
Upwind turbines with 40 dBA masking	59	65	67
Considering Only General Source Characteristics			
Nonimpulsive source	58	65	68
Impulsive source	53	57	60

spectral response is typical of homes undergoing impulsive loading (from the MOD-1 or a few downwind turbines) compared with random excitation (sources such as a single upwind turbine or many downwind ones). Figure 6-5 plots these two typical transfer or acoustic transmissibility functions. As we can see, impulsive loading is characterized by much higher acoustic transmissibilities above about 10 Hz in comparison to random, external acoustic loads. The details related to the physics responsible for these curves are discussed in [1]. Using each of the transfer functions plotted in Figure 6-5, we modified and replotted the original frequency weighting of the LSL parameter in Figure 6-6. An interior estimate of the PLSL level is calculated by applying the appropriate weighting curve of Figure 6-6 (impulsive or nonimpulsive) to an externally measured 1/3-octave band pressure spectrum.

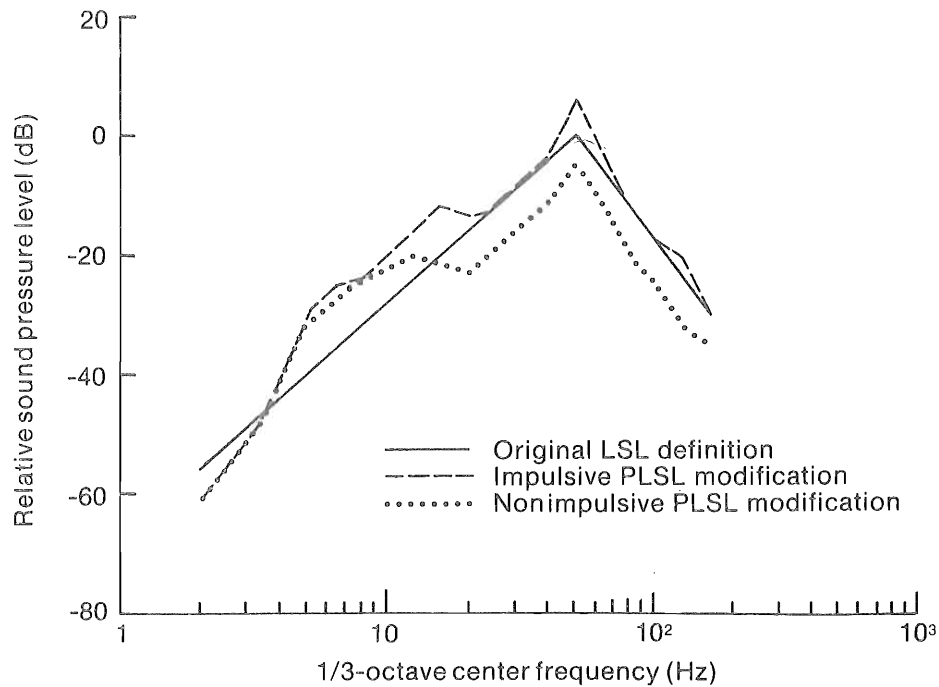
#### 6.2.2.2 Establishing a Reference External Acoustic Loading

The method of estimating a representative PLSL value requires a suitable measure of the external acoustic loading spectrum. Since most homes are located at some distance from the nearest wind turbine(s), a method must be devised to provide a reference spectrum that takes into account situations in which atmospheric refraction and surface reflection combine to increase the observed levels above that expected from spatial divergence alone. In order to achieve a "figure-of-merit" PLSL value for a single MOD-2 turbine, a



008328

Figure 6-5. Typical Indoor/Outdoor Transmissibility Functions for Impulsive and Nonimpulsive Acoustic Loadings



008329

Figure 6-6. Modification of Original LSL Frequency Weighting for Impulsive and Nonimpulsive PLSL Measurements

reference distance of 1 km (approximately 10D) was chosen. Table 6-4 lists the 1983 MOD-2 PLSL<sub>eq</sub> and PLSL<sub>10</sub> values at the reference distance of 1 km propagated by spatial divergence alone and with an additional 15 dB of terrain/atmospheric focusing as a worst-case estimate. The worst-case 1982 MOD-2 run (ST25-1) and the 35- and 23-RPM cases from the MOD-1 are also listed for comparison in Table 6-4.

**6.3 Estimating the Community Annoyance Potential of Both an Individual MOD-2 Turbine and Clusters of Turbines**

Community annoyance related to the acoustic emissions of a single MOD-2 turbine has two sources: (1) emissions in the high-frequency range generally heard outdoors or through open windows, and (2) interior annoyance arising from structural loading by acoustic energy in the low-frequency range. We discuss both sources below.

**6.3.1 Annoyance Potential from High-Frequency-Range Emissions**

From the results of our measurements of the high-frequency characteristics discussed in Section 4.0, we have reached the following conclusions.

- (1) The aural identification of a single turbine or a cluster of MOD-2 turbines as the source of HF, broadband sounds can be expected, on the average, 1.2-1.5 km (4000-5000 ft) downwind of the nearest turbine. This recognition distance depends on the state of the acoustic environment at the observer's location and the distance to the nearest turbine.

**Table 6-4. Predicted Interior LSL (PLSL) Values at 1 km from the MOD-2 Turbine (1983 Configuration)**

Run Number	PLSL <sub>eq</sub> (dB)	PLSL <sub>eq</sub> +15 (dB)	PLSL <sub>10</sub> (dB)	PLSL <sub>10</sub> +15 (dB)
A03-1	37	52	39	54
A03	41	56	43	58
A05	39	54	44	59
A14-1	42	57	45	60
A14-2	40	55	43	58
A15-1	44	59	47	62
A18	43	58	46	61
A11	43	58	46	61
Means	41	56	44	59
<u>1982 MOD-2 (severe off-design operation)</u>				
ST25-1	56	71	60	75
<u>MOD-1 (worst cases)</u>				
35-RPM	65	80	68	83
23-RPM	54	69	58	73

- (2) While the broadband sounds modulated at the blade passage frequency can often be distinguished above local acoustical background at distances exceeding 1.6 km (1 mile) under the right atmospheric conditions (i.e., low wind speeds in the vicinity of the observer), there appears to be a very low probability of community annoyance from a single MOD-2 turbine at distances beyond 1 km (0.6 mile). Typical  $L_{eq}$  levels measured at the Goodnoe Hills Site and 0.9 km downwind of Turbine No. 2 were 43-45 dBA for representative recording periods of 6 hours, which included a wide range of inflow conditions. The corresponding  $L_{10}$  and  $L_{90}$  levels were 53 and 43 dBA, respectively.
- (3) A series of narrowband (12.5-Hz resolution) analyses of the high-frequency portion of the radiated spectrum taken covering a range of inflow conditions showed no persistent tonal (discrete frequency) noise. This indicates that the mechanical noise sources are well controlled, making the rotor's aerodynamically generated sounds the dominant HF source.

### 6.3.2 Interior Annoyance Potential of Low-Frequency-Range Emissions

Using the PLSL metric discussed in Section 6.2, we concluded that the likelihood of interior annoyance resulting from acoustical loading produced by 1983 MOD-2 LF emissions on homes located a kilometer or more away is very remote. Even under the worst generation and propagation conditions (a home located where a combination of terrain reflection and atmospheric refraction is producing 15 dB of enhancement), it is unlikely that the turbine would be detectable within a home with the windows closed a kilometer or more away.

## 7.0 CONCLUSIONS

### 7.1 High-Frequency-Range Acoustic Characteristics

At the Goodnoe Hills site, the average audible range of a single MOD-2 turbine was found to be about 1.2-1.5 km (4000-5000 ft). A polynomial which describes the average fall-off with distance for the Goodnoe Hills site is

$$L_{eq}(A) = -3.89454 x^4 + 46.6729 x^3 - 191.884 x^2 + 287.151 x - 28.4 ,$$

where  $L_{eq}(A)$  is the equivalent sound pressure level in dB and  $x$  is the  $\log_{10}$  of the downwind distance in feet. When multiple turbines were operating, the turbine noise level experienced by an observer is dominated by the nearest turbine.

The  $L_{eq}(A)$  at a distance of 1.5 rotor diameters (1.5D, 137 m or 450 ft) from the rotor plane was found to vary, primarily with the hub-height wind speed. This variation in dB can be expressed to within  $\pm 0.5$  dB over a wind-speed range of 6-15 m/s by

$$L_{eq}(A) = 1/2 U_H + 57 ,$$

where  $U_H$  is the hub wind speed in m/s.

A comparison of the 1982 and 1983 turbine configurations revealed an apparent upper-band-limiting of the 1983 emissions as a result of the vortex generator installation and pitch schedule modifications.

No significant, steady tone noise components were found in the high-frequency-range narrowband (25-Hz) spectra. This indicates that the mechanical noise sources are well controlled, and there appear to be no discrete aeroacoustic sources of consequence.

### 7.2 Low-Frequency-Range Acoustic Characteristics

The variances observed of the the ensemble mean and the first three statistical moments of randomly sampled, low-frequency acoustic emission spectra in 1/3-octave band resolution were found to be adequately explained via a linear, multivariate regression model, with the following inflow scales as the most efficient predictors:

- A mean wind speed at a height within the rotor disk layer
- The gradient Richardson number stability parameter (Ri) measured across the rotor disk layer
- The Monin-Obukov length scale,  $L$
- The vertical or upwash turbulence integral scale,  $I_w^z$ .

Comparisons made between the 1982 and 1983 emissions showed that the 1983 turbine was far more acoustically sensitive to inflow stability.

The physics of the rotor-turbulence interaction are such that unsteady blade loads are the most common source of radiated low-frequency acoustic emissions and much of the rotor aeroelastic response. We can achieve a high correlation with the former using bulk scaling measures of the inflow, so this technique might be successfully extended to the latter. This would allow a given rotor aeroelastic response to be expressed directly in terms of surface-layer turbulence bulk properties.

The common origin of the rotor low-frequency acoustic and aeroelastic responses was demonstrated by space-time correlation measurements. We found that observed flap and chordwise bending moments, blade normal forces, and the 8-Hz band, radiated acoustic pressures were similarly correlated over time periods of 65-75 ms. These periods suggest that the unsteady processes responsible for the fluctuations take place over a rotor travel distance of about 5 m for the MOD-2 blade.

### 7.3 Comparisons of MOD-2 Low-Frequency Emission Characteristics with Those of the MOD-1

Measurements of the MOD-2 showed that the 1983 turbine configuration produced less coherent (impulsive) low-frequency acoustic radiation than the 1982 version and much less than the MOD-1 turbine operating at either 35 or 23 RPM under the worst impulsive conditions. The degree of coherency (impulsiveness) in the 1983 turbine emissions was found to be strongly related to the vertical atmospheric stability (Richardson number), the vertical or upwash turbulence scale length,  $I_w^z$ , and the blade loading, as indicated by the mean axial velocity.

It is clear in 1982, the MOD-2 rotor instabilities associated with unstable, high-velocity inflows were responsible for producing low-frequency acoustic emissions that resembled those of the downwind MOD-1 turbine under the worst impulsive conditions. A definite improvement was made in the levels and impulsiveness of the LF emissions by the addition of the vortex generators and pitch schedule changes.

### 7.4 Community Annoyance Potential of a Single MOD-2 Turbine

While the broadband sounds modulated at the blade passage frequency can often be distinguished above the local acoustical background at distances exceeding 1.6 km (1 mile) under the right atmospheric conditions, there appears to be a very low probability that community annoyance will result from a single MOD-2 turbine in the 1983 configuration beyond a distance of 1 km. Even under the worst generation and propagation conditions (a home located where a combination of terrain reflection and atmospheric refraction produces 15 dB of enhancement), it is unlikely that the turbine noise would be detectable within a home with closed windows a kilometer or more away.

## 8.0 RECOMMENDATIONS

We strongly recommend that the techniques developed for the acoustic characterization of the MOD-2 Unit No. 2 at Goodnoe Hills be applied to the one remaining MOD-2 turbine currently operating in California (Unit No. 5). This will permit the following to be accomplished:

- (1) A verification of the atmospheric surface-layer bulk properties as accurate predictors of ensemble statistical distributions of low-frequency acoustic emissions
- (2) Comparisons of the statistically derived acoustic response functions for the Goodnoe and Solano Hills sites
- (3) Detailed comparisons of the turbulent inflow properties for the two regimes.

We further recommend that the techniques developed for the MOD-2 turbine be applied to a range of wind turbine designs and sizes in order to isolate critical scaling parameters to be used in predicting acoustic noise and in developing control strategies.

## 9.0 REFERENCES

1. Kelley, N.D., H.E. McKenna, R.R. Hemphill, C.L. Etter, R.L. Garrelts, and N.C. Linn, Acoustic Noise Associated with the MOD-1 Wind Turbine: Its Source, Impact and Control, SERI/TR-635-1156, Golden, CO: Solar Energy Research Institute (February 1985), 262 pp.
2. Hubbard, H.H., K.P. Shepherd, and F.W. Grosveld, Sound Measurements of the MOD-2 Wind Turbine Generator, NASA CR-165752, Hampton, VA: NASA Langley Research Center (July 1981), 29 pp.
3. Stephens, D.G.; K.P. Shepherd, H.H. Hubbard, and F.W. Grosveld, Guide to the Evaluation of Human Exposure to Noise from Large Wind Turbines, NASA TM-83288, Hampton, VA: NASA Langley Research Center (March 1982), 70 pp.
4. Shepherd, K.P., Detection of Low Frequency Impulsive Noise from Large Wind Turbines, NASA CR-172511, Hampton, VA: NASA Langley Research Center (January 1985), 23 pp.
5. Hemphill, R.R., An Acoustic Ranging Technique with Application to Assessment of Low-Frequency Acoustic Noise of Wind Turbines, SERI/TP-215-1954, Golden, CO: Solar Energy Research Institute (May 1983), 10 pp.
6. Kelley, N.D., H.E. McKenna, and E.W. Jacobs, Observed Acoustic and Aeroelastic Spectral Responses of a MOD-2 Turbine Blade to Turbulence Excitation, SERI/TP-214-2374, Golden, CO: Solar Energy Research Institute (June 1984), 7 pp.
7. Kelley, N.D. A Proposed Metric for Assessing the Potential of Community Annoyance from Wind Turbine Low-Frequency Noise, SERI/TP-217-3261, Golden, CO: Solar Energy Research Institute (October 1987), 9 pp.
8. Simms, D.A., N.D. Kelley, H.E. McKenna, and E.W. Jacobs, A Comparison of Micrometeorological Measurements Made from a Tethered Balloon and a Meteorological Tower, SERI Technical Report, in preparation.
9. Panofsky, H.A., and J.A. Dutton, Atmospheric Turbulence, New York: John Wiley & Sons, Inc. (1984) 397 pp.
10. Homicz, G.F., Broadband and Discrete Frequency Noise Radiation from Subsonic Rotors, Ph.D. Dissertation, Ithaca, NY: Cornell University (1973).
11. Homicz, G.F., and A.R. George, "Broadband and Discrete Frequency Radiation from Subsonic Rotors," J. of Sound and Vibration, Vol. 36 (1974), pp. 151-177.
12. George, A.R., and S.T. Chou, "Comparison of Broadband Noise Mechanisms, Analyses, and Experiments on Helicopters, Propellers, and Wind Turbines," presented at AIAA 8th Aeroacoustics Conference, Paper No. AIAA-83-0690, Atlanta, GA, 11-13 April 1983.

13. Monin, A.S., and A.M. Obukhov, "Basic Regularity in Turbulent Mixing in the Surface Layer of the Atmosphere," Trudy Geophys. Inst. ANSSSR, No. 24, as referenced by J.L. Lumley and H.A. Panofsky in The Structure of Atmospheric Turbulence, New York: John Wiley & Sons, Inc. (1964), 239 pp.
14. Monin, A.S., and A.M. Yaglom, Statistical Fluid Mechanics, Vol. I, J.L. Lumley, ed., Cambridge, MA: The MIT Press (1971), 769 pp.
15. Businger, J.A., J.C. Wyngaard, Y. Izumi, and E.F. Bradley, "Flux-Profile Relationships in the Atmospheric Surface Layer," J. Atmospheric Science, Vol. 28 (1971), pp. 181-189.
16. Kaimal, J.C., "Turbulence Spectra, Length Scales and Structure Parameters in the Stable Surface Layer," Boundary-Layer Meteorology, Vol. 4 (1973), pp. 289-309.
17. George, A.R., and Y.N. Kim, "High-Frequency Broadband Rotor Noise," AIAA Journal, Vol. 15, No.4 (April 1977), pp. 538-545.
18. Hojstrup, J., "A Simple Model for the Adjustment of Velocity Spectra in Unstable Conditions Downstream of an Abrupt Change in Roughness and Heat Flux," Boundary-Layer Meteorology, Vol. 21 (1981), pp. 341-356.
19. Kelley, N.D., H.E. McKenna, and R.R. Hemphill, "A Methodology for Assessment of Wind Turbine Noise Generation," J. Solar Engineering, Vol. 104 (May 1982), pp. 112-120.
20. Wyngaard, J.C., "On Surface-Layer Turbulence," in Workshop on Micrometeorology, D.A. Haugen, ed., Boston, MA: American Meteorological Society (1973), pp. 101-149.
21. International Organization for Standardization (ISO), Draft Proposal for "Acoustics Methods for Describing Infrasound," ISO/DIS 7196, Geneva, Switzerland: ISO.
22. Tokita, Y., A. Oda, and K. Shimizu, "On the Frequency Weighting Characteristics for Evaluation of Infra and Low Frequency Noise," Proc. 1984 Conf. on Noise Control Engineering, G.C. Maling, Jr., ed., Poughkeepsie, NY: Institute of Noise Control Engineering (1984), pp. 917-920.
23. American National Standards Institute (ANSI), "American National Standard Specification for Sound Level Meters," ANSI S1.4-1983, New York, NY: ANSI (1983).
24. Robin Towne, Assoc., Environmental Study of Low Frequency Noise and Vibration, A Report to the Portland General Electric Co., Portland, OR: Robin Towne Assoc. (1974), 144 pp.
25. Kelley, N.D., A Detailed Examination of the Goodnoe Hills Microscale Turbulence Structure and Its Impact on Aeroacoustic Noise Generation, SERI Technical Report, (a proposed report).

26. Ffowcs Williams, J.E., and D.L. Hawkings, "Theory Relating to the Noise of Rotating Machinery," J. Sound and Vibration, Vol. 10 (1969), pp. 10-21.

<b>Document Control</b> <b>Page</b>	1. SERI Report No. TR-217-3036	2. NTIS Accession No.	3. Recipient's Accession No.
4. Title and Subtitle The MOD-2 Wind Turbine: Aerocoustical Noise Sources, Emissions, and Potential Impact		5. Publication Date January 1988	
		6.	
7. Author(s) N.D. Kelley, H. McKenna, E. Jacobs, R. Hemphill,		8. Performing Organization Rept. No.	
9. Performing Organization Name and Address Solar Energy Research Institute 1617 Cole Boulevard Golden, Colorado 80401-3393		10. Project/Task/Work Unit No. WE721201	
		11. Contract (C) or Grant (G) No. (C) (G)	
12. Sponsoring Organization Name and Address		13. Type of Report & Period Covered Technical Report	
		14.	
15. Supplementary Notes			
16. Abstract (Limit: 200 words)  This report summarizes research into characteristics of acoustic noise emissions of the DOE/NASA MOD-2 wind turbine. The results of this study showed that the MOD-2 noise levels are well below annoyance thresholds within residential structures a kilometer or more from the turbine rotor. It was also found that the inflow turbulent structure has a major influence on the level and characteristics of the low-frequency-range (2-150 Hz) acoustic emissions which, in turn, have implications for the associated structural response of the rotor assembly. The high-frequency-range (A-weighted) levels were found to vary primarily with the mean hub-height wind speed. The rotor inflow turbulence characteristics at the Goodnoe Hills site were found to be controlled almost entirely by the diurnal variation in the vertical stability of the first 100 m of the atmospheric boundary layer.			
17. Document Analysis a. Descriptors Wind power ; wind turbines ; acoustic measurements ; turbulence  b. Identifiers/Open-Ended Terms   c. UC Categories 60			
13. Availability Statement National Technical Information Service U.S. Department of Commerce 5285 Port Royal Road Springfield, Virginia 22161		19. No. of Pages 211	
		20. Price A10	